

**PHYS 578A : Special Topics in Theoretical Physics**  
**Quantum Information and Simulation for Scientific Applications**  
**Spring 2024**

Martin J. Savage<sup>1</sup>

<sup>1</sup> *The InQuBator for Quantum Simulation (IQuS), Department of Physics,  
University of Washington, Seattle, WA 98195-1550, USA*

(Dated: June 19, 2024)

This document contains all of the material associated with the 2024 offering of PHYS 578A **Quantum Information and Simulation for Scientific Applications**, that was offered during the Spring of 2024. This is a variant of the material from the Spring of 2022 and 2023. This was the third time the course was offered. The referencing remains quite poor, apologies to all, but they will continue to be improved during later offerings.

These notes bring together results and understandings arrived at by our community of scientists. They have been formed from discussions, teachings, collaborations, workshops, conferences, programs, publications, and an uncountable number of conversations with others.

Confession: In this area, I can point to opportunities that I missed as a junior scientist, or ones that I simply did not appreciate the depth and importance of because of my lack of wisdom. This includes not absorbing the importance of quantum information to fundamental physics while I was a graduate student at Caltech in the last 1980's, where both Feynman and Gell-Mann paved the way in this area and taught advanced graduate classes. From this, I learned that when accomplished scientists are thinking about "odd things", one should always pay attention! Further, I learned that having/making the time to think about odd things, is also an important part of being a scientist.

## Contents

<b>I. Introduction</b>	4
A. Welcome	4
B. Code of Conduct	4
C. Where did the course come from?	4
D. Objective: QIS to SM	5
E. Objective: SM to QIS	5
F. Quantum Information	6
1. 20th Century and Entanglement	6
2. Our Universe, pure state and unitary evolution	6
3. Subsystems of our universe	7
4. Life	7
5. Classical, Quantum	8
6. Implication	10
7. Quantum Correlations	11
8. Understanding this aspect of the Standard Model	11
9. Quantum Teleportation	11
G. Classical Limits, Complexity and Quantum Simulation	13
1. Feynman and Computing	13
H. Classical Difficulties	16

1. Signal-To-Noise in Statistical Sampling used in Classical Simulations, e.g., Nucleons in Lattice QCD	17
2. Sign Problems	20
I. Related Comments on Scientific Applications	20
J. Some Words about Quantum Simulation	21
<b>II. Quantum Circuits for Digital Quantum Simulation</b>	22
A. 1-qubit	22
B. 2-qubits	25
1. Molmer-Sorensen Gate	27
2. Controlled Operators	29
C. Hamiltonian Evolution	31
D. Qutrits	32
1. Givens Rotations	33
<b>III. Entanglement Measures</b>	34
A. Pure and Mixed Ensembles	35
B. Separability	35
C. Schmidt Decomposition	37
D. Entanglement Entropy	38
E. Rényi Entropy	39
F. Distillable Entanglement	39
G. Concurrence	40
H. Partial Transpose and Negativity	41
I. N-Tangle	42
J. Entanglement Witness	42
<b>IV. Lattice Scalar Field Theory and Quantum Simulation</b>	42
A. One Lattice Site	45
B. Two Lattice Sites	45
C. Four Lattice Sites	47
D. Arbitrary Number of Lattice Sites	48
E. Lattice Scalar Field Theory ala Jordan, Lee and Preskill (JLP)	50
F. The Quantum Fourier Transform	55
1. The “Usual” (Un-Twisted) Quantum Fourier Transform	55
2. The Symmetric-Symmetric QFT (SSQFT) [1]	58
G. Quantum Circuits for Scalar Field Theory in JLP Basis	59
1. Time Evolution of Scalar Field Theory in JLP Basis	61
2. Scalar Field Theory - $d$ -Dimensions	63
H. Sequency in Quantum Simulations	64
I. Adiabatic Preparation of the Vacuum of Scalar Field Theory	66
1. Preparing the Vacuum of Non-Interacting Scalar Field Theory - Somma Inflation	67
2. Preparing the Vacuum of Interacting Scalar Field Theory - Adiabatic Evolution [2]	68
3. Dark States from Adiabatic Evolution	69
J. Wavepacket Preparation in Lattice Scalar Field Theory (Jordan, Lee, Preskill [2])	73
K. Particle Detection and S-Matrix Elements (Jordan, Lee, Preskill [2])	75
<b>V. Time Evolution of Quantum Systems</b>	76
A. Trotterized Time Evolution	78

B. Higher-Order Trotterization	81
C. Randomly-Ordered Trotterization	83
D. qDrift [3]	85
E. Linear Combination of Unitaries (LCUs)	86
F. Quantum Imaginary Time Evolution (QITE)	89
G. Other	90
<b>VI. Quantum Simulations of Lattice Gauge Theories</b>	90
A. Fermions in 1+1 Dimensions	90
1. Time Evolution of Free fermions using a JW Mapping	94
B. Yukawa Theory in 1+1 Dimensions: 1 Fermion and 1 Scalar	97
C. 1+1 QED - The Schwinger Model in the Continuum	98
D. The Lattice Schwinger Model in $A_0 = 0$ Gauge	101
1. Eliminating the (Spatial) Gauge-Field from the Outset : A Non-Local Mapping of the Schwinger Model using Axial Gauge: $A_x = 0$	105
2. More than one species: $e^-$ and $\mu^-$	106
3. Background Charges	108
4. Quantum Circuits	109
E. Non-Abelian Gauge Theories in 1+1 Dimensions	110
1. The Extension to SU(3) in 1+1D	113
F. Yang-Mills Lattice Gauge Theory in Higher Dimensions	114
1. Plaquettes	114
2. In the Beginning....There was One Plaquette of Glue	119
3. Global Basis	119
4. Measurement Error Mitigation	122
5. Dynamic Decoupling	123
6. Pauli-Twirling or Randomized Compiling	124
7. Decoherence Renormalization	124
8. Local Basis	125
9. Insights from SU(2) Lattice Gauge Theory	127
<b>VII. Applied Quantum Computational Complexity</b>	127
A. Stabilizer States	128
1. Stabilizer States for Qubit Systems	128
2. Qutrits	129
3. Stabilizer States for Qutrit Systems	131
B. Magic	134
1. Magic for Qubit Systems	134
2. Magic for Qutrit Systems	134
C. The Entanglement Power and Magic Power of Unitary Operators	135
<b>VIII. Assignment-1</b>	136
A. A One-Qubit Effective Hamiltonian and Time Evolution	136
B. State Preparation: A Real Function on Two Qubits	136
<b>IX. Assignment-2</b>	137
A. Question 1: Entanglement	137
B. Question 2: Non-Interacting and Interacting Scalar Field Theory	137
<b>X. Assignment-3</b>	138

A. Question 1: Time Evolution	138
<b>XI. Assignment-4</b>	139
A. Question 1: The Schwinger Model	139
<b>A. Gell-Mann Matrices</b>	140
1. Side Note	140
<b>References</b>	140

## I. INTRODUCTION

### A. Welcome

Welcome to QIS and Simulation for Scientific Applications! This is the third time this course has been offered, with the first version in 2022, and second in 2023.

### B. Code of Conduct

It is important to have a code of conduct (CoC) at any gathering that is understood by everyone. I would like you all to read the CoC of the Physics Department, the UW and of IQuS, think about its contents, what it means and agree to abide by them. This is important.

<https://iqus.uw.edu/about-us/code-of-conduct/>

<https://phys.washington.edu/code-conduct-uw-department-physics>

These are works in progress and continue to evolve as we all continue to better understand the essential rules of engagement, what is appropriate behavior and what is not, as we strive to move toward a more inclusive and diverse community.

### C. Where did the course come from?

This course naturally emerged from growing activity in the area of *quantum information science and engineering* in the UW's Physics Department, and more generally the UW, and is focused on the interface of QIS and fundamental physics, particularly Standard Model Physics (and beyond). Specifically, since about 2016, the QIS activity in US nuclear and particle physics has grown, driven by progress in multiple related areas, and by the challenges in these areas that clearly require QIS to be addressed.

My background in Standard Model and its descendent effective field theories, including nuclear forces, including more than 15 years of using classical HPC for lattice QCD simulations of single-meson and baryon, multi-meson and few-nucleon systems, including light nuclei with a great group of colleagues in the NPLQCD collaboration (which included Silas - who many of you know). A “feeling” of starting to feel the physical limits of classical computing for certain important aspects of simulations of such systems in the mid 2010s aligned well with the first appearances of quantum computers/devices with sufficiently long coherence times that elementary calculations became possible (around 2016). In particular, the nuclear physics community assessed the exascale HPC resources required to accomplish its objectives [4], and found that some lay beyond what could be expected to be accomplished with exascale computing resources, which generally fell into two categories 1) finite fermion density systems, and 2) real-time dynamics.

#### D. Objective: QIS to SM

While the ultimate goal of this endeavor is to be able to both reliably compute the static properties and dynamics of Standard Model systems from baryogenesis to the properties of dense matter, and to integrate our existing expertise to advance the understanding and applications of QIS, we are at the early stages along the path toward making this a reality. The present period in the evolution of this field, where the quantum devices are limited by short coherence times, limited size and noisy qubits (Noisy Intermediate-Scale Quantum – NISQ [5] as coined by John Preskill), is one of learning and understanding how we can design and control quantum devices in a way to solve our scientific problems. At a practical level, from a theorists point of view, this is an iterative process (as is usually the evolution of all research), where we understand and implement computations with available devices and algorithms, identify ways to make such simulations/calculations more precise to be impactful (usually faster and bigger), and work with experimentalists and developers to make more effective devices, codes and algorithms.

It is important to say that while the focus of this course is Standard Model physics, the contents are generally applicable to all quantum simulations, from exotic materials through to fluids. I have chosen to use the context of the Standard Model because, a) it is what I know best, and b) it has all of the relevant degrees of freedom and challenges that are present in all other domains, e.g., fermions, bosons, Majorana particles, etc.

As with classical simulations, it is highly desirable to minimize that tasks that are asked of the computer during any given simulation. For example, if the system has a symmetry, it is efficient to build that symmetry into the simulation from the outset. Quantum simulations are no different in this regard. It is the last stages of evolution, not the first, where a large capable quantum computer performs end-to-end simulations, and so building in “physics”, or performing “physics-aware” simulations is important. The ability to optimally use a large-scale computer is developed step-by-step, it is an “adiabatic” process where the scientists evolve with the hardware, and vice versa.

#### E. Objective: SM to QIS

Of course, predictions for Standard Model physics provide only one motivation, and the development of new technologies for sensing, communication and general purpose computing is a high priority, but very importantly, complementary and synergistic. The development of the understanding, algorithms and implementation of quantum simulations for Standard Model physics relevant to high-energy physics and nuclear physics research priorities also align well with those in materials, fluids and other domain sciences, but also with error-correction, communication and more, and as such this course is applicable, possibly with *some* translation, to general scientific applications.

An interesting area of such application is in programmable quantum sensors. One has an array of qubits (or qudits), to which a set of unitary operations are applied to entangle the system in such a way to increase its sensitivity to something in the “environment”, such as magnetic field. As just one example, it turns out that the encoding (and decoding) stages (unitaries) can utilize Hamiltonians that are of similar form to those used to describe nuclear many-body systems, thereby making a connection, in this instance, between spin-squeezing and multi-nucleon structure, see Ref. [6] and references therein.

## F. Quantum Information

### 1. 20th Century and Entanglement

Perhaps a somewhat bizarre statement to start with is that in the same way that one does not *understand* quantum mechanics, one does not *understand* quantum information, for the same reasons. Quantum mechanics is a consistent description of how our universe works at a fundamental level, and we continue to strive to understand *why* that is. BUT, during the 20th century, we have developed a great understanding of the applications of quantum mechanics to many important challenges in science and technology (and implications) specifically related to local processes. There has been remarkable progress in understanding and engineering basic aspects of entanglement (and coherence) and its implications for quantum many-body systems, and hence “technology”, since around the mid 1990s, and this is now rapidly growing.

Entanglement and coherence are features of quantum mechanics whose impact and utility are only now becoming a main-stream focus of research in the domain sciences, as part of the research and development (R and D) pipeline toward a robust component of the quantum technology supply chain. This is, of course, built upon the “wonderment” of entanglement famously discussed by Einstein, Podolsky and Rosen (EPR) in 1935, and the important theoretical progress in exposing quantum correlations starting, in effect, with the work by Bell in the 1964, and programs of remarkable pioneering experiments starting in the 1970s.

While nuclear and particle physics are exciting areas of scientific exploration that have been active research areas for decades, with the latter emerging from the former about sixty years ago, entirely new research activities are under development to understand, utilize and contribute to QIS in relevant systems [7–15]. The same is true for advances in machine learning and artificial intelligence (ML/AI), but that is not the topic of this course.

### 2. Our Universe, pure state and unitary evolution

Assuming unitary time-evolution of our universe from its beginning via Hamiltonian dynamics, we have arrived in/at the universe that we have today. It is reasonable to assume that the (closed) universe can be described by a pure wavefunction that has been evolving from some initial condition until present day.<sup>1</sup>

Low-energy interactions are determined with high precision by the Standard Model (with critical aspects of the neutrino sector, and the Dark Matter and Dark Energy sectors being exceptions, as is also true of what lies beyond the Standard Model), which is to be considered a low-energy effective field theory (EFT) relevant below some high energy scale, which now exceeds several TeV (as probed by experiment). We do not have a unique calculable theory of quantum gravity (coupled to matter fields), but assume that it satisfies basic attributes, and we do have a successful low-energy EFT. A cartoon of the desired connection between the Standard Model and the dynamics of large systems via quantum simulation is shown in Fig. 1.

---

<sup>1</sup> A pure state means that there is a single quantum wavefunction  $|\psi\rangle$  that completely describes the universe, as opposed to the universe being in a mixed-state where some number of quantum wavefunctions  $|\psi_i\rangle$ , with probability  $p_i$ , form an ensemble.

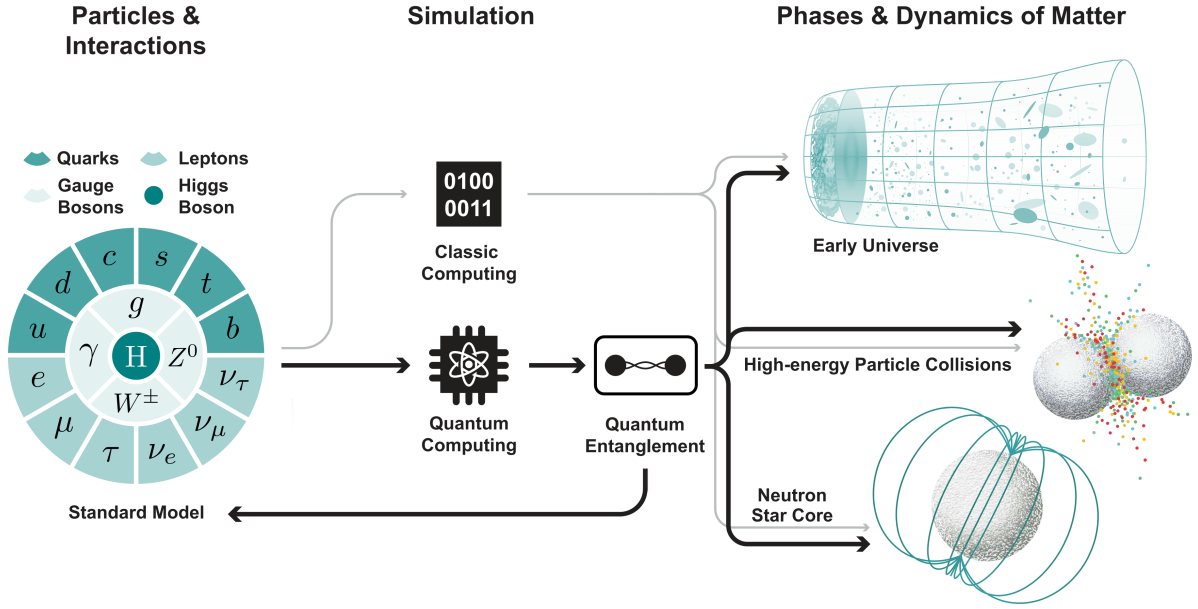


FIG. 1: Simulating the dynamics of extreme physical environments (right) emerging from the SM of quarks, leptons, gauge fields, and the Higgs boson (left) requires large-scale classical or quantum simulations (center). Quantum entanglement and coherence utilized by quantum computers are expected to enable progress while providing new insights into the SM itself. This figure was created by Christian Bauer, Zohreh Davoudi, Natalie Klco and myself [13].

### 3. Subsystems of our universe

The (small) subsystems of the universe that we can experience and manipulate are “embedded” in this universe, where we do not have access to most of the degrees of freedom. For instance, when performing electron-electron collisions, the cosmic microwave background radiation is not considered, and this does not limit our ability to calculate reaction rates. This is despite the fact that it is present as “a background” during “state preparation” of the electron beams, during the interaction in the collision region, and during the detection/measurement of the scattered final state(s).

### 4. Life

From the view point of a large biological system comprised of a very large number of fundamental particle that is continually interacting with its environment, the question becomes how does one start from the wavefunction of the universe that is undergoing unitary evolution, and after some time end up with (small) biological systems that can build devices to change their (immediate) environment to their advantage in an essentially classical way?

Of course, this is complicated by the fact that one cannot understand a more complicated theory (quantum systems) from a less complicated theory (classical systems). The collections of atoms in biological systems that work together to form self-sustaining systems with controllable membranes, interact with their environment (the atoms and fundamental particles) to “make decisions” about how to change in such a way to stay together and thrive as a system (i.e. make money, find food, buy cars, reproduce, etc.).

As an interesting side note, the astrobiology definition of life is reserved for systems that have control over their membranes. For this to be the case, there is a minimum electronic complexity that is required for this to be possible, which means the existence of elements beyond hydrogen and helium. In the context of nuclear physics, this means the stability of the ground states of nuclei including nitrogen, carbon and oxygen (and of course electrons!). In the context of the standard model, this means that the parameters of the Standard Model, i.e. the dimensionless parameters, such as the ratios of quark masses to the scale of strong interactions, which translates to the numerical values of the Yukawa couplings, the Higgs vacuum expectation value (VEV), and the strong coupling at the electroweak scale, are such that these nuclei are stable. The NPLQCD lattice QCD collaboration, now among others, studies the properties of light nuclei as a function of light-quark masses, for example Refs. [16–25], in an effort to determine of the parameters of the Standard Model are finely tuned with regard to, for example, the existence of biological membranes. These lattice QCD calculations are demanding because of the current methods employed for classical simulations of quarks, with the resulting sign problems, and equivalent signal-to-noise problems (we will discuss these more shortly).

### 5. Classical, Quantum

Now we think about systems of decreasing scale.



FIG. 2: Pacman in action.

At the classical level, the picture that we all have in our head of a biological system to first approximation is *Pacman* (system-1), see Fig. 2, that moves around consuming parts of its environment, for example, eats an apple and then biologically extracts useful nutrients from the apple and expels the rest back into the environment. In the back of our (classical) minds we have the system and environment “tensor-produced” together, and the biological Hamiltonian evolving the initial tensor-product into a final and different tensor-product of states.

At the quantum level, generally, we have the system entangled with its environment. Interactions with the environment, including non-locality through entanglement, can induce a change in the quantum state/dynamics of the system. It is the case that the nature of changes to a quantum system is richer than those of a classical system. The information processing that a quantum system can engage in exceeds that of which a classical system can engage in, and has elements that are simply “different”.

From a more Standard Model Physics point of view, there are quantum correlations between the states of two or more spatially separated systems that differ from those possible from classical mechanics alone, and therefore there is the potential for more information and information processing. To be a bit more precise, the information in a classical system is in the classical values and

correlations within the system, while the information in a quantum system is in the quantum properties and correlations within itself and the correlations with other quantum systems outside.....the last part of which is profoundly different.

### Setting conventions, and a well-known example from Wiki

To finish this part of the introduction, and to also set qubit conventions, it is worth simply reviewing the violation of local realism in quantum mechanics, as can be found on the Wikipedia page for **Bell's Theorem**, by simple manipulations of the **GHZ** (Greenberger, Horne, and Zeilinger) state. A 3-qubit GHZ state is a linear combination  $|\psi\rangle = (|000\rangle - |111\rangle)/\sqrt{2}$ . We will work with the qubit basis

$$\begin{aligned} \text{basis} &= \{ |0\rangle, |1\rangle \} \\ \hat{X}|0\rangle &= |1\rangle, \quad \hat{X}|1\rangle = |0\rangle, \quad \hat{Y}|0\rangle = +i|1\rangle, \quad \hat{Y}|1\rangle = -i|0\rangle \\ \hat{Z}|0\rangle &= +|0\rangle, \quad \hat{Z}|1\rangle = -|1\rangle, \end{aligned} \quad (1)$$

which, in this basis, <sup>a</sup> naturally leads to the matrix representations

$$\hat{X} = \begin{pmatrix} 0 & 1 \\ 1 & 0 \end{pmatrix}, \quad \hat{Y} = \begin{pmatrix} 0 & -i \\ i & 0 \end{pmatrix}, \quad \hat{Z} = \begin{pmatrix} +1 & 0 \\ 0 & -1 \end{pmatrix}, \quad |0\rangle \rightarrow \begin{pmatrix} 1 \\ 0 \end{pmatrix}, \quad |1\rangle \rightarrow \begin{pmatrix} 0 \\ 1 \end{pmatrix} \quad (2)$$

For example, if an electron is prepared in a linear combination of the eigenstates of the  $\hat{Z}$  operator,  $|e\rangle = \alpha|0\rangle + \beta|1\rangle$ , when a measurement is performed on this state corresponding to the action of the  $\hat{Z}$  operator, the resulting outcomes are  $\hat{Z} \rightarrow +1$  with probability  $|\alpha|^2$  and  $-1$  with probability  $|\beta|^2$ , and importantly, only a  $\pm 1$  will be obtained in each measurement performed on a "fresh" member of an ensemble of electrons prepared in this state. Further, all subsequent measurements on that same electron will yield the same value as measured initially. Of course, the same is true for measurements about any axis (after appropriate rotations). <sup>b</sup>

<sup>a</sup> Note that this convention used in the classic QIS textbook by Nielsen and Chuang [26], but is opposite to that that used by those of us trained as NP and HEP.

<sup>b</sup> Projectors are used to implement measurements, e.g.,  $\hat{\Lambda}_0 = |0\rangle\langle 0|$  acts on  $|e\rangle$  to collapse the wavefunction under measurement of eigenvalue  $+1$  to produce a normalized wavefunction  $|\chi\rangle = \hat{\Lambda}_0|e\rangle/\sqrt{\langle e|\hat{\Lambda}_0|e\rangle}$ , obtained with probability  $p_0 = \langle e|\hat{\Lambda}_0|e\rangle$ .

The following "sidebar" discussing a GHZ state demonstrates an example of the new features that are available to use for computations and simulation. It shows multi-body entanglement among three particles, electrons or qubits. This is just one example of quantum correlations, that lie outside of what can be accomplished classically, that we are in the process of understanding and utilizing in simulations of physics systems (which, of course, have such correlations within them, generally).

### A GHZ State

We imagine preparing the 3-qubit GHZ state and distributing each particle to distant laboratories, where measurements corresponding to the action of the Pauli operators can be performed. For example, for electrons we imagine the spin carrying this information, and that the spins of the 3 electrons are prepared in the GHZ state. Pauli measurements are performed using, at least conceptually, a modern-version of the Stern-Gerlach apparatus where the deflection of the beam in a magnetic-field gradient is determined by the alignment with regard to the gradient. A measurement of each  $\hat{Z}$  will produce a value of  $\pm 1$  (that is what each laboratory will measure) with equal probability, but that all three labs will either measure 0 or 1 in each element of the ensemble, and so when they get together or have a phone call to compare results, they will have measured either 000 or 111 only, and with equal probability. Consider the measurements of the form,

$$\hat{X} \otimes \hat{Y} \otimes \hat{Y} |\psi\rangle = \frac{1}{\sqrt{2}} \left[ \hat{X}|0\rangle \otimes \hat{Y}|0\rangle \otimes \hat{Y}|0\rangle - \hat{X}|1\rangle \otimes \hat{Y}|1\rangle \otimes \hat{Y}|1\rangle \right] = +|\psi\rangle , \quad (3)$$

and similarly for  $\hat{Y}\hat{X}\hat{Y}$  and  $\hat{Y}\hat{Y}\hat{X}$ . One can imagine arguing classically, assuming local realism, that it might then be consistent to assign a variable that determines the outcome at each site when  $X$  or  $Y$  is measured. In this case, one would then suggest that, for example,  $\hat{X}_a|\psi\rangle = \eta_a^{(\hat{X})}|\psi\rangle$ . By taking products of the outcomes of measurements of  $\hat{X}\hat{Y}\hat{Y}$ ,  $\hat{Y}\hat{X}\hat{Y}$  and  $\hat{Y}\hat{Y}\hat{X}$ , that leads to  $\eta_1^{(\hat{X})}\eta_2^{(\hat{X})}\eta_3^{(\hat{X})} (\eta_1^{(\hat{Y})}\eta_2^{(\hat{Y})}\eta_3^{(\hat{Y})})^2 > 0$ , such local realism leads to  $\eta_1^{(\hat{X})}\eta_2^{(\hat{X})}\eta_3^{(\hat{X})} > 0$ . In fact, explicit calculation leads to  $\hat{X}^{\otimes 3}|\psi\rangle = -|\psi\rangle$ , which is a contradiction.

An obvious consequence of this is that, for this wavefunction, if one of the labs measures 1, then the wavefunction collapses to  $|111\rangle$ , which is unentangled, and if the lab measures 0, the wavefunction collapses to  $|000\rangle$ , which is also unentangled. So, one concludes that there is no 2-body entanglement in this GHZ state.

### 6. Implication

This simple and well known example highlights that entanglement enables an entirely different set of correlations between quantum systems that do not exist classically. As these correlations have physical consequences for the outcomes of experiments with structures beyond those obtainable from classical mechanics alone, systems and devices can use them (in their structure and in their sensing) to respond to their environment to which they can be (likely) entangled. Making use of these correlations is a different matter, and in this instance, would require classical (at least) communication between the systems.

To connect back to our previous discussions, if you (as an example) are a system that is tensor producted with the rest of the universe, and then you receive one of the spins in a GHZ-state (described above) from the environment, your response based upon making Pauli measurements will depend upon information that is fundamentally quantum (entanglement) through the quantum correlations with the environment, and is not obtainable from classical physics (local realism) alone. The important question to then ask is how much information is in such correlations and potential suite of measurements of particles/sensing from the environment, and how can that be processed (using entanglement) and transmitted by a quantum system (in its own self interest?)? This defines the field of quantum information science.

### *7. Quantum Correlations*

For classical physics, information that enters a sub-system from the environment can be extracted from the values of measurements, while for quantum systems, the beyond-classical quantum information resides in the correlations with other quantum sub-systems. Accordingly, there is a much larger volume of information that can reside in quantum correlations between systems than the individual systems themselves. A big question that we will address at some level are how does one harvest and utilize quantum information, and for this course we are focused toward simulations of systems of physical interest and importance.

### *8. Understanding this aspect of the Standard Model*

Taking one step further toward the topic of this course, as all systems that we are familiar with in the everyday world are described with high precision by the Standard Model of particle physics and its low-energy effective field theory descendants. The Standard Model is constructed in terms of quantum gauge field theories with specific matter content, and therefore understanding and controlling the behavior of (quantum) sub-systems of our universe requires understanding the quantum information and correlation structures of quantum field theories (and better understanding certain quantum field theories themselves). This has many tentacles that we will encounter in this course, including in the nature of fundamental physics (HEP), in the structure of matter (CM) and the technology that can be created, in nuclear physics through the structure and dynamics of dense matter and complex many-body systems.

### *9. Quantum Teleportation*

Quantum teleportation is a simple and beautiful demonstration of some of the features and capabilities of quantum mechanics, which is remarkable in its own right, but also something we will integrate into our quantum simulation algorithms for simulating larger systems, and is central to quantum communication. The following “sidebar” provides the classic demonstration of quantum teleportation. This is a well-known protocol that can be found in elementary texts on QIS. It requires a knowing what a CNOT-gate does and what a Hadamard gate does, which we will discuss in this example.

### Quantum Teleportation

Consider two laboratories A and B that receive entangled photons (two state systems = “qubits”) from an EPR source with wavefunction  $|\psi\rangle$ , and A also has a single qubit prepared in an unknown state,  $|\phi\rangle$ ,

$$\begin{aligned} |\phi\rangle &= \alpha|0\rangle + \beta|1\rangle , \quad |\psi\rangle = \frac{1}{\sqrt{2}} [ |00\rangle + |11\rangle ] \\ |\phi\rangle \otimes |\psi\rangle &= \frac{1}{\sqrt{2}} [ \alpha|000\rangle + \alpha|011\rangle + \beta|100\rangle + \beta|111\rangle ] . \end{aligned} \quad (4)$$

The combined wavefunction of the systems is the tensor product of the two,  $|\phi\rangle \otimes |\psi\rangle$ , where laboratory A can manipulate the first 2 qubits, while laboratory B can manipulate the third. Alice (who is the experimentalist in laboratory-A) then applies a sequence of two operators to her two qubits, First the two-qubit entangling gate CNOT, controlled on the system to be teleported, and then a Hadamard gate on that same qubit. These operators entangle the physics qubit with the Bell pair which are distributed (far apart?), but remain quantum correlated. The action of the CNOT gate, controlled on qubit-1 and acting on qubit-2, is of the form

$$\begin{aligned} \text{CNOT}_{12} &= \hat{\Lambda}_0 \otimes \hat{I}_2 + \hat{\Lambda}_1 \otimes \hat{X} \\ \hat{\Lambda}_0 &= |0\rangle\langle 0| , \quad \hat{\Lambda}_1 = |1\rangle\langle 1| . \end{aligned} \quad (5)$$

I will denote the single-qubit Hadamard-gate as  $\hat{H}$  at the moment, but might change later to mitigate confusion with the Hamiltonian:

$$\begin{aligned} \hat{H}|0\rangle &= \frac{1}{\sqrt{2}} [ |0\rangle + |1\rangle ] , \quad \hat{H}|1\rangle = \frac{1}{\sqrt{2}} [ |0\rangle - |1\rangle ] \\ \hat{H} &= \frac{1}{\sqrt{2}} \begin{pmatrix} 1 & 1 \\ 1 & -1 \end{pmatrix} . \end{aligned} \quad (6)$$

We then have that

$$\begin{aligned} (\hat{H} \otimes \hat{I} \otimes \hat{I}) (\text{CNOT}_{12} \otimes \hat{I}) |\phi\rangle \otimes |\psi\rangle &= \frac{1}{2} [ \alpha(|000\rangle + |100\rangle + |011\rangle + |111\rangle) \\ &\quad + \beta(|010\rangle - |110\rangle + |001\rangle - |101\rangle) ] \\ &= \frac{1}{2} [|00\rangle \otimes (\alpha|0\rangle + \beta|1\rangle) + |01\rangle \otimes (\alpha|1\rangle + \beta|0\rangle) \\ &\quad + |10\rangle \otimes (\alpha|0\rangle - \beta|1\rangle) + |11\rangle \otimes (\alpha|1\rangle - \beta|0\rangle)] \\ &= |\Psi\rangle . \end{aligned} \quad (7)$$

Measurements made by Alice are implemented with projectors. By performing measurements of along the z-axis of both qubits and finding 00 collapses the wavefunction with the projector  $\hat{\Lambda}_{00} = |00\rangle\langle 00|$ , with probability  $\langle\Psi|\hat{\Lambda}_{00} \otimes \hat{I}|\Psi\rangle$ , which in this case is  $\frac{1}{4}$ . The post-collapse wavefunction is then  $|00\rangle \otimes (\alpha|0\rangle + \beta|1\rangle)$ . Now, measuring an ensemble of such states provides the four possible outcomes with equal probabilities of  $\frac{1}{4}$ , but different wavefunctions in laboratory B (where Bob runs the experiments). To uniquely recover the state in B from each measurement in A, a **classical communication** (CC) from Alice to Bob that transmits just 2 numbers, 00, 01, 10 or 11 for each entangled pair, is required. For Bob to recover the state from Alice, the corresponding **local operations** (LO) that Bob must execute on the single qubit in B are 00 :  $\hat{I}$ , 01 :  $\hat{X}$ , 10 :  $\hat{Z}$  and 11 :  $\hat{Y}$ .

This is an amazing result, that you have seen many time before. The quantum correlations in the Bell-pair that is distributed between laboratories A and B can be used via **local operation and classical communication** (LOCC) by Alice to be able to send only 2 bits of classical information to Bob for him to be able to fully recover the quantum state that Alice has (and may or may not know what it is) by a local operation that depends upon the sent classical information. This is true for any distance separation between Alice and Bob, as long as classical communication is possible.

## G. Classical Limits, Complexity and Quantum Simulation

### 1. Feynman and Computing

In his classic paper published in 1982, *Simulating Physics with Computers* [27], Feynman discusses the limitations of classical computing, and indicates that quantum computer are required to simulate important aspects of physically relevant quantum systems. Conceptually, this remarkable work/insight is a natural (substantial) extension of an understanding that Feynman is famous for expressing (reminding us) of that *one cannot understand a more fundamental theory with a less fundamental theory*. Translating this into the computing sense, this means simulating a given quantum system using a classical computer versus a quantum computer. While computing has a long history, including remarkable *pre-history*, including **Babbage's difference engine** of the 1820's, which was the first computer, "digital" (classical) computing started early in the 20th Century. After the development of the first integrated circuit in the 1970s, a period of exponential growth in transistor density and the number of transistors that can be successfully fabricated in silicon, we have laptops, cell phones and supercomputers of today. Initially, single integrated CPUs gave way to large-scale homogeneous systems of CPUs with on-chip memory, then heterogeneous systems with CPU, GPU, etc. But fundamentally, all of these increasing complex compute architectures are classical in the sense that they do not utilize entanglement and coherence. They can efficiently manipulate and store binary numbers of "0"s and "1"s, but they are unable to "**efficiently**" simulate certain aspects of a general quantum systems. This then moves us toward a discussion of what is easy (efficient) and what is hard (inefficient) to compute.

### Complexity in (Scientific) Computation

A discussion of computational complexity is embedded in a much larger discussion about what is computable. We take a *non-computer science* perspective on this consideration, and address this matter from a somewhat practical standpoint. If we take wish to compute properties of any finite size quantum system, then we are compelled to ask questions such as:

1. how much (classical or quantum) memory will be required to contain and operate on all elements of the system (the dimensionality of the Hilbert space and the memory required to perform the necessary operations on that Hilbert space)?
2. the number of operations and compute time required to initialize the state?
3. the number of operations and compute time necessary to evolve the system from an initial to final state?
4. with a finite compute resource, what is the "closest" system (to the target system) that can be simulated (defined by smallest systematic error(s))?

Such questions are in the context of simulating aspects of the universe - infinite spatial volume (for practical purposes of the Standard Model without gravity) and a continuous spacetime - with finite resources. Further, from a computational point of view, these questions are in the context of scaling simulations with system size, i.e., how do the requirements change as the size of a system, for example, double or triple?

These question are also framed in the context of real-world constraints. In performing such simulations, one has a finite number of team members, each can contribute a certain number of hours per week for a set number of weeks or months. Further, other real-world constraints, such as the amount of computational resources have been "awarded" to the project by the computing centers, and over what period of time.

We are all too familiar with the limits our laptops. For a small system, requiring just a few operations, computations run very quickly, within the blink of an eye, but as we study systems with increasing numbers of degrees of freedom, the computation requires increasing time. At some system size, the computation time takes major *jumps* as the system no longer fits into cache, then into RAM and requires addressing hierarchically slower memory systems. Eventually the system no longer fits into the computer and the time to solution tends to infinity. So while computations have been performed with precision on systems up to certain sizes, there is a very clear limit for each laptop, depending on the CPU, GPU, motherboard, memory, memory buses etc.

For some important calculations, larger computers are an answer (brute force). Comprised of many independent compute nodes connected by fast interconnects (communication fabric), larger problems can be solved by connecting together, say, 1 million compute nodes with a low-latency communication fabric that has the same topology as the physics problem one is trying to solve. For lattice QCD, as an example, this can provide polynomial scaling of required resources with increasing system size. If the memory is  $\times 2$  as large then a systems of  $\times n$  can be simulated with polynomially scaling time, etc. In fact, the needs to lattice QCD research motivated a hardware development project that pioneered a number of computing attributes, including on-chip memory (for a nice review, see Ref. [28]).

The most successful method for simulating (non-perturbative) field theories is to discretize the theory using a hyper-cubic grid, such as shown in Fig. 3. As computer memory is finite, to perform simulations, the problem that we solve on the computers will be different from that desired, because it must be formed from a finite number of degrees of freedom. It will necessarily involve only a finite

part of space that is discretized by a lattice spacing, evolved for a finite length of time (usually with finite steps). For physical systems, fine discretizations of the systems and small time steps will enable computations of low-energy aspects of any theory that is gapped<sup>2</sup> with converging precision. Typically, the best layouts (mappings) are ones that maximally respect the symmetries

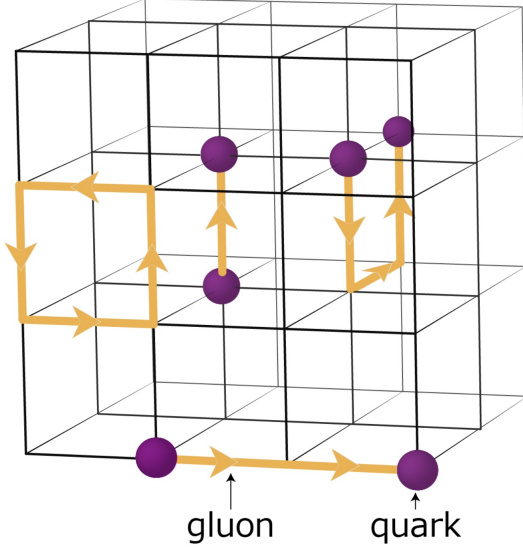


FIG. 3: Simulating non-perturbative quantum fields in our spacetime using a grid of points in four dimensions. For quantum chromodynamics, the quark fields reside on lattice sites, while the gluons reside on the links between sites.

of the theory, and for field theories Lorentz invariance is fundamental. While this is not preserved exactly due to the lattice spacing, it can be recovered in the continuum limit.

The question then becomes, how do the required resources scale with increasing system size? There are a number of different quantities to consider. Lets think about trying to simulate a system with  $N_{\text{sys}}$  degrees of freedom over some physical time interval (intrinsic time)  $T_{\text{sys}}$ . As both of these quantities becomes very large (asymptotically large), this will require some classical memory size  $N_{\text{comp}}$  and some compute time (wall-clock time)  $T_{\text{comp}}$  on a classical computer to arrive at a result that is within some tolerance,  $\epsilon$ , of the true result (and it is non-trivial to understand what this actually is). The deviation between the computed result and the true result is called the **error**<sup>3</sup>. From a computer science (CS) point of view, if  $N_{\text{comp}} \sim (N_{\text{sys}})^\alpha$  and  $T_{\text{comp}} \sim (T_{\text{sys}})^\beta$  **for a fixed error**, then the computation(s) can be performed efficiently. That is to say, it can be performed in polynomial-scaling amounts of time on a deterministic Turing machine, and resides in **P** and **PSPACE**. In contrast, if the time to solution scales greater than any polynomial, then the problem resides in **NP**. If the problem resides within **P**, then it can be performed efficiently at scale, with an error that can be quantified and reduced with more computing. If the problem resides outside of **P**, then this cannot be accomplished. Many classic examples of such problems are known, for instance the **Traveling Salesman Problem** that asks “What is the route between multiple cities that a salesman should take to minimize fuel costs?”. For a salesman starting in a city and traveling

<sup>2</sup> If a system is not gapped, then even at low-energies the finite volume of the simulated region will generally lead to power-law systematic errors, as opposed to exponentially small errors.

<sup>3</sup> From a physics standpoint, this is a systematic error in the simulation. As errors in the computation vanish, this systematic error represents the total error associated with the simulation.

to  $N$  other cities, there are  $(N - 1)!$  different ways that the cities can be visited, and the fuel cost is to be computed for each path. Sterlings formula gives a classical compute time that scales as  $N! \rightarrow \exp[N(\log N - 1)]$ .

We have made remarkable progress in simulating aspects of quantum systems with classical computers, and we have recently entered the **exascale era** of super computing (1 Exa =  $10^3$  Peta =  $10^6$  Tera =  $10^9$  Giga). The point I want to make here is that complexity classes and asymptotic scaling are good to know about, however,

1. they are not that relevant for simulating small-*ish* systems,
2. they are very relevant for simulations using present-day classical HPC computers,
3. but they are not relevant for present-day quantum simulations using quantum computers

The history of computing has shown that we can make great progress in computing properties of systems with classical computing, and particularly in problems that lie outside of **P**. In the context of quantum simulations, the quantum chemists articulated this a few years ago, as they realized that the polynomial terms and coefficients in the scaling of quantum resource estimates for quantum simulations can matter. For what we will do, we will not be constrained in what we tackle by asymptotic scalings, because there is an enormous amount of physics to be learned before the limitations of asymptotic scaling properties manifest themselves. From the practical standpoint, we will tackle problems until we can no longer make progress. Historically, this attitude has served scientists well in utilizing computers, in some ways based upon the old adage that “necessity is the motherhood of invention”.

An important aspect of this, that is not included in the complexity class analysis related to physical systems, is that with an error bound  $\epsilon$ , we are free to change the theory we are simulating using the computer by an amount that maintains  $\epsilon$ . Much of progress in simulating nuclear and particle physics on the 20th and 21st Centuries was a partnership between computation and theory (and experiment), in which effective field theories (EFTs) describing observables over some limit regime or parameter set of the full theory, enabled a hierarchy of interactions to be rigorously identified. The leading-order (LO) interactions are simulated with computers, and the higher-order corrections are then included in perturbation theory. A prime example of this is the “partnership” between heavy-quark effective field theory (HQEFT) and lattice QCD, or between chiral perturbation theory ( $\chi$ PT) and lattice QCD.

## H. Classical Difficulties

It is worth reminding ourselves of some the difficulties encountered in simulating quantum field theories using classical computers, which roughly fall into two categories for the Standard Model:

1. finite density
2. real-time evolution

I wish to discuss this with a little detail because the implications are not restricted to classical computing. They also impact quantum simulation because of the ensemble averaging nature of quantum computation. In quantum computation, excited states contribute high-frequency components to a time-evolving wavefunction, which in many cases, need to be “filtered out” to gain access to the target physics observables which appear with lower frequencies.

Evolution in imaginary time ( $t \rightarrow -i\tau$ ) can be used effectively with classical computers to find the ground states of some complex systems. Instead of working in Minkowski space, the theory is

formulated in Euclidean space, so that a unitary time-evolution operator is instead a non-unitary operator that differentially suppresses high-energy states, e.g.,

$$\begin{aligned}\hat{U}(t_M)|\psi\rangle &= e^{-i\hat{H}t_M} \sum_n c_n |\phi_n\rangle = \sum_n c_n e^{-iE_n t_M} |\phi_n\rangle \\ \rightarrow \hat{U}_E(t_E)|\psi\rangle &= e^{-\hat{H}t_E} \sum_n c_n |\phi_n\rangle = \sum_n c_n e^{-E_n t_E} |\phi_n\rangle .\end{aligned}\quad (8)$$

In Euclidean space, after a time period defined by the gaps in the system, the system has been "purified" into its ground state, with exponentially small systematic errors, but with an exponentially-small amplitude. The overall amplitude, defined by  $c_0$  is *a priori* unknown unless the theory is already solved. From a field theory point of view, correlations between operators - correlation functions - are computed in the region outside of the light cone. The issue of analytic continuation back to Minkowski space from Euclidean is easy for single particle systems, challenging and manageable for 2-body systems (Luscher, and many others), but generally is very challenging for arbitrary n-body correlation functions.

However, in general it looks like it should be easy to compute ground states of systems. Unfortunately, life is not so simple..... As the exact calculations of many-body systems beyond just a handful of degrees of freedom, lies beyond what can be classically computed (consider what would be required to be stored to provide a complete wavefunction of an n-body state - grows exponentially with the number of degrees of freedom), statistical sampling of configurations (of fields/particle) is, instead, employed. For QFT, it is snap-shots of the vacuum that are created by sampling from the exponential of the Euclidean-space action,  $e^{-S_E}$  (these snapshots are stored in computer memory or drives). These samples of the ground-state wavefunction are used, in a statistical way, to determine expectation values of operators. The quality of the calculation,  $\epsilon$ , is determined by the quality of the sampling (Ergodic or close proximity), the volume size, lattice spacing, parameter tunings, **AND** importantly the statistical properties of the correlation functions themselves. Following pioneering work by Georgio Parisi [29], by Peter Lepage [30], and the NPLQCD collaboration <sup>4</sup> for nuclei [19], a range of behaviors are found for correlation functions in lattice QCD (and in statistical spin systems), that render some calculations practical and some impractical.

### 1. Signal-To-Noise in Statistical Sampling used in Classical Simulations, e.g., Nucleons in Lattice QCD

Through statistical sampling, one can generate an ensemble of snapshots of the gauge field vacuum, most commonly without background fields or chemical potentials, { gf<sub>i</sub> }, where the index  $i$  runs from 1 to  $N_{\text{cfg}}$ . These represent a thermal distribution in Euclidean space, distributed to recover  $e^{-S_E}$  through Monte Carlo accept/reject algorithms, such as molecular dynamics using Metropolis type conditions.

To form vacuum <sup>5</sup> expectation values of an operator, one evaluates the observable for each member of the ensemble, and then averages the result. This can be shown to be rigorous methodology to recover VEVs, including correlation functions defined by specific quantum numbers. Imagine that we are interested in the mass of the nucleon. From the previous discussion, we know that

---

<sup>4</sup> <https://www.ub.edu/nplqcd/>

<sup>5</sup> The vacuum is the ground state of a strongly interaction system is not the trivial vacuum. For QCD, the vacuum has a non-zero expectation value of  $\langle \bar{\psi}\psi \rangle = \langle \Omega | \bar{\psi}\psi | \Omega \rangle$  and a non-zero vacuum energy density,  $\epsilon_{\text{vac}}$ . because the wavefunction is not simply empty space with all fields in the perturbative ground state, but involves non-trivial configurations.

at large Euclidean times, the correlation function with quantum numbers of a single nucleon will decay exponentially as the  $C_N(t) \sim Z_N e^{-M_N t} + \dots$  where the ellipsis denote contributions from higher mass states such as nucleon+pion, or nucleon resonances. Because we cannot solve QCD, nor analytically determine the vacuum state of generally any strongly interacting field/spin theory, we do NOT have the unique form of operators to create and destroy a nucleon. Further, the underlying hyper-cubic lattice violates continuous rotational symmetry, and so we only have operators that have some overlap with the nucleon, but they also overlap with other states also - in general all of the states with the lattice quantum number of the operator that reside in the lattice. For all practical purposes, these correspond to the form of local or de-localized operators from 3-quark operators or multi-quark-multi-gluon operators with the same quantum numbers. Let us not worry about the exact forms, and generically think about a  $qqq$  operator,  $\hat{O}_{qqq}(\mathbf{x}, t)$ , that annihilates some state at position  $\mathbf{x}$  and time  $t$  that depends upon the gluon configuration. The nucleon correlation function from this operator, projected to zero three-momentum, is given by

$$\begin{aligned} C_N(t) &= \sum_{\mathbf{x}} \langle \Omega | \hat{O}_{qqq}(\mathbf{x}, t) \hat{O}_{qqq}^\dagger(\mathbf{0}, 0) | \Omega \rangle \rightarrow \sum_{\mathbf{x}, \phi_N} \langle \Omega | \hat{O}_{qqq}(\mathbf{x}, t) | \phi_N \rangle \langle \phi_N | \hat{O}_{qqq}^\dagger(\mathbf{0}, 0) | \Omega \rangle \\ &= \bar{Z} \sum_{\phi_N} e^{-E_{\phi_N} t} |\langle \Omega | \hat{O}_{qqq}(\mathbf{0}, 0) | \phi_N \rangle|^2 = Z_N e^{-M_N t} + Z_{N^*} e^{-M_N^* t} + Z_{N\pi} e^{-E_{N\pi} t} + \dots \quad (9) \end{aligned}$$

where the sum is over all states with the quantum numbers of a single baryon, of which the nucleon at rest is the lightest, and the dominant state at late times. The overlap of the interpolating operator onto the single nucleon state,  $\langle \Omega | \hat{O}_{qqq}(\mathbf{0}, 0) | \phi_N \rangle$ , is generally an unknown complex number (for some arbitrary set of global quantum numbers).

In a classical lattice QCD simulation, the actual numerical evaluation is accomplished by ensemble averaging, which involves evaluating quark propagators and contracting them together in all possible ways allowed by the symmetries:

$$C_N(t) = \langle \Omega | \hat{O}_{qqq}(\mathbf{x}, t) \hat{O}_{qqq}^\dagger(\mathbf{0}, 0) | \Omega \rangle \rightarrow \frac{1}{N_{\text{cfg}}} \sum_i i \langle \hat{O}_{qqq}(\mathbf{x}, t) \hat{O}_{qqq}^\dagger(\mathbf{0}, 0) \rangle_i . \quad (10)$$

With such contractions, there are only intermediate states that are “accessible” with 3-quarks, and hence the lowest state, consistent with above, is the single nucleon states. It is worth noting that confinement plays a major role in this analysis, as there are no free single or 2-quark states.

To recover the nucleon mass from calculations such as these, one notes that for  $c(t) \sim Z e^{-Mt}$  (the form at late times - determined by the gaps in the theory) that, as an example,

$$\frac{c(t)}{c(t + \delta t)} = e^{+M\delta t} , \quad \frac{1}{\delta t} \log \frac{c(t)}{c(t + \delta t)} = M , \quad (11)$$

and hence by measuring the (late time) correlation function at two times, the mass of the ground state can be estimated.

However, with any statistical evaluation, one must pay attention to the underlying statistical distributions. If the distribution is non-Gaussian, then one can anticipate the calculations taking longer to converge than naively expected, and perhaps may require the use of robust statistical methods rather than simply forming average values. In particular, if distributions that are contributing to the expectation values have long tails, then samples in the tails require significantly more time to sample efficiently (in general, and if they actually are convergent), and alternate (robust) estimators, such as the median and median-absolute-deviation (mad), may be better choices of estimators [31].

Let us consider the variance of the nucleon correlation function, which is determined by the VEV of  $|\hat{O}_{qqq}(\mathbf{x}, t) \hat{O}_{qqq}^\dagger(\mathbf{0}, 0)|^2 = \hat{O}_{qqq}^\dagger(\mathbf{x}, t) \hat{O}_{qqq}(\mathbf{x}, t) \hat{O}_{qqq}^\dagger(\mathbf{0}, 0) \hat{O}_{qqq}(\mathbf{0}, 0)$ . The structure of this is

interesting because, upon contracting the quark lines between the initial and final states, one sees that only intermediate states accessible to 3-quarks **and** 3-anti-quarks (and arbitrary gluons) are allowed. Inserting a complete set of states, the hadronic states that will contribute are interacting states of  $N\bar{N}$ ,  $3\pi$ , etc,

$$\begin{aligned}
 C_{q^3\bar{q}^3}(t) &= \sum_{\mathbf{x}} \langle \Omega | \hat{O}_{qqq}^\dagger(\mathbf{x}, t) \hat{O}_{qqq}(\mathbf{x}, t) \hat{O}_{qqq}^\dagger(\mathbf{0}, 0) \hat{O}_{qqq}(\mathbf{0}, 0) | \Omega \rangle \\
 &\rightarrow \sum_{\mathbf{x}, \chi_{q^3\bar{q}^3}} \langle \Omega | \hat{O}_{qqq}^\dagger(\mathbf{x}, t) \hat{O}_{qqq}(\mathbf{x}, t) | \chi_{q^3\bar{q}^3} \rangle \langle \chi_{q^3\bar{q}^3} | \hat{O}_{qqq}^\dagger(\mathbf{0}, 0) \hat{O}_{qqq}(\mathbf{0}, 0) | \Omega \rangle \\
 &= \overline{Z} \sum_{\chi_{q^3\bar{q}^3}} e^{-E_{\chi_{q^3\bar{q}^3}} t} |\langle \Omega | \hat{O}_{qqq}^\dagger(\mathbf{0}, 0) \hat{O}_{qqq}(\mathbf{0}, 0) | \chi_{q^3\bar{q}^3} \rangle|^2 \\
 &= Z_{q^3\bar{q}^3}^{(0)} e^{-E_{q^3\bar{q}^3}^{(0)} t} + Z_{q^3\bar{q}^3}^{(1)} e^{-E_{q^3\bar{q}^3}^{(1)} t} + \dots \rightarrow Z_{3\pi} e^{-E_{3\pi} t} + Z_{N\bar{N}} e^{-E_{N\bar{N}} t} + \dots , \quad (12)
 \end{aligned}$$

The interesting, and computationally limiting aspect of this is that in QCD, the lowest energy configuration is  $3\pi$ , with an energy of  $\sim 3m_\pi$  in the limit of non-interacting pions (and simply  $E_{3\pi}$  when interactions are considered), where  $3m_\pi \sim 420$  MeV, while the energy associated with the nucleon mass is  $E_{N\bar{N}} \sim M_N + M_{\bar{N}}$  which is  $\sim 1880$  MeV (for physical values of the quark masses). This means that while the single-nucleon correlation function is falling with  $\sim e^{-M_N t}$ , its standard deviation is falling as  $\sim e^{-3M_\pi t/2}$ . Relatively, the “signal” (mean value) is decaying exponentially compared to the “noise” (standard deviation). A suppression of this problem that has been algorithmically employed in LQCD calculations is that  $Z_{3\pi} \ll Z_{N\bar{N}}$ , and so at short and intermediate times the  $3\pi$  component is negligible, but eventually, at long times, it dominates the variance of the correlation function sampling. As this is the variance correlation function, it can be used to define the signal-to-noise (StoN) ratio, where the noise is defined by the standard deviation of the correlation function measurements,

$$\begin{aligned}
 \text{StoN} &= \frac{C_N(t)}{\sqrt{C_{q^3\bar{q}^3}(t)}} \rightarrow \frac{Z_N}{\sqrt{Z_{N\bar{N}}}} e^{-(M_N - \frac{1}{2}E_{N\bar{N}})t} \sim 1 \text{ as } t \rightarrow 0 \\
 &\rightarrow \frac{Z_N}{\sqrt{Z_{3\pi}}} e^{-(M_N - \frac{1}{2}E_{3\pi})t} \sim e^{-(M_N - \frac{3}{2}m_\pi)} \text{ as } t \rightarrow \infty , \quad (13)
 \end{aligned}$$

When statistically evaluated with  $N$  samples, there is a  $1/\sqrt{N}$  that multiplies this form <sup>6</sup> This behavior means that there is a limit to the temporal extent to which signal can be extracted with meaning, to the time where the standard deviation and mean are comparable. This makes it challenging to explore such systems with small gaps ... i.e. nuclei with bindings that are  $\sim$  MeV compared to nuclei with masses that are many GeV, where the StoN ratio scale exponentially with system size [19],

$$\text{StoN} = \sim e^{-A(M_N - \frac{3}{2}m_\pi)t} \text{ as } t \rightarrow \infty , \quad (14)$$

where  $A$  is the number of nucleons. This is modified when discussing hyperons containing strange quarks, see NPLQCD [33] and subsequent works.

What does this mean for quantum simulation? With the many differences, there are similarities that will likely provide a challenge to quantum simulations of nuclear systems. High mass states give rise to high-frequency oscillations while low mass states give low-frequency oscillations. StoN

---

<sup>6</sup> In reality, the statistical behavior is rich, involving circular statistics and such. See Ref. [32].

problems in Euclidean space correspond to sign-problems in Minkowski space. We will explore this further later. This represents an issue for quantum simulations of QCD and other confining theories, particularly with composite Goldstone modes, that remains to be yet identified as a limitation, but at some point will.

## 2. Sign Problems

Let's start by reminding ourselves what a sign problem is. There are many simple systems that exhibit sign problems, and can be understood by considering the following example. Considering numerically evaluating

$$I = \int_0^{2\pi} d\phi e^{ik\phi} , \quad (15)$$

for  $k \neq 0$  and  $k \in \mathbb{Z}$ . We know that this integral is identically zero for  $k \neq 0$  (and = 1 for  $k = 0$ ), but when performing a statistical evaluation, each of the contributions has magnitude 1. To obtain an estimation that is exponentially close to the correct result requires exponentially large numbers of measurements.

For quantum field theories, using the Lagrange density path integral technology to determine observables, such as S-matrix elements, masses and so forth, the evaluation involves a sum over all possible paths, weighted by  $e^{iS}$ , providing results that are dominated by paths near a minimum of the action. But it is for the reason shown in the simple model, that Euclidean space formulation is used for numerical simulation because an exponential suppression of deviations from minima of the action is explicit in the sampling,  $e^{-S}$ . This transformation and numerical implementation is great when the action is a real number. However, when there are chemical potentials and finite density systems as asymptotic states, an imaginary contribution to the action is present.

$$Z \sim \int \mathcal{D}\phi e^{-S_E(\phi, \partial\phi) + i\mu_Q \hat{Q}(\phi, \partial\phi)} . \quad (16)$$

For sufficiently small  $\mu_Q$ , this is relatively benign and can be handled with brute force, massive statistics, but for larger values of the chemical potential, or baryon number, the rapidly rotating complex phase renders the evaluation impossible, and naively requiring exponentially large statistical samples. The problem of circular statistics becomes overwhelming once the phase wraps around the circle, leading to an impossible inversion.

A side note, we see that in unitary time evolution, the action of the evolution operator will in general generate a sum of exponentials with phases corresponding to the energy eigenvalues of the system. Something that has not had much attention paid to it in the literature is the impact of imperfect operators, and signal-to-noise issues in time evolution in general. Clearly, there are important studies that need to be undertaken in this particular area.

## I. Related Comments on Scientific Applications

In considering applying quantum simulation to quantum field theories and quantum many-body systems, there is no need to re-invent *most of* the wheel. Many aspects of the process and analytic techniques are already in place from the decades of numerical simulation using classical computing, and that can be *ported* over to quantum simulation without much modification. There are certainly many important new features and fundamental differences that have to be invented and handled also - which is what this course is about.

For example, for QFT, we know how to discretize spacetime, the quark and gluon field, we know about finite-volume (FV) effects and have the technology of EFT developed, and we have a lot of experience with doublers. We understand lattice spacing artifacts for 4-dimensional simulations. We understand sampling from non-Gaussian distributions. We recognize the importance of a complete quantification of uncertainties and error estimated. For quantum simulation, we need to provide reliable technology and algorithms, with error estimates at finite sample size, for time-evolution, for 3+1 dimensional systems, for finite Hilbert spaces, and the systematic error associated with each truncation and mapping that is employed in quantum simulation.

The concept of co-design is essential to advancing our field. So when we design quantum circuits to simulate our systems, we should always be looking for ways that might help us .... i.e., if the hardware had a certain feature - and then let our experimental colleagues know what that feature is - and they, or we together, might be able to develop that technology.

Finally, much of the work in any one science domain will have applicability, either direct or indirect, in all of the other science domains. However, for example, the quantum chemists are not going to solve QCD because the problems are so very different. The algorithms, conceptual thinking, error correction protocols and control of hardware, on the other hand, are of direct benefit. The same is true in the other direction.

### J. Some Words about Quantum Simulation

Quantum simulations correspond to faithfully or approximately simulating a physically interesting quantum systems using a different quantum system. Analog quantum simulators simulate a physical system using its internal Hamiltonian after a suitable mapping and preparing of an initial state. The “goodness” of the simulation is determined both by how well the system can be initialized and of the mapping of Hamiltonians between systems. An example of such a simulator is an early cold-atom system (with tweezers, etc). In contrast, a digital quantum computer is one with which a physical systems can be mapped onto a quantum register, and a sequence of gates (unitary operations) from a universal gate set can be applied in some sequence to evolve the system from some initial state, prepared with some fidelity, to some final state. Ideally, after a given gate-sequence, the quantum register remains in that quantum state until acted on again. With such systems, there is a well-defined path forward for improving the simulation (i.e., reducing  $\epsilon$ ). Examples of such systems are the superconducting quantum computers of IBM and the trapped-ion quantum computers of IonQ and Quantinuum. Hybrid systems have elements of some or all of these integrated together, including classical computing resources, providing a larger range of capabilities than each one individually. In this course, I am going to focus on digital quantum simulation. However, there are rapid advances in analog and hybrid simulation, e.g., cold-atom systems from Quera or Atom Computing, in fact there is an apparent convergence in device capabilities so that in the future, such distinctions are becoming less impactful.

In general, all simulations will be hybrid simulations. In the case of digital quantum computers, they will always be embedded in an classical HPC ecosystem, for control purposes, for circuit preparation, for circuit measurement and post-processing, for error correction. In this sense, what we mean by a digital quantum computer really is a hybrid system.

Figure 4 displays a cartoon of a target physics curve and a result with associated uncertainties. In simulation, quantum or classical, most of the computing resources are expended in determining a complete quantification of uncertainties (or errors). In the current era of quantum simulation, the largest uncertainties are from the quantum devices, not the theory or mappings. This is changing, and at some point, like HPC, the hardware errors will become the sub-dominant source of errors, and other sources will become the limitations. It is important to keep this in mind when setting

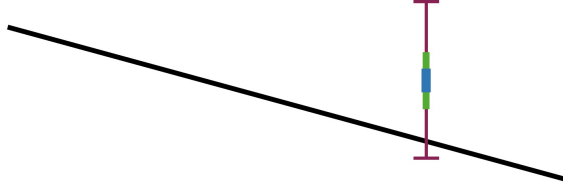


FIG. 4: A cartoon of a target physics curve and a result with associated uncertainties (errors).

up for simulations using quantum computers!

## II. QUANTUM CIRCUITS FOR DIGITAL QUANTUM SIMULATION

At the heart of every quantum simulation using a digital quantum computer are quantum circuits that are composite applications of unitary operations from a universal gate-set. They are constructed in such a way to reproduce a target unitary evolution with some level of precision  $\epsilon$  (systematic error), that can be systematically decreased as desired.<sup>7</sup>

### A. 1-qubit

To set convention for what follows, we first consider a single qubit, which generally can be in the state  $|\psi\rangle = c_0|0\rangle + c_1|1\rangle$ , with a generalized set of Pauli operators  $\hat{A}_i = \{\hat{I}, \hat{X}, \hat{Y}, \hat{Z}\}$ . The states of  $|0\rangle$  and  $|1\rangle$  are eigenstates of the  $\hat{Z}$  operator. We have previously discussed the actions of  $\hat{A}_i$  on a single qubit.

$$\hat{X}|\psi\rangle = c_0|1\rangle + c_1|0\rangle, \quad \hat{Y}|\psi\rangle = i c_0|1\rangle - i c_1|0\rangle, \quad \hat{Z}|\psi\rangle = c_0|0\rangle - c_1|1\rangle. \quad (17)$$

These are unitary operators, as the norm of the state before and after their application is the same. Arbitrary rotations of the qubit can be implemented using the well-known rotation operators for SU(2) (acting on the fundamental representation in the case of a qubit),

$$\hat{U}(\boldsymbol{\theta}) = e^{-i\mathbf{T}\cdot\boldsymbol{\theta}}, \quad T^i = \frac{1}{2}\sigma^i, \quad (18)$$

where  $\boldsymbol{\theta} = \theta\mathbf{n}$ , where  $\mathbf{n}$  is the axis about which the rotation by  $\theta$  is taking place, and the  $T^a$  are the generators of SU(2) (proportional to the Pauli matrices).<sup>8</sup> There are many practically useful parameterizations of the rotation operator, for example,

$$\hat{U}(\boldsymbol{\theta}) = e^{-i\mathbf{T}\cdot\boldsymbol{\theta}} = e^{-iT^z\eta_z} \cdot e^{-iT^y\eta_y} \cdot e^{-iT^x\eta_x}, \quad (19)$$

where the angles  $\eta_i$  must be determined in terms of the  $\theta_i$  (because of the non-commutativity of the generators). It is generally convenient, for SU(2), with some exceptions, to use the Euler

<sup>7</sup> If a device has large systematic errors in its operation, from the quality of the gate set or underlying hardware, then an infinitely precise gate sequence (prepared by the user) does not improve the quality of the simulations beyond the capabilities of the device.

<sup>8</sup> In these notes, we will interchangeably change notation between, for example,  $\hat{\sigma}^x = \hat{X}$ , and between their associated matrix representations.

representation of the rotational operator,

$$\begin{aligned}\hat{U}(\alpha, \beta, \gamma) &= R_z(\gamma).R_y(\beta).R_z(\alpha) = e^{-i\frac{1}{2}\sigma^z\gamma}.e^{-i\frac{1}{2}\sigma^y\beta}.e^{-i\frac{1}{2}\sigma^z\alpha} \\ &= \begin{pmatrix} e^{-i(\alpha+\gamma)/2} \cos \frac{\beta}{2} & -e^{+i(\alpha-\gamma)/2} \sin \frac{\beta}{2} \\ +e^{-i(\alpha-\gamma)/2} \sin \frac{\beta}{2} & e^{+i(\alpha+\gamma)/2} \cos \frac{\beta}{2} \end{pmatrix} ,\end{aligned}\quad (20)$$

where the phases  $\alpha, \gamma$  lie between 0 and  $2\pi$ , while the rotation about the y-axis lies between 0 to  $\pi$ .

Each technology company, start-up, university group that is creating algorithms and software for running quantum computers is free to choose its own (sets of) conventions, and also to utilize the fact that overall phase in a quantum wavefunction does not have measurable consequences. We are considering, and will be using, Google's **cirq** [34] and IBM's **qiskit** [35], but you are free to use any software packages that you wish in solving problems.

The IBM interface, **qiskit**, for ease of implementation retains an overall phase, and has representation (with  $\alpha = \lambda, \gamma = \phi$ )

$$e^{+i(\alpha+\gamma)/2}\hat{U}(\alpha, \beta, \gamma) \rightarrow \hat{U}(\theta, \phi, \lambda)^{(\text{qiskit})} = \begin{pmatrix} \cos \frac{\theta}{2} & -e^{+i\lambda} \sin \frac{\theta}{2} \\ +e^{+i\phi} \sin \frac{\theta}{2} & e^{+i(\lambda+\phi)} \cos \frac{\theta}{2} \end{pmatrix} .\quad (21)$$

In building circuits, we can use built-in functions that the software has, such as  $U(\theta, \phi, \lambda)$ , or we can apply the operations sequentially to recover the Euler product <sup>9</sup>. This rotation operator provides the most general rotation on the Bloch-sphere. Under a general rotation in qiskit, the  $|0\rangle$  is transformed into

$$\hat{U}^{\text{qiskit}}|0\rangle = \cos \frac{\theta}{2}|0\rangle + e^{+i\phi} \sin \frac{\theta}{2}|1\rangle .\quad (22)$$

There are other gates that are essential in building circuits, including the Hadamard, the phase-gate  $\hat{S}$  and the T-gate  $\hat{T}$ ,

$$\hat{H} = \frac{1}{\sqrt{2}} \begin{pmatrix} 1 & 1 \\ 1 & -1 \end{pmatrix} , \quad \hat{S} = \begin{pmatrix} 1 & 0 \\ 0 & i \end{pmatrix} , \quad \hat{T} = \begin{pmatrix} 1 & 0 \\ 0 & e^{i\pi/4} \end{pmatrix} .\quad (23)$$

It is important to note that operations that involve the Clifford gates, without the T-gates, can be shown to be classically efficient (**Gottesman-Knill theorem** [36]). The Clifford group can be generated with the Pauli's, S-gate and CNOT-gate. Circuits using only the Clifford gates are called **stabilizer circuits**, relevant for error correction.

The actions of these are “nice”, e.g.,  $\hat{S}|k\rangle = i^k|k\rangle$ . They are used in sequences to recover arbitrary SU(2) rotations. The **Solovay–Kitaev theorem** from 1995 and 1997 [26, 37]: If one has a finite set of SU(2) operators that generate a dense set on SU(2), then a sequence of gates that can be applied to perform an arbitrary transformation that is within  $\epsilon$  of the desired transformation scales as  $\sim \mathcal{O}(\log^\alpha \frac{1}{\epsilon})$ . Of course, one can find more complex circuits, but there exists gate sets for which  $\alpha = 1$ . In some sense, one can define a universal single-qubit gate-set by one that satisfies this scaling.

In terms of rotation operators,

$$\hat{H} = \hat{X}.R_y\left(\frac{\pi}{2}\right) = e^{i\frac{\pi}{2}}R_z\left(\frac{\pi}{2}\right).R_x\left(\frac{\pi}{2}\right).R_z\left(\frac{\pi}{2}\right) , \quad \hat{S} = e^{i\frac{\pi}{4}}R_z\left(\frac{\pi}{2}\right) , \quad \hat{T} = e^{i\frac{\pi}{8}}R_z\left(\frac{\pi}{4}\right) .\quad (24)$$

---

<sup>9</sup> The right-most operator corresponds to the first circuit element.

Composites can be formed by repeated applications of these gates, e.g.,

$$R_x\left(\frac{\pi}{4}\right) = e^{-i\frac{\pi}{8}} \hat{H} \hat{T} \hat{H} . \quad (25)$$

For example,

$$\hat{T} \hat{H} \hat{T} \hat{H} = e^{i\pi/4} \left( \hat{I} \cos^2 \frac{\pi}{8} - i \sin \frac{\pi}{8} \left( \hat{X} \cos \frac{\pi}{8} + \hat{Y} \sin \frac{\pi}{8} + \hat{Z} \cos \frac{\pi}{8} \right) \right) . \quad (26)$$

We see that by using the SU(2) commutation relations, we can use the universal gate-set, by repeated applications, to recover any desired SU(2) rotation within a given  $\epsilon$ . Polynomial increases in the number of gates applied furnishes exponential convergence in the rotation operator (**Solovay–Kitaev theorem**).

In reality, accomplishing this is more complex than it sounds, but an efficient, exponentially converging algorithm for implementing without the need for ancilla qubits is presented in a paper by Ross and Selinger [38] from 2014. For instance, there are two different rotation axes defined by the operators  $THTH$  and  $HTHT$ ,  $\mathbf{n}_1$  and  $\mathbf{n}_2$ ,

$$\hat{U}_{\mathbf{n}_i} = \hat{I} \cos \eta - i \sin \eta \boldsymbol{\sigma} \cdot \mathbf{n}_i . \quad (27)$$

Figure 5 shows an excerpt from the paper by Ross and Selinger [38] which presents details of the construction of a rotation about the z-axis,  $R_z(\frac{\pi}{128})$ , in terms of a **Solovay–Kitaev** decomposition.

Part of the computation involves decomposing the target rotation into Euler angles about these two axes (in analogy with defining any given arbitrary rotation by rotations about the  $y$ - and  $z$ -axes),

$$\hat{U}_{\text{target}} = e^{i\alpha} R_1(\beta).R_2(\gamma).R_3(\rho) , \quad (28)$$

using projections

$$\text{Tr}[U_{\text{target}}]/2 = \cos \theta_{\text{target}} , \quad \text{Tr}[\hat{X} U_{\text{target}}]/2 = -i \sin \theta_{\text{target}} \mathbf{n}_x^{\text{target}} , \quad \dots \quad (29)$$

on Eq. (27), and by determining the number of applications of each operator required to approach the target rotation within  $\epsilon$ . This is iterative tree’ing task and requires serious coding and algorithms.

In present day quantum computers, with addressable hardware, pulses, laser or microwave, are applied to the qubits or qudits to apply gates. The duration, magnitude and pulse shape determines the response of the qubit and the effective digital unitary operation. As such, it is determining these pulses and pulse sequences that is the actual “behind the scenes” classical computations to design the required unitary operators,

$$\hat{U}(t) \rightarrow \hat{U}(\alpha, \beta, \gamma) . \quad (30)$$

Just to close out this section with a general result. If we want to switch between representations, it can be shown that (with ”quadrant issues” that can be resolved),

$$e^{i(\alpha_1 \hat{X} + \alpha_2 \hat{Y} + \alpha_3 \hat{Z})} = e^{i\theta_3 \hat{Z}} e^{i\theta_2 \hat{Y}} e^{i\theta_1 \hat{Z}} , \quad (31)$$

with

$$\begin{aligned} \theta_1 &= \frac{1}{2} \left( \tan^{-1} \left( \frac{\alpha_3}{\alpha_1} \tan \alpha_r \right) - \tan^{-1} \left( \frac{\alpha_2}{\alpha_1} \right) \right) \\ \theta_3 &= \frac{1}{2} \left( \tan^{-1} \left( \frac{\alpha_3}{\alpha_1} \tan \alpha_r \right) + \tan^{-1} \left( \frac{\alpha_2}{\alpha_1} \right) \right) \\ \tan^2 \theta_2 &= \frac{\alpha_1^2 + \alpha_2^2}{(\alpha_r \cot \alpha_r - i\alpha_3)^2} . \end{aligned} \quad (32)$$



In terms of the  $T^a$ , for  $SU(2)$ , there is only 1 generator,  $\hat{J}_z$  that commutes with the Casimir,  $\hat{J}^2 = \sum_i \hat{J}_i^2$ , in  $SU(3)$  there are 2,  $\hat{I}_z$  and  $\hat{Y}$ , and in  $SU(4)$  there are 3, and generally the dimensionality of the Cartan sub-algebra equals the number of diagonal generators minus 1. Therefore, we know that for  $SU(4)$  there are three generators acting between the spaces that the  $\hat{K}_j$  act in, and that commute with each other. Counting the number of independent angles that we have in such a construction, each  $\hat{K}_j$  has 3 angles, so there are 12 angles in the single qubit rotations, and there are 3 defining the Cartan part, and so we have  $12 + 3 = 15$ , which is the correct number.

Because we have set up the circuit so that the  $\hat{K}_j$  act on the individual qubits, it will be entangling gates that implement the Cartan sub-algebra,  $\hat{X}\hat{X}$ ,  $\hat{Y}\hat{Y}$  and  $\hat{Z}\hat{Z}$ . Considering the operators defining the Cartan sub-algebra to begin with,

$$\begin{aligned}\hat{X}\hat{X} &= \hat{X} \otimes \hat{X} = (\hat{X} \otimes \hat{I}) \cdot (\hat{I} \otimes \hat{X}) = \hat{X}_1 \hat{X}_2 \\ &= \begin{pmatrix} 0 & 1 \\ 1 & 0 \end{pmatrix} \otimes \begin{pmatrix} 0 & 1 \\ 1 & 0 \end{pmatrix} = \begin{pmatrix} 0 & 0 & 0 & 1 \\ 0 & 0 & 1 & 0 \\ 0 & 1 & 0 & 0 \\ 1 & 0 & 0 & 0 \end{pmatrix} \\ \hat{Y}\hat{Y} &= \begin{pmatrix} 0 & 0 & 0 & -1 \\ 0 & 0 & 1 & 0 \\ 0 & 1 & 0 & 0 \\ -1 & 0 & 0 & 0 \end{pmatrix} \\ \hat{X}\hat{X} \cdot \hat{Y}\hat{Y} &= \begin{pmatrix} -1 & 0 & 0 & 0 \\ 0 & 1 & 0 & 0 \\ 0 & 0 & 1 & 0 \\ 0 & 0 & 0 & -1 \end{pmatrix} = \hat{Y}\hat{Y} \cdot \hat{X}\hat{X} \\ [\hat{X}\hat{X}, \hat{Y}\hat{Y}] &= 0 ,\end{aligned}\tag{35}$$

and similarly for the other two commutators.<sup>10</sup> This seems a little odd at first, but

$$\begin{aligned}\hat{X}\hat{X} \cdot \hat{Y}\hat{Y} &= \hat{X}\hat{Y} \otimes \hat{X}\hat{Y} = \left( \frac{1}{2}\{\hat{X}, \hat{Y}\} + \frac{1}{2}[\hat{X}, \hat{Y}] \right) \otimes \left( \frac{1}{2}\{\hat{X}, \hat{Y}\} + \frac{1}{2}[\hat{X}, \hat{Y}] \right) \\ &= -\hat{Z} \otimes \hat{Z} = \hat{Y}\hat{Y} \cdot \hat{X}\hat{X} ,\end{aligned}\tag{37}$$

due to the vanishing of the anti-commutators, i.e.,  $\hat{X}\hat{Y} = i\hat{Z}$  and  $\hat{Y}\hat{X} = -i\hat{Z}$ . We see the signs cancel for the reverse ordering, and hence the operators commute.

We already know how to implement  $SU(2)$  transformations on one qubit, so what remains is to implement the rotations associated with the Cartan sub-algebra,

$$\hat{C} = e^{-i\frac{1}{2}(\theta_7 \hat{X}\hat{X} + \theta_8 \hat{Y}\hat{Y} + \theta_9 \hat{Z}\hat{Z})} ,\tag{38}$$

---

<sup>10</sup> For clarity in what “ $\otimes$ ” means:

$$\hat{X} \otimes \hat{Z} = \begin{pmatrix} 0 & 0 & 1 & 0 \\ 0 & 0 & 0 & -1 \\ 1 & 0 & 0 & 0 \\ 0 & -1 & 0 & 0 \end{pmatrix} .\tag{36}$$

By explicit construction, it is straightforward to show that

$$\begin{aligned} e^{-i\frac{1}{2}\alpha Z \otimes Z} &= \text{CNOT}(1, 2). (\hat{I} \otimes R_z(\alpha)). \text{CNOT}(1, 2) \\ e^{-i\frac{1}{2}\beta X \otimes X} &= \hat{H}_1. \hat{H}_2. \text{CNOT}(1, 2). (\hat{I} \otimes R_z(\beta)). \text{CNOT}(1, 2). \hat{H}_1. \hat{H}_2 \\ e^{-i\frac{1}{2}\gamma Y \otimes Y} &= \hat{S}_1. \hat{S}_2. \hat{H}_1. \hat{H}_2. \text{CNOT}(1, 2). (\hat{I} \otimes R_z(\gamma)). \text{CNOT}(1, 2). \hat{H}_1. \hat{H}_2. \hat{S}_1^\dagger. \hat{S}_2^\dagger \quad , \end{aligned} \quad (39)$$

as shown in Fig. 7, each with gate counts of 2 CNOTs, 1 single-qubit rotation about the z-axis

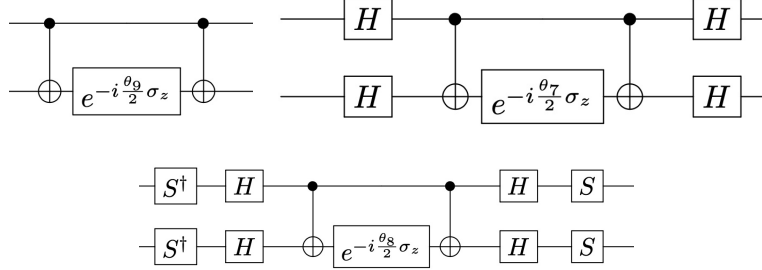


FIG. 6: Quantum circuits for the Cartan sub-algebra. Here we have that  $\alpha = \theta_9$  in Eq. (39),  $\beta = \theta_7$  and  $\gamma = \theta_8$ .

and 0, 4, 8 single qubit gates. If this is how a general SU(4) transformation was implemented, by sequential application of these circuits, 6 CNOTs, 3 single qubit rotations and 12 single qubit gates would be required. However, it was figured out a long time ago by Dawson and Vidal [40], that in fact the Cartan unitary can be implemented with the circuit shown in Fig. 7, requiring only 3 CNOTs, 5 single qubit rotations and 3 single qubit gates. It is the case that the entangling gates are

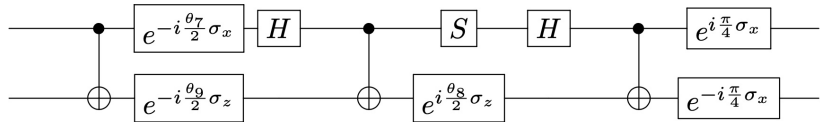


FIG. 7: Efficient quantum circuit for the Cartan sub-algebra, with  $\alpha = \theta_9$  in Eq. (39),  $\beta = \theta_7$  and  $\gamma = \theta_8$ .

more computationally demanding, and hence with lower fidelity and requiring longer application times, and so the reduced CNOT count is very helpful. Note that the naive implementation uses single-qubit rotations about the z-axis and appropriate changes of basis, while the Dawson-Vidal circuit uses rotations about the x-axis and z-axis.

### 1. Molmer-Sorensen Gate

There are an infinite number of potential ways to entangle 2 qubits, and on trapped-ion systems, it turns out that the Molmer-Sorensen (MS) gate can be implemented with the hardware as a fundamental 2-qubit interaction. The physics of the implementation is that for trapped ions, ions trapped by background fields in a local harmonic trap, laser light excites the atom, but at the same time the atom recoils, exciting it into a vibrational mode of the trap. It is this combination that entangles the ions.

IonQ implements a native gate

$$R_{\hat{X}\hat{X}}\left(\frac{\pi}{2}\right) = e^{-i\frac{\pi}{4}\hat{X}\otimes\hat{X}}, \quad (40)$$

which is related to the CNOT-gate by single qubit operations and phases. The CNOT gate can be recovered from the MS gate via [41]<sup>11</sup>,

$$\text{CNOT}_{12} = e^{-i\pi/4} \left(R_y(-\frac{\pi}{2})\otimes\hat{I}\right) \left(R_x(-\frac{\pi}{2})\otimes\hat{I}\right) \left(\hat{I}\otimes R_x(-\frac{\pi}{2})\right) R_{\hat{X}\hat{X}}\left(\frac{\pi}{2}\right) \left(R_y(+\frac{\pi}{2})\otimes\hat{I}\right) \quad (41)$$

There are generalized MS (GMS) gates, which implement gates with continuous rotation angle,  $\chi_{ij}$ ,

$$XX_{ij}(\chi_{ij}) = e^{-i\frac{\chi_{ij}}{2}\hat{X}\otimes\hat{X}}, \quad (42)$$

between the  $i^{\text{th}}$  and  $j^{\text{th}}$  qubits, recovering the MS gate when  $\chi = \pi/2$ . With the GMS gate, the Cartan sub-algebra of SU(4) can be implemented straightforwardly.

Let us explore a little more what the GMS-gate does,

$$\hat{X}\otimes\hat{X} = \begin{pmatrix} 0 & 0 & 0 & 1 \\ 0 & 0 & 1 & 0 \\ 0 & 1 & 0 & 0 \\ 1 & 0 & 0 & 0 \end{pmatrix}, \quad e^{-i\frac{\alpha}{2}\hat{X}\otimes\hat{X}} = \begin{pmatrix} \cos\frac{\alpha}{2} & 0 & 0 & -i\sin\frac{\alpha}{2} \\ 0 & \cos\frac{\alpha}{2} & -i\sin\frac{\alpha}{2} & 0 \\ 0 & -i\sin\frac{\alpha}{2} & \cos\frac{\alpha}{2} & 0 \\ -i\sin\frac{\alpha}{2} & 0 & 0 & \cos\frac{\alpha}{2} \end{pmatrix}, \quad (43)$$

which evolves

$$(c_{00}, c_{01}, c_{10}, c_{11}) \rightarrow \left(c_{00}\cos\frac{\alpha}{2} - ic_{11}\sin\frac{\alpha}{2}, c_{01}\cos\frac{\alpha}{2} - ic_{10}\sin\frac{\alpha}{2}, c_{10}\cos\frac{\alpha}{2} - ic_{01}\sin\frac{\alpha}{2}, c_{11}\cos\frac{\alpha}{2} - ic_{00}\sin\frac{\alpha}{2}\right), \quad (44)$$

which mixes  $|00\rangle$  with  $|11\rangle$ , and mixes  $|01\rangle$  with  $|10\rangle$ .

In fact, the state of the system is that of the electronic degrees of freedom with the vibrational degrees of freedom, e.g.,  $|01\rangle\otimes|n\rangle$ , and because of the recoil of the atoms, one should consider the tower of states

$$\dots|00\rangle\otimes|n-1\rangle, |01\rangle\otimes|n-1\rangle, |10\rangle\otimes|n-1\rangle, |11\rangle\otimes|n-1\rangle, |00\rangle\otimes|n\rangle, |01\rangle\otimes|n\rangle, |10\rangle\otimes|n\rangle, |11\rangle\otimes|n\rangle, |00\rangle\otimes|n+1\rangle, |01\rangle\otimes|n+1\rangle, |10\rangle\otimes|n+1\rangle, |11\rangle\otimes|n+1\rangle, \dots \quad (45)$$

along with the Hamiltonian describing the evolution of the system,

$$\begin{aligned} H_0 &= \nu \left(a^\dagger a + \frac{1}{2}\right) + \frac{\omega_{01}}{2} \sum_i \hat{Z}_i \\ H_I &= \sum_i \frac{\Omega_i}{2} \left(\sigma_i^+ e^{i(\eta_i(a+a^\dagger)-\omega_i t)} + \text{h.c.}\right) \end{aligned}, \quad (46)$$

where  $\nu$  is the trap frequency,  $a$  annihilates vibrational quanta in the trap,  $\omega_{01}$  is the energy difference between the single-particle electronic spin states.  $H_I$  includes the interactions between the  $i^{\text{th}}$  spin and the vibrational degrees of freedom, where  $\sigma_i^+$  denotes the raising operator on the  $i^{\text{th}}$  spin, and  $\frac{1}{2}(\hat{X} + i\hat{Y})$ . Figure 8 shows a cartoon of the ideal electron-vibrational levels in a trapped-ion system that enables the implementation of a GMS-gate. A set of laser frequencies acting for a well-defined length of time can induce the GMS-gate amplitudes between  $|00\rangle$  and  $|11\rangle$ , with sub-leading corrections in the expansion, and an analogous set of lasers frequencies induces the  $|01\rangle$  and  $|10\rangle$  amplitudes.

---

<sup>11</sup> The article referred to, Ref. [41], provides a very nice compilation of gate structures.

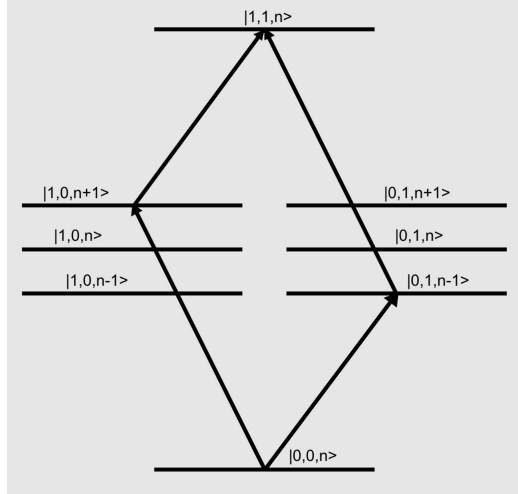


FIG. 8: A cartoon of the electronic-vibrational levels of ions in a trap, and the de-tuned electronic transition to implement a generalized Molmer-Sorenson gate. (Wikipedia).

## 2. Controlled Operators

With two qubits, we can consider the situation where the operations on one qubit are controlled by the state of other qubits. For example, we can have the rotation performed on qubit-2 be determined by the state of qubit-1. The generalization of this concept extends to systems with n-qubits, where the state of the  $n^{\text{th}}$  qubit depends upon the state of  $n - 1^{\text{th}}$  qubits. We have seen this with the CNOT gate, which is a controlled-X-gate. In the case of rotations, an example of which is shown in Fig. 9, transforms the state  $|00\rangle$  into

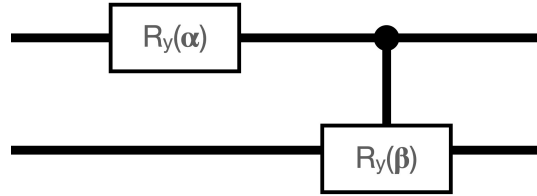


FIG. 9: Circuit showing qubit-2 controlled by a rotated qubit-1.

$$\begin{aligned} |\psi'\rangle &= \left( \hat{\Lambda}_0 \otimes \hat{I} + \hat{\Lambda}_1 \otimes \hat{R}_y(\beta) \right) \left( \hat{R}_y(\alpha) \otimes \hat{I} \right) |\psi\rangle, \\ |00\rangle &\rightarrow \cos \frac{\alpha}{2} |00\rangle + \sin \frac{\alpha}{2} |10\rangle \rightarrow \cos \frac{\alpha}{2} |00\rangle + \sin \frac{\alpha}{2} \cos \frac{\beta}{2} |10\rangle + \sin \frac{\alpha}{2} \sin \frac{\beta}{2} |11\rangle . \end{aligned} \quad (47)$$

While this circuit maps this initial state to 3 states in the 4-dimensional Hilbert space, it is insufficient to map to all of the states. i.e. it is insufficient to produce an arbitrary real function through-out the Hilbert space starting from  $|00\rangle$ . After all, we are only using two angles, and defining three real amplitudes! To define an arbitrary real-valued wavefunction from this initial state, three angles are required – one for each amplitude (with the state normalized to unity). To do this, we introduce another control on qubit-1, denoted by an open circle acting on qubit-1, as shown in Fig. 10. The combined operators are denoted by an open circle with a dot in it, as shown

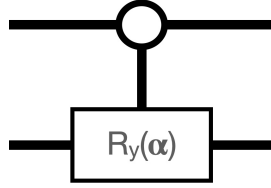


FIG. 10: The sample of a y-rotation controlled on qubit-1 performing a non-trivial rotation when qubit-1 is in  $|0\rangle$ .

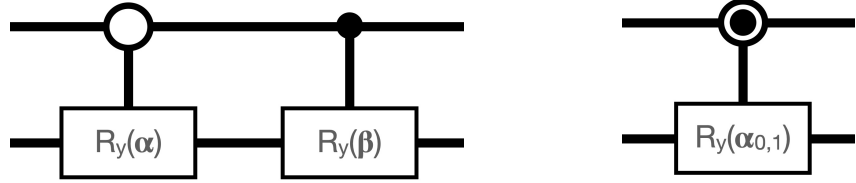


FIG. 11: The general controlled operation. The left panel shows the two controlled operations that are denoted by that in the right panel with lower-indices.

in Fig. 11.

A circuit that allows all of the states in the Hilbert space to be "accessed" from  $|00\rangle$  is shown in Fig. 12. The action of this circuit, acting left to right is

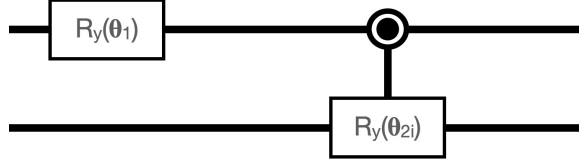


FIG. 12: A circuit to initialize an arbitrary real function on two qubits, requiring three independent angles, e.g.,  $\theta_1$ ,  $\theta_{20}$ ,  $\theta_{21}$ .

$$\begin{aligned}
 |\psi'\rangle &= (\hat{\Lambda}_0 \otimes \hat{R}_y(\theta_{20}) + \hat{\Lambda}_1 \otimes \hat{I}) (\hat{\Lambda}_0 \otimes \hat{I} + \hat{\Lambda}_1 \otimes \hat{R}_y(\theta_{21})) (\hat{R}_y(\theta_1) \otimes \hat{I}) |\psi\rangle , \\
 &= (\hat{\Lambda}_0 \otimes \hat{R}_y(\theta_{20}) + \hat{\Lambda}_1 \otimes \hat{R}_y(\theta_{21})) (\hat{R}_y(\theta_1) \otimes \hat{I}) |\psi\rangle , \\
 |00\rangle &\rightarrow \cos \frac{\theta_1}{2} |00\rangle + \sin \frac{\theta_1}{2} |10\rangle \\
 &\rightarrow \cos \frac{\theta_1}{2} \left( \cos \frac{\theta_{20}}{2} |00\rangle + \sin \frac{\theta_{20}}{2} |01\rangle \right) + \sin \frac{\theta_1}{2} \left( \cos \frac{\theta_{21}}{2} |10\rangle + \sin \frac{\theta_{21}}{2} |11\rangle \right) \\
 &\rightarrow \cos \frac{\theta_1}{2} \cos \frac{\theta_{20}}{2} |00\rangle + \cos \frac{\theta_1}{2} \sin \frac{\theta_{20}}{2} |01\rangle + \sin \frac{\theta_1}{2} \cos \frac{\theta_{21}}{2} |10\rangle + \sin \frac{\theta_1}{2} \sin \frac{\theta_{21}}{2} |11\rangle , \quad (48)
 \end{aligned}$$

which with three independent angles, is sufficient to initialize an arbitrary real function across the Hilbert space with unit norm. There is a nice physical picture to be considered, as sketched in

Fig. 13. In binary, the states are in ascending order, with the lowest two determined by  $\cos \theta_1$  and the upper two by  $\sin \theta_1$  (the red-dashed lines). Upon subdivision, the asymmetry between the lower two is determined by  $\theta_{20}$  and between the upper two by  $\theta_{21}$  (the teal-solid lines).

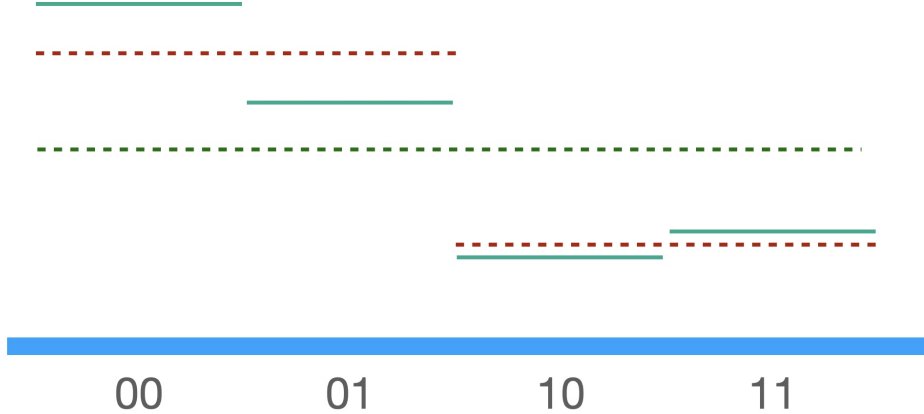


FIG. 13: A cartoon of a real wavefunction on two qubits (initialized as in Eq. (48)).

The counting of angles seems a little odd at first because it disagrees with the general number of SU(4) angles. But it is important to keep in mind that this is not a general real symmetric transformation, but only the one that connects to  $|00\rangle$ , and so the number is less (3 and not 9). <sup>12</sup>

Another point to note for practical purposes, is that instead of starting from one state in the Hilbert space, if the target wavefunction has support throughout most of the space, it can be more convenient to start from the wavefunction with equal amplitudes for all states. This is accomplished by first applying Hadamard gates to all qubits.

$$\hat{H}^{\otimes 2}|00\rangle = \frac{1}{2} [ |00\rangle + |01\rangle + |10\rangle + |11\rangle ] \quad , \quad (49)$$

then applying the circuit shown in Fig. 12 (for which the three angles are expected to be smaller if the target state is close to that in Eq. (49)).

### C. Hamiltonian Evolution

One important unitary that we will encounter many times during this course is that of unitary time evolution, with real and symmetric Hamiltonians,

$$\hat{U}(t) = e^{-i\hat{\mathcal{H}}t} \quad . \quad (50)$$

As the physical system is unchanged by arbitrary local unitary transformations among the basis states,  $\hat{\mathcal{H}} \rightarrow \hat{U}\hat{\mathcal{H}}\hat{U}^\dagger$ , the Hamiltonian can be transformed into one that can be decomposed onto a reduced set of SU(N) generators. <sup>13</sup> For instance, for SU(2), the three angles required to define

<sup>12</sup> For example, if we had started from the state  $|11\rangle$  (or any of the 3 other states), the same real wavefunction would have required 3 different angles,  $\theta'_1, \theta'_{2i}$ .

<sup>13</sup> Diagonalization of the n-dimensional Hamiltonian provides n eigenstates. For CP, T conserving Hamiltonians, an SO(n) transformation is sufficient to express any state in the Hilbert space in terms of these eigenstates. In such rotated bases, the Hamiltonian is real and symmetric.

the unitary operation is reduced to 2, corresponding to, for example,  $\hat{X}$  and  $\hat{Z}$ . Generally,

$$\begin{aligned} SU(2) &: 3 \rightarrow 2 \\ SU(3) &: 8 \rightarrow 5 \\ SU(4) &: 15 \rightarrow 9 \\ SU(N) &: N^2 - 1 \rightarrow \frac{1}{2}N(N + 1) - 1 \quad , \end{aligned} \quad (51)$$

corresponding to keeping the real-valued generators, and so the number of angles that need to be determined is smaller than for an arbitrary unitary operation for any given  $N$ . This can be taken into account when designing quantum circuits. For example,

$$\hat{\mathcal{H}} = \begin{pmatrix} 1 & 4 \\ 4 & 5 \end{pmatrix} = 3\hat{I} + 4\hat{X} - 2\hat{Z} \quad , \quad (52)$$

and the relations in Eqs. (31) and (32) can be used to define unitary time-evolution.

#### D. Qutrits

If we wish to think more generally, and in particular about what type of quantum hardware could be optimal or more efficient, to address a certain system, then we should think beyond qubits, and think generally about qudits (for a recent review of qudits, see Ref. [42]). Qudits are objects supporting a  $d$ -dimensional discrete Hilbert space, a generalization of a qubit.  $SU(d)$  transformations connect the states of a qudit, and our discussions about  $SU(2)$  transformations for qubits must be generalized to  $SU(d)$ . It turns out that  $SU(2)$  is more closely related to  $U(1)$  than it is to  $SU(3)$ ,  $SU(4)$ , ..., which seems like an odd statement, and one that is not immediately obvious, but keep it in mind as we go forward.

The simplest qudit beyond the qubit is a *qutrit* that supports  $d = 3$  quantum states, canonically denoted by  $m = \pm 1, 0$ . From a familiar hardware point of view, qutrits are supported in superconducting "qubit" systems, as they can be in states with  $\pm 1$  or zero units of flux, and trapped ion species can support, for example, two  $S$ -states + 1  $D$  state, which can be connected via RF+optical photons.

Any arbitrary  $SU(3)$  transformation, that is appropriate for qutrits, can be written as

$$\hat{U}_3 = e^{-i\alpha\lambda_3}e^{-i\beta\lambda_1}e^{-i\gamma\lambda_3}e^{-i\theta\lambda_4}e^{-ia\lambda_3}e^{-ib\lambda_1}e^{-ic\lambda_3}e^{-i\phi\lambda_8} \quad , \quad (53)$$

with the number of angles corresponding to the number of generators, and where I have taken the liberty of replacing the usual  $\lambda_5$  with  $\lambda_4$ , and  $\lambda_2$  with  $\lambda_1$  (compared with the usual convention). The reason for this particular choice of generators is that on some hardware it is easier to implement  $\hat{X}$ -rotations between pairs of states, rather than  $\hat{Y}$ -rotations.<sup>14</sup> As a reminder, the explicit rotation

<sup>14</sup> The choice of generators to implement the transformations does not impact the "physics", and is entirely a choice. However, just as the choice of basis determines the amount of labor required to accomplish a calculation, the same is true for the representation of transformations.

matrices are:

$$\begin{aligned} e^{-i\theta\lambda_4} &= \begin{pmatrix} \cos\theta & 0 & -i\sin\theta \\ 0 & 1 & 0 \\ -i\sin\theta & 0 & \cos\theta \end{pmatrix}, \quad e^{-i\beta\lambda_1} = \begin{pmatrix} \cos\beta & -i\sin\beta & 0 \\ -i\sin\beta & \cos\beta & 0 \\ 0 & 0 & 1 \end{pmatrix} \\ e^{-i\alpha\lambda_3} &= \begin{pmatrix} e^{-i\alpha} & 0 & 0 \\ 0 & e^{i\alpha} & 0 \\ 0 & 0 & 1 \end{pmatrix}, \quad e^{-i\phi\lambda_8} = \begin{pmatrix} e^{-\frac{i\phi}{\sqrt{3}}} & 0 & 0 \\ 0 & e^{-\frac{i\phi}{\sqrt{3}}} & 0 \\ 0 & 0 & e^{\frac{2i\phi}{\sqrt{3}}} \end{pmatrix}. \end{aligned} \quad (54)$$

Now, there are further simplifications because the Hamiltonian is real and symmetric, and as such, it does not map out all possible SU(3) rotations, but just a 5-dimensional subset. In particular

$$\alpha = c, \quad \gamma = a + \sqrt{3}\phi, \quad \beta = b, \quad , \quad (55)$$

giving

$$\hat{U}_3^{(\text{sym.H})} = e^{-ic\lambda_3}e^{-ib\lambda_1}e^{-ia\lambda_3}e^{-i\sqrt{3}\phi\lambda_3}e^{-i\theta\lambda_4}e^{-ia\lambda_3}e^{-ib\lambda_1}e^{-ic\lambda_3}e^{-i\phi\lambda_8}. \quad (56)$$

### 1. Givens Rotations

Thinking in terms of hardware, it is difficult to think about generic SU(3) transformations, but much easier to think about sequences of SU(2) transformations between two of the three levels. We have, in fact, used this in constructing our general SU(3) transformation. For example  $\lambda_4$  is a real matrix that connects state-1 with state-3 only, and similarly  $\lambda_2$  connects state-1 with state-2 only. Exponentiation of these generators, only induces rotations between 2 of the 3 states.

We can define  $\hat{X}$ -type and  $\hat{Y}$ -type Givens operators for a single qutrit, of the form

$$\begin{aligned} \mathcal{X}_{12} &= \begin{pmatrix} 0 & 1 & 0 \\ 1 & 0 & 0 \\ 0 & 0 & 0 \end{pmatrix}, \quad \mathcal{X}_{13} = \begin{pmatrix} 0 & 0 & 1 \\ 0 & 0 & 0 \\ 1 & 0 & 0 \end{pmatrix}, \quad \mathcal{X}_{23} = \begin{pmatrix} 0 & 0 & 0 \\ 0 & 0 & 1 \\ 0 & 1 & 0 \end{pmatrix} \\ \mathcal{Y}_{12} &= \begin{pmatrix} 0 & -i & 0 \\ i & 0 & 0 \\ 0 & 0 & 0 \end{pmatrix}, \quad \mathcal{Y}_{13} = \begin{pmatrix} 0 & 0 & -i \\ 0 & 0 & 0 \\ i & 0 & 0 \end{pmatrix}, \quad \mathcal{Y}_{23} = \begin{pmatrix} 0 & 0 & 0 \\ 0 & 0 & -i \\ 0 & i & 0 \end{pmatrix}, \end{aligned} \quad (57)$$

and the associated diagonal phase operators

$$\mathcal{Z}_3 = \begin{pmatrix} 1 & 0 & 0 \\ 0 & -1 & 0 \\ 0 & 0 & 0 \end{pmatrix}, \quad \mathcal{Z}_8 = \frac{1}{\sqrt{3}} \begin{pmatrix} 1 & 0 & 0 \\ 0 & 1 & 0 \\ 0 & 0 & -2 \end{pmatrix}. \quad (58)$$

These are obviously directly related to the Gell-Mann matrices, but with different labeling that is more intuitive in this setting. The associated unitary transformations that mix states of a qutrit are,

$$G_{ij}^{\hat{X}}(\alpha) = e^{-i\frac{\alpha}{2}\hat{X}_{ij}}, \quad G_{ij}^{\hat{Y}}(\alpha) = e^{-i\frac{\alpha}{2}\hat{Y}_{ij}}. \quad (59)$$

In the same way that we have controlled operators between 2 qubits, and multiply controlled operations between n qubits, we can have the same type of operations among qutrits. However, the notation becomes a bit more deliberate because the projections (controls) depend upon the state of the control qutrit. As an example, Fig. 14 shows a generic Givens rotation controlled on

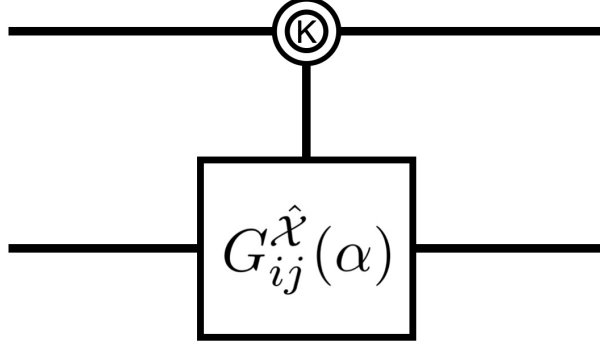


FIG. 14: Example of a controlled-Givens rotation. The control is on the  $K$  state of qutrit-1, generating a rotation between states  $i, j$  on qutrit-2, the general case of that given in Eq. (60).

the  $k$ -state of qutrit-2 inducing a rotation between states  $l, m$ . The form of the operator induced by controlled-Givens rotation in Fig. 14 is, for example, for an  $\hat{X}$ -type of operator, with  $k = 3$  and  $l, m = 1, 2$  is,

$$\begin{aligned}\hat{U}(\alpha; 3; 12) &= \left( \hat{I} - \hat{\Lambda}_3 \right) \otimes \hat{I} + \hat{\Lambda}_3 \otimes G_{12}^{\hat{X}}(\alpha) \\ \hat{\Lambda}_3 &= |3\rangle\langle 3| = \begin{pmatrix} 0 & 0 & 0 \\ 0 & 0 & 0 \\ 0 & 0 & 1 \end{pmatrix}.\end{aligned}\quad (60)$$

This discussion generalizes straightforwardly to qudits for arbitrary  $d$ . There remains freedom in how to define the diagonal generators. Generalizing the Gell-Mann convention is the simplest, for example for SU(4), the diagonal generators are written as

$$\mathcal{Z}_3 = \begin{pmatrix} 1 & 0 & 0 & 0 \\ 0 & -1 & 0 & 0 \\ 0 & 0 & 0 & 0 \\ 0 & 0 & 0 & 0 \end{pmatrix}, \quad \mathcal{Z}_8 = \frac{1}{\sqrt{3}} \begin{pmatrix} 1 & 0 & 0 & 0 \\ 0 & 1 & 0 & 0 \\ 0 & 0 & -2 & 0 \\ 0 & 0 & 0 & 0 \end{pmatrix}, \quad \mathcal{Z}_{15} = \frac{1}{\sqrt{12}} \begin{pmatrix} 1 & 0 & 0 & 0 \\ 0 & 1 & 0 & 0 \\ 0 & 0 & 1 & 0 \\ 0 & 0 & 0 & -3 \end{pmatrix}. \quad (61)$$

However, it can be more convenient to use the Hadamard-Walsh basis, directly related to sequency corresponding to discrete Fourier analysis used in signal processing,

$$w_1 = \frac{1}{2} \begin{pmatrix} 1 & 0 & 0 & 0 \\ 0 & 1 & 0 & 0 \\ 0 & 0 & 1 & 0 \\ 0 & 0 & 0 & 1 \end{pmatrix}, \quad w_2 = \begin{pmatrix} 1 & 0 & 0 & 0 \\ 0 & 1 & 0 & 0 \\ 0 & 0 & -1 & 0 \\ 0 & 0 & 0 & -1 \end{pmatrix}, \quad w_3 = \begin{pmatrix} 1 & 0 & 0 & 0 \\ 0 & -1 & 0 & 0 \\ 0 & 0 & -1 & 0 \\ 0 & 0 & 0 & 1 \end{pmatrix}, \quad w_4 = \begin{pmatrix} 1 & 0 & 0 & 0 \\ 0 & -1 & 0 & 0 \\ 0 & 0 & 1 & 0 \\ 0 & 0 & 0 & -1 \end{pmatrix} \quad (62)$$

which have norm 1.

### III. ENTANGLEMENT MEASURES

I would like to start this week by introducing and discussing relevant aspects of entanglement and entanglement measures. The reason for this is that, along with coherence, they are the features that quantum computers have control over that are inaccessible to classical computers. It is these features that we need to learn how to use in computations and simulations in order to be able to accomplish more than classical computing alone.

### A. Pure and Mixed Ensembles

A key aspect of quantum mechanics is ensemble measurement. That is to say that, for example, a laboratory receives (or creates) a number  $N$  quantum systems on which they can perform measurements. The ensembles can be **pure** by which we mean that each element of the ensemble is in identically the same quantum state,  $|\psi\rangle$ , and hence with density matrix  $\hat{\rho} = |\psi\rangle\langle\psi|$ . Or they can be **mixed** by which we mean that the ensemble contains elements in different quantum states  $|\phi_j\rangle$ . Consider performing experiments sequentially, element by element, on a mixed ensemble, there is a probability  $p_j$  that a given element will be in  $|\phi_j\rangle$ , and hence the corresponding density matrix is

$$\hat{\rho} = \sum_j p_j |\phi_j\rangle\langle\phi_j| , \quad p_j \geq 0 , \quad \sum_j p_j = 1 . \quad (63)$$

It is the probability-weighted average of the contributing pure-state density matrices. When considering discussions and developments about entanglement in “the literature”, it might be helpful to keep this picture in mind.

In performing quantum simulation using quantum computers or simulators, ensemble measurements correspond to executing quantum circuits (for digital simulations) multiple times, forming the target observables, and then ensemble averaging. Practical limitations include the amount of access time on a given device, device errors and mitigation strategies.

### B. Separability

Consider a situation in which there are two (collaborating) laboratories, lab-A and lab-B<sup>15</sup>, that share components of elements of an ensemble. The simplest picture to keep in mind is that there is a **source** that sequentially creates quantum states (either the same pure state (a pure ensemble) or a selection of a number of different pure states (a mixed ensemble)) and sends parts to lab-A and other parts to lab-B.

For **pure states**, if the wavefunction can be written as a tensor product,

$$|\Psi\rangle = |\psi_A\rangle \otimes |\psi_B\rangle , \quad (64)$$

then the state is unentangled and separable. Measurements and operations that are performed on the part of the wavefunction in lab-A have no quantum correlations with measurements and operations performed in lab-B. If it cannot be written in this way, then it is entangled and not separable.

For **mixed states**, the analogous statement is that if all elements of the ensemble can be written as tensor products,

$$|\Phi_j\rangle = |\phi_{j,A}\rangle \otimes |\phi_{j,B}\rangle , \quad (65)$$

then the ensemble is unentangled and separable. On the other hand, if some of the elements cannot be written in this way, i.e. not all elements are tensor-product states, then the ensemble is **entangled, but may or may not be separable**. This depends upon the nature of the quantum correlations. The fact that a mixed ensemble may be separable does not mean that it is

---

<sup>15</sup> Of course, the common QIS language for this situation is lab-A=Alice and lab-B=Bob. We will use this notation interchangeably.

not entangled. However, the absence of correlations beyond those possible with classical physics does not mean that the ensemble is not entangled—entanglement can be obscured by separability.

To be more concrete, let's consider the density matrix associated with an ensemble of two-qubit systems, with some prepared as Bell pairs and some prepared as randomly aligned states. This is known as a *Werner State* [43]. This is perhaps the simplest system with which to begin to understand that impact that **noise** can have on quantum correlations. In any measurement that the labs are performing on a given element of the ensemble, there is a probability  $p$  that they are performing measurements on a Bell-pair and a probability  $1 - p$  that they are performing measurements on a randomly aligned state. Explicitly,

$$\begin{aligned} p : |\Phi_1\rangle &= \frac{1}{\sqrt{2}} [ |00\rangle + |11\rangle ] , \\ \frac{1}{4}(1-p) : |00\rangle &, \\ \frac{1}{4}(1-p) : |01\rangle &, \\ \frac{1}{4}(1-p) : |10\rangle &, \\ \frac{1}{4}(1-p) : |11\rangle &. \end{aligned} \quad (66)$$

The density matrix  $\rho_{AB}$ , as given in Eq. (63), of this system is

$$\begin{aligned} \hat{\rho}_{AB} &= p|\Phi_1\rangle\langle\Phi_1| + (1-p)\frac{1}{4}I_4 , \\ \hat{\rho}_{AB} &= \begin{pmatrix} \frac{1+p}{4} & 0 & 0 & \frac{p}{2} \\ 0 & \frac{1-p}{4} & 0 & 0 \\ 0 & 0 & \frac{1-p}{4} & 0 \\ \frac{p}{2} & 0 & 0 & \frac{1+p}{4} \end{pmatrix} , \end{aligned} \quad (67)$$

in the basis  $\{|00\rangle, |01\rangle, |10\rangle, |11\rangle\}$ . It is straightforward to show that this density matrix can also be written as, where we use the notation, for example,  $\rho(|00\rangle) = |00\rangle\langle 00|$ ,

$$\begin{aligned} \hat{\rho}_{AB} &= \frac{p}{2} [ \rho(|++\rangle_x) + \rho(|--\rangle_x) + \rho(|+-\rangle_y) + \rho(|-+\rangle_y) ] \\ &\quad + \frac{1-p}{4} (\rho(|00\rangle) + \rho(|11\rangle)) \\ &\quad + \frac{1-3p}{4} (\rho(|01\rangle) + \rho(|10\rangle)) , \\ \text{with } |\pm\rangle_x &= \frac{1}{\sqrt{2}} [ |0\rangle \pm |1\rangle ] , \quad |\pm\rangle_y = \frac{1}{\sqrt{2}} [ |0\rangle \pm i|1\rangle ] . \end{aligned} \quad (68)$$

The important point to note about this mathematical relation is that it involves only tensor-product states - which means that the system is separable **while containing elements in the ensemble that are entangled**. In order for this to be a **valid** density matrix, **all** of the coefficients in Eq. (68) must be  $0 \leq p_i \leq 1$ , and this is true **iff**  $p \leq \frac{1}{3}$ . For  $p \leq \frac{1}{3}$ , the density matrix of this entangled state has a convex decomposition in terms of tensor-product states, and hence does not exhibit quantum correlations between measurements in lab-A and lab-B, and is separable. On the other hand, for  $p > \frac{1}{3}$ , the system **cannot** be written as a convex decomposition, there is no density matrix that can be formed from tensor-product states alone, and therefore the system is not separable. Summary:

- $p = 0$ : classical and separable

- $0 < p \leq \frac{1}{3}$ : mixed ensemble containing entangled states, but the system is separable
- $p > \frac{1}{3}$ : mixed ensemble containing entangled states and the system is not separable
- $p = 1$ : pure state, entangled and not separable

It is important to note that the ensemble is unchanged by the ability to re-decompose the density matrix into only tensor-product states for  $p < \frac{1}{3}$ . This does not mean that the ensemble changes, or the states are physically changed – they are not. However, it does mean that, from a quantum correlation perspective, all correlations are consistent with classical physics. For example,  $|\psi\rangle = |01\rangle$  is classically correlated, i.e., lab-A always measures 0 and lab-B always measures 1 and there is no wavefunction collapse or randomness in measurement.

This example does illustrate the complications that arise when analyzing mixed states. Of course, any real system that we make in the laboratory is a mixed state due to interactions with the environment that are always present at some level. This example provides a small window into how entanglement in quantum many-body systems can be obscured by noise.

### C. Schmidt Decomposition

One important result of broad implication and application is the **Schmidt Decomposition**. Consider two Hilbert spaces  $A$  and  $B$ . There exist bases (that can be obtained by transformations that are local to the two spaces), denoted by  $\{|n_A\rangle\}$  and  $\{|n_B\rangle\}$ , such that any **pure state** can be written as

$$|\Psi\rangle = \sum_n^{\text{Min}(\dim(A), \dim(B))} \lambda_n |n_A\rangle \otimes |n_B\rangle , \quad (69)$$

where  $\lambda_i$  can be taken to be real and positive. If there is only one non-zero  $\lambda_i$ , the system has Schmidt-rank 1 (or Schmidt number), and is (obviously) separable. If the Schmidt rank is greater than 1, then it is not separable. The density matrix from the wavefunction in Eq. (69) is

$$\hat{\rho}_{AB} = \sum_{n,n'} \lambda_n \lambda_{n'} |n_A\rangle \otimes |n_B\rangle \langle n'_A| \otimes \langle n'_B| . \quad (70)$$

Using this definition and bases, and “tracing out” or “tracing over” space B,<sup>16</sup> gives

$$\hat{\rho}_A = \text{Tr}_B \hat{\rho}_{AB} = \sum_{n_A} \lambda_n^2 |n_A\rangle \langle n_A| , \quad (71)$$

with an analogous expression for  $\hat{\rho}_B$ ,

$$\hat{\rho}_B = \text{Tr}_A \hat{\rho}_{AB} = \sum_{n_B} \lambda_n^2 |n_B\rangle \langle n_B| . \quad (72)$$

Therefore, in this basis, the eigenvalues of the density matrices are the same for both spaces (with additional zeros present for asymmetric spaces).

No matter the complexity of the entanglement, if we project to one of the spaces, the reduced density matrix in that space has the same eigenvalues as the reduced density matrix in the other space. This definition does not extend beyond two subsystems (or bipartitions).

---

<sup>16</sup>  $\text{Tr}_B \hat{O} = \sum_k \langle k_B | \hat{O} | k_B \rangle$

#### D. Entanglement Entropy

Entanglement entropy for quantum systems is based upon Shannon Entropy in classical information theory. Imagine an ensemble of bits sent between labs A and B, in which only 0 is transmitted each time. The system is perfectly ordered. As there is no structure or randomness in the signal, no information can be transmitted. In contrast, signals that contain both 0 and 1 can carry (meaningful!) information.

A pure state is one in which only one independent state, entangled among subsystems or not, defines an ensemble. As there is a basis (in the full system) in which the outcome of a measurement is unique and identical for each element in the ensemble, no information can be conveyed by such measurements on the full system. The system is perfectly ordered. Thus the entanglement entropy of the full system vanishes, by design. For a pure state, the Schmidt decomposition in Eq. (69) indicates that the entanglement entropy in Eq. (73) between any two parts of the system, A and B, can be computed using the reduced density matrix for either A or B, resulting in the same result. The reduced density matrix for each space represents a mixed ensemble, generated by the tracing procedure. For a mixed state, with density matrix  $\rho$ , the Von Neumann (Entanglement) Entropy is defined as

$$S(\hat{\rho}) = -\text{Tr}[\hat{\rho} \log_2 \hat{\rho}] = -\sum_i \omega_i \log_2 \omega_i = -\sum_i p_i \log_2 p_i , \quad (73)$$

where  $\omega_i$  are the eigenvalues of  $\hat{\rho}$  ( $\omega_i = \lambda_i^2$  in the Schmidt decomposition). The act of tracing over degrees of freedom in a given system generally changes a pure (entangled) ensemble into a mixed ensemble.

For a quantum many-body system of interest, the Von Neumann entropy can be considered for any bipartition of interest. It is one numerical quantity that provides a measure of the entanglement between sub-regions of a more complete system (in a pure state). Explicitly, if the state of the full system (pure state) was an unentangled tensor product (classical),  $|\psi_{BA}\rangle = |\psi_A\rangle \otimes |\psi_B\rangle$ , then tracing over B would leave A in a pure state, and vice versa. The entanglement entropy of the reduced density matrix vanishes. Therefore, the larger the value of  $S(\hat{\rho}_A)$ , the more entangled is the AB system. In other words, the more mixed the reduced system is, the larger the entanglement between the regions in the full system.

As an example, consider the pure state of two qubits (which we can distribute to lab-A and lab-B),

$$|\psi\rangle = \frac{7}{10}|00\rangle + \frac{1}{10}|01\rangle + \frac{1}{10}|10\rangle + \frac{7}{10}|11\rangle , \quad (74)$$

The reduced density matrix for region A is,<sup>17</sup>

$$\begin{aligned} \hat{\rho}_A &= \text{Tr}_B[|\psi\rangle\langle\psi|] = \left(\frac{7}{10}|0\rangle + \frac{1}{10}|1\rangle\right)\left(\frac{7}{10}\langle 0| + \frac{1}{10}\langle 1|\right) + \left(\frac{1}{10}|0\rangle + \frac{7}{10}|1\rangle\right)\left(\frac{1}{10}\langle 0| + \frac{7}{10}\langle 1|\right) \\ &= \frac{1}{50} \begin{pmatrix} 25 & 7 \\ 7 & 25 \end{pmatrix} = \frac{1}{2} \left( \hat{I} + \frac{7}{25} \hat{X} \right) , \end{aligned} \quad (75)$$

which is the density matrix associated with a two-species mixed state, each appearing with equal probability, with wavefunctions

$$|\phi_1\rangle = \frac{1}{\sqrt{50}} [7|0\rangle + |1\rangle] , \quad |\phi_2\rangle = \frac{1}{\sqrt{50}} [|0\rangle + 7|1\rangle] . \quad (76)$$

---

<sup>17</sup>  $\text{Tr}_B[|\psi\rangle\langle\psi|] = {}_B\langle 0|\psi\rangle\langle\psi|0\rangle_B + {}_B\langle 1|\psi\rangle\langle\psi|1\rangle_B$ .

The associated entanglement entropy of region A is  $S(\hat{\rho}_A) = 0.942$  (from eigenvalues of  $\hat{\rho}_A$  of 0.64 and 0.36, satisfying  $\text{Tr}\hat{\rho} = 1$ ), while the maximal possible value is 1 obtained when the eigenvectors of  $\hat{\rho}_A$  have eigenvalues of  $p = 1/2$ . Therefore, the AB system is nearly maximally entangled between A and B.

### E. Rényi Entropy

The Rényi Entropy is a generalization of the Von Neumann entropy that we have just discussed,

$$H_r(\hat{\rho}) = \frac{1}{1-r} \log_2 \left( \sum_j p_j^r \right) . \quad (77)$$

This is useful in some applications and areas, we will not be making much use of it in this course. It also becomes the Von Neumann entropy in the limit  $r \rightarrow 1$ .<sup>18</sup>

### F. Distillable Entanglement

There are different “types” of entanglement. Some entanglement within a system, or subsystem, may be convertible into entangled Bell pairs (of photons), but this is not assured, and this leads to the concept of bound entanglement and distillable entanglement. Just like bound state particles have negative energy and are localized in space, there are systems in which more entanglement is required in their formation than can be converted into Bell-pairs of photons. These are important aspects of quantum many-body systems. Distillable entanglement can be moved around within an ensemble to form a reduced number of highly entangled states, such as Bell pairs. We can think of an ensemble comprised of a large number of photons entangled between beams A and B (heading in different directions), and it has been known for a long time now that protocols exist involving operations on a number N pairs of the ensemble, to produce K pairs that are more entangled. That is to say that one can start with a mixed-state of photons that do not violate Bells inequalities, perform operations on the ensemble, and form a reduced ensemble of pure states that violate Bells inequalities.

As an example, consider an initial density matrix corresponding to the Werner state in Eq. (67). The fidelity of this initial state is defined by

$$F = \langle \Phi_1 | \hat{\rho}_{AB} | \Phi_1 \rangle = \frac{1}{4} (1 + 3p) . \quad (78)$$

Recall that for  $p \leq 1/3$  the state was separable, which means in this case the ensemble cannot be distinguished from a classical one. Thus, distillation of entanglement is not possible. However, for  $p > 1/3$  it is. The BBPSSW protocol [44] is such that lab-A takes two qubits from the ensemble, and lab-B takes the two corresponding qubits it has. Each acts with a CNOT-gate controlled on their first qubit targeted on their second qubit. The second qubit is measured in both labs. They then talk on the phone - classical communication - and keep the first qubit if the measurements are 00 or 11, and discard if 01 or 10. The probability of success and the post distillation fidelity are:

$$p_{\text{success}} = F^2 + \frac{2}{3}F(1-F) + \frac{5}{9}(1-F)^2 , \quad F_{\text{out}} = \frac{F^2 + \frac{1}{9}(1-F)^2}{F^2 + \frac{2}{3}F(1-F) + \frac{5}{9}(1-F)^2} . \quad (79)$$

---

<sup>18</sup>  $r = 1 - \epsilon$ ,  $\sum_j p_j^r = \sum_j p_j p_j^{-\epsilon} = \sum_j p_j e^{-\epsilon \log p_j} = \sum_j p_j - \epsilon p_j \log p_j = 1 - \epsilon \sum_j p_j \log p_j$ .

Figure 15 shows the outcome of the BBPSSW acting on the Werner state with probability  $p$ .

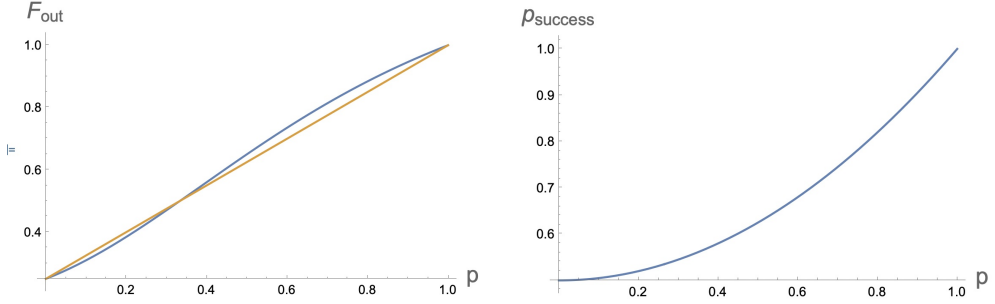


FIG. 15: The fidelity of the density matrix after BBPSSW distillation (left panel), and the probability of success in each two-qubit selection process.

Initial states that do not have the form of the Werner state can be Pauli-twirled into such a form.

The Entanglement of Distillation,  $D(\rho_{AB})$  is the maximum fraction of singlets that can be extracted – distilled from  $n$  copies of  $\rho_{AB}$  by CLOCC(Collective Local Operations Classical Communications). This is analogous to the Free-energy of a system, and is sometimes called the Free Entanglement. The process of distillation is irreversible, as  $N$  elements of the ensemble are required to produce  $K$  Bell pairs.

We will discuss later the entanglement required to produce an ensemble, the entanglement of formation,  $E_f(\hat{\rho}_{AB})$ , and as such the difference between this and the distillable entanglement is called Bound Entanglement (as it cannot be converted into free entanglement).

## G. Concurrence

Consider a 2-qubit spin system, with a general wavefunction of the form

$$|\psi_{AB}\rangle = \alpha|00\rangle + \beta|01\rangle + \gamma|10\rangle + \delta|11\rangle . \quad (80)$$

The concurrence [45] of this state is defined as

$$C(|\psi_{AB}\rangle) = |\langle\psi_{AB}|\hat{Y}^{\otimes 2}|\psi_{AB}\rangle^*| = 2|\alpha\delta - \beta\gamma| , \quad (81)$$

and we generically define the state  $|\tilde{\psi}_{AB}\rangle = \hat{Y}^{\otimes 2}|\psi_{AB}\rangle^*$  (alternately,  $\rho \rightarrow \hat{Y}^{\otimes 2}\rho\hat{Y}^{\otimes 2}$ ).

We can recall the logic we developed for utility of the entanglement entropy of the reduced density matrix, i.e. a tensor-product state leaves a pure density matrix upon tracing over one of the bipartitions. It can be shown that

$$C(|\psi_{AB}\rangle) = \sqrt{2(1 - \text{Tr}\hat{\rho}_A^2)} , \quad (82)$$

where  $\hat{\rho}_A$  is the reduced density matrix for A.<sup>19</sup> Analogous to the entanglement entropy, if the reduced density matrix of A corresponds to a pure state, then  $\text{Tr}\hat{\rho}_A^2 = 1$  and  $C(|\psi_{AB}\rangle) = 0$ . Therefore,  $C(|\psi_{AB}\rangle)$  provides a measure of the entanglement between A and B. This is a different measure than entanglement entropy,  $-\text{Tr}\hat{\rho}_A \log_2 \hat{\rho}_A$ .

<sup>19</sup> For the sake of manipulation  $1 \rightarrow (|\alpha|^2 + |\beta|^2 + |\gamma|^2 + |\delta|^2)^2$ .

A less obvious construction for the concurrence is in terms of the eigenvalues of  $\hat{\rho}_{AB}$ ,

$$C(|\psi_{AB}\rangle) = \text{Max}(0, \lambda_1 - \lambda_2 - \lambda_3 - \lambda_4) , \quad (83)$$

where  $\lambda_i$  are the square roots of the eigenvalues of  $\rho_{AB}\tilde{\rho}_{AB}$ , and where  $\lambda_1 \geq \lambda_2 \geq \lambda_3 \geq \lambda_4$ .

Interestingly, and we will return to this shortly, the negativity,  $\mathcal{N}(\rho_{AB})$  (the upper limit to distillable entanglement) is bounded above by the concurrence,  $\mathcal{N}(\rho_{AB}) \leq C(\rho_{AB})$ .

For a general mixed state of 2 qubits, the entanglement of formation,  $E_f(\rho_{AB})$ , is directly related to  $C = C(|\psi_{AB}\rangle)$  by [45, 46],

$$E_f(\rho_{AB}) = h\left(\frac{1 + \sqrt{1 - C^2}}{2}\right) , \quad h(x) = -x \log_2 x - (1 - x) \log_2(1 - x) . \quad (84)$$

### H. Partial Transpose and Negativity

The partial transpose of a system's density matrix with respect to a subsystem is another useful entanglement measure to consider, i.e., the initial and final states of a subsystem are being exchanged. In the setting of quantum field theory, this corresponds to time-reversing parts of the system. A partial transpose (PT) with respect to system B is denoted by

$$\hat{\rho}_{AB} \rightarrow \hat{\rho}_{AB}^{\Gamma_B} , \quad \langle i_A, j_B | \hat{\rho}_{AB}^{\Gamma_B} | k_A, l_B \rangle = \langle i_A, l_B | \hat{\rho}_{AB} | k_A, j_B \rangle . \quad (85)$$

While the eigenvalues of  $\hat{\rho}_{AB}$  are positive definite quantities, bounded by unity, as they correspond to coefficients in a spectral decomposition, the sum of eigenvalues of  $\hat{\rho}_{AB}^{\Gamma_B}$  remains unity (time reversal is an anti-unitary operation invariant under tracing), the eigenvalues themselves can be negative. For the same reasons discussed above, a tensor-product state is invariant under PT, and therefore remains positive definite.

The negativity is defined to be the sum of the negative eigenvalues under PT,

$$\mathcal{N}(\hat{\rho}_{AB}) = \sum_i |\omega_i| \theta(-\omega_i) = \sum_j^{negatives} |\omega_j| , \quad (86)$$

where the  $\omega_i$ 's are the eigenvalues of  $\hat{\rho}_{AB}^{\Gamma_B}$ . The negativity can also be written as a 1-norm,

$$\begin{aligned} \mathcal{N}(\hat{\rho}_{AB}) &= \frac{1}{2} \left( \|\hat{\rho}_{AB}^{\Gamma_B}\|_1 - 1 \right) = \frac{1}{2} \left( \sum_i |\omega_i| - 1 \right) \\ &= \frac{1}{2} \left( \sum_i \omega_i + 2 \sum_i |\omega_i| \theta(-\omega_i) - 1 \right) = \sum_i |\omega_i| \theta(-\omega_i) . \end{aligned} \quad (87)$$

Consider a Bell state

$$|\psi\rangle = \frac{1}{\sqrt{2}} [ |00\rangle + |11\rangle ] , \quad \hat{\rho} = \frac{1}{2} [ |00\rangle\langle 00| + |00\rangle\langle 11| + |11\rangle\langle 00| + |11\rangle\langle 11| ] , \quad (88)$$

which has eigenvalues or 1, 0, 0, 0 as it is a pure state. PT on the state with respect to system B gives

$$\hat{\rho}^{\Gamma_B} = \frac{1}{2} [ |00\rangle\langle 00| + |01\rangle\langle 10| + |10\rangle\langle 01| + |11\rangle\langle 11| ] , \quad (89)$$

which has eigenvalues  $-\frac{1}{2}, \frac{1}{2}, \frac{1}{2}, \frac{1}{2}$ , and hence negativity,  $\mathcal{N} = \frac{1}{2}$ .

The log-negativity,  $E_{\mathcal{N}}(\rho_{AB})$  is perhaps more useful because it is an additive quantity, i.e. the log-negativity is additive for tensor-product states,

$$E_{\mathcal{N}}(\rho_{AB}) = \log_2 \|\hat{\rho}_{AB}^{\Gamma_B}\|_1 = \log_2 (2\mathcal{N} + 1) . \quad (90)$$

**This quantity can be shown to provide an upper bound to the distillable entanglement.**

The negativity and log-negativity vanish for a system that is PPT (positive PT), but that does not imply separability because of bound entanglement. If the system is NPT, then it is not separable (as one cannot have negative eigenvalues from the tensor product of density matrices).

**PPT is a necessary but not sufficient condition for separability.** However, in the special cases of **qubit-qubit** and **qubit-qutrit** two-body systems, PPT has been shown to be necessary and sufficient for separability.

## I. N-Tangle

Entanglement in quantum many-body systems extends beyond two-body entanglement, as we have seen, and therefore measures of multi-body entanglement are also important. As a generalization of concurrence, for an N-qubit system, with N-even, the **N-tangle** is defined to be

$$\tau_N(|\psi\rangle) = |\langle\psi|\tilde{\psi}\rangle|^2 , \quad |\tilde{\psi}\rangle = \hat{Y}^{\otimes N} |\psi\rangle^* . \quad (91)$$

Extending this definition, the **n-tangle** of a N-body systems can be defined as

$$\tau_n(|\psi\rangle) = |\langle\psi|\tilde{\psi}\rangle|^2 , \quad |\tilde{\psi}\rangle = \hat{Y}_{i_1} \hat{Y}_{i_2} \dots \hat{Y}_{i_n} |\psi\rangle^* , \quad (92)$$

where the  $i_1, i_2, \dots, i_n$  define the bodies in the N-body system that have been selected. For example, the 4-qubit GHZ state is invariant under  $\hat{Y}^{\otimes 4}$ , and therefore has 4-tangle of  $\tau_4 = 1$ . Interestingly, its  $\tau_3 = \tau_2 = 0$ , so while it has 4-body entanglement, it does not have 3-body or 2-body entanglement.

Consider a 3-body system, A B C. We define the 2-tangle between any two systems by tracing over the third and then forming the 2-tangle, which reduces to the square of the concurrence between the two in the reduced system. For the 3-body system, the average 2-tangle is defined to be  $\langle\tau_2\rangle = (C_{AB}^2 + C_{BC}^2 + C_{AC}^2)/3$ . We define the bipartite entanglement between A and BC, and the associated 3-tangle, by

$$C_{A(BC)} = \sqrt{2(1 - \text{Tr}\rho_A^2)} , \quad \tau_3 = C_{A(BC)}^2 - C_{AB}^2 - C_{AC}^2 . \quad (93)$$

## J. Entanglement Witness

This is to add to our vocabulary .... an **Entanglement Witness** is a Hermitian operator (observable) that is + for every separable state, but - for some entangled states.

## IV. LATTICE SCALAR FIELD THEORY AND QUANTUM SIMULATION

Let us now begin our journey toward the quantum simulation of quantum fields. We are in the enviable situation of knowing a lot about quantum field theory, the convenient language that we use to describe the fundamental forces of nature. Great progress has been made in analytic and numerical studies of quantum fields in order to make predictions to compare with experiment. From your QFT courses, you know that QFT represents one of the most significant advances in

fundamental physics, the unification of special relativity and quantum mechanics, and as such, is necessarily the language and framework of quantum information, and all of the associated theoretical developments. So far, we have not considered the finite speed of light in any of our discussions.

I do not wish to reproduce or demonstrate results you have already seen in your QFT courses, but will start quite quickly into the lattice field theory framework, which is directly applicable to quantum simulation. Furthermore, it remains the only formal framework with which to formulate quantum field theory non-perturbatively. A great deal can be learned from the study of scalar field theory, just as we do from perturbative QFT. It is also the quantum field theory that has been studied extensively in QIS, and provides the only example of which a “beginning to end” analysis has been performed for quantum simulation and complexity classes, by Jordan, Lee and Preskill [2, 47, 48]. Remarkably, they have shown that interacting scalar field theory ( $\lambda\phi^4$ ) is **BQP-complete**. That is to say that any problem that resides in **BQP**<sup>20</sup> can be mapped with polynomial quantum resources to computations in  $\lambda\phi^4$ , and in particular the S-matrix in the presence of classical sources. Therefore, studying the quantum simulation of quantum field theories, while having a particular target of Standard Model physics, is also a study, in this case, of methodology that can address all systems that are efficiently simulatable with quantum computers.

The most general Lagrange density describing one real scalar field that is renormalizable in 3+1 dimensions is,

$$\mathcal{L} = \frac{1}{2}\partial_\mu\phi\partial^\mu\phi - \frac{1}{2}m^2\phi^2 - \frac{\lambda}{4!}\phi^4 = T - V , \quad (94)$$

where the field  $\phi$ , mass  $m$  and coupling  $\lambda$  are all bare parameters that dictate all of the S-matrix of scalar field theory (including renormalization). No further parameters are required to absorb divergences from quantum fluctuations. The generating functional from which all n-point correlation functions within the theory can be derived is,

$$Z[J] = \frac{\int \mathcal{D}\phi e^{i\int d^n x \mathcal{L} + J(x)\phi(x)}}{\int \mathcal{D}\phi e^{i\int d^n x \mathcal{L}}} , \quad (95)$$

and, for example, the vacuum k-point correlation functions are defined via,

$$\begin{aligned} G_k(x_1, \dots, x_k) &= \langle \Omega | \hat{T}[\phi(x_1) \dots \phi(x_k)] | \Omega \rangle = \frac{\int \mathcal{D}\phi e^{i\int d^n x \mathcal{L}} \phi(x_1) \dots \phi(x_k)}{\int \mathcal{D}\phi e^{i\int d^n x \mathcal{L}}} \\ &= (-i)^k \frac{\delta^k Z[J]}{\delta J(x_1) \dots \delta J(x_k)} . \end{aligned} \quad (96)$$

As quantum computers perform unitary operations on states, the natural framework for such systems is Hamiltonian dynamics and the wavefunctions of QFTs. Most undergraduate and graduate courses in QFT are designed to address physics that is amenable to perturbation theory, and are oriented toward the foundations of the Standard Model of particle physics, which is one of the remarkable accomplishments of 20<sup>th</sup> Century physics. This is captured by the Lagrange formulation of the path integral, which is particularly convenient for non-Abelian gauge theories. As a result, less attention has been paid to Hamiltonian dynamics of QFTs.

The Hamiltonian density for one real scalar field, corresponding to the Lagrange density given in Eq. (94), is

$$\mathcal{H} = \frac{1}{2}\hat{\Pi}^2 + \frac{1}{2}|\nabla\hat{\phi}|^2 + \frac{1}{2}m^2\hat{\phi}^2 + \frac{\lambda}{4!}\hat{\phi}^4 = \hat{T} + \hat{V} , \quad (97)$$

---

<sup>20</sup> Bounded polynomially-scaling quantum resources: problems that can be simulated with a bounded error  $\epsilon$  with polynomial-scaling quantum resources.

which actually provides the starting point for deriving the path integral for Lagrangian formulation. The "new" element here is the conjugate momentum,  $\hat{\Pi}$ , the conjugate momentum to the field  $\hat{\phi}$ , with an equal-time commutation relation,

$$\left[ \hat{\phi}(\mathbf{x}), \hat{\Pi}(\mathbf{y}) \right] = i\hbar\delta^3(\mathbf{x} - \mathbf{y}) , \quad (98)$$

which is to be thought of the same ways as  $[\hat{x}, \hat{p}] = i\hbar$  in non-relativistic quantum mechanics. For everything that follows, we will work with  $\hbar = 1$ . It is easy to conclude, generalizing to functions in the  $|\phi\rangle$  basis, that

$$\hat{\Pi}(\mathbf{x}) = -i\hbar\frac{\delta}{\delta\phi(\mathbf{x})} , \quad (99)$$

For simulations of this and all field theory, we need to work with a finite system that can be accommodated with our classical or quantum computer, and thus is not exactly what we want to simulate in nature. However, if we do things correctly, the numerical evaluations will be perturbatively close to what we actually want, that we can use our understanding of QFT to perform extrapolations and interpolations to make reliable predictions. For example, it is known, that using a hyper-cubic spacetime lattice grid on which to define the fields, is such a construction that leads to continuum limit and infinite volume results in a controllable way, with reliable error estimation. For classical simulations, this has been studied in detail, and for quantum simulations it is the pioneering works of Jordan, Lee and Preskill [2, 47, 48] that have accomplished the heroic task of a complete quantification of systematic errors in quantum simulation. Working with a finite grid of points in the x,y,z directions, separated by a distance  $a$  in all directions (isotropic lattice), the corresponding lattice Hamiltonian in  $n = d + 1$  dimensions is,<sup>21</sup>

$$H^{\text{latt.}} = a^d \sum_{\mathbf{x}} \frac{1}{2}\hat{\Pi}^2 - \frac{1}{2}\hat{\phi}\nabla^2\hat{\phi} + \frac{1}{2}m_0^2\hat{\phi}^2 + \frac{\lambda_0}{4!}\hat{\phi}^4 , \quad (100)$$

and the simplest definition of the  $\nabla^2\phi$  is through the simplest finite-difference operator, defined by appealing to the continuum limit of a function

$$\begin{aligned} \phi(x+y) &= \phi(x) + y_j\nabla_j\phi(x) + \frac{1}{2}y_jy_k\nabla_j\nabla_k\phi(x) + \dots \\ \phi(x-a) &= \phi(x) - a\nabla_x\phi(x) + \frac{1}{2}a^2\nabla_x^2\phi(x) + \dots \\ \phi(x+a) &= \phi(x) + a\nabla_x\phi(x) + \frac{1}{2}a^2\nabla_x^2\phi(x) + \dots \\ \phi(x+a) + \phi(x-a) - 2\phi(x) &= a^2\nabla_x^2\phi(x) + \dots , \end{aligned} \quad (101)$$

which recovers the correct Laplacian in the continuum limit. Therefore,

$$\begin{aligned} H^{\text{latt.}} &= a^d \sum_{\mathbf{x}} \left( \frac{1}{2}\hat{\Pi}^2 - \frac{1}{2a^2}\hat{\phi}(x) \sum_j^d (\hat{\phi}(x + \boldsymbol{\mu}_j) + \hat{\phi}(x - \boldsymbol{\mu}_j)) + \frac{1}{2} \left( m_0^2 + \frac{2d}{a^2} \right) \hat{\phi}^2 \right. \\ &\quad \left. + \frac{\lambda_0}{4!}\hat{\phi}^4 \right) . \end{aligned} \quad (102)$$

The parameters in the Hamiltonian density that are entered into any simulation code (bare lattice parameters), for running on classical or quantum computers, are *apriori* unknown, and are fit to

---

<sup>21</sup> We have used the vanishing of surface terms to write  $|\nabla\hat{\phi}|^2 = -\phi\nabla^2\phi$ .

at least two independent experimental results, such as the mass of the physical scalar particle and the  $\phi\phi \rightarrow \phi\phi$  scattering cross section.<sup>22</sup> After rescaling fields and couplings, the lattice spacing can be set equal to unity.

### A. One Lattice Site

Consider non-interacting scalar field theory at one lattice site, with the Hamiltonian density from Eqs. (100) and (102) of,

$$H_1 = \frac{1}{2}\hat{\Pi}^2 + \frac{1}{2}m^2\hat{\phi}^2 , \quad (103)$$

which we identify with the 1-dim harmonic oscillator (HO) with

$$\begin{aligned} \hat{\phi} &= \frac{1}{\sqrt{2m}}(\hat{a} + \hat{a}^\dagger) , \quad \hat{\Pi} = -i\sqrt{\frac{m}{2}}(\hat{a} - \hat{a}^\dagger) \\ [\hat{\phi}, \hat{\Pi}] &= +i[\hat{a}, \hat{a}^\dagger] = i , \\ H_1 &= m\left(\hat{a}^\dagger\hat{a} + \frac{1}{2}\right) . \end{aligned} \quad (104)$$

The quanta in the field have fixed energy,  $\omega = m$  (with units restored becomes  $\hbar\omega = mc^2$ ) , and we can add as many quanta as we like as the system is bosonic. The states of the field at this one site are defined by occupation numbers,  $|n\rangle$  with the usual ladder operations,  $a^\dagger|n\rangle = \sqrt{n+1}|n+1\rangle$  and  $a|n\rangle = \sqrt{n}|n-1\rangle$ , and the field wavefunction is

$$\langle\phi|n\rangle = \psi_n(\phi) = \frac{1}{\sqrt{2^n n!}}\left(\frac{m}{\pi}\right)^{1/4} e^{-\frac{1}{2}m\phi^2} H_n(\sqrt{m}\phi) , \quad (105)$$

with energy  $E_n = (n + \frac{1}{2})m$ , and  $H_n(x)$  are the Hermite polynomials. One sees, as expected, that the field is fluctuating around zero with a variance that depends on the number of quanta,  $\langle\phi^2\rangle = n + \frac{1}{2}$ .

Beyond a single lattice site, boundary conditions (BC) must be specified in order to be able to define derivatives. The most common BC is periodic boundary conditions (PBC), such that  $\phi(x=L) = \phi(x=0)$ . This is a choice, but any choice that displays the correct infinite volume limit is legitimate.

### B. Two Lattice Sites

For two lattice sites with PBCs, from Eqs. (100) and (102), the Hamiltonian is

$$\hat{H}_2 = \frac{1}{2}\hat{\Pi}_1^2 + \frac{1}{2}\hat{\Pi}_2^2 + \frac{1}{2}m^2\hat{\phi}_1^2 + \frac{1}{2}m^2\hat{\phi}_2^2 + (\hat{\phi}_1 - \hat{\phi}_2)^2 , \quad (106)$$

where

$$\begin{aligned} -\frac{1}{2}\sum \hat{\phi}_j(\hat{\phi}_{j+1} + \hat{\phi}_{j-1} - 2\hat{\phi}_j) &= -\frac{1}{2}\left(\hat{\phi}_1(\hat{\phi}_0 + \hat{\phi}_2 - 2\hat{\phi}_1) + \hat{\phi}_2(\hat{\phi}_1 + \hat{\phi}_3 - 2\hat{\phi}_2)\right) \\ &= -\frac{1}{2}\left(\hat{\phi}_1(\hat{\phi}_2 + \hat{\phi}_0 - 2\hat{\phi}_1) + \hat{\phi}_2(\hat{\phi}_1 + \hat{\phi}_3 - 2\hat{\phi}_2)\right) \\ &= +(\hat{\phi}_1 - \hat{\phi}_2)^2 , \end{aligned} \quad (107)$$

---

<sup>22</sup> This tuning procedure introduce systematic errors set by the lattice spacing. The results of simulations are performed at a fixed lattice spacing, while the observables that the bare couplings are tuned to, experimental observables, are only known in the continuum.

as  $\hat{\phi}_0 \rightarrow \hat{\phi}_2$  and  $\hat{\phi}_3 \rightarrow \hat{\phi}_1$  for PBCs. Redefining the fields into linear combinations

$$\hat{\chi}_1 = \frac{1}{\sqrt{2}} (\hat{\phi}_1 + \hat{\phi}_2) , \quad \hat{\chi}_2 = \frac{1}{\sqrt{2}} (\hat{\phi}_1 - \hat{\phi}_2) , \quad (108)$$

which trivially transforms the conjugate momentum operators, decouples the system into

$$\hat{H}_2 = \frac{1}{2} \hat{\Pi}_{\chi_1}^2 + \frac{1}{2} \hat{\Pi}_{\chi_2}^2 + \frac{1}{2} m^2 \hat{\chi}_1^2 + \frac{1}{2} (m^2 + 4) \hat{\chi}_2^2 , \quad (109)$$

providing a tensor product basis set  $|n_{\chi_1}\rangle \otimes |n_{\chi_2}\rangle$ , with energies  $\omega_i = \{m, \sqrt{m^2 + 4}\}$ . Interestingly (at this point), when written in terms of the two allowed momenta of the two site system,  $k = 0, \pi$ , these energies correspond to <sup>23</sup>

$$\omega_1 = \sqrt{m^2 + 0} , \quad \omega_2 = \sqrt{m^2 + 4 \sin^2 \frac{\pi}{2}} . \quad (110)$$

The ground state for the two-site system is  $|0\rangle \otimes |0\rangle$ , and its inner product providing the  $\phi$ -space wavefunction is, from Eq. (105) (with  $m \rightarrow \omega$ ),

$$\begin{aligned} \psi_{\text{GS}}(\phi_1, \phi_2) &= \langle \phi_1, \phi_2 | (|0\rangle_{\chi_1} \otimes |0\rangle_{\chi_2}) = \left( \frac{m\sqrt{m^2 + 4}}{\pi^2} \right)^{1/4} e^{-\frac{1}{4}m(\phi_1 + \phi_2)^2 - \frac{1}{4}\sqrt{m^2 + 4}(\phi_1 - \phi_2)^2} \\ &= \left( \frac{m\sqrt{m^2 + 4}}{\pi^2} \right)^{1/4} e^{-\frac{1}{2}\Phi^T K \Phi} , \\ \Phi &= \begin{pmatrix} \phi_1 \\ \phi_2 \end{pmatrix} , \quad K = \frac{1}{2} \begin{pmatrix} m + \sqrt{m^2 + 4} & m - \sqrt{m^2 + 4} \\ m - \sqrt{m^2 + 4} & m + \sqrt{m^2 + 4} \end{pmatrix} , \end{aligned} \quad (111)$$

where the fields have been brought together into a vector, and the argument of the exponential is not the contraction of the field vectors and a  $2 \times 2$  matrix,  $K$ . This generalizes straightforwardly to systems with multiple lattice sites. To understand the entanglement in the quantum vacuum state between the fields at the sites,

$$|\psi_{\text{GS}}\rangle = \int d\phi_1 d\phi_2 |\phi_1, \phi_2\rangle \psi_{\text{GS}}(\phi_1, \phi_2) , \quad (112)$$

for which it is clear that is more than a single tensor-product state in field space contributing. This should be contrasted with the vanishing entanglement between the  $\chi_{1,2}$  fields (in the same state, defined by vanishing mode occupation numbers, but in terms of different variables) in momentum space, i.e., the momentum-space modes are unentangled while field-space modes are entangled.

---

<sup>23</sup> To make a direct connection to momentum space, the momentum eigenfunctions in this lattice with PBCs are of the form  $\frac{1}{\sqrt{2}} e^{ikx}$ , with sites  $x = 0, 1$ . Inserting explicit values of  $k = 0, \pi$  gives:  $\frac{1}{\sqrt{2}} (\phi(0) + \phi(1))$  for  $k = 0$  and  $\frac{1}{\sqrt{2}} (\phi(0) - \phi(1))$  for  $k = \pi$ . The energy of such a state with momentum  $k$  is  $\sqrt{m^2 + 4 \sin^2 \frac{k}{2}}$ .

### C. Four Lattice Sites

It now seems straightforward to extend this discussion to four spatial lattice sites. The Hamiltonian in Eqs. (100) and (102) becomes,

$$\begin{aligned}
H_4 &= \sum_j^4 \frac{1}{2} \left( \hat{\Pi}_j^2 + m^2 \hat{\phi}_j^2 \right) - \frac{1}{2} \phi_j (\phi_{j+1} + \phi_{j-1} - 2\phi_j) \\
&= \frac{1}{2} \sum_j^4 \hat{\Pi}_j^2 \\
&\quad + \frac{1}{2} m^2 \frac{1}{4} (\phi_1 + \phi_2 + \phi_3 + \phi_4)^2 + \frac{1}{2} (m^2 + 2) \frac{1}{2} (\phi_1 - \phi_3)^2 \\
&\quad + \frac{1}{2} (m^2 + 2) \frac{1}{2} (\phi_2 - \phi_4)^2 + \frac{1}{2} (m^2 + 4) \frac{1}{4} (\phi_1 - \phi_2 + \phi_3 - \phi_4)^2 \\
&= \frac{1}{2} \sum_j^4 \hat{\Pi}_j^2 \\
&\quad + \frac{1}{2} (m^2 + 4 \sin^2 \frac{0}{2}) \frac{1}{4} (\phi_1 + \phi_2 + \phi_3 + \phi_4)^2 + \frac{1}{2} (m^2 + 4 \sin^2 \frac{\pi}{4}) \frac{1}{2} (\phi_1 - \phi_3)^2 \\
&\quad + \frac{1}{2} (m^2 + 4 \sin^2 \frac{\pi}{4}) \frac{1}{2} (\phi_2 - \phi_4)^2 + \frac{1}{2} (m^2 + 4 \sin^2 \frac{\pi}{2}) \frac{1}{4} (\phi_1 - \phi_2 + \phi_3 - \phi_4)^2 , \quad (113)
\end{aligned}$$

corresponding to (linear combinations of) states with momenta  $k = 0, \pm \frac{\pi}{4}, \pm \frac{\pi}{2}$ . Written in terms of Fourier transforms,

$$\begin{pmatrix} \chi_1 \\ \chi_2 \\ \chi_3 \\ \chi_4 \end{pmatrix} = \frac{1}{2} \begin{pmatrix} 1 & 1 & 1 & 1 \\ 1 & i & -1 & -i \\ 1 & -i & -1 & +i \\ 1 & -1 & 1 & -1 \end{pmatrix} \begin{pmatrix} \phi_1 \\ \phi_2 \\ \phi_3 \\ \phi_4 \end{pmatrix} , \quad (114)$$

with eigenenergies

$$m, \sqrt{m^2 + 4 \sin^2 \frac{\pi}{4}}, \sqrt{m^2 + 4 \sin^2 \frac{\pi}{4}}, \sqrt{m^2 + 4 \sin^2 \frac{\pi}{2}} = m, \sqrt{m^2 + 2}, \sqrt{m^2 + 2}, \sqrt{m^2 + 4} \quad (115)$$

The wavefunction has the expected form

$$\begin{aligned}
\psi_{\text{GS}}(\phi_1, \phi_2, \phi_3, \phi_4) &\sim e^{-\frac{1}{2} \Phi^T K \Phi} \\
K &= \begin{pmatrix} K_0 & K_1 & K_2 & K_3 \\ K_1 & K_0 & K_1 & K_2 \\ K_2 & K_1 & K_0 & K_1 \\ K_3 & K_2 & K_1 & K_0 \end{pmatrix} \\
K_0 &= \frac{1}{4} \left( m + 2\sqrt{m^2 + 2} + \sqrt{m^2 + 4} \right) \rightarrow m , \quad K_1 = K_3 = \frac{1}{4} \left( m - \sqrt{m^2 + 4} \right) \rightarrow -\frac{1}{2m} \\
K_2 &= \frac{1}{4} \left( m - 2\sqrt{m^2 + 2} + \sqrt{m^2 + 4} \right) \rightarrow -\frac{1}{4m^3} . \quad (116)
\end{aligned}$$

#### D. Arbitrary Number of Lattice Sites

Labeling the spatial sites from  $n = 0, 1, \dots, L - 1$ , for a total of  $L$ -sites, we found that the non-interacting 1-dim Hamiltonian takes the form

$$H_L = \sum_{j=0}^{L-1} \frac{1}{2} \left( \hat{\Pi}_j^2 + m^2 \hat{\phi}_j^2 \right) - \frac{1}{2} \phi_j (\phi_{j+1} + \phi_{j-1} - 2\phi_j) , \quad (117)$$

using the trivial finite-difference operator description for  $\nabla^2 \phi$ . With PBCs imposing the constraint that  $kL = n2\pi$  (where  $n = 0, 1, \dots, L - 1$ ), the discrete momentum and energy associated with this system are

$$\begin{aligned} k &\rightarrow 0, \pm \frac{2\pi}{L}, \pm \frac{4\pi}{L}, \pm \frac{6\pi}{L}, \dots \pm \left( \pi - \frac{2\pi}{L} \right), +\pi \\ E &\rightarrow \sqrt{m^2 + 4 \sin^2 \frac{k}{2}} = m, \sqrt{m^2 + 4 \sin^2 \frac{\pi}{L}}, \sqrt{m^2 + 4 \sin^2 \frac{2\pi}{L}} \dots \sqrt{m^2 + 4} . \end{aligned} \quad (118)$$

The first line of Eq. (118) represents just one way to uniformly ‘sample’ momentum space, and other ways could have been chosen. The relation between the momentum eigenstates,  $\chi_k$  and the position eigenstates  $\phi_j$  is via Fourier transform,

$$\begin{aligned} \chi_k &= \frac{1}{\sqrt{L}} \sum_{j=0}^{L-1} \phi_j e^{-ikj} \\ \chi &= \mathbf{V} \cdot \phi , \quad \mathbf{V} = \frac{1}{\sqrt{L}} e^{-i\mathbf{k} \cdot \mathbf{j}} . \end{aligned} \quad (119)$$

So, for example, for the  $L = 4$  defining the  $\mathbf{E}$  matrix to be the matrix of energy eigenvalues of the finite-difference lattice operator,

$$\begin{aligned} \mathbf{E} &= \text{diag} \left( \sqrt{m^2 + 2}, m, \sqrt{m^2 + 2}, \sqrt{m^2 + 4} \right) , \quad V = \frac{1}{2} \begin{pmatrix} 1 & i & -1 & -i \\ 1 & 1 & 1 & 1 \\ 1 & -i & -1 & i \\ 1 & -1 & 1 & -1 \end{pmatrix} \\ \mathbf{K} &= \mathbf{V}^\dagger \cdot \mathbf{E} \cdot \mathbf{V} , \end{aligned} \quad (120)$$

where we have re-ordered the basis compared to the analysis above.<sup>24</sup> The ground state wavefunction is

$$\begin{aligned} |\psi_{\text{gs}}\rangle &= |\psi_{\chi_0}\rangle_0 \otimes |\psi_{\chi_1}\rangle_0 \otimes |\psi_{\chi_2}\rangle_0 \otimes \dots \otimes |\psi_{\chi_{L-1}}\rangle_0 \\ \langle \chi_0, \chi_1, \dots, \chi_{L-1} | \psi_{\text{gs}} \rangle &= \frac{(\det \mathbf{E})^{1/4}}{\pi^{L/4}} e^{-\frac{1}{2} \chi^T \mathbf{E} \chi} , \\ \langle \phi_0, \phi_1, \dots, \phi_{L-1} | \psi_{\text{gs}} \rangle &= \frac{(\det \mathbf{K})^{1/4}}{\pi^{L/4}} e^{-\frac{1}{2} \phi^T \mathbf{K} \phi} . \end{aligned} \quad (122)$$

---

<sup>24</sup> The ordering we have used is

$$k = -\left(\pi - \frac{2\pi}{L}\right), \dots -\frac{6\pi}{L}, -\frac{4\pi}{L}, -\frac{2\pi}{L}, 0, +\frac{2\pi}{L}, +\frac{4\pi}{L}, +\frac{6\pi}{L}, \dots +\left(\pi - \frac{2\pi}{L}\right), +\pi . \quad (121)$$

To find the 2-point correlation function in the vacuum state, we note that  $\mathbf{K}^{-1} = \mathbf{V}^\dagger \cdot \mathbf{E}^{-1} \cdot \mathbf{V}$  (trivially), and thus

$$\begin{aligned} C_{\alpha\beta} &= \langle \psi_{\text{gs}} | \phi_\alpha \phi_\beta | \psi_{\text{gs}} \rangle = \left[ \frac{1}{2} \mathbf{K}^{-1} \right]_{\alpha\beta} \\ &= \sum_n \frac{(V^\dagger)_{\alpha n} (V)_{n\beta}}{2E_n} = \frac{1}{L} \sum_k \frac{e^{ik(\alpha-\beta)}}{2\sqrt{m^2 + \hat{k}^2}} \\ \hat{k} &= 2 \sin \frac{k}{2} . \end{aligned} \quad (123)$$

In the limit of vanishing lattice spacing and infinite spatial extent,  $L \rightarrow \infty$ , this reduces to the well-known form from scalar field theory,

$$C_{\alpha\beta} \rightarrow \frac{1}{2\pi} K_0(m|\alpha - \beta|) \rightarrow \frac{1}{\sqrt{8\pi}} \frac{e^{-m|\alpha - \beta|}}{\sqrt{m|\alpha - \beta|}} , \quad (124)$$

where  $K_0(mx)$  is a modified Bessel function of the second kind.

During this discussion we have been using a self-consistent construction between the field defined in position space  $\phi(x)$  and in momentum space  $\chi(k)$ , which are related by spatial Fourier transform. We have exploited the fact that we can construct the exact wavefunction for the non-interacting theory by recognizing we can write the Hamiltonian in terms of coupled HOs, that are decoupled in momentum space, and hence the wavefunction is a tensor product in momentum space. However, when considering interactions, by including the  $\lambda\phi^4$  term, the wavefunction no longer decouples into a tensor product, and the momentum modes are all coupled. Even worse than this, the couplings between modes in momentum space are non-local, as can be seen from considering the momentum conserving  $\delta$ -function,  $\delta^3(\mathbf{P}_{\text{tot}} - \sum_j \mathbf{k}_j)$ . In general, in momentum space, we have n-body nonlocal couplings between modes, which puts this formulation into the QMA complexity class, and not efficient for a quantum computer — in the most general sense. Therefore, we must look for a different formulation.

It is interesting at this point to inject some known QIS results. In 2004, after a period of development, the paper: *The Complexity of the Local Hamiltonian Problem*, by Julia Kempe, Alexei Kitaev and Oded Regev, quant-ph/0406180. FSTTCS 2004: Foundations of Software Technology and Theoretical Computer Science, edited by K. Lodaya and M. Mahajan (Springer Berlin Heidelberg, Berlin, Heidelberg, 2005) pp. 372–383, appeared in the arXiv [49, 50]. They showed that a general  $k$ -local Hamiltonian problem for  $k \geq 2$  is QMA-complete. This implies that the resources required to find the ground state of a system with a general 2-qubit (two-body) interaction and larger, scales in such a way to make it generically beyond the capability of quantum computers, even ideal ones. This sounds daunting and possibly a point in which we give up, but one recalls again that the complexity class is for the worst case problem, and in this case includes gapless theories. Interestingly, it also means that any QMA problem can be mapped with polynomial resources to a general 2-local Hamiltonian. From the standpoint of simulating the fundamental forces off Nature, the theories that we have to solve are specific ones, Abelian and. non-Abelian gauge theories constructed from local and global symmetries with specific particle content. So while a general theory with interactions may be beyond the realm of quantum computing at scale, this does not mean that this statement is applicable to simulating Nature's fundamental forces.

### E. Lattice Scalar Field Theory ala Jordan, Lee and Preskill (JLP)

Given what we have learned, let's attempt to reformulate. As we know from field theory, typically, we can work with an operator construction and formulate QFT that way, or we can consider the Feynman construction in the way that he developed the path integral. To do this with registers of qubits or qudits, we must give up on considering a continuous field at each lattice site at the moment, and think about discrete systems only. Recovering the infinite-volume limit in the continuum, within a tolerance  $\epsilon$ , is required to make connection with nature and experiment.<sup>25</sup> Instead of having a continuous real number at each lattice site, there will be a quantum register with a given number of states in the Hilbert space. The JLP construction has  $n_s$  states in the Hilbert space from  $n_Q$  qubits,  $n_s = 2^{n_Q}$ . For a 3-dim spatial lattice with extent  $L = Na$  ( $N$  sites in each direction) and with  $n_Q$  qubits at each site, there are a total of  $N^3 \times n_Q$  qubits.

The JLP papers [2, 47, 48] define the “Gold Standard” for analysis of QFT for quantum simulation. [S. P. Jordan, K. S. M. Lee, and J. Preskill, Quantum Inf. Comput. 14, 1014 \(2014\).](#) [S. P. Jordan, K. S. M. Lee, and J. Preskill, Science 336, 1130 \(2012\).](#) One of the main observations is that, when working in the basis of eigenstates of  $\hat{\phi}$ , only the  $\nabla^2\phi$  term connects adjacent Hilbert spaces and corresponds to a phase because  $\hat{\phi}|\phi\rangle = \phi|\phi\rangle$ . This is nice because the action of the mass operator and  $\lambda\phi^4$  simply produce the value of the field raised to some power,

$$\left( \frac{1}{2}m^2\hat{\phi}^2 + \frac{\lambda}{4!}\hat{\phi}^4 \right) |\phi\rangle = \left( \frac{1}{2}m^2\phi^2 + \frac{\lambda}{4!}\phi^4 \right) |\phi\rangle , \quad (125)$$

and correspond to a constant times the identity operator in field space. Further, they observed that the quantum Fourier transform is efficient, and can be used to evaluate  $\hat{\Pi}^2$  efficiently.

Returning to the 1-site scalar field theory, consider now the digitized version, where the continuous real values of the scalar field are truncated and **digitized** onto a finite dimensional Hilbert space, supported by some qubits or some qudits. The word “digitization” is used to distinguish the impact of mapping to a discrete Hilbert space from the discretization that results from mapping the spacetime continuum to a grid of points. At present, we are only considering the values of the field  $\phi$  at a single lattice site, for example,  $\phi(x = 0)$ . Previously, the value of the field could assume any real number, but now it to only take a range of discrete values from  $-\phi_{\max}$  to  $+\phi_{\max}$ . It is bounded at a minimum and maximum value, that we are free to define in any way we like (subsequently, we will tune these values for optimal convergence), and we have chosen to make it symmetric about zero, to be consistent with the  $\phi \rightarrow -\phi$  symmetry of the Hamiltonian. The value of the field  $\phi$  for any state in the Hilbert space,  $|j\rangle$  for  $j \in [0, n_s - 1]$  is

$$\phi = -\phi_{\max} + j\delta_\phi , \quad \delta_\phi = \frac{2\phi_{\max}}{n_s - 1} , \quad j \in [0, n_s - 1] , \quad (126)$$

where  $\delta_\phi$  is the interval in field space between the states in the Hilbert space. This mapping naturally aligns the field with the states in the Hilbert space in a linear way, symmetric about  $\phi = 0$ .

The next objective is to evaluate the action of the conjugate momentum operator,  $\hat{\Pi}^2$ , specifically matrix elements in field space.<sup>26</sup>

$$\langle \phi' | \hat{\Pi}^2 | \phi \rangle . \quad (127)$$

---

<sup>25</sup> We should keep in mind that there are an arbitrary number of ways to encode a real function onto qubits, and hence an arbitrary number of ways to map scalar field theory to qubits or qudits. We will discuss alternative mappings later.

<sup>26</sup> For the conjugate momentum operator, we must not get confused about what we just learned about momentum-space, although aspects are relevant.

While this does not immediately come to mind, it is worth reminding ourselves of the Nyquist-Shannon sampling theorem. This is best accomplished at a practical level with consideration of a bounded and localized function (in both position and momentum spaces) over some interval, a Gaussian, and we will be interested in expectation values of *nice* functions, e.g.,

$$\begin{aligned} \sum_{\phi} \phi^2 e^{-\alpha\phi^2/2} &= \sum_{j=0}^{n_s-1} (-\phi_{\max} + j\delta_{\phi})^2 e^{-\alpha(-\phi_{\max} + j\delta_{\phi})^2/2} \\ &= \sum_{j=-\infty}^{\infty} (-\phi_{\max} + j\delta_{\phi})^2 e^{-\alpha(-\phi_{\max} + j\delta_{\phi})^2/2} + \mathcal{O}\left(e^{-\alpha\phi_{\max}^2/2}\right) . \end{aligned} \quad (128)$$

Using the *Poisson resummation formula*,

$$\begin{aligned} \sum_{j=-\infty}^{\infty} f(j) &= \int_{-\infty}^{\infty} dx f(x) \sum_{j=-\infty}^{\infty} \delta(x-j) = \int_{-\infty}^{\infty} dx f(x) \sum_{p=-\infty}^{\infty} e^{i2\pi px} \\ &= \int_{-\infty}^{\infty} dx f(x) + \sum_{p \neq 0} \int_{-\infty}^{\infty} dx f(x) e^{i2\pi px} , \end{aligned} \quad (129)$$

and (for the Gaussian)

$$\int dx e^{-\delta^2 \alpha x^2/2} e^{i2\pi px} \sim e^{\frac{-8\pi^2 p^2}{\delta^2 \alpha}} , \quad (130)$$

shows that uniform sampling of a smooth bounded function with finite support, and uniform sampling of the bounded function with finite support in momentum space assure that discrete sums converge faster than polynomial to the continuum value. The  $1/\delta^2$  factor in the argument of the exponential provides the non-polynomial convergence with increasing sampling. Therefore, the estimate of the  $\langle \psi | \phi^2 | \psi \rangle$  from the digitized wavefunction converges to the value from the continuous wavefunction as

$$\sum_{\phi} \phi^2 e^{-\alpha\phi^2/2} \rightarrow \int d\phi \phi^2 e^{-\alpha\phi^2/2} + \mathcal{O}\left(e^{-\alpha\phi_{\max}^2/2}\right) + \mathcal{O}\left(e^{-\frac{8\pi^2}{\delta_{\phi}^2 \alpha}}\right) , \quad (131)$$

which converges faster than any polynomial expansion in  $\delta_{\phi}$ . With the JLP construction, as we will discuss, this result can be achieved in both spaces,  $\phi$  and  $\Pi$ , providing exponential convergence for both types of required matrix elements efficiently. Therefore, the impact of digitization can be rendered negligible compared to the other (well known) systematic errors in using a lattice to simulate a quantum field theory.<sup>27</sup>

The maximum value of the **conjugate momentum** supported in the finite Hilbert space is set by  $\delta_{\phi}$ . Drawing analogy between spatial lattice spacing  $a$ , and field spacing  $\delta_{\phi}$ , the discrete values of momentum in the conjugate space **can be**,

$$\begin{aligned} k_{\max} &= \frac{\pi}{\delta_{\phi}} \\ k_{\phi} &= -\frac{\pi}{\delta_{\phi}} + p \frac{2\pi}{\delta_{\phi} n_s} , \quad p = 1, 2, \dots n_s \\ &= \frac{1}{\delta_{\phi}} \left\{ -\pi + \frac{2\pi}{n_s}, -\pi + \frac{4\pi}{n_s}, \dots, +\pi \right\} , \end{aligned} \quad (132)$$

---

<sup>27</sup> For much of what follows, I have collaborated with Natalie Klco, and some of the results can be found in Ref. [1]. Our efforts were to understand the JLP body of work [2, 47, 48], and to make efforts toward performing simulations with present-day quantum computers, *circa* 2019.

which you will note is asymmetrically distributed in momentum space. For example, for  $n_s = 4$ , the conjugate-momentum states are:  $-\frac{\pi}{2\delta_\phi}, 0, \frac{\pi}{2\delta_\phi}, \frac{\pi}{\delta_\phi}$ . Hence, this choice of momentum modes breaks the symmetry between  $\phi$ -space and  $\Pi$ -space digitization, and also breaks parity-symmetry in  $\Pi$ -space, an undesirable situation that we will return to soon.

The commutation relation  $[\phi, \Pi] = i$ , led us to  $\hat{\Pi} = -i\frac{\delta}{\delta\phi}$  for a continuous field, which under digitization can be replaced by the simplest finite-difference operator

$$\begin{aligned} \hat{\Pi} \rightarrow \hat{\Pi}_{FD} &= -i\frac{1}{\delta_\phi}(\phi_{j+1} - \phi_j) , \quad \hat{\Pi}^2 \rightarrow \hat{\Pi}_{FD}^2 = -\frac{1}{\delta_\phi^2}(\phi_{j+1} + \phi_{j-1} - 2\phi_j) \\ \langle \phi' | \hat{\Pi}_{FD}^2 | \phi \rangle &= \frac{1}{\delta_\phi^2} \begin{pmatrix} 2 & -1 & 0 & 0 & \cdots & -1 \\ -1 & 2 & -1 & 0 & \cdots & 0 \\ 0 & -1 & 2 & -1 & \cdots & 0 \\ \vdots & & & & & \\ -1 & 0 & 0 & \cdots & -1 & 2 \end{pmatrix} = V^\dagger \cdot \hat{P}^2 \cdot V , \\ \hat{P} &= \text{diag}\left(\frac{2}{\delta_\phi} \sin \frac{k_\phi \delta_\phi}{2}\right) , \quad V = \frac{1}{\sqrt{n_s}} e^{-i\mathbf{k}\cdot\mathbf{j}} , \end{aligned} \quad (133)$$

that is constructed explicitly with PBCs in field space (at the single lattice site) in the definition of  $\nabla\phi$  at the edges of field space. This is the analog of momentum-space modes with PBCs at the spatial edges of the lattice.

This is the "natural" construction when working with a finite-difference operator for the discretized field. As with any finite-difference operator, there are associated discretization (digitization in this case) errors. In lattice QCD, with discretization in position space, there are well-studied lattice artifacts, and which naively scale as  $a^n$ . They can, in principle, be systematically removed order-by-order using the Symanzik (improved) action [51, 52] in simulations with additional tunings.

In our situation, as was noted by JLP, we can actually do much (parametrically) better. The point is that the finite-difference operator  $\hat{P}$  does not uniformly sample in momentum space, due to the modification from  $k \rightarrow \frac{2}{\delta_\phi} \sin \frac{k_\phi \delta_\phi}{2}$ . JLP noted that the Quantum Fourier Transform (QFT) is efficient, and means that we can apply any operator we want in  $\hat{\Pi}$ -space as long as the correct commutation relation is recovered in the case  $\delta_\phi \rightarrow 0$  limit. In particular, they noted that using

$$\langle \phi' | \hat{\Pi}_{\text{exact}}^2 | \phi \rangle = V^\dagger \cdot \hat{P}^2 \cdot V \quad \text{with} \quad \hat{P} \rightarrow \text{diag}(k_\phi) , \quad (134)$$

instead of the finite-difference relation, leads to the vanishing of all power-law corrections of the form  $\delta_\phi^n$ , and leaving only exponential corrections to the matrix elements. The matrix remains Toeplitz, but is now dense, as opposed to a limited band structure of the finite-difference operator. For  $n_s = 8$  corresponding to 3 qubits, we find that

$$\langle \phi' | \hat{\Pi}_{\text{exact}}^2 | \phi \rangle = \frac{1}{\delta_\phi^2} \begin{pmatrix} 3.39 & -2.11 & 0.617 & -0.361 & 0.308 & -0.361 & 0.617 & -2.11 \\ -2.11 & 3.39 & -2.11 & 0.617 & -0.361 & 0.308 & -0.361 & 0.617 \\ 0.617 & -2.11 & 3.39 & -2.11 & 0.617 & -0.361 & 0.308 & -0.361 \\ -0.361 & 0.617 & -2.11 & 3.39 & -2.11 & 0.617 & -0.361 & 0.308 \\ 0.308 & -0.361 & 0.617 & -2.11 & 3.39 & -2.11 & 0.617 & -0.361 \\ -0.361 & 0.308 & -0.361 & 0.617 & -2.11 & 3.39 & -2.11 & 0.617 \\ 0.617 & -0.361 & 0.308 & -0.361 & 0.617 & -2.11 & 3.39 & -2.11 \\ -2.11 & 0.617 & -0.361 & 0.308 & -0.361 & 0.617 & -2.11 & 3.39 \end{pmatrix} \quad (135)$$

Now that we realize that we have significant freedom in how we set the problem up in both  $\phi$  and  $\Pi$ -space, let us return to our previous use of PBCs. It turns out that in  $\Pi$ -space, this is

not quite optimal, as the momentum modes are not symmetrically positioned in Fourier-space, breaking a discrete symmetry of the Hamiltonian,  $\hat{\Pi} \rightarrow -\hat{\Pi}$  (in the same way we centered the field  $\phi$  so that the symmetry  $\phi \rightarrow -\phi$  is explicit). Having a mapping that does not respect the symmetries of the Hamiltonian is not a good way to proceed (this is an understatement). This symmetry can be restored by working with a different set of conjugate momentum modes:

$$\begin{aligned} k_{\max} &= \frac{\pi}{\delta_\phi} \\ k_\phi^\Delta &= -\frac{\pi}{\delta_\phi} + \left(p - \frac{1}{2}\right) \frac{2\pi}{\delta_\phi n_s} , \quad p = 1, 2, \dots, n_s \\ &= \frac{1}{\delta_\phi} \left\{ -\pi + \frac{\pi}{n_s}, -\pi + \frac{3\pi}{2n_s}, -\frac{\pi}{n_s}, +\frac{\pi}{n_s}, \dots, +\pi - \frac{\pi}{n_s} \right\} , \end{aligned} \quad (136)$$

which is now symmetrically distributed about  $k = 0$ . For example, for  $n_s = 4$ , the conjugate-momentum states are:  $-\frac{3\pi}{4\delta_\phi}, -\frac{\pi}{4\delta_\phi}, \frac{\pi}{4\delta_\phi}, \frac{3\pi}{4\delta_\phi}$ .

We can understand how these modes are established by recalling that in defining the BCs of the field, there is freedom in defining the continuation around the lattice (the phase picked up when traveling “around the world”), and in particular, a phase can be included,

$$\phi(n_s) = e^{i\eta} \phi(0) , \quad (137)$$

which is particularly relevant for evaluating derivatives. With such a phase, the nominal quantization condition becomes <sup>28</sup>

$$kL = 2\pi q \rightarrow 2\pi q + \eta , \quad (140)$$

accommodating the shift in momentum that we have used.<sup>29</sup> Using the JLP construction, we readily know the diagonal elements of the operator  $\hat{P}$  (which now excludes zero) with a modified Fourier transform matrix, only changing the sign of elements corresponding to  $\Pi(n_s) = \Pi(0)$ . The finite-difference operator subject to twisted-BCs in Eq. (137),  $\eta = \pi$ , becomes (the extreme off-diagonal elements are different),

$$\begin{aligned} \langle \phi' | \hat{\Pi}_{FD}^{2,\Delta} | \phi \rangle &= \frac{1}{\delta_\phi^2} \begin{pmatrix} 2 & -1 & 0 & 0 & \cdots & +1 \\ -1 & 2 & -1 & 0 & \cdots & 0 \\ 0 & -1 & 2 & -1 & \cdots & 0 \\ \vdots & & & & & \\ +1 & 0 & 0 & \cdots & -1 & 2 \end{pmatrix} = V_\Delta^\dagger \cdot \hat{P}_\Delta^2 \cdot V_\Delta , \\ \hat{P}_\Delta &= \text{diag} \left( \frac{2}{\delta_\phi} \sin \frac{k_\phi^\Delta \delta_\phi}{2} \right) , \quad V_\Delta = \frac{1}{\sqrt{n_s}} e^{-i\mathbf{k}^\Delta \cdot \mathbf{j}} , \end{aligned} \quad (141)$$

---

<sup>28</sup> By using a mode expansion

$$\phi(x) = \sum_k e^{+ikx} A_k , \quad (138)$$

and requiring that  $\phi(L) = e^{i\eta} \phi(0)$ , e.g., in 1D,

$$e^{ikL} = e^{i\eta} , \quad kL = \eta + 2\pi n . \quad (139)$$

<sup>29</sup> These correspond to *twisted* boundary conditions (TBCs) that have been successfully used in many areas of physics, including in lattice QCD, for example, Refs. [53–58], and condensed matter physics. Interestingly, NPLQCD introduced i-PBCs [57] in an effort to eliminate the lowest few shells of finite-volume effects in bound systems in lattice QCD computations of light nuclei, e.g., Ref. [22]. See, <https://www.ub.edu/nplqcd/>.

with  $k_\phi^\Delta$  given in Eq. (136). Using the exact (JLP) conjugate-momentum eigenvalues leads to

$$\hat{P}_\Delta^{\text{exact}} = \text{diag}(\ k_\phi^\Delta \ ) ,$$

$$\langle \phi' | \hat{\Pi}_{\text{exact}}^{2,\Delta} | \phi \rangle = \frac{1}{\delta_\phi^2} \begin{pmatrix} 3.24 & -1.95 & 0.436 & -0.138 & 0 & 0.138 & -0.436 & 1.95 \\ -1.95 & 3.24 & -1.95 & 0.436 & -0.138 & 0 & 0.138 & -0.436 \\ 0.436 & -1.95 & 3.24 & -1.95 & 0.436 & -0.138 & 0 & 0.138 \\ -0.138 & 0.436 & -1.95 & 3.24 & -1.95 & 0.436 & -0.138 & 0 \\ 0 & -0.138 & 0.436 & -1.95 & 3.24 & -1.95 & 0.436 & -0.138 \\ 0.138 & 0 & -0.138 & 0.436 & -1.95 & 3.24 & -1.95 & 0.436 \\ -0.436 & 0.138 & 0 & -0.138 & 0.436 & -1.95 & 3.24 & -1.95 \\ 1.95 & -0.436 & 0.138 & 0 & -0.138 & 0.436 & -1.95 & 3.24 \end{pmatrix} \quad (142)$$

To make explicit the impact of this twisting and associated redefinitions, Fig. 16 shows the systematic error associated with digitization as a function of the number of states for different tunings of  $\phi^{\max}$  for the HO. One expects to see a lower limit set by the truncation of the wavefunction and to scale as a Gaussian of  $\phi^{\max}$ , which becomes (exponentially) saturated as the number of states increases. With a particular and effective tuning of  $\phi^{\max}$ , the precision of the ground state energy

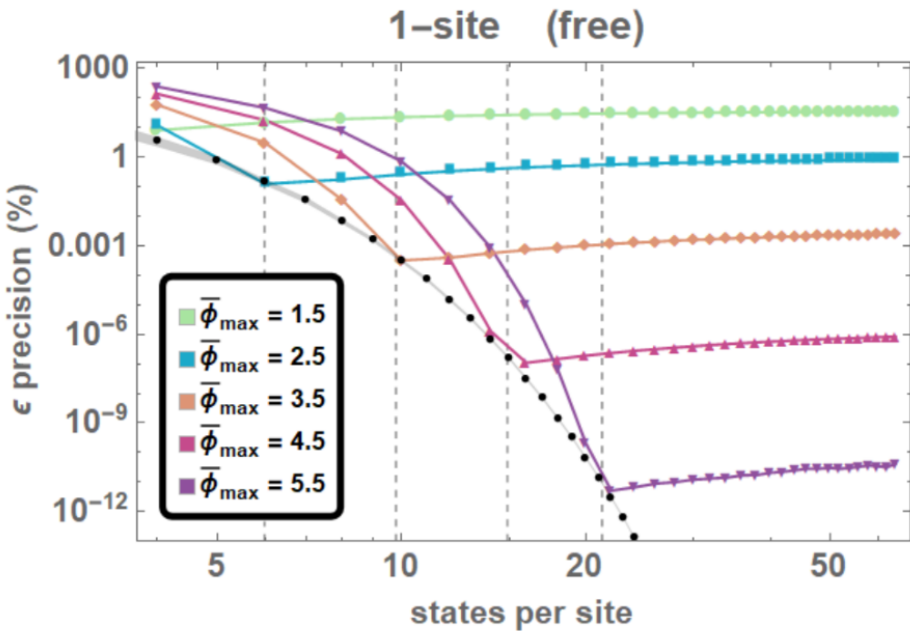


FIG. 16: The precision of calculations of the ground-state energy of the HO. The expectations for an ideal quantum computer for different values of  $\phi_{\max}$  as a function of the number of states. The vertical gray-dashed lines correspond to the location of inflection points predicted by the NS sampling theorem for the indicated values of  $\phi_{\max}$ . A fit to the grey points calculated at the NS saturation point indicates  $\epsilon \sim (1.8(2) \times 10^3) 2^{-2.234(4)n_s}$ , quantifying the double-exponential scaling between  $\epsilon$  and  $n_Q$ . This image is reproduced from Ref. [1].

is explored as a function of the number of states in Fig. 17 for different implementations of  $\hat{\Pi}$ . The JLP implementation in Fourier space is found to be the most effective, without polynomial systematic errors.

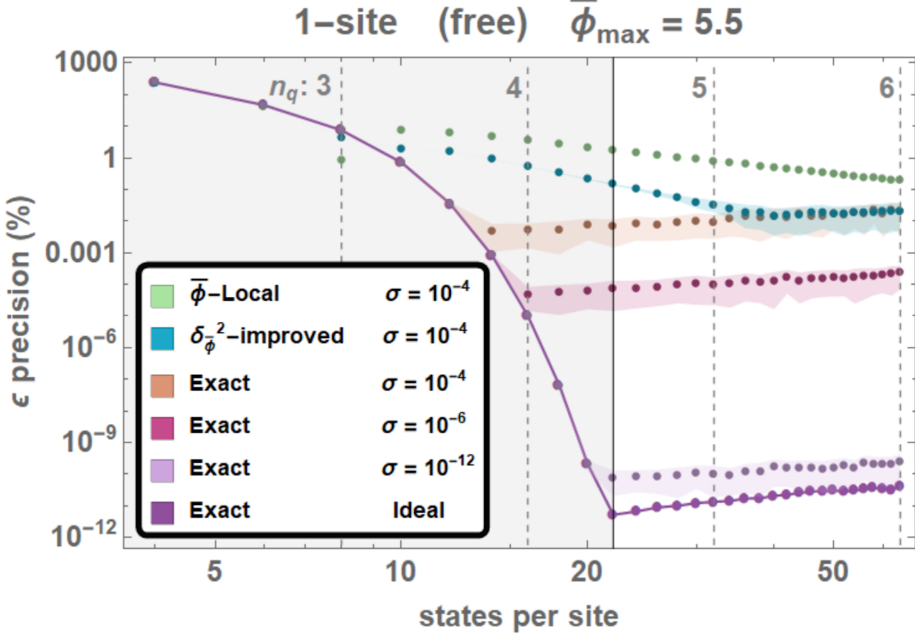


FIG. 17: The precision of the ground-state energy of the HO for unimproved, improved and exact conjugate-momentum operators, over a range of digitizations of  $\bar{\phi}$  with different levels of gate noise. The light-green points correspond to implementing the finite-difference conjugate-momentum operator, the light-blue corresponds to the  $\mathcal{O}(\delta_{\phi}^2)$ -improved conjugate-momentum operator, and the purple-points correspond to the exact conjugate-momentum operator. Gaussian noise with a width  $\sigma$  is added to the diagonal elements of the eigenvalues of the conjugate momentum operators. The maximum value of the field is fixed to be  $\bar{\phi}_{\max} = 5.5$ , enabling a precision of  $\sim 10^{-12}$  for an ideal quantum computer. The vertical light-gray dashed lines correspond to the number of qubits associated with the number of states, while the solid darker-gray line corresponds to the naïve estimate of saturation of the NS sampling bound based upon the properties of the HO ground state wavefunction. For the computational errors anticipated in the NISQ-era, 4 qubits are seen to be sufficient to eliminate the digitization of the scalar field as a source of important error. From reference [1].

## F. The Quantum Fourier Transform

All of the above observations and manipulations are pinned upon the ability to work in  $\hat{\Pi}$ -space as efficiently, and with the same flexibility, as in  $\hat{\phi}$ -space. In classical calculations, this is not the case, where Fourier transform over the complete lattice volume are impractically expensive. The same is true for quantum simulations, but we have been assuming that QFTs in each local Hilbert space can be done efficiently, and that we will require at most  $\mathcal{O}(V)$  of them in any application of the Hamiltonian.

For our purposes, with the shifted field variables to satisfy the  $\hat{\Pi} \leftrightarrow -\hat{\Pi}$  symmetry of the Hamiltonian, the standard QFT must be modified in order to be helpful. It turns out that this is straightforward.

### 1. The “Usual” (Un-Twisted) Quantum Fourier Transform

The usual QFT can be constructed simply, with all states indexed starting at 0, for which the position-space register of  $n_Q$  qubits becomes organized as,  $|x_0\rangle \otimes |x_1\rangle \otimes \dots \otimes |x_{n_Q-1}\rangle$ . Any state

in this  $n_s = 2^{n_Q}$  dimensional Hilbert space can be located via its binary decomposition,

$$x = \sum_{i=0}^{n_Q-1} x_i 2^i = x_0 + 2x_1 + 4x_2 + \dots + 2^{n_s-1} x_{n_Q-1} = 0, 1, 2, \dots, n_Q - 1 , \quad (143)$$

and similarly for  $k$ .<sup>30</sup> The states in the space can be compactly written in binary, e.g., for 3-qubits we have 8 states in the Hilbert space labeled by  $x = x_2 x_1 x_0 = 000, 001, 010, \dots, 111$ . The QFT maps between position space and momentum space via the linear map

$$|x\rangle = \frac{1}{\sqrt{n_s}} \sum_{k=0}^{n_s-1} e^{i \frac{2\pi}{n_s} kx} |k\rangle , \quad (144)$$

where both  $|x\rangle = |0\rangle, |1\rangle, \dots, |7\rangle$  and  $|k\rangle = |0\rangle, |1\rangle, \dots, |7\rangle$ .

All of the “content” in the QFT is in the phase factors, and the binary representation is efficient (as can be found, for instance, in Nielsen and Chuang [26]),

$$\frac{2\pi}{2^{n_Q}} kx = \frac{2\pi}{2^{n_Q}} \left( \sum_{i=0}^{n_Q-1} k_i 2^i \right) \left( \sum_{j=0}^{n_Q-1} x_j 2^j \right) = 2\pi \sum_{i,j}^{n_Q-1} x_i k_j 2^{i+j-n_Q} . \quad (145)$$

If  $i+j-n_Q \geq 0$ , this contributes a phase of  $2\pi$ , and hence can be replaced by zero in the argument of the exponential. In the case of  $n_Q = 3$ , there are nontrivial contributions from  $i = 0, j = 0, 1, 2$  and  $i = 1, j = 0, 1$  and  $i = 2, j = 0$ , and hence nontrivial phases

$$e^{i2\pi k_0 \left( \frac{x_0}{8} + \frac{x_1}{4} + \frac{x_2}{2} \right)} e^{i2\pi k_1 \left( \frac{x_0}{4} + \frac{x_1}{2} \right)} e^{i2\pi k_2 \left( \frac{x_0}{2} \right)} . \quad (146)$$

The QFT can now be written as

$$|x\rangle = \frac{1}{\sqrt{n_s}} \sum_{k_0=0}^1 \sum_{k_1=0}^1 \dots \sum_{k_{n_Q-1}=0}^1 e^{i2\pi k_0 \left( \frac{x_0}{2^{n_Q}} + \dots + \frac{x_{n_Q-2}}{4} + \frac{x_{n_Q-1}}{2} \right)} e^{i2\pi k_1 \left( \frac{x_0}{2^{n_Q-1}} + \dots + \frac{x_{n_Q-2}}{2} \right)} \dots e^{i2\pi k_{n_Q-1} \frac{x_0}{2}} |k\rangle , \quad (147)$$

where we have used

$$\sum_{k=0}^{n_s-1} = \sum_{k_0=0}^1 \sum_{k_1=0}^1 \dots \sum_{k_{n_Q-1}=0}^1 . \quad (148)$$

Examining the simplest contribution, from the highest-k qubit and the lowest-x qubit, gives

$$\sum_{k_{n_Q-1}=0}^1 e^{i2\pi k_{n_Q-1} \frac{x_0}{2}} |k_{n_Q-1}\rangle = |0\rangle + e^{i\pi x_0} |1\rangle = \sqrt{2} \hat{H} |x_0\rangle$$

$$e^{i\pi x_0} = 1 \text{ for } x_0 = 0 , = -1 \text{ for } x_0 = 1 , \quad (149)$$

---

<sup>30</sup> Note that in this notation, the “geometry” factors have been factored, leaving  $k$  to be an integer defining the states in momentum space.

and the next simplest contribution,<sup>31</sup> from the next-to-highest-k qubit and the next-to-lowest-x qubit, gives

$$\sum_{k_{n_Q-2}=0}^1 e^{i2\pi k_{n_Q-2}(\frac{x_0}{4} + \frac{x_1}{2})} |k_{n_Q-2}\rangle = |0\rangle + e^{i\pi x_1} e^{i\pi \frac{x_0}{2}} |1\rangle = \left[ C\tilde{R}(\frac{1}{2}) \right]_{01} \cdot \hat{H} |x_1\rangle$$

$$\tilde{R}(\theta) = \begin{pmatrix} 1 & 0 \\ 0 & e^{i\pi\theta} \end{pmatrix} = e^{i\theta/2} R_z(-\theta)$$

$$e^{i\pi x_1} e^{i\pi \frac{x_0}{2}} = 1 \text{ for } x_1 x_0 = 00, = -1 \text{ for } x_1 x_0 = 10$$

$$= i \text{ for } x_1 x_0 = 01, = -i \text{ for } x_1 x_0 = 11, \quad (151)$$

where the controlled-rotation on  $|x_1\rangle$  is controlled by the initial value of  $|x_0\rangle$ . This means that in the ordering operations in the quantum circuit, this controlled operation is implemented before the Hadamard gate is applied to the  $|x_0\rangle$  qubit. We note the interchange of ordering of the registers between the spaces. The largest x-qubit corresponds to the smallest k-qubit, and so a swap is performed at the end to restore the conventional ordering. The generalization of these two examples to larger systems is obvious, and leads to the usual QFT circuit shown in Figure 18.<sup>32</sup>

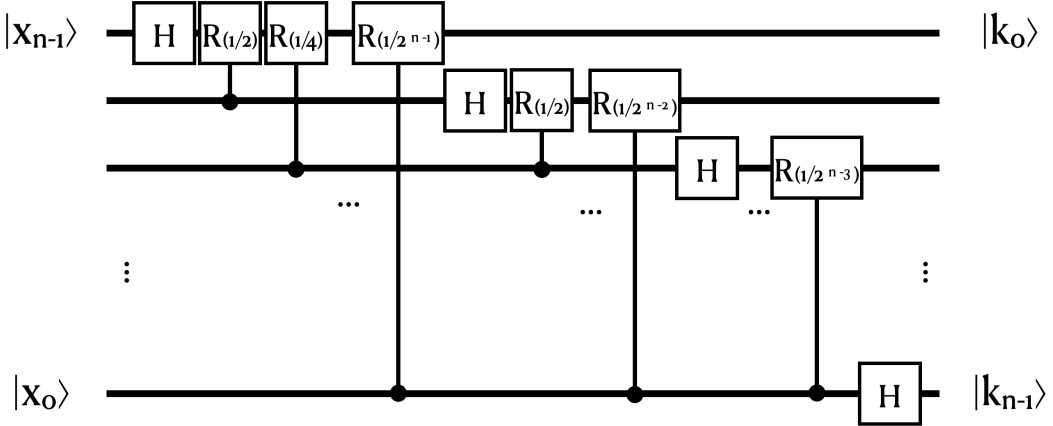


FIG. 18: The standard QFT for  $n$  qubits. The rotation matrix is given in Eq. 151, and is controlled with projectors in the usual way,

<sup>31</sup> For  $n_Q = 3$ , this reads

$$\sum_{k_2=0}^1 e^{i2\pi k_2 \frac{x_0}{2}} |k_2\rangle = |k_2=0\rangle + e^{i\pi x_0} |k_2=1\rangle = \sqrt{2} \hat{H} |x_0\rangle. \quad (150)$$

This is interpreted as that the qubit is initially in state  $|x_0\rangle$ . A Hadamard gate is applied, which puts the state into  $|0\rangle + |1\rangle$  if  $|x_0\rangle = |0\rangle$  and  $|0\rangle - |1\rangle$  if  $|x_0\rangle = |1\rangle$ . In terms of coefficients in the wavefunction,  $|\psi\rangle = \alpha|0\rangle + \beta|1\rangle$ , the action of the Hadamard generates coefficients of  $\frac{1}{\sqrt{2}}(\alpha + \beta)$  for  $|0\rangle$  and  $\frac{1}{\sqrt{2}}(\alpha - \beta)$  for  $|1\rangle$ , and so one interprets  $|0\rangle$  as the  $k = 0$  state and  $|1\rangle$  as the  $k = 1$  state, with coefficients corresponding to the Fourier transform of  $|\psi\rangle$ .

<sup>32</sup> Most likely this is completely obvious, but in some sense, the notation is somewhat confusing as the qubits are “simply” qubits, and are unchanged, and it is their “denoting” is being overloaded. The amplitudes of the qubits in the wavefunction are changing via the unitary operations that are being applied. What I mean by this is a qubit on a quantum register remains in place and is not being moved around within the register, but its amplitude means different things before and after the sequence of unitary operations, and that is what the labeling of the qubit is keeping track of.

The standard swap-operation is shown in Figure 19.

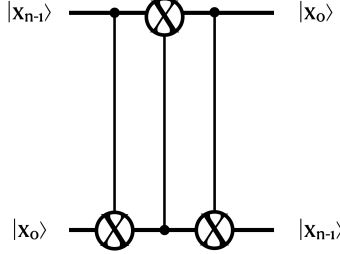


FIG. 19: A swap operation. This can be applied after the QFT to restore the original ordering of qubits in the register if so desired.

As an example, consider a two-qubit system, and the Fourier transform of four states.

$$\begin{aligned}
 |\psi\rangle &= \alpha|00\rangle + \beta|01\rangle + \gamma|10\rangle + \eta|11\rangle , \\
 &\rightarrow \frac{1}{\sqrt{2}} [\alpha(|00\rangle + |10\rangle) + \beta(|01\rangle + |11\rangle) + \gamma(|00\rangle - |10\rangle) + \eta(|01\rangle - |11\rangle)] , \\
 &\rightarrow \frac{1}{\sqrt{2}} [\alpha(|00\rangle + |10\rangle) + \beta(|01\rangle + i|11\rangle) + \gamma(|00\rangle - |10\rangle) + \eta(|01\rangle - i|11\rangle)] , \\
 &\rightarrow \frac{1}{2} [|00\rangle(\alpha + \beta + \gamma + \eta) + |01\rangle(\alpha - \beta + \gamma - \eta) + |10\rangle(\alpha + i\beta - \gamma - i\eta) + |11\rangle(\alpha - i\beta - \gamma + i\eta)] , \\
 &\rightarrow \frac{1}{2} [|00\rangle(\alpha + \beta + \gamma + \eta) + |10\rangle(\alpha - \beta + \gamma - \eta) + |01\rangle(\alpha + i\beta - \gamma - i\eta) + |11\rangle(\alpha - i\beta - \gamma + i\eta)] ,
 \end{aligned} \tag{152}$$

from which we should note the ordering of momenta.

To implement the QFT in  $\hat{\Pi}$ -space in a way that satisfies the symmetry,  $\hat{\Pi} \leftrightarrow -\hat{\Pi}$ , requiring a symmetric distribution in both spaces) a shift in both  $x$  and  $k$  from the usual QFT is required. This was introduced in reference [1].

## 2. The Symmetric-Symmetric QFT (SSQFT) [1]

We want to work with basis vectors that are indexed symmetrically about the origin to naturally preserve the symmetries of the Hamiltonian,

$$\begin{aligned}
 \bar{x} &= -\frac{n_s - 1}{2}, \dots, +\frac{n_s - 1}{2} , \\
 \bar{k} &= -\frac{n_s - 1}{2}, \dots, +\frac{n_s - 1}{2} .
 \end{aligned} \tag{153}$$

The SSQFT is therefore defined to be

$$\begin{aligned}
 |\bar{x}\rangle &= \frac{1}{\sqrt{n_s}} \sum_{\bar{k}=-\frac{n_s-1}{2}}^{+\frac{n_s-1}{2}} e^{i\frac{2\pi}{n_s}\bar{k}\bar{x}} |\bar{k}\rangle \\
 &= \frac{1}{\sqrt{n_s}} \sum_{k=0}^{n_s-1} e^{i\frac{2\pi}{n_s}(k-\frac{n_s-1}{2})(x-\frac{n_s-1}{2})} |k\rangle ,
 \end{aligned} \tag{154}$$

where it has been written in terms of the usual QFT phases and offsets in both spaces. The phase(s) of the exponential can be expanded as

$$\begin{aligned}
& \pi \frac{1}{2^{n-1}} \left( k_0 + 2k_1 + \dots + 2^{n-1}k_{n-1} - 2^{n-1} + \frac{1}{2} \right) \left( x_0 + 2x_1 + \dots + 2^{n-1}x_{n-1} - 2^{n-1} + \frac{1}{2} \right) \\
& \pi \left[ \frac{kx}{2^{n-1}} - \left( 1 - \frac{1}{2^n} \right) (k_0 + 2k_1 + \dots + 2^{n-1}k_{n-1}) - \left( 1 - \frac{1}{2^n} \right) (x_0 + 2x_1 + \dots + 2^{n-1}x_{n-1}) \right. \\
& \quad \left. + \left( 1 - \frac{1}{2^n} \right) \left( 2^{n-1} - \frac{1}{2} \right) \right] \\
& \rightarrow \pi \left[ \frac{kx}{2^{n-1}} - \left( \left( 1 - \frac{1}{2^n} \right) x_0 - \frac{1}{2^n} (2x_1 + 4x_2 + \dots + 2^{n-1}x_{n-1}) \right) \right. \\
& \quad \left. - \left( \left( 1 - \frac{1}{2^n} \right) k_0 - \frac{1}{2^n} (2k_1 + 4k_2 + \dots + 2^{n-1}k_{n-1}) \right) - \left( 1 - \frac{1}{2^{n+1}} \right) \right] , \tag{155}
\end{aligned}$$

where factors of  $2\pi N$  have been dropped, and we have assumed that  $n \geq 2$ . We see that the circuit modifications are straightforward. There are only non-trivial single qubit transformation before and after the QFT required for the modification, along with a global phase factor. For example,

$$\begin{aligned}
& \exp \left( -I\pi \left( \left( 1 - \frac{1}{2^n} \right) x_0 - \frac{1}{2^n} (2x_1 + 4x_2 + \dots + 2^{n-1}x_{n-1}) \right) \right) \rightarrow \\
& R_0 \left( - \left( 1 - \frac{1}{2^n} \right) \right) . R_1 \left( \frac{1}{2^{n-1}} \right) . R_2 \left( \frac{1}{2^{n-2}} \right) . \dots . R_{n-1} \left( \frac{1}{2} \right) , \tag{156}
\end{aligned}$$

acting on the  $x$ -register (i.e. before the usual QFT) as denoted by the subscript on the rotation matrix operator. Similarly for the other non-trivial phase, but this acts on the  $k$ -register after the QFT, but has an identical form. So the complete quantum circuit is the same as before with pre- and post-single qubit phase factors, as shown in Fig. 20.

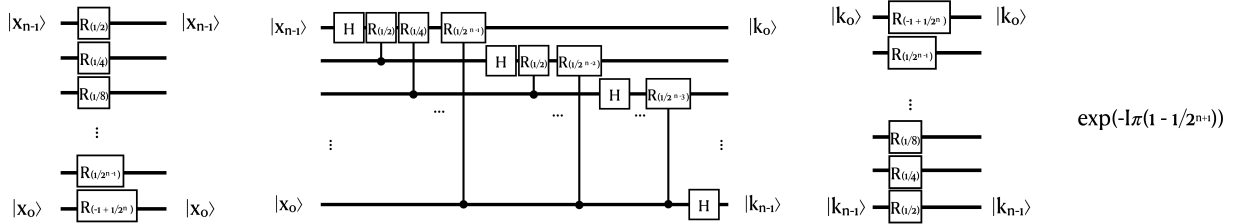


FIG. 20: The symmetric-symmetric QFT (SSQFT). The swap gate follows at the far right to return to the original ordering (if required).

### G. Quantum Circuits for Scalar Field Theory in JLP Basis

In order to provide explicit examples of quantum circuits that are required to simulate the evolution of scalar field theory, we consider explicitly a single site of the HO and  $\lambda\phi^4$  using  $n_Q = 3$  qubits, as explicitly constructed in Ref. [1]. With  $n_s = 8$  states,  $\phi$  is sampled at the field and conjugate-momentum values, Eq. (126) and Eq. (136),

$$\phi = \{\pm 1, \pm \frac{5}{7}, \pm \frac{3}{7}, \pm \frac{1}{7}\} \phi_{\max} , \quad k_\phi = \{\pm \frac{7}{8}, \pm \frac{5}{8}, \pm \frac{3}{8}, \pm \frac{1}{8}\} \frac{\pi}{\delta_\phi} , \quad \delta_\phi = \frac{2\phi_{\max}}{7} , \tag{157}$$

and symmetric sampling in both spaces is being used (including twisted BCs in  $\hat{\Pi}$ -space) to preserve the discrete symmetries of the Hamiltonian. The superscript  $\Delta$  on  $k_\phi^\Delta$  will be dropped from this point forward for ease of notation. Importantly, recall that the operators associated with these values are diagonal matrices in their perspective spaces.

The simplest way to proceed is to project the field onto Pauli matrices, and the operator decomposition of the Hamiltonian for this system is straightforward. It is useful to extend the basis of Pauli operators to include the identity matrix,  $\bar{\sigma} = (\hat{X}, \hat{Y}, \hat{Z}, \hat{I})$ , and to define the general tensor product of  $n_Q = 3$  operators  $T^{ijk} = \bar{\sigma}^i \otimes \bar{\sigma}^j \otimes \bar{\sigma}^k$ ,

$$T^{ijk} = \bar{\sigma}^i \otimes \bar{\sigma}^j \otimes \bar{\sigma}^k , \quad \text{Tr} [ T^{ijk} T^{i'j'k'} ] = 8 \delta^{ii'} \delta^{jj'} \delta^{kk'} , \quad (158)$$

where the orthogonality of the  $T^{ijk}$  is helpful in decomposing the Hamiltonian into qubit operators. It is straightforward to show that,

$$\begin{aligned} \hat{\phi} &= -\frac{\phi_{\max}}{7} \left( \hat{I} \otimes \hat{I} \otimes \hat{Z} + 2\hat{I} \otimes \hat{Z} \otimes \hat{I} + 4\hat{Z} \otimes \hat{I} \otimes \hat{I} \right) \\ \hat{\phi}^2 &= \frac{4\phi_{\max}^2}{49} \left( \hat{I} \otimes \hat{Z} \otimes \hat{Z} + 2\hat{Z} \otimes \hat{I} \otimes \hat{Z} + 4\hat{Z} \otimes \hat{Z} \otimes \hat{I} + \frac{21}{4}\hat{I} \otimes \hat{I} \otimes \hat{I} \right) \\ \hat{\phi}^4 &= \left( \frac{4\phi_{\max}^2}{49} \right)^2 \left( \frac{53}{2}\hat{I} \otimes \hat{Z} \otimes \hat{Z} + 29\hat{Z} \otimes \hat{I} \otimes \hat{Z} + 46\hat{Z} \otimes \hat{Z} \otimes \hat{I} + \frac{777}{16}\hat{I} \otimes \hat{I} \otimes \hat{I} \right) \\ \hat{\Pi} &= -\frac{\pi}{8\delta_\phi} \left( \hat{I} \otimes \hat{I} \otimes \hat{Z} + 2\hat{I} \otimes \hat{Z} \otimes \hat{I} + 4\hat{Z} \otimes \hat{I} \otimes \hat{I} \right) \\ \hat{\Pi}^2 &= \frac{\pi^2}{16\delta_\phi^2} \left( \hat{I} \otimes \hat{Z} \otimes \hat{Z} + 2\hat{Z} \otimes \hat{I} \otimes \hat{Z} + 4\hat{Z} \otimes \hat{Z} \otimes \hat{I} + \frac{21}{4}\hat{I} \otimes \hat{I} \otimes \hat{I} \right) , \end{aligned} \quad (159)$$

where we use the (remainingly odd) notation of  $\hat{Z}|0\rangle = +|0\rangle$  and  $\hat{Z}|1\rangle = -|1\rangle$ . This results can be found by multiplication of operators, or by repeating the trace against  $\sigma$  matrices. The  $\hat{\phi}$  and  $\hat{\phi}^2$  operators act in  $|\phi\rangle$ -space, and the  $\hat{\Pi}$  and  $\hat{\Pi}^2$  operators act in  $|\Pi\rangle$ -space.

We see from this list of operator matrix elements in the two spaces that only phases from, 1-body  $\hat{Z}$  and 2-body  $\hat{Z}\hat{Z}$  operators, appear when the system is limited to 3 qubits. This is remarkably efficient. Using the simple construction for exponentials of  $\hat{Z}\hat{Z}$  operators,

$$e^{-i\frac{\theta}{2}\hat{Z}\otimes\hat{Z}} = \text{CNOT}_{12}.R_{2,z}(\theta).\text{CNOT}_{12} , \quad (160)$$

the required circuits can be constructed. It is helpful to note that these three operators commute with each other, and there are no errors introduced by implementing them sequentially and not simultaneously. It is also the case that  $\lambda\phi^4$  term commutes with the  $\phi^2$  term, so these can be split analogously. As the  $\hat{\Pi}$  term and  $\phi^n$  do not commute in general, they cannot be applied sequentially without systematic errors arising. The question is..... how do we actually accomplish time-evolution now that we have determined the digitized mapping of fields onto a quantum register? I wish to give a rigorous method that has been shown to converge, but which has been improved upon, and we will come to that at a somewhat later date.

If we have the quantum register of the  $\phi$  field prepared in any given initial state,  $|\psi\rangle_0$ , how do we evolved it forward in time? Let us not worry about how we prepared this state, we have already seen ways to do this (including in Homework). The question is - what happens next?

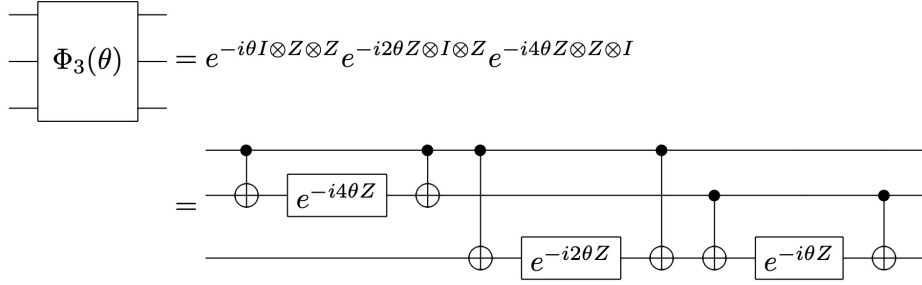


FIG. 21: A quantum circuit for implementing the  $\hat{\phi}^2$  or  $\hat{\Pi}^2$ . The generalization to include the  $\lambda\phi^4$  operator is clear. There are more efficient circuits possible by using GHZ transformations.

### 1. Time Evolution of Scalar Field Theory in JLP Basis

Writing the general Hamiltonian in the form of

$$\hat{H} = \hat{K} + \hat{V}, \quad (161)$$

where both  $\hat{K}$  and  $\hat{V}$  do not depend explicitly on time, the time evolution of  $|\psi\rangle_0$  is “simply” given by

$$|\psi\rangle(t) = \hat{U}(t) |\psi\rangle_0, \quad \hat{U}(t) = e^{-i\hat{H}t}. \quad (162)$$

In general, we do not know how to create a circuit that directly recovers this unitary evolution, and certainly becomes intractable as the number of qubits tends to infinity. For  $n_Q = 3$  it can be accomplished because there are only 63 angles that need to be determined in  $SU(8)$ <sup>33</sup>. The well-known, default, and in many instances best way to proceed is to use Trotterization or higher-order corrected versions, Suzuki-Trotter, and beyond. Trotterized time-evolution has been established to be efficient for time evolving quantum wavefunctions forward in time using quantum computers [59].

It is (exactly) true that (without errors as we have not partitioned the operator in the exponent),

$$\hat{U}(t) = e^{-i\hat{H}T} = \left[ e^{-i\hat{H}\Delta t} \right]^{T/\Delta t}, \quad (163)$$

for any arbitrary  $\Delta t$ ,  $T$  and  $\hat{H}$ . When a circuit for the complete  $\hat{H}$  cannot be identified, the unitary operator can be decomposed into manageable parts. In particular, by taking the limit of small time increments that sum to accomplish the desired evolution,

$$\hat{U}(t) = e^{-i\hat{H}T} = \lim_{\Delta t \rightarrow 0} \left[ e^{-i(\hat{K} + \hat{V})\Delta t} \right]^{T/\Delta t}. \quad (164)$$

Because of its non-uniqueness, and hence range of quantum resource requirements, it is valuable to consider the ways to isolate and separate terms while converging to the correct time evolution as  $\Delta t \rightarrow 0$ . One can show by simple expansion and collection of terms that the leading-order (LO) Trotter expansion is

$$e^{-i\hat{K}\Delta t} e^{-i\hat{V}\Delta t} = e^{-i(\hat{K} + \hat{V})\Delta t} + \mathcal{O}(\Delta t^2). \quad (165)$$

<sup>33</sup> For  $SU(N)$ , there are  $N^2 - 1$  generators and hence angles required to implement an arbitrary unitary. For example, for one qubit :  $SU(2)$  there are 3  $\hat{T}^a$ ; for two qubits :  $SU(4)$  there are 15  $\hat{T}^a$ ; for three qubits :  $SU(8)$  there are 63  $\hat{T}^a$ ; for four qubits :  $SU(16)$  there are 255  $\hat{T}^a$ , etc.

By considering how this will be employed via Eq. (164), LO Trotter leads to  $\mathcal{O}(\Delta t)$  systematic errors in the time-evolution operator (because it is applied  $T/\Delta t$  times during the evolution). <sup>34</sup> One can consider an arbitrary number of higher-order variants on this decimation, including 2nd-order Trotter

$$\begin{aligned} e^{-i\hat{K}\Delta t/2} e^{-i\hat{V}\Delta t} e^{-i\hat{K}\Delta t/2} &= e^{-i(\hat{K} + \hat{V})\Delta t} + \mathcal{O}(\Delta t^3) \\ e^{-i\hat{V}\Delta t/2} e^{-i\hat{K}\Delta t} e^{-i\hat{V}\Delta t/2} &= e^{-i(\hat{K} + \hat{V})\Delta t} + \mathcal{O}(\Delta t^3) , \end{aligned} \quad (166)$$

which give rise to  $\mathcal{O}(\Delta t^2)$  systematic errors in the time-evolution operator. Of course, the coefficient of the  $\mathcal{O}(\Delta t^n)$  errors matters, and as it would vanish identically if the operators commuted, it has associated powers of the operators and at least one power of  $[\hat{K}, \hat{V}]$ .

In the case of scalar field theory, the question becomes about the separation of terms in the Hamiltonian and the associated circuits. We have already considered a circuit that recovers both terms, one in  $|\phi\rangle$  space and one in  $|\Pi\rangle$  space.

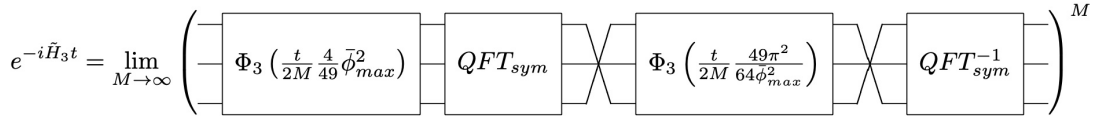


FIG. 22: The time-evolution operator for a HO digitized on  $n_Q = 3$  qubits at leading order in a Trotter expansion.  $M$  is an integer corresponding to the number of Trotter steps to evolve from  $t = 0$  to  $t = T$ . QFT represents a Symmetric-Symmetric Quantum Fourier Transform (SSQFT) (discussed in Sec. IV F 2). The quantum circuit implementing the three-qubit function  $\Phi_3$  is given in Fig. (21), and the inclusion of the  $\lambda\phi^4$  terms is straightforward.

The discussion that we have just detailed for the system digitized onto  $n_Q = 3$  generalizes to an arbitrary number of qubits, with the only increase in complexity associated with number of 1-body and 2-body operators. In Table I, we show the gate counts required for the application of a single Trotter step for the HO ( $\lambda = 0$ ). One of the many beautiful aspects of the JLP construction is

Basis	$n_Q$	0-body	1-body	2-body	3-body	4-body	5-body	6-body	$QFT$	CNOTs
JLP	2	1	8	2					✓	8
	3	1	14	6					✓	24
	4	1	20	12					✓	48
	5	1	26	20					✓	80
	6	1	32	30					✓	120
	$JLP\ n_Q$	1	$6n_Q - 4$	$2 * \binom{n_Q}{2}$					✓	$8\binom{n_Q}{2}$

TABLE I: Resource requirements for one step in the Trotterized time evolution of a HO in the field-digitization JLP basis. CNOT counts are based upon a standard multi-Pauli implementation requiring  $2(k-1)$  CNOTs for each  $k$ -body operator. When a QFT is required (JLP), the standard CNOT counts of  $2\binom{n_Q}{2}$  for this operation (and its inverse) are included.

that there are no 3-body or higher operators, and consequently the gate count scales quite benignly with increasing digitization.

<sup>34</sup> Experience shows that in many situations relevant for simulating systems of fundamental particles, LO Trotterization is optimal when considering required quantum resources and propagation/accumulation of systematic errors.

## 2. Scalar Field Theory - d-Dimensions

So far, we have explored how to set up and time evolve an interacting scalar field theory at one spatial site. This corresponds to linear (non-interacting) and non-linear (interacting) HOs. We will return to Trotterization and other methods for time evolution soon, but to complete discussions of  $\lambda\phi^4$ , time-evolution in the theory defined in d-spatial dimensions should be considered. JLP [2] explained how this is straightforward.

The target Hamiltonian for quantum simulation in three dimensions has the form

$$\begin{aligned} H &= \frac{1}{2} \sum_{\mathbf{n}}^{L-1, L-1, L-1} \left( \hat{\Pi}_{\mathbf{n}}^2 + m^2 \hat{\phi}_{\mathbf{n}}^2 - \sum_{j=x,y,z} \hat{\phi}_{\mathbf{n}} (\hat{\phi}_{\mathbf{n}+\mu_j} + \hat{\phi}_{\mathbf{n}-\mu_j} - 2\hat{\phi}_{\mathbf{n}}) \right) \\ &= \frac{1}{2} \sum_{\mathbf{n}}^{L-1, L-1, L-1} \left( \hat{\Pi}_{\mathbf{n}}^2 + (m^2 + 6) \hat{\phi}_{\mathbf{n}}^2 - \sum_{j=x,y,z} \hat{\phi}_{\mathbf{n}} (\hat{\phi}_{\mathbf{n}+\mu_j} + \hat{\phi}_{\mathbf{n}-\mu_j}) \right) , \end{aligned} \quad (167)$$

where  $\mu_j$  is a unit vector in the  $j^{\text{th}}$ -direction (this is the minimal finite-difference operator implementing the  $\nabla^2\phi$  in the continuum). The notable modifications to the form of Hamiltonian in Eq. (167) in changing the number of spatial dimensions from  $d = 0$  to  $d = 3$  are slight and straightforward to implement. The first is that the summation of the Hamiltonian density extends over all of the lattice sites in the spatial volume, to give the discrete approximation to the Hamiltonian,

$$H = \int d^3\mathbf{x} \mathcal{H}(\mathbf{x}) \rightarrow \sum_{j=x,y,z} \mathcal{H}^{\text{latt.}}(\mathbf{j}) . \quad (168)$$

The second is that the mass that appears at each spatial site now depends upon the number of spatial-dimensions,  $m^2 \rightarrow m^2 + 2d$  to absorb terms from the discretized  $\nabla^2\phi$  operator. The third is the appearance of terms that couple spatial sites which involves a sum over the action of  $\nabla^2\phi$  in each of the spatial directions at each of the spatial points in the lattice. Therefore, the only aspect in Eq. (167) that we have not encountered previously is the contribution from the last term,  $\sum_{j=x,y,z} \hat{\phi}_{\mathbf{n}} (\hat{\phi}_{\mathbf{n}+\mu_j} + \hat{\phi}_{\mathbf{n}-\mu_j})$ . As JLP pointed out, it is straightforward to evaluate the contributions from this term in the  $|\phi\rangle$ -basis. Recall that at each site, when digitized onto 3-qubits for example, we have the field operator:

$$\hat{\phi} = -\frac{\phi_{\max}}{7} \left( \hat{I} \otimes \hat{I} \otimes \hat{Z} + 2\hat{I} \otimes \hat{Z} \otimes \hat{I} + 4\hat{Z} \otimes \hat{I} \otimes \hat{I} \right) , \quad (169)$$

and longer strings for a more dense sampling of the  $\phi$  field. For demonstrative purposes, in  $d = 1$ , the  $\hat{\phi}_j \hat{\phi}_{j+1}$  term becomes

$$\hat{\phi}_j \hat{\phi}_{j+1} \rightarrow \left( \frac{\phi_{\max}}{7} \right)^2 \left( \hat{I} \otimes \hat{I} \otimes \hat{Z} + 2\hat{I} \otimes \hat{Z} \otimes \hat{I} + 4\hat{Z} \otimes \hat{I} \otimes \hat{I} \right) \otimes \left( \hat{I} \otimes \hat{I} \otimes \hat{Z} + 2\hat{I} \otimes \hat{Z} \otimes \hat{I} + 4\hat{Z} \otimes \hat{I} \otimes \hat{I} \right) , \quad (170)$$

that acts on the 6-qubits describing the field at the 2 sites (for this digitization). The generalization to d-dims involves a straightforward sum of “two-site” contributions In the evolution operator, these terms introduce operators of the form  $\hat{Z} \otimes \hat{Z}$ , which are, once again, (two-qubit) phases multiplying the wavefunction which can be implemented straightforwardly.

It is worth dwelling on the form for these terms and the Hamiltonian in general. The first two terms in the Hamiltonian are the sum of contributions from individual sites, with wavefunctions

digitized with some level of resolution. We have seen that their contributions can be computed efficiently with the use of QFT in their respective field spaces, and with double-exponential convergence with increasing numbers of qubits. With the quantum circuits required for their implementation individually confined to each spatial site, all such operations can be performed on a quantum device in parallel. Further, we have just seen that the contributions from the  $\nabla^2\phi$  operator involves nearest neighbor interactions only (in the minimal implementation, without spatial smearing), and gives rise to phases in the wavefunction (only). Therefore, in  $d = 1$ , a complete Trotter step can be implemented in two steps, that is to say that it can be accomplished in two-steps of large-scale parallel operations on pair-wise local sites.

It is important to recognize that a quantum Fourier transform (QFT) over the spatial volume is not required. The QFTs that have to be performed are local to each spatial site in evaluating the action of  $\hat{\Pi}^2$ . So the total cost of computing scales only with the spatial volume of the lattice (times the number of Trotter steps). Further, *it is all about phases* with no other operator structures to consider (modulo the QFT).

A final comment is that the qubit requirements scale trivially from those required to simulate one spatial site, without any further/hidden costs. The number of qubits is

$$N_Q = n_Q \times L^3 , \quad (171)$$

So we have all of the ingredients to perform the time evolution of a d-dim scalar field theory with a bounded error,  $\epsilon$ , including with  $\lambda\phi^4$  interactions. Lattice scalar field theory, as we discussed in week-1 of this course, is in the **BQP-complete** complexity class [48], and therefore its simulation is expected to be efficient using quantum computers. The challenge that we now must confront is preparing the initial state of lattice scalar field theory on a quantum register.

However, before that, it might be useful to make a small technical detour to show how the “B” in **BQP** can be helpful in how quantum circuits are designed.

## H. Sequency in Quantum Simulations

From a physic perspective, considering all of the machinery that we have used in formulating effective field theory descriptions of nature, a target physical observable will typically be dominated by field configurations that lie within a given region. Low-energy electroweak interactions do not require knowledge or simulation capabilities at the Planck scale, for instance. The same logic also applies within lattice scalar field theory, where a simulation of low-energy scattering at some-level of precision,  $\epsilon$ , for instance, does not require knowing about the behavior/structure of high-energy field configurations (after renormalization). This means that in evaluating contributions from operators in processes restricted to certain regimes, further approximations likely exist that are consistent with a total error bounded by  $\epsilon$ .

In digital signal processing, discrete transform play a central role, and it turns out that they are useful in the present context because of the digitization of the scalar field and quantum simulation more generally. They are used on the engineering side of quantum computing and simulation extensively. A particularly useful set of transforms is the Walsh-Hadamard transforms, which constitute a digital version of the Four transform. Figure 23 shows the lowest-*sequency* Walsh functions. These are particularly useful in mapping between a digitization of a smooth function, such as the lattice scalar field  $\phi$ , and string of Pauli- $\hat{Z}$  operators.

Consider a single lattice point digitized onto four qubits,  $\phi = \phi_{\max}\{-1, -\frac{13}{15}, -\frac{11}{15}, \dots, +\frac{11}{15}, +\frac{13}{15}, +1\}$ . This has a mapping onto strings of Pauli- $\hat{Z}$  operators

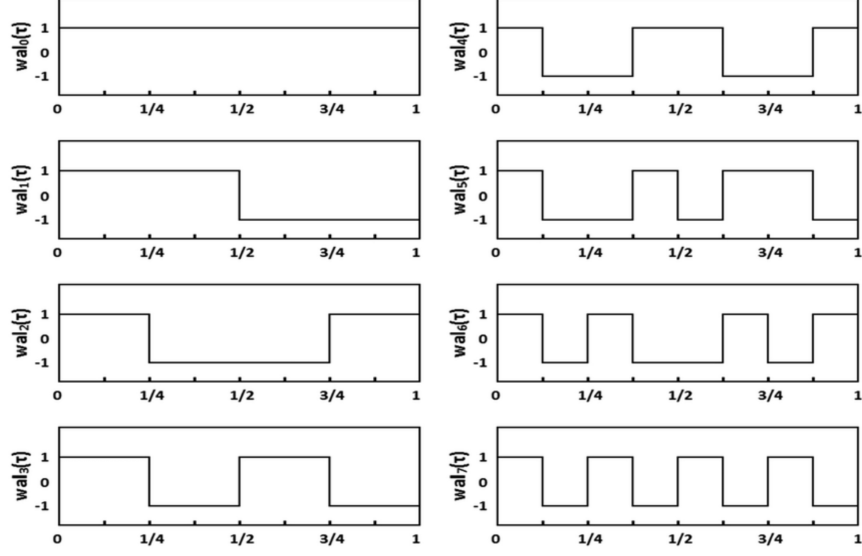
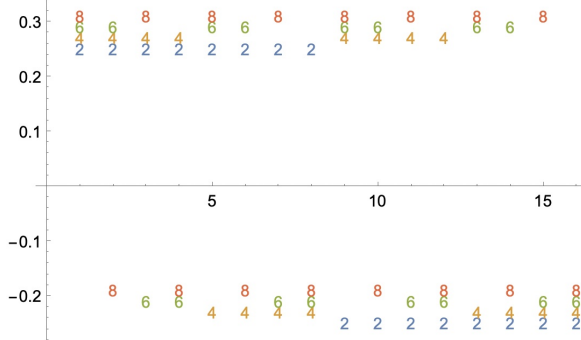


FIG. 23: The lowest-sequence Walsh functions.

(which is particularly simple),

$$\hat{\phi} = -\frac{32}{15}\phi_{\max} \left[ \hat{Z}\hat{I}\hat{I}\hat{I} + \frac{1}{2}\hat{I}\hat{Z}\hat{I}\hat{I} + \frac{1}{4}\hat{I}\hat{I}\hat{Z}\hat{I} + \frac{1}{8}\hat{I}\hat{I}\hat{I}\hat{Z} \right], \quad (172)$$

which correspond to the  $2^1, 2^2, 2^3, 2^4$  labels of Walsh-Hadamard vectors for  $2^4$  states. Figure 24

FIG. 24: The four Walsh-Hadamard sequence functions contributing to the decomposition of the four-qubit digitization of  $\phi$ , given in Eq. (172). The functions have been displaced in the vertical direction by a small amount for display purposes.

shows the four Walsh-Hadamard sequence functions contributing to the decomposition of the four-qubit digitization of  $\phi$ . The important aspect of this decomposition is the hierarchy in the coefficients of the Pauli operators. The lowest sequence contribution has the largest amplitude, while the highest sequence contribution has the smallest.<sup>35</sup>

With an established hierarchy in contributions from operators, quantum simulations can be simplified (substantially) by first performing simulations with the leading operator to produce

<sup>35</sup> An explicit example of such hierarchies can be found in the appendix of a paper I wrote with Natalie Klco [60]. We considered a Gaussian distribution digitized onto four qubits, and examined hierarchies in the sequence distribution.

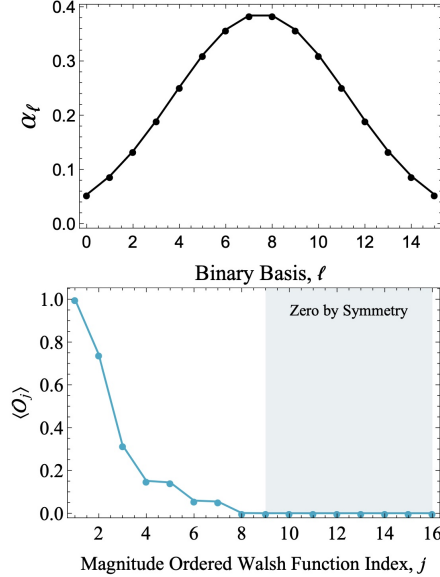


FIG. A1. (upper) Probabilities,  $|\psi_\ell|^2$ , associated with the Gaussian wavefunction prepared on four qubits with the parameters defined in Eq. (A1). (lower) The expectation values of  $O_j$ , calculated using the natural-ordered WHT of Eq. (A2) and sorted by magnitude.

FIG. 25: The expectation values of Pauli- $\hat{Z}$  strings in a Gaussian wavefunction distributed across  $n_Q = 4$  qubits [60].

the leading-order determination of the observable of interest, with systematic refinements (with increasing quantum resource requirements) provided by including higher orders. This is a technique that can be applied to any smooth function for which there is a limited region of support in sequency space.

One reason to think about this is in the context of error-correction. For low-energy simulations, exhibiting such sequency hierarchies, some qubits are more important than others, in the sense that some need to have high fidelity, while others can have low fidelity. If mapped in such a way that the latter qubits make small contributions to the observables of interest, they do not “corrupt” the bounded error budget. Therefore, in such systems, not all logical qubits need to have high fidelity. It is likely that in early simulations, only a small fraction of accessible qubits will be error corrected, and there is likely a way to map problems of interest in such a way to optimize production when using such heterogeneous registers.

## I. Adiabatic Preparation of the Vacuum of Scalar Field Theory

Preparation of the initial quantum states for subsequent quantum simulation is a major area of research for essentially all important problems. Preparing states in order to be able to determine or bound the ground state of a complex many-body system is also a critical problem by itself. In the context of lattice scalar field theory, JLP [2] showed that this can be accomplished by initializing the register into the ground state of the non-interacting theory, and then using adiabatic time evolution to evolve from the ground state of the free theory to that of the interacting theory. Therefore, there are two important steps to initializing the register—a) preparing the non-interacting state and b) adiabatic evolution to the interacting state.

### 1. Preparing the Vacuum of Non-Interacting Scalar Field Theory - Somma Inflation

Before considering state preparation for lattice scalar field theory in three dimensions, let us with the simple case of preparing the ground state of non-interacting scalar field theory in zero-spatial dimensions, a HO. Let us imagine we have  $\phi$  on the one site digitized with  $n_Q$ -qubits. The previously developed quantum circuits can be used to initialize any real function across the register, including that of a Gaussian wavefunction, with a mean location and width, and with a  $\phi_{\max}$  for the field. The number of angles that are required to be determined in order to initialize this state using that circuit is  $N_\theta = 2^{n_Q} - 1$ . This is an extensive number that grows with the volume of the Hilbert space dimensionality, and clearly this exact initialization becomes impractical for registers with large numbers of qubits. It is interesting to note, from the previous section on sequency, that approximate initialization, i.e., establishing a wavefunction that is within some tolerance of the target Gaussian is possible with fewer operations/angles.

There are two improvements over the naive exact digitization initialization across the entire space that we now consider. One is by Rolando Somma [61]. A summary of this algorithm is that if one has a register  $n_Q$  qubits corresponding to  $n_s$  states in the Hilbert space, a Gaussian can be initialized on a small subsection of the Hilbert space with a small number of rotation angles, which can then be evolved straightforwardly to the desired size/support in the entire space. Because this evolution can be Trotterized, it is efficient for quantum computers. For a given mean location and narrow width (compared with the extent of the space), a parametrically smaller number of angles need to be determined to initialize this state. Because its support is distributed over a reduced number of states in the space, the precision of the digitized wavefunction after inflation to its full size,  $\epsilon$ , is determined by the number of states supporting the initial wavefunction and not the number of states in the Hilbert space.

Let us begin by understanding the underlying physics of the method. In the continuum,

$$\psi(x, t=0) = \left( \frac{1}{2\pi\sigma^2} \right)^{1/4} e^{-\frac{1}{4}\frac{x^2}{\sigma^2}}, \quad (173)$$

which is the ground state of a HO. Recall that the propagator for a non-relativistic particle of mass,  $m$ , with Hamiltonian  $\hat{H} = \hat{p}^2/(2m)$  is given by

$$K(x, t; x', 0; m) = \langle x | \hat{U}(t) | x' \rangle = \sqrt{\frac{m}{i2\pi t}} e^{\frac{im(x-x')^2}{t}}. \quad (174)$$

This form can be used to evolve the initial wavefunction forward in time with  $\hat{H} = \hat{p}^2$  by setting  $m = \frac{1}{2}$ . After time  $t$ , the wavefunction becomes

$$\begin{aligned} \psi(x, t) &= \langle x | \hat{U}(t) | \psi \rangle = \langle x | e^{-i\hat{p}^2 t} | \psi \rangle = \left( \frac{\sigma^2}{2\pi} \right)^{1/4} \frac{1}{\sqrt{\sigma^2 - it}} e^{-\frac{1}{4}\frac{x^2}{\sigma^2 - it}} \\ &= \frac{e^{i\frac{t}{2\sigma^2}}}{\sqrt{\sigma^4 + t^2}} e^{-i\frac{1}{4}\frac{x^2 t}{\sigma^4 + t^2}} \left( \frac{\sigma^2}{2\pi} \right)^{1/4} e^{-\frac{1}{4}\frac{x^2 \sigma^2}{\sigma^4 + t^2}}, \end{aligned} \quad (175)$$

which is of the form: i) a time-dependent phase independent of  $x$ , ii) a time-dependent phase that depends upon  $x$ , and iii) a broadened Gaussian function of width

$$\sigma(t) = \sigma^2 + \frac{t^2}{\sigma^2}. \quad (176)$$

Because time-evolution resides in **BQP**, this evolution is efficient. So the idea of *Somma Inflation* is to initialize a Gaussian with support over a small number of states, requiring a manageable number

of angles and circuit elements, then to time-evolve forward using a free Hamiltonian, which creates a Gaussian of much larger support in the space. As there is no free lunch, the fidelity of the inflated wavefunction is limited by the fidelity of the initial state, which is set by the number of states in its initial support. This is an efficient way to initial a Gaussian wavefunction. In actually preparing the wavefunction with limited support, a generic circuit has most of the qubits that are spatially far from the center wavefunction in the Hilbert space set to  $|0\rangle$ . As a result, the control structures on those qubits can be set to zero. So the localization of the wavefunction helps in reducing the overhead involved in the state preparation.

## 2. Preparing the Vacuum of Interacting Scalar Field Theory - Adiabatic Evolution [2]

The previous section showed how to efficiently prepare a single site in the ground state of a HO, either by brute-force, or by various truncations, or using Somma-inflation. As a step toward field theory, neglecting the coupling between spatial sites (and hence spatial entanglement), the previous single-site discussions generalize straightforwardly to a large number of uncoupled HOs. They also generalize to a large number of coupled HOs essentially in a well-defined, but somewhat more complex way. The entanglement between sites requires more complex circuitry, but this is aided by the discrete translation invariance of the lattice system, and the ability to re-arrange circuits to explicitly take advantage of the exponential dependence of the correlation functions [62–65]. Consequently, ground-state wavefunctions of non-interacting lattice scalar field theory can be prepared efficiently on quantum registers.

The next step in the preparation is to transform the wavefunctions of non-interacting lattice scalar field theory into the ground state wavefunctions of the interacting theory, and more generally, prepare scattering states of the interacting theory. This was solved in the JLP papers by using adiabatic evolution. Consider a one dimensional system to evolve from the ground state with  $\lambda = 0$  to the ground state with  $\lambda \neq 0$ ,

$$\begin{aligned} H_i &= \frac{1}{2}\hat{\Pi}^2 + \frac{1}{2}m^2\hat{\phi}^2 \\ H_f &= \frac{1}{2}\hat{\Pi}^2 + \frac{1}{2}m^2\hat{\phi}^2 + \frac{\lambda}{4}\hat{\phi}^4 \quad , \end{aligned} \quad (177)$$

where unitary evolution will be performed on the initially-prepared ground state wavefunction of  $H_i$  to adiabatically evolve it to the ground state of  $H_f$  via some path in a parameter space of a fictitious “time”  $s$  from  $s = 0$  to  $s = S$ ,

$$\begin{aligned} H(s) &= A(s)H_i + B(s)H_f \\ A(0) &= 1 \quad , \quad B(0) = 0 \quad , \quad A(S) = 0 \quad , \quad B(S) = 1 \quad , \quad A(s) + B(s) = 1 \quad , \end{aligned} \quad (178)$$

which is equivalent, in this case, to evolving the quartic coupling,  $\lambda(s)$  from  $\lambda(0) = 0$  to  $\lambda(S) = \lambda$ . This is sometimes called “adiabatic switching”.

The evolved wavefunction is of the form

$$|\psi(S)\rangle = \mathcal{P} \left[ e^{-i \int_0^S ds \hat{H}(s)} \right] |\psi(0)\rangle \quad , \quad (179)$$

where the path-ordering operator is the same as time-ordering if  $s$  were a time variable. Performing a Trotter expansion of this evolution operator with respect to  $s$ , over  $s$ -intervals that are small compared to the “change of the Hamiltonian”, this evolved wavefunction becomes,

$$|\psi(S)\rangle = \hat{U}(S, S - \delta s) \hat{U}(S - \delta s, S - 2\delta s) \dots \hat{U}(\delta s, 0) |\psi(0)\rangle + \mathcal{O}(\delta s) \quad , \quad (180)$$

where we require that

$$\delta s \langle \psi(s) | \frac{\delta \hat{H}(s)}{\delta s} | \psi(s) \rangle \ll 1 , \quad (181)$$

The adiabatic theorem tells us that after the evolution, the system will be in the ground state of the interacting theory, with quantifiable systematic errors. The physics behind the adiabatic evolution is well known to us. The Hamiltonian must change sufficiently slowly that the modes supporting the observable(s) of interest have time to "sample" the slightly modified Hamiltonian over enough time to "adjust" themselves. Notice that this conditions is related to variation of the expectation value of the variation of the Hamiltonian in the state of interest. It is not in some generic state, but the specific target state. Once again, this is pointing toward an effective field theory analysis and mindset. This is well known technology, and within QIS systematic errors are now being fully quantified.

Every physical system of interest, has a different spectrum, and hence has a different construction that will be required in order to evolve from a state that can be easily prepared on a device, to the one that has the full set of target interactions, that takes us beyond the limits of classical computing. While we can derive compelling analytic expressions that provide guides to estimating errors, reliable computation will require tuning for each system to determine the necessary decimation of the path in s-space to arrive at the ground state of the target theory with the precision that we require (to perform the desired computations with the target precision (specified by the science objective)). To say a few more words on this subject that connect to adiabatic evolution in other systems, we can consider a general system, and instantaneous eigenstates. Under adiabatic evolution, the wavefunction of the evolving system can be written in terms of the instantaneous eigenstates of the system multiplied by complex phases,

$$\begin{aligned} \hat{H}(t) |\psi_n(t)\rangle &= E_n(t) |\psi_n(t)\rangle , \quad |\psi(t)\rangle = \sum_n c_n(t) |\psi_n(t)\rangle \\ c_k(t) &= c_k(0) e^{-i\theta_k(t)} e^{-i\gamma_k(t)} , \end{aligned} \quad (182)$$

where the two phases originate from two different aspects of the evolution

$$\theta_k(t) = \int_0^t dt' E_k(t') , \quad (183)$$

where  $\theta_k(t)$  is the phase that one expects to arrive at from naively extending time-independent evolution. However, the naivety has lead to an error, as there is a further contribution from the time-evolution of the instantaneous state itself,

$$\gamma_k(t) = -i \int_0^t dt' \langle \psi_k | \dot{\psi}_k \rangle(t') , \quad (184)$$

being Berry's phase. Many interesting things are possible by integrating the wavefunction around paths that bring it back to itself, but that is beyond what we are discussing at the moment. Because  $|\dot{\psi}_k\rangle$  has to be imaginary to preserve unitarity, the extra factor of  $i$  ensures that  $\gamma$  is real.

To provide some more intuition about adiabatic evolution, and some unusual features that can result and potentially be useful, in the next section we consider *Adiabatic Evolution and Dark States*.

### 3. Dark States from Adiabatic Evolution

Dark states are important generally in QIS systems, with interesting physics emerging from adiabatic evolution of Hamiltonia. Let us consider them in the context of spin-systems (to provide a

concrete example), and more broadly, in the context of quantum computers and communication. In particular, their potential use in the (somewhat stealthy) movement of information within a quantum system. This is sufficiently bizarre and interesting that it might have applications for simulating quantum field theories, but this remains to be determined.

Lets start by considering a systems of 3 spins in a quantum register with a total z-component of spin  $s_z = \frac{1}{2}$ . The possible basis states for this system are (and I am changing notation from binary to " $\uparrow$ " and " $\downarrow$ "),

$$\text{basis} = \{ |\downarrow\uparrow\uparrow\rangle, |\uparrow\downarrow\uparrow\rangle, |\uparrow\uparrow\downarrow\rangle \} , \quad (185)$$

that are evolved by a time-dependent Hamiltonian of the form,

$$H(t) = K(t) \frac{1}{2} (\hat{X}_1 \hat{X}_2 + \hat{Y}_1 \hat{Y}_2) + L(t) \frac{1}{2} (\hat{X}_2 \hat{X}_3 + \hat{Y}_2 \hat{Y}_3) . \quad (186)$$

The Hamiltonian is slowly evolved in time from one nearest-neighbor interaction (2-3) to the other nearest-neighbor interaction (1-2), while at no time is there a 1-3 interaction, i.e., only local interactions present.

The action of the operators on any of the basis states is well understood and simple,

$$\begin{aligned} \hat{O}|\uparrow\downarrow\rangle &= |\downarrow\uparrow\rangle, \quad \hat{O}|\downarrow\uparrow\rangle = |\uparrow\downarrow\rangle, \quad \hat{O}|\downarrow\downarrow\rangle = 0, \quad \hat{O}|\uparrow\uparrow\rangle = 0, \\ \hat{O} &= \frac{1}{2} (\hat{X}\hat{X} + \hat{Y}\hat{Y}) = \hat{\sigma}^+ \hat{\sigma}^- + \hat{\sigma}^- \hat{\sigma}^+, \end{aligned} \quad (187)$$

from the relations to ladder operators,  $\hat{X} = \hat{\sigma}^- + \hat{\sigma}^+$  and  $\hat{Y} = i(\hat{\sigma}^- - \hat{\sigma}^+)$ .

To analyze this system, we begin by determining the instantaneous eigenstates of the Hamiltonian at any given time,  $t$ ,

$$\hat{H}(t)|\psi_n(t)\rangle = \begin{pmatrix} 0 & K(t) & 0 \\ K(t) & 0 & L(t) \\ 0 & L(t) & 0 \end{pmatrix} \begin{pmatrix} \alpha(t) \\ \beta(t) \\ \gamma(t) \end{pmatrix} = E_n(t)|\psi_n(t)\rangle , \quad (188)$$

where  $n = 1, 2, 3$ , and  $\alpha, \beta, \gamma$  are the (time-dependent) coefficients of the basis states. The eigenvalues of the Hamiltonian matrix are  $\lambda = 0, \pm\sqrt{K^2 + L^2} = 0, \pm F$ , with eigenvectors,

$$\psi_{+F} = \frac{1}{F\sqrt{2}} \begin{pmatrix} K \\ +F \\ L \end{pmatrix}, \quad \psi_0 = \frac{1}{F} \begin{pmatrix} L \\ 0 \\ -K \end{pmatrix}, \quad \psi_{-F} = \frac{1}{F\sqrt{2}} \begin{pmatrix} K \\ -F \\ L \end{pmatrix}. \quad (189)$$

The physics we working toward is the following: if we initially prepare the system in the  $E = 0$  state, and adiabatically evolve from  $L = F, K = 0$  to  $K = F, L = 0$ , then the  $\downarrow$  will move from site-1 to site-3, without it ever being in site-2. This is despite the fact that there are only ever two-body interactions, both involving site-2!! This seems quite counter-intuitive, but is in fact well known.

Let us make this more explicit via a gauge transformation between basis states. To change bases from the coordinate basis give in Eq. (185), to the basis defined by the instantaneous eigenstates, we perform a unitary transformation defined by the instantaneous eigenvectors,

$$\begin{aligned} \hat{U}_0 \hat{H} \hat{U}_0^\dagger &= \begin{pmatrix} +F & 0 & 0 \\ 0 & 0 & 0 \\ 0 & 0 & -F \end{pmatrix}, \quad \hat{U}_0 = \frac{1}{F\sqrt{2}} \begin{pmatrix} K & F & L \\ \sqrt{2}L & 0 & -\sqrt{2}K \\ K & -F & L \end{pmatrix} \\ \Phi_{\text{adiab}} &= \begin{pmatrix} c_{+F} \\ c_0 \\ c_{-F} \end{pmatrix} = \hat{U}_0 \psi . \end{aligned} \quad (190)$$

The coefficients  $c_i$  in  $\Phi_{\text{adiab}}$  are defined in the basis of instantaneous eigenstates,

$$\{ |\psi_{+F}\rangle, |\psi_0\rangle, |\psi_{-F}\rangle \} , \quad (191)$$

and are the amplitudes of the instantaneous eigenstates in any given wavefunction written in terms of the spin-basis in Eq. (185). The equations of motion for  $\Phi_{\text{adiab}}$  are found from

$$\begin{aligned} (i\partial_t - \hat{H})\psi &= 0, \\ \hat{U}_0 (i\partial_t - \hat{H})\hat{U}_0^\dagger \hat{U}_0\psi &= 0, \\ (i\partial_t - \hat{U}_0 \hat{H} \hat{U}_0^\dagger + i\hat{U}_0 \partial_t \hat{U}_0^\dagger) \Phi_{\text{adiab}} &= (i\partial_t - \hat{H}_{\text{adiab}}) \Phi_{\text{adiab}} = 0 . \end{aligned} \quad (192)$$

Explicit evaluation gives, where we have defined the constrained evolution such that  $\partial_t F^2 = K\partial_t K + L\partial_t L = 0$ ,

$$i\hat{U}_0 \partial_t \hat{U}_0^\dagger = \frac{i}{\sqrt{2}F^2} \begin{pmatrix} 0 & K\partial_t L - L\partial_t K & 0 \\ L\partial_t K - K\partial_t L & 0 & L\partial_t K - K\partial_t L \\ 0 & K\partial_t L - L\partial_t K & 0 \end{pmatrix} . \quad (193)$$

Defining a variable  $\gamma$  using  $\tan \gamma = K/L$ , we have that  $F^2 \partial_t \gamma = L\partial_t K - K\partial_t L$ ,<sup>36</sup> and hence

$$i\hat{U}_0 \partial_t \hat{U}_0^\dagger = -\frac{i\partial_t \gamma}{\sqrt{2}} \begin{pmatrix} 0 & 1 & 0 \\ -1 & 0 & -1 \\ 0 & 1 & 0 \end{pmatrix} , \quad (195)$$

leading to

$$\hat{H}_{\text{adiab}} = \begin{pmatrix} +F & -\frac{i\partial_t \gamma}{\sqrt{2}} & 0 \\ \frac{i\partial_t \gamma}{\sqrt{2}} & 0 & \frac{i\partial_t \gamma}{\sqrt{2}} \\ 0 & -\frac{i\partial_t \gamma}{\sqrt{2}} & -F \end{pmatrix} . \quad (196)$$

As expected, the when the time derivative is small compared to the gaps between the eigenstates, the loss from the instantaneous eigenstates is suppressed.

Specifically, if the system is initially in the  $E = 0$  state and slowly evolved, it will remain in the  $E = 0$  state as  $\partial_t \gamma / F \rightarrow 0$ ,

$$\psi_0 = \frac{1}{F} \begin{pmatrix} L \\ 0 \\ -K \end{pmatrix} , \quad (197)$$

which evolves adiabatically from

$$\psi_0(0) = \begin{pmatrix} 1 \\ 0 \\ 0 \end{pmatrix} \rightarrow \psi_0(\infty) = \begin{pmatrix} 0 \\ 0 \\ -1 \end{pmatrix} . \quad (198)$$

---

<sup>36</sup> Writing the relation in terms of the angle makes the system straightforward to consider geometrically, including

$$\partial_t \tan \gamma = \frac{\partial_t K}{L} - \frac{K\partial_t L}{L^2} = \frac{\partial_t \gamma}{\cos^2 \gamma} = \frac{F^2}{L^2} \partial_t \gamma . \quad (194)$$

The subtle point about this evolution is that at no time during the evolution is there an amplitude to be found in the second spin-basis state. To give concrete examples, consider the Hamiltonian matrix and evolution operator (Trotterized)

$$\begin{aligned}\hat{H}(t) &= \begin{pmatrix} 0 & \kappa t & 0 \\ \kappa t & 0 & 1 - \kappa t \\ 0 & 1 - \kappa t & 0 \end{pmatrix} \\ \hat{U}(T = 1/\kappa) &= \prod_{n=0}^{n=T/\delta t} e^{-iH(n\delta t)\delta t} ,\end{aligned}\quad (199)$$

which is a linear time evolution of the Hamiltonian from beginning to end. The system is then evaluated at times between  $t = 0, 1/\kappa$ . Starting in  $\psi_0$ , the results for  $\kappa = 0.05$  and  $\delta t = 0.5$ , and hence 40 steps to complete the transition, are shown in Fig. 26, along with the evolution using two other values  $\kappa$ . One sees that the probability of site-2 being  $\downarrow$  diminishes with decreasing  $\kappa$ , as

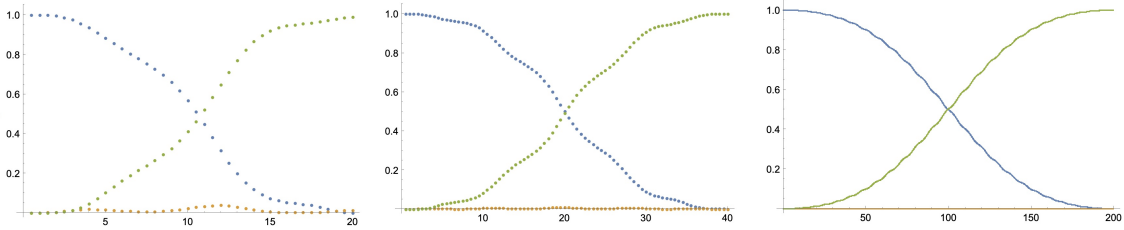


FIG. 26: The probabilities of finding the system in each of the states as a function of normalized transition time. Left panel shows  $\kappa = 0.05$ , middle panel shows  $\kappa = 0.025$  and right panel shows  $\kappa = 0.005$ .

expected.

This is the concept of a Dark State. The Hamiltonian does not couple 1-3, and only couples 1-2 and 2-3, yet during adiabatic evolution of the Hamiltonian from all one type of coupling to all of the other type of coupling, the wavefunction evolves from site-1 to site-3 with vanishing amplitude at site-2 for all times. If you only had access to site-2, you would never know that the quantum information is passing through site-2 in transiting from site-1 to site-3. This concept is used in communication, and is termed a **3-Spin 1-Leaf-Node**

Generalizing this to 4-spins, and generically higher, consider a Hamiltonian of the form

$$\hat{H} = \begin{pmatrix} 0 & K & 0 & 0 \\ K & 0 & L & L \\ 0 & L & 0 & 0 \\ 0 & L & 0 & 0 \end{pmatrix} , \quad (200)$$

in the basis

$$\text{basis} = \{ |\downarrow\uparrow\uparrow\rangle, |\uparrow\downarrow\uparrow\rangle, |\uparrow\uparrow\downarrow\rangle, |\uparrow\uparrow\uparrow\downarrow\rangle \} , \quad (201)$$

where is comprised of spin interactions, generalizing the Hamiltonian we considered for 3 spins, but in a particular way. The spin of the 4th site is also couple to the 2nd site, and not to the 3rd, i.e. we have 1-2, 2-3, 2-4 couplings (i.e., the connectivity is beginning to look like a leaf or tree). The instantaneous eigenvectors of this Hamiltonian are

$$\begin{aligned}v_1 &= \frac{1}{\sqrt{2}F_2} ( 2L, 0, -K, -K )^T , \quad v_2 = \frac{1}{\sqrt{2}} ( 0, 0, 1, -1 )^T , \\ v_3 &= \frac{1}{\sqrt{2}F_2} ( K, -F_2, L, L )^T , \quad v_4 = \frac{1}{\sqrt{2}F_2} ( K, +F_2, L, L )^T ,\end{aligned}\quad (202)$$

with  $F_2 = \sqrt{K^2 + 2L^2}$ , and with eigenvalues,  $0, 0, -F_2, +F_2$ , respectively. As such linear combinations of  $v_{1,2}$  are also eigenvectors. In analogy with the 3-spin system,  $v_1$  is a Dark State for this 4-spin system. The initial state  $v_{1i} = |\downarrow\uparrow\uparrow\uparrow\rangle$  adiabatically evolves into the entangled state

$$v_{1f} = \frac{1}{\sqrt{2}} (|\uparrow\uparrow\downarrow\uparrow\rangle + |\uparrow\uparrow\uparrow\downarrow\rangle) , \quad (203)$$

without any spin-down amplitude at site-2 (the "node" of the leafing/treeing). This is a **4-Spin 2-Leaf-Node** configuration.

### J. Wavepacket Preparation in Lattice Scalar Field Theory (Jordan, Lee, Preskill [2])

If we wish to determine scattering matrix elements and dynamics from quantum simulations (in Minkowski space), a situation/configuration has to be set up that resembles corresponding experiments that would be performed in the laboratory. That is to say, just like experiments performed at colliders or fixed-target experiments, a well-defined initial state that has localized packets in momentum space and position space is created, and then evolved forward in time till the configurations move through an interaction region and once again are well separated. At CERN, or RHIC, this involves colliding beams of high-energy protons or nuclei with highly instrumented regions of spacetime, in which members of the two ensembles interact with each other, in many instances in a highly-inelastic process to produce a final state of many particles with a distribution of energy and momenta. These particles leave the collision region and enter the detection regions. Ultimately, we wish to perform simulations of these entire processes from beginning to end, to include quantum coherence and entanglement, and we are now starting down that path. For our purposes, we need to understand basic elements of what is required to initialize one wavepacket and two isolated wavepackets in the interacting field theory.

Our previous discussions and developments, have indicated the path we should take/start down, and that is to identify a localized wavepacket in the non-interacting theory, and then adiabatically evolved it from the non-interacting theory to interacting theory. This is the path that JLP developed in their seminal paper. Lets again work with a lattice field theory in 1-dim for simplicity, where we know that the vacuum state is given by

$$\begin{aligned} |\psi_{\text{gs}}\rangle &= |\psi_{\chi_0}\rangle_0 \otimes |\psi_{\chi_1}\rangle_0 \otimes |\psi_{\chi_2}\rangle_0 \otimes \dots |\psi_{\chi_{L-1}}\rangle_0 \\ \langle \chi_0, \chi_1, \dots \chi_{L-1} | \psi_{\text{gs}} \rangle &= \frac{(\det \mathbf{E})^{1/4}}{\pi^{L/4}} e^{-\frac{1}{2} \boldsymbol{\chi}^T \mathbf{E} \boldsymbol{\chi}} \\ \langle \phi_0, \phi_1, \dots \phi_{L-1} | \psi_{\text{gs}} \rangle &= \frac{(\det \mathbf{K})^{1/4}}{\pi^{L/4}} e^{-\frac{1}{2} \boldsymbol{\phi}^T \mathbf{K} \boldsymbol{\phi}} , \end{aligned} \quad (204)$$

where  $\mathbf{E}$  is the diagonal matrix of energy eigenvalues following the lattice dispersion relation. Therefore, the wavefunction in momentum space is a product of Gaussians with different widths. A single particle state of definite momentum, and hence maximally indefinite location, is one in which one of the momentum space HOs is excited with a single quanta, e.g.,

$$|p\rangle \sim a^\dagger(p) |\psi_{\text{gs}}\rangle \sim |\psi_{\chi_0}\rangle_0 \otimes |\psi_{\chi_1}\rangle_0 \otimes \dots |\psi_{\chi_p}\rangle_1 \otimes \dots |\psi_{\chi_{L-1}}\rangle_0 , \quad (205)$$

where the field operator,  $\phi(x)$ , is defined in terms of these annihilation and creation operators,

$$\begin{aligned} \phi(x) &= \int \frac{dk}{(2\pi) 2\omega_k} \left( a(k) e^{-ikx} + a^\dagger(k) e^{ikx} \right) , \\ \left[ a(k), a^\dagger(q) \right] &= (2\pi) 2\omega_k \delta(k - q) . \end{aligned} \quad (206)$$

This is true for any allowed momentum in the spatial volume. Therefore, the most general single particle state is a linear superposition of momentum eigenstates,

$$|\Psi\rangle = \int \frac{dk}{(2\pi) 2\omega_k} g(k) a^\dagger(k) |\psi_{gs}\rangle , \quad (207)$$

for some function  $g(k)$  that we are free to choose. Keep in mind that this is the most general **single**-particle state (in the non-interacting theory). It is straightforward to show that  $\langle p|\Psi\rangle = g(p)$  where  $|p\rangle = a^\dagger(p)|0\rangle$ .

Given that the momentum-space wavefunctions are,

$$\langle \chi|n\rangle = \psi(\chi) = \frac{1}{\sqrt{2^n n!}} \left( \frac{E_p}{\pi} \right)^{1/4} e^{-\frac{1}{2} E_p \chi^2} H_n \left( \sqrt{E_p} \chi \right) , \quad (208)$$

the only modification to the wavefunction with the additional quanta is a replacement of the form,  $H_0(\sqrt{E_p} \chi_p) \rightarrow H_1(\sqrt{E_p} \chi_p)$  (and recalling that  $H_0(x) = 1$ ).

The profile in momentum space that we would like is such that the particles lie within some resolution of the beam energy,  $\Delta p$ . Choosing, **for example**, a localized momentum-space profile of the form,

$$g(k; p) \sim e^{-\frac{1}{2}(k-p)^2/\sigma_p^2} , \quad (209)$$

and switching back to discrete (latticized) system, the  $\chi$ -space wavefunction becomes

$$\langle \chi_0, \chi_1, \dots, \chi_{L-1} | \psi_{1;g} \rangle \sim e^{-\frac{1}{2} \mathbf{x}^T \mathbf{E} \mathbf{x}} \sum_k g(k; p) H_1 \left( \sqrt{E_k} \chi_k \right) , \quad (210)$$

and the field space wavefunction can be recovered, as before,

$$\chi_k = \frac{1}{\sqrt{L}} \sum_{j=0}^{L-1} \phi_j e^{-ikj} , \quad \mathbf{x} = \mathbf{V} \cdot \boldsymbol{\phi} , \quad \mathbf{V} = \frac{1}{\sqrt{L}} e^{-i\mathbf{k} \cdot \mathbf{j}} . \quad (211)$$

With the localized profile in momentum space, a wavefunction that is localized in  $\phi$  space will result from a Fourier Transform, with appropriate complex phases, with a width that is set by  $1/\sigma_p$  in Eq. (209).

This is quite a useful expression and relation to have. While we have not presented quantum circuits to initialize complex functions onto a quantum register directly (nothing in principle stopping this), we have discussed initializing real functions. So, in the spatial volume (not conjugate momentum space), we can initialize the momentum space wavefunction and then QFT back to  $\phi$ -space. This might violate some of the features we have been expounding upon that permits efficient computation, but this is likely not the case. As a wavepacket is localized in  $\phi$ -space, not all of the lattice volume has to be modified, only the sites where there is support. So we will only seek to modify a finite region of the lattice volume, which will introduce truncation error set by the  $1/\sigma_p$ .

In reality, in a simulation, a significant amount of effort will be required to tune the system so that wavepackets are isolated prior to collision, that the time between initialization and collision is sufficiently short that the packets have not spread "too much" before classical impact.

To arrive at a wavepacket in the interacting theory, a wavepacket in the noninteracting theory is first constructed in  $\phi$ -space, as just described. Now, unlike the vacuum state, which is an eigenstate of the Hamiltonian, the wavepacket is not, and it evolves in time, beyond a simple time-dependent phase. This makes preparation of the wavepacket a little more complicated.

Lets return to non-relativistic quantum mechanics, and consider the evolution of a simple 1-dim wavepacket. Such a state could be,

$$|\psi(0)\rangle \sim \int \frac{dk}{(2\pi)^3} g(k) |k\rangle = \int \frac{dk}{(2\pi)^3} e^{-\frac{1}{2}k^2/\sigma^2} |k\rangle , \quad (212)$$

where  $g(k)$  is a function localized in momentum space, for instance a Gaussian. Under time evolution of a free (non-interacting) Hamiltonian, this evolves to

$$|\psi(t)\rangle = \hat{U}(t)|\psi(0)\rangle = \int \frac{dk}{(2\pi)^3} e^{-itk^2/(2m)} e^{-\frac{1}{2}k^2/\sigma^2} |k\rangle \sim \frac{1}{\sqrt{1+it\sigma^2/m}} , \quad (213)$$

which corresponds to a system with a width that is increasing with time. As we know from the usual spreading of wavepackets. On the other hand if we did little steps forward and little steps backward in time, then we would not have changed the width of the wavepacket at all!

$$|\psi(t)\rangle = \hat{U}(\delta t)\hat{U}(-\delta t)\dots\hat{U}(\delta t)|\psi(0)\rangle , \quad T = \sum_n \delta t , \quad (214)$$

where the system is evolved over a total time duration of  $T$ . So, for adiabatic evolution, the system is evolved forward and backward in time, while switching the Hamiltonian, which will take the system into the interacting theory, but without damaging the initial localization of the wavepacket **too much**. The amount of (unwanted) spreading of the wavepacket can be quantified, and naturally depends on the size of  $\delta t$ . For instance, for linear evolution (as a simple example),

$$e^{-i\delta t(\hat{H}_0\frac{\delta t}{T}+(1-\frac{\delta t}{T})\hat{H}_I)} \dots e^{+i\delta t(\hat{H}_0(1-3\frac{\delta t}{T})+3\frac{\delta t}{T}\hat{H}_I)} e^{-i\delta t(\hat{H}_0(1-2\frac{\delta t}{T})+2\frac{\delta t}{T}\hat{H}_I)} e^{+i\delta t(\hat{H}_0(1-\frac{\delta t}{T})+\frac{\delta t}{T}\hat{H}_I)} e^{-i\delta t\hat{H}_0} \quad (215)$$

for sufficiently large  $T$ , and sufficiently small  $\delta t$ , the system is evolved adiabatically from a wavepacket in  $H_0$  which we know how to prepare efficiently, to one of the interacting theory  $H_I$ , which we do not know how to directly prepare. As long as the Hamiltonian is "nice", this is a method that can be used to prepare a localized wavepacket in  $\lambda\phi^4$ .

To determine S-matrix elements, preparation of two localized wavepackets that have equal and opposite momenta and are well-separated from each other (so that they collide at some point in the future) is required. The fact that they are localized and the vacuum state is translationally invariant, means that they can both be prepared without interference, either in momentum space, or by direct construction on  $\phi$ -space. Corrections to the construction of the second wavepacket are additive to the error of preparing the first wavepacket (as the system initially is a tensor product).

This is a brief description of wavepacket preparation. At this point in time, efforts are being made to prepare wavepackets in quantum simulations, both using quantum simulators and computers. Successful demonstrations have been shown in spin- $\frac{1}{2}$  systems.

## K. Particle Detection and S-Matrix Elements (Jordan, Lee, Preskill [2])

In the previous sections, we sketched how to initialize one or more tensor-product wavepackets in an interacting theory, with the intent of preparing states on a quantum device that can be used to simulate particle scattering and enable the computation of S-matrix elements. After initializing our quantum register, the system is evolved forward in time well beyond the classical time required for the center of the wavepackets to coincide, corresponding to a classical scattering time, and long enough for the scattering states to evolve into non-interacting localized states.

We know from our non-relativistic quantum mechanics experience that the cross-sections, and hence S-matrix elements, can be determined from the ratio of particle fluxes entering our detectors

to the fluxes entering the collision(s). This is easy to visualize for elastic processes, for instance neutron-proton or electron-electron scattering, but becomes “messy” when considering the collision of two 100 TeV protons, which gives rise to jets which subsequently fragment into hadrons, with the possibility of thousands of pions being produced. Nonetheless, ratios of fluxes at asymptotically-large distances into a given solid-angle (or, equivalently, penetrating a region of the surface of a large sphere around the scattering center) is sufficient (neglecting infrared complications with massless particles, such as photons, in this discussion .... that can be handled).

One way to think about this is that our quantum simulation is simply mimicking the real world, and we should incorporate “detectors”<sup>37</sup> into our simulations that operate in the same way as experimental detectors. For example, in some region of the simulation, we could have a set of qubits connected to an “ammeter” that records the amount of current “entering the qubits”, which is then promptly removed from the simulation. This would be the measure of flux entering the “detectors”. This is not how we do things at the moment, as detectors are complicated many-body systems themselves, but is currently one of the forefront matters being considered for next generation simulations.

It is helpful to think again in 1-dim. Imagine we have evolved through a collision and want to know “what happened”. One way to answer this is to recognize the fact that once the particles/wavepackets have separated, we can adiabatically return to the non-interacting theory and ask about the population of all of the momentum eigenstates. Reversing the process used to create the incident wavepackets will reveal a generally complicated occupation of states in momentum space. At late times, all wavepackets will be far from the scattering center and far from themselves, and there is meaning to selecting sub-regions of the spatial volume to quantum Fourier transform for analysis in momentum space. This also has not yet been accomplished in a quantum simulation. So there is an enormous amount of creativity that remains to be delivered into designing detection algorithms for efficient quantum simulations of scattering in important systems in nuclear and particle physics. And once again, much of this thinking was already anticipated in the work of JLP.

## V. TIME EVOLUTION OF QUANTUM SYSTEMS

One of the major “jumps forward” in simulation enabled by quantum computing is the time evolution of quantum many-body systems, including quantum field theories. Being efficient for quantum computers, it resides in the **BQP** complexity class, making it, in some sense, the easy part of a quantum simulation (with state preparation, generically residing in **QMA** being the difficult part formally). There are a number of distinct approaches to time evolution, but at the heart is a commonality of discretizing time. As a result, there are different optimizations that can be done that depend upon what you want to accomplish, and in particular, it is important to know what you want to do/have at the end of a simulation.

Time discretization is nothing new, it is a fundamental part of any classical or quantum simulation. For classical lattice field theory simulations that are carried out in Euclidean space, there are both isotropic and an-isotropic lattices that are used. An anisotropic discretization is conceptually “nicer” as it involves a finer resolution of time, but has challenges associated with tuning the increased number of lattice parameters, the increased computational cost of more lattice sites, and modifications to the Symanzik action or other methods to systematically mitigate discretization artifacts. The discussion is essentially the same for quantum simulations, but with quantum

---

<sup>37</sup> We are imagining systems of qubits or qudits that have functionality of a particle detector.

devices currently at a more primitive stage of development, equivalent algorithms suitable for ideal quantum devices behave differently on current, NISQ-era, hardware.

Conceptually, in time evolution, we wish to be able to perform a finite set of quantum operations on an initial state (that has already been prepared), and evolve the initial state into a final state that is within  $\epsilon$  (to be defined) of the target quantum state, corresponding to an application of the exact time evolution operator (of nature),

$$\begin{aligned} |\psi(t)\rangle_{\Delta T, \text{device}} &= \hat{U}_{\Delta T, \text{device}} |\psi(0)\rangle \\ |\psi(t)\rangle_{\text{nature}} &= \hat{U}_{\text{nature}} |\psi(0)\rangle \\ \|\ |\psi(t)\rangle_{\Delta T, \text{device}} - |\psi(t)\rangle_{\text{nature}} \| &\leq \mathcal{O}(\epsilon) , \end{aligned} \quad (216)$$

where we need to define what we mean by  $\|\ |\chi\rangle \|$ . Implicit in this construction is the assumption that the initial state is prepared within  $\mathcal{O}(\epsilon)$  of the target initial state. From the viewpoint of a team of scientists, developers and engineers interested in simulating a set of observables, for instance within some energy interval, it is not obvious that this is in fact the correct metric to guide the development of quantum simulations for a given scientific application, and in fact it generally is not.

Typically, in scientific communities, there are one or more programs with well-defined scientific objectives defined by current understanding and estimated paths forward to improve understanding and predictive capabilities. This is a community understanding, at some level, arising from available and planned experimental facilities and expected data sets during the near-term. This loosely defines sets of simulations that are desirable to perform in order to best optimize the scientific impact of overall program. Thus, the relevant metrics for computation are set by the appropriate observables during the near-term period, and their required precision, as defined by a complete, robust and reproducible quantification of uncertainties.<sup>38</sup> Therefore, it is the scientific objectives that provide the targets for simulations, and it is the required/target uncertainties in a set of observables that drives the algorithm and computational hardware development. This is of course, greatly enhanced by contributions from developers, computer scientists and so forth, but the generic arguments and scaling of generic problems that define some of the discussions must give way to discussions of "what is required" to obtain a limited number of specialized quantities with target precisions. That is to say that, it is the science program that defines sets of observables  $\{\mathcal{O}_i\}$  with target precisions  $\{\epsilon_i^{\text{target}}\}$  to be determined within a certain time frame through simulation. This means that not only do the (quantum) simulations be completed by then, but also the formal framework and error-analysis protocols all be in place to be able to robustly estimate the  $\{\epsilon_i^{\text{compute}}\}$ .

Let us consider the potential impact of an "EFT-oriented thinking" on how to proceed. We know that all of the theories that we have identified as describing nature are EFTs, including the SM of particle physics. This means that there is a limited range of applicability of the theory, outside of which predictions become unreliable and deviate from observations of nature. For lattice simulations, the UV cut-off imposed by the lattice spacing provides an energy scale near and above which the results of simulations are unrelated to the target theory/real world. Far below the UV

---

<sup>38</sup> As with experiment, computations and simulations require independent verification and validation. This means that sufficient resources must be available to independent teams of scientists working on the same set of problems, and that codes are not shared until fully-verified and validated, algorithms should be different where possible (made challenging by differing resource requirements), and activities should be "stove-piped" as much as possible. In addition, while challenging and involving significant overhead, it is important to employ *blinding* in simulations to mitigate the ever-present sociological pressures to produce "the best result" defined by the smallest error-bar, particularly a concern for simulations aimed at verification with experimental data. In some sense, the quantum equivalent of this "phenomenon" can already be seen in the drive toward quantum advantage.

cut off, they are expected to become arbitrarily close to nature as the simulation is systematically improved. This indicates, that we do not need to know the wavefunction in the UV, and only need to have good control over the IR components, up to an energy scale relevant to the observables of interest. Further, generic statements about the deviation of the wavefunction and scalings are only relevant as far as they impact observables of interest.<sup>39</sup>

### A. Trotterized Time Evolution

In an ideal world, we would be able to construct "the" evolution operator,  $\hat{U}(t)$  defined over some macroscopic time scale(s), and evolve our system forward in a single application. A challenge to this is that the exponentiation of an operator includes an arbitrary number of applications, and generally, for QCD, this moves from short-distance nearest-neighbor interactions that are well known in terms of quarks and gluons, to the structure of nuclear and materials that are non-trivial complex quantum many-body systems with phases that depend on external macroscopic conditions. As such, it is overly optimistic for us to expect to be able to develop an efficient single-application evolution operator. But we do expect that once we know that form of the dynamics, we can perform a finite set of operations on our system and approximate the actual dynamics of the system. We also know that the challenge in simulating quantum systems, as Feynman made clear, is that entanglement and coherence are attributes that make classical computation difficult, and are attributes that also present challenges for quantum simulations. Thus, the challenge is to identify a set of finite steps of time evolution to arrive at a desired final state within the prescribed error budget.

Our present experience in simulating (very) small instances of lattice quantum field theories repeatedly show that the simplest approach to time evolution is usually, and quite surprisingly, the "best" approach. Let us consider the simplest path forward - **Trotter Evolution**. If we have a Hamiltonian that maps efficiently into a quantum circuit (and we can figure out what that is), then the evolution can be implemented without time-discretization, and then that is all we need to know to time evolve our system without introducing further errors. If the Hamiltonian is comprised of a series of operators that do not commute, then generally we do not know how to efficiently find a quantum circuit for time evolution, and we break down the evolution into a series of steps that approximate the true evolution, and which can be systematically improved. Before considering the general case, let us consider two such operators, as we have previously discussed in the context of lattice scalar field theory, and a Hamiltonian of the form  $\hat{H} = \hat{K} + \hat{V}$ , corresponding to kinetic and potential energy terms. The evolution operator can be approximated by

$$\begin{aligned}\hat{U}(t) &= e^{-i\hat{H}t} = 1 - i\hat{H}t - \frac{1}{2}\hat{H}^2t^2 - \frac{i}{3!}\hat{H}^3t^3 + \dots \\ &= 1 - i(\hat{K} + \hat{V})t - \frac{1}{2}(\hat{K}^2 + \hat{V}^2 + \hat{K}\hat{V} + \hat{V}\hat{K})t^2 - \frac{i}{3!}(\hat{K} + \hat{V})^3t^3 + \dots .\end{aligned}\quad (217)$$

---

<sup>39</sup> Somewhat of an analog in classical computing can be found in comparing the performance of, say, `linpack` Vs application code performance. They are not unrelated, but for a domain scientist, the priority is the performance of the application code, generically the *time to solution*. Further, it is generally the case that a specialized code written to determine specific observables will outperform code written for general applicability to many different problems - an empirical fact of life.

If we do not know the circuit for  $e^{-it\hat{H}}$ , but do know circuits for  $e^{-it\hat{V}}$  and  $e^{-it\hat{K}}$ , then,

$$\begin{aligned}
 \hat{U}_{\hat{V}}(t) &= e^{-i\hat{V}t} = 1 - i\hat{V}t - \frac{1}{2}\hat{V}^2t^2 - \frac{i}{3!}\hat{V}^3t^3 + \dots \\
 \hat{U}_{\hat{K}}(t) &= e^{-i\hat{K}t} = 1 - i\hat{K}t - \frac{1}{2}\hat{K}^2t^2 - \frac{i}{3!}\hat{K}^3t^3 + \dots \\
 \hat{U}_{\hat{K}}(t)\hat{U}_{\hat{V}}(t) &= 1 - i(\hat{K} + \hat{V})t - \frac{1}{2}(\hat{K}^2 + \hat{V}^2 + 2\hat{K}\hat{V})t^2 + \dots \\
 &= 1 - i(\hat{K} + \hat{V})t - \frac{1}{2}(\hat{K}^2 + \hat{V}^2 + \hat{K}\hat{V} + \hat{V}\hat{K} + [\hat{K}, \hat{V}])t^2 + \dots \\
 &= e^{-i(\hat{K} + \hat{V})t} e^{-\frac{t^2}{2}[\hat{K}, \hat{V}]} + \mathcal{O}(t^3), \\
 &= e^{-i[(\hat{K} + \hat{V})t - i\frac{t^2}{2}[\hat{K}, \hat{V}]]} + \mathcal{O}(t^3). \tag{218}
 \end{aligned}$$

At small times, this product of operators reproduces the desired unitary evolution, but becomes arbitrarily incorrect at large times (defined by internal time scales). By splitting the argument of the exponential, the time evolution is that of a time dependent Hamiltonian with an extra term given by the commutator.

Consider the application of these circuits multiple times, with incremental time steps, during the desired time interval,

$$\begin{aligned}
 \hat{U}_{\hat{K}}(\delta t)\hat{U}_{\hat{V}}(\delta t) &= e^{-i[(\hat{K} + \hat{V})\delta t - i\frac{(\delta t)^2}{2}[\hat{K}, \hat{V}]]} + \mathcal{O}((\delta t)^3), \\
 &= 1 - i(\hat{K} + \hat{V})\delta t - \frac{(\delta t)^2}{2}(\hat{K} + \hat{V})^2 - \frac{(\delta t)^2}{2}[\hat{K}, \hat{V}], \\
 [\hat{U}_{\hat{K}}(\delta t)\hat{U}_{\hat{V}}(\delta t)]^n &= 1 - i(\hat{K} + \hat{V})n\delta t - n\frac{(\delta t)^2}{2}(\hat{K} + \hat{V})^2 - n\frac{(\delta t)^2}{2}[\hat{K}, \hat{V}] - \frac{n(n-1)}{2}(\hat{K} + \hat{V})^2(\delta t)^2 + \mathcal{O}((\delta t)^3) \\
 &= 1 - i(\hat{K} + \hat{V})n\delta t - \frac{(n\delta t)^2}{2}(\hat{K} + \hat{V})^2 - \frac{(n\delta t)^2}{2n}[\hat{K}, \hat{V}] + \mathcal{O}((\delta t)^3) \\
 \left[\hat{U}_{\hat{K}}\left(\frac{T}{n}\right)\hat{U}_{\hat{V}}\left(\frac{T}{n}\right)\right]^n &= e^{-i(\hat{K} + \hat{V})T - [\hat{K}, \hat{V}]\frac{T^2}{2n}} + \dots, \quad \delta t = T/n. \tag{219}
 \end{aligned}$$

By doing this we have reduced the magnitude of the commutator term by  $1/n$ , the number of Trotter steps. This is great news!! But now a dose of reality.

Typically, when implementing the circuits for  $\hat{K}, \hat{V}$ , there are two-qubit entangling gates in one or both. These are one of the limiting factors in NISQ-era hardware - the entangling gates are relatively lower-fidelity and take longer to implement. This means that simulation outputs are noisier, and that circuit depths are limited by the number of entangling operations that can be implemented while the device is coherent. There are ways for mitigating the former, and recent results have demonstrated that error-correction protocols can lengthen coherence times. Therefore, there is a practical limit to the number of Trotter steps that can be applied for a given process on any given quantum device. With an infinite number of Trotter steps, the wavefunction can be recovered with precision that scales as  $1/N_{\text{Trotter}}$  in principle. To keep track of quantum resource costs, if  $\hat{K}, \hat{V}$  require  $N_{\hat{K}}^{c\times}, N_{\hat{V}}^{c\times}$  CNOTs respectively, then  $N_{\text{Trotter}}$  requires  $N_{\text{Trotter}}(N_{\hat{K}}^{c\times} + N_{\hat{V}}^{c\times})$  CNOTs total, and produces a result with a theory-systematic fractional error that scales as  $T/N_{\text{Trotter}} = \Delta T$ . Importantly, for a given Trotter step, the systematic error is not anticipated to increase with increasing number of applications, but as we have just discussed, the device error will grow to the point of failure at some number of time steps (where failure denotes obtaining results that no longer are related to the actual system being simulated). Figure 27 provides a classical simulation of the resulting total error resulting from Trotter errors and statistically distributed circuit element errors

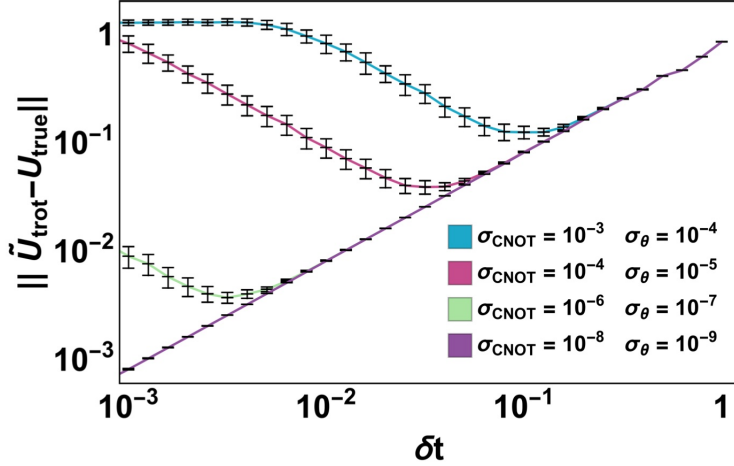


FIG. 17: Distance measure (Schatten 1-norm) between the noisily-Trotterized and exactly-digitized time evolution operator (after step (3) and (1) of Fig. 1, respectively) as a function of the Trotter step size,  $\delta t$ , for an integrated evolution time of  $T_f = 1$ . The noisy, first-order Trotterized propagator,  $\hat{U}_{\text{trot}}$  is implemented with sampled error rates on 1- and 2-qubit gates set by  $\sigma_\theta$  and  $\sigma_{\text{CNOT}}$ , respectively. The digitization scheme is defined by  $n_Q = 3$  and  $\bar{\phi}_{\max} = 3.0$ . From right-to-left, the calculations deviate from the ideal result in the top-to-bottom order of the legend with the last calculation at  $\sigma_{\text{CNOT}} = 10^{-8}$  maintaining visual agreement for the entire plotted domain.

FIG. 27: The overall Trotterization error from a circuit with non-zero CNOT errors [1].

in a particular model that was considered in work with Natalie Klco [1]. From the Fig. 27 caption (from the paper), the Schatten 1-norm was used to define the error in the evolution. Typically, when considering the errors in evolving a quantum system, a norm of the error (i.e. a metric) is required to define how well or how poorly the evolution is actually reproducing the true system evolution. For the case at hand, the difference between unitary operators (which is not unitary) is useful, and the Schatten p-norm for the difference of evolution operators is a measure of distance between what we have and what we want,

$$\begin{aligned} d\hat{U} &= \hat{U}_{\text{Trott.}} - \hat{U}_{\text{exact}} \\ \|d\hat{U}\|_p &= \left( \text{Tr}|d\hat{U}|^p \right)^{1/p}, \end{aligned} \quad (220)$$

and we have chosen to use the 1-norm.

In the above development, we chose an initial ordering of  $\hat{U}_{\hat{K}}(\frac{T}{n}) \hat{U}_{\hat{V}}(\frac{T}{n})$ , but in fact this choice was arbitrary - there is no physics reason motivating this choice, and so the other ordering, for instance, has exactly the same resource requirement <sup>40</sup>, and gives

$$\left[ \hat{U}_{\hat{V}}\left(\frac{T}{n}\right) \hat{U}_{\hat{K}}\left(\frac{T}{n}\right) \right]^n = e^{-i(\hat{K}+\hat{V})T + [\hat{K}, \hat{V}] \frac{T^2}{2n}} + \dots, \quad (221)$$

where the commutator contributes with the opposite sign. The difference between these results can be used to provide an estimate for the magnitude of Trotter errors.

<sup>40</sup> This is not complete true, as circuit elements in the last step that do not alter probabilities can be dropped in some cases.

This also points us toward another way of thinking about mitigating such Trotter errors. We can imagine a situation where we alternate, with 50% probability which circuit ordering we run for each member of the ensemble, say  $10^3$  shots. So observables that are computed with the two different wavefunctions will differ by the commutator, with a "+" or "-" sign depending on which is chosen, and the average value of the observable across the ensemble will not have linear dependence on the commutator,

$$\begin{aligned}\langle O \rangle_{\text{ensemble}} &= \frac{1}{2} \langle O(1 + \mathcal{O}(\hat{K}, \hat{V}) \frac{T^2}{n}) \rangle + \frac{1}{2} \langle O(1 - \mathcal{O}(\hat{K}, \hat{V}) \frac{T^2}{n}) \rangle + \dots \\ &= \langle O \rangle + \dots .\end{aligned}\quad (222)$$

While this is correct, it now relies on statistical averaging over all the members of the ensemble, and not in correcting each member of the ensemble. If the distributions of results are too wide (as defined by how much the evolution operator wraps around the circle), then this averaging will be slowly converging and potentially pathological, with the potential to wrap around the circle leading to catastrophic failure of the method. It is better to try to mitigate theory errors for each member of the ensemble if this is practical. Presently, we can run using millions of shots and a thousands CNOT gates,<sup>41</sup> so statistical methods are currently being pursued (if you have enough money). These include transforming coherent errors into statistical errors via *Pauli-Twirling*, which has been shown to be very effective.

Extending this LO Trotter analysis to 3 operators, it is easy to show that

$$\left[ \hat{U}_{\hat{A}}\left(\frac{T}{n}\right) \hat{U}_{\hat{B}}\left(\frac{T}{n}\right) \hat{U}_{\hat{C}}\left(\frac{T}{n}\right) \right]^n = e^{-i(\hat{A}+\hat{B}+\hat{C})T - [\hat{A},\hat{B}] \frac{T^2}{2n} - [\hat{A},\hat{C}] \frac{T^2}{2n} - [\hat{B},\hat{C}] \frac{T^2}{2n}} + \dots , \quad (223)$$

which generalizes to an arbitrary Hamiltonian comprised of  $N_{\text{ops}}$  terms to,

$$\begin{aligned}\hat{H} &= \sum_j h_j \\ \left( \prod_j e^{-ih_j T/n} \right)^n &= \left( e^{-ih_1 T/n} e^{-ih_2 T/n} \dots e^{-ih_{N_{\text{ops}}} T/n} \right)^n \\ &= e^{-iT\hat{H}-\frac{T^2}{2n}\sum_{j>i}[\hat{h}_i,\hat{h}_j]} + \dots .\end{aligned}\quad (224)$$

As the number of operators contributing to the Hamiltonian grows, so does the expected magnitude of the error envelope, determined by the sum of commutators.

## B. Higher-Order Trotterization

In the previous section, the behavior and convergence of LO Trotterization, and the potential for sampling techniques to mitigate some Trotter errors were explored. In this section, systematic mitigation(s) of Trotter errors for each member of the ensemble is developed. This is a subject that has been studied extensively in the literature. There are a number of effective techniques available, and reality dictates that each method should be evaluated for each problem at hand. For introductions to these methods, see Refs. [66–68].

---

<sup>41</sup> Up until 2023, circuits with hundreds of CNOT gates were possible, after error mitigation. This changed at the end of 2023, where it became possible to implement thousands of CNOT gates. See, for example, recent work by IQuS [65].

Building upon LO Trotter evolution, linear thinking leads directly to formulating the cancellation of commutators in the Trotter expansion. From above, LO Trotter evolution is enacted by,

$$\left[ \hat{U}_{\hat{K}}\left(\frac{T}{n}\right) \hat{U}_{\hat{V}}\left(\frac{T}{n}\right) \right]^n = e^{-i(\hat{K}+\hat{V})T - [\hat{K},\hat{V}]\frac{T^2}{2n}} + \dots , \quad (225)$$

and assuming that we know the commutator and an associated quantum circuit can be designed that is efficient,

$$\left[ \hat{U}_{\hat{K}}\left(\frac{T}{n}\right) \hat{U}_{\hat{V}}\left(\frac{T}{n}\right) \right]^n e^{+[\hat{K},\hat{V}]\frac{T^2}{2n}} = e^{-i(\hat{K}+\hat{V})T} + \dots . \quad (226)$$

If this is available to us, then this is effective, but generally, the commutators are complicated and their associated quantum circuits are unable to be efficiently constructed. Examples of such implementations on quantum computers have been demonstrated and are effective.

Perhaps the most straightforward improvement can be achieved by using 2nd-order (next-to-leading order, NLO) Trotterization, in which,

$$\begin{aligned} S_2(t) &= \hat{U}_{\hat{K}}(t/2)\hat{U}_{\hat{V}}(t)\hat{U}_{\hat{K}}(t/2) = 1 - i(\hat{K} + \hat{V})t - \frac{1}{2}(\hat{K}^2 + \hat{V}^2 + \hat{K}\hat{V} + \hat{V}\hat{K})t^2 + \dots \\ &= 1 - i(\hat{K} + \hat{V})t - \frac{1}{2}(\hat{K} + \hat{V})^2 t^2 + \dots \\ &= e^{-i(\hat{K}+\hat{V})t} + \mathcal{O}(t^3) = e^{-i(\hat{K}+\hat{V})t + R_3 t^3 + R_5 t^5} + \dots . \end{aligned} \quad (227)$$

The systematic error from Trotterization has been parametrically reduced by splitting one of the unitary operators. This requires more circuit elements, but the circuits are already known from LO, and we can make a choice as to which to split, and thus typically the one with the fewer entangling gates is chosen.

This NLO result straightforwardly generalizes to multiple operators,

$$\begin{aligned} \hat{H} &= \sum_j h_j \\ \hat{U}(t) &\rightarrow \left( e^{-ih_{N_{ops}}T/n/2} \dots e^{-ih_2T/n/2} e^{-ih_1T/n} e^{-ih_2T/n/2} \dots e^{-ih_{N_{ops}}T/n/2} \right)^n , \end{aligned} \quad (228)$$

with NLO errors that scale as  $T^3/n^2$  (as opposed to  $T^2/n$  at LO). This procedure can be used to systematically eliminate successively higher-order Trotter errors, to NNLO and higher, and this has been studied extensively.

Consider the following,

$$S_{4,a}(t) = S_2(st) \cdot S_2((1-2s)t) \cdot S_2(st) , \quad (229)$$

where  $S_2$  is defined in Eq. (227), and determine if there is a value of  $s$  for which the evolution is further parametrically improved. Multiplying out the exponentials to sufficiently high orders reveals

$$S_{4,a}(t) = S_2(st) \cdot S_2((1-2s)t) \cdot S_2(st) = e^{-i(\hat{K}+\hat{V})t + t^3 R_3(2s^3 + (1-2s)^3) + t^5 R_5} + \dots , \quad (230)$$

and so there is a value of  $s$  for which the coefficient of  $t^3 R_3$  vanishes,

$$2s^3 + (1-2s)^3 = 0 , \quad 2^{1/3}s = 2s - 1 , \quad s = \frac{1}{2 - 2^{1/3}} = 1.351207192 = s_0 , \quad (231)$$

which then provides an evolution operator of the form

$$S_{4,a}(t) = S_2(s_0 t).S_2((1 - 2s_0)t).S_2(s_0 t) = e^{-i(\hat{K} + \hat{V})t + t^5 R_5} + \dots . \quad (232)$$

It is interesting to think about the form of this a little more. With  $s_0 = 1.3512 > 0.5$ , there is a relative sign in the evolution operators in the product  $S_2(s_0 t).S_2((1 - 2s_0)t).S_2(s_0 t)$ . The first evolution goes beyond the time that is required, the 2nd goes backward by a large amount, and the third forward to the desired time,  $t$ .

We can go further and consider another 4th order corrected discretization, via <sup>42</sup>

$$S_{4,b}(t) = [S_2(st)]^2.S_2((1 - 4s)t).[S_2(st)]^2 = e^{-i(\hat{K} + \hat{V})t + t^5 R_5} + \dots , \quad (233)$$

where solutions to

$$4s^3 + (1 - 4s)^3 = 0, \quad 4^{1/3}s = 4s - 1, \quad s = \frac{1}{4 - 4^{1/3}} = 0.41449077 = s_1 , \quad (234)$$

are required. Here, the terms in the product of operators do not overshoot the target time, all of the evolution lies between  $t = 0$  and  $t = t$ . The extension to higher orders is now clear, so for instance,

$$S_6(t) = S_4(st)^2.S_4((1 - 4s)t).S_4(st)^2 = e^{-i(\hat{K} + \hat{V})t + t^7 R_7} + \dots , \quad (235)$$

where now instead of solving a cubic polynomial, we are required to solve a quintic polynomial.

An interesting corollary, if you will, is related to mapping out group spaces, by implementing unitary evolution via commutators. It follows straightforwardly from what we have already done

$$\begin{aligned} \hat{U}_{\hat{K}}(t)\hat{U}_{\hat{V}}(t) &= e^{-i[(\hat{K} + \hat{V})t + i\frac{t^2}{2}[\hat{K}, \hat{V}]]} + \mathcal{O}(t^3) \\ \hat{U}_{\hat{K}}(-t)\hat{U}_{\hat{V}}(-t)\hat{U}_{\hat{K}}(t)\hat{U}_{\hat{V}}(t) &= e^{t^2[\hat{K}, \hat{V}]} + \mathcal{O}(t^3) , \end{aligned} \quad (236)$$

from which we see that we can actually exploit the non-commutativity if we so desire.

### C. Randomly-Ordered Trotterization

Our previous discussion naturally leads toward considering statistical methods that evolves each member of the ensemble in ways that are determined statistically and without bias. As the corrections to Trotter evolution involve commutators of operators, we expect that the ensemble average of randomly ordered unitaries will provide estimates of operators that are closer to the true value than from any one particular ordering of operators.

The algorithm for implementing this is straightforward. The time interval is decimated into time steps,  $\Delta T = T/n$ , and each ordering of the evolution operator is selected at random,

$$\hat{U}_{\mathbf{a}^i}(\Delta T) = \hat{U}_{a_1^i}(\Delta T)\hat{U}_{a_2^i}(\Delta T)\dots\hat{U}_{a_K^i}(\Delta T) , \quad \hat{H} = \sum_j^K h_j , \quad (237)$$

for  $K$  operators comprising the Hamiltonian. For each element of the ensemble and random ordering of the  $K$  operators is chosen, by  $\{\mathbf{a}^i\}$ , from which observables are computed and stored,

---

<sup>42</sup> Keep in mind that  $S_2(st)$  is nonlinear in time.

giving rise to an ensemble of observables. Ideally, this would be repeated at least  $K!$  times **per Trotter step** to begin to have sampling of all possible  $K!$  orderings of operators. As the number of Trotter steps grows, the number of samples increases linearly.

This scheme is quite effective compared to other schemes that you might imagine. One reason for this is because, at each sample, it is the other of operators that is selected randomly and not the operators themselves. That is to say that each operator appears once and only once at each Trotter step, and situations such as only having one operator contribute multiple times is excluded.

As a concrete example of this evolution, consider the evolution of a single plaquette of SU(3) Yang-Mills flux truncated at the **8** irreducible representation, with Hamiltonian,

$$H = \frac{g^2}{2} \begin{pmatrix} 0 & 0 & 0 \\ 0 & \frac{16}{3} & 0 \\ 0 & 0 & 12 \end{pmatrix} + \frac{3}{g^2} \hat{I}_3 - \frac{1}{2g^2} \begin{pmatrix} 0 & \sqrt{2} & 0 \\ \sqrt{2} & 1 & \sqrt{2} \\ 0 & 0\sqrt{2} & 0 \end{pmatrix}, \quad (238)$$

At each Trotter step, a random triplet of integers is created that denotes the ordering of the three operators. The observables computed are the vacuum-to-vacuum amplitude and the energy in the electric field, starting from an empty vacuum states. For the sake of demonstration, the strong coupling has been set to  $g = 1$ . Figure 28 shows the results of the evolution for exact fixed-order Trotter and statistically-ordered Trotter evolution. For a large enough Trotter step,

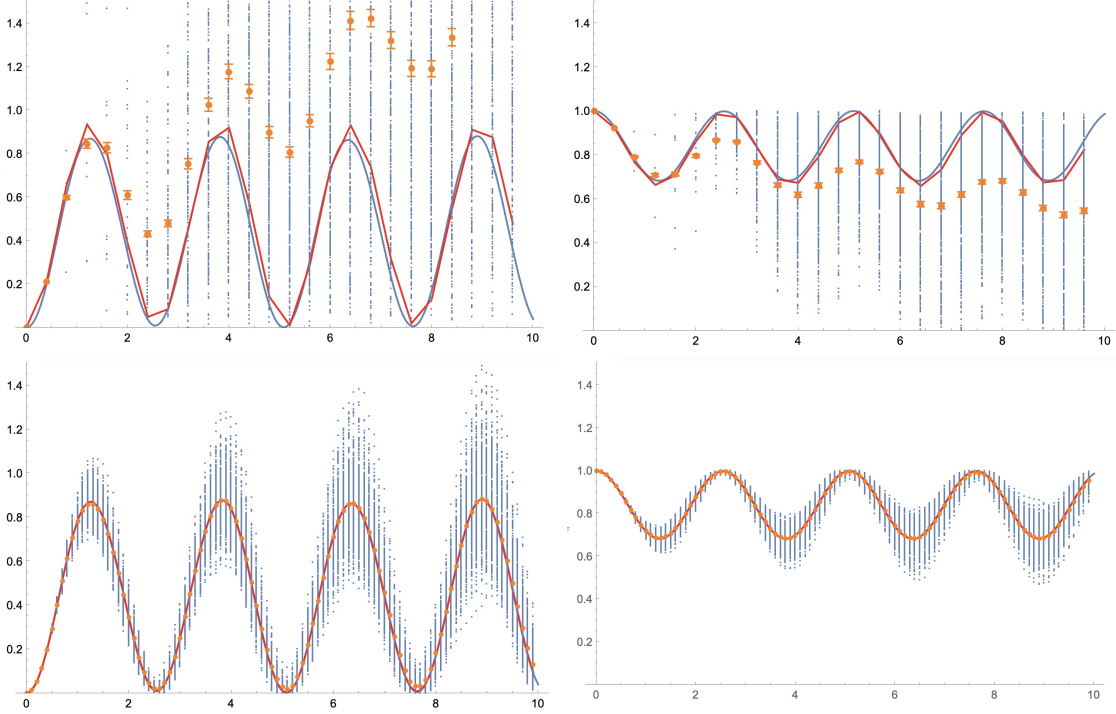


FIG. 28: Statistical sampling of the Trotterized evolution operator associated with one plaquette of SU(3) Yang-Mills flux truncated at **8** (as given in Eq. (238)) for  $\Delta T = 0.4$  (upper panels) and  $\Delta T = 0.1$  (lower panels). The left panels show the energy in the electric field and the right panels show the vacuum-to-vacuum persistence probability. The solid blue lines are the exact time evolution, while the red curves correspond to the result from a fixed-ordering LO Trotter evolution. The blue points correspond to the results obtained by statistically sampling the Trotter ordering at each Trotter step, i.e., a different order for each student step, for 400 evolution trajectories. The orange points with error bars correspond to the mean of the 400 trajectories.

the statistically-ordered sampling with generate samples that *warp around the circle* resulting in

statistically averaging an ensemble with a sign problem and mean zero. This corresponds to loss of any meaningful quantum evolution. Decreasing step size will bring the sampling to within an arc of the circle, allowing for a meaningful mean and variance to be determined. This behavior is becoming visible in the results displayed in Fig. 28.

#### D. qDrift [3]

Trotterized time evolution provides one way to evolve an ensemble of states forward in time. The quantum circuit required to perform a macroscopic time step generally require super-polynomial amounts of classical computing to determine, i.e., to determine the rotations angles of a general  $SU(2^{nQ})$  circuit, but circuits for implementing much smaller circuits associated with smaller components of the Hamiltonian can typically be found. The quantum state resulting from their implementation becomes increasingly close to the target wavefunction as the time steps become smaller, but with the associated cost of increasing numbers of circuit elements/operations. In the NISQ-era, we have noisy quantum devices of intermediate scale with short (but increasing) coherence times, but with gate-application times that permit large numbers of measurements, particularly for the superconducting devices. Therefore, it is possible to “trade off” the circuit depth for the ensemble size in a way to minimize the over all error in the measurement of one or more observables. This, once again, is an example of tuning that can be done prior to large-scale production.

One should keep in mind when trading off the quantum-volume of simulations with the size of the ensemble that one (very loosely speaking) is on the path toward classical statistical Monte-Carlo sampling to evaluate observables of the quantum system, and the pathologies of classical evaluations of quantum observables that have led us toward quantum simulations become increasingly present. These include sign problems and signal-to-noise problems.

The essential issue that we face with decimated time evolution is made clear in LO Trotter,

$$\begin{aligned}\hat{U}_1 &= \hat{U}_{\hat{K}}(t)\hat{U}_{\hat{V}}(t) = e^{-i[(\hat{K}+\hat{V})t+i\frac{t^2}{2}[\hat{K},\hat{V}]] + \mathcal{O}(t^3)} , \\ \hat{U}_2 &= \hat{U}_{\hat{V}}(t)\hat{U}_{\hat{K}}(t) = e^{-i[(\hat{K}+\hat{V})t-i\frac{t^2}{2}[\hat{K},\hat{V}]] + \mathcal{O}(t^3)} ,\end{aligned}\quad (239)$$

and the differences between the operator orderings is a hint as to how we may be able to systematically reduce their impact in estimating observables.

One such mitigation strategy is **qDrift** [3]. The qDrift protocol, created by Earl Campbell is one (nice) way to accomplish an ensemble averaging of the evolution operator at each time step that reduces systematic errors introduced by Trotterization. Working with a Hamiltonian of the form,

$$\hat{H} = \sum_j h_j \hat{H}_j , \quad (240)$$

where the coefficients of the terms,  $h_j$  are defined so that the largest eigenvalue of  $\hat{H}_j$  is unity. Generally, the commutators of the operator set are unknown or unrealistically challenging to determine, and as such it is impractical to work to higher orders in a Trotterized expansion as we examined previously. When the operator set becomes large, it also becomes impossible to identify a unique, or a set of optimal, orderings of operators to minimize the Trotter error. However under unbiased sampling of orderings, the mean value of expectation values of observables should reproduce the expected ensemble average without decimation, as the contributions from commutators will statistically average to zero.

A probability distribution is created for the operator set defined by the coefficients defining the Hamiltonian in Eq. (240). The probability of selecting  $\hat{H}_j$ , normalized by the sum of the  $h_j$ , is

$$p_j = \frac{h_j}{\Lambda} , \quad \Lambda = \sum_j h_j . \quad (241)$$

For each member of the ensemble, and at each time-step, a classical computer is used to select  $\hat{H}_j$ , using the probability distribution defined by the  $p_j$ , to produce a sequence of  $N$  ordered  $j$ 's to form the product of unitary operators,

$$\hat{U}_{\mathbf{j}}(t) = \prod_j e^{-i\Lambda \hat{H}_j t/N} . \quad (242)$$

The subscript on  $\hat{U}_{\mathbf{j}}(t)$  denotes the fact that this product results from one set of samplings of the probability distribution. Notice that the time steps are now  $t/N$ , where  $N$  is the number of times that operators are selected during the interval, meaning that each operator is used to evolve the system forward over a time interval  $\delta t = t/N$ . This construction is such that effective the path integral is being performed, over the time interval  $t$  that is divided into  $N$  steps. It turns out that to reach a target error in the evolution,  $\epsilon$ , the number of steps scales as

$$N = \frac{2\Lambda^2 t^2}{\epsilon} , \quad (243)$$

resulting from the diffusion-like nature of the evolution. Note that the number of decimations scales as  $1/\epsilon$  as opposed to a naive estimate of  $1/\epsilon^2$ . For any realistic simulation, the resulting statistical distribution of such a process has to be examined and tuned - both for the time-step  $t$  and the number of qDrift steps. While this is a formally convergent protocol, there are a number of limitations that are encountered when this algorithm is implemented.

For the systems that we have explored qDrift, mainly simulations of the low-dimensional field theories, it performs less well than Trotter evolution for finite statistics because the fluctuations at the time intervals practical today are too large. It is possible, and perhaps likely, that for simulations of the future with higher fidelity gates and qubits, that this could become a preferred algorithm.

Figure 29 shows the same example as we considered above but including the results from the qDrift algorithm. In this analysis of qDrift I did not decrease the sampling step by the number of operators and increase the operator density corresponding. The reason for this is the increase in circuit depth, which I wanted to keep to be comparable for the two methods. Clearly, by decreasing the Trotter step for each operator to increase the sampling rate leads to estimates that are closer to the true value. One of the defects of minimal-qDrift is that there is a non-zero probability of the same operator appearing many times, and in fact all of the time, which leads to extreme outlying trajectories. There have been a number of suggestions for improving this, including constraining the total time duration that any operator can appear to be to that of its expected value.

### E. Linear Combination of Unitaries (LCUs)

The Linear Combination of Unitaries (LCU) protocol was introduced 10 years ago by Andrew Childs and Nathan Wiebe [69]. It is of broad applicability in a number of contexts, but most notably in time evolution. The main point is that the sum of unitary operators is generically not a unitary operator itself, and as such cannot be implemented directly in a quantum circuit. However, insight in this method is that it can be implemented if the system is embedded into a larger

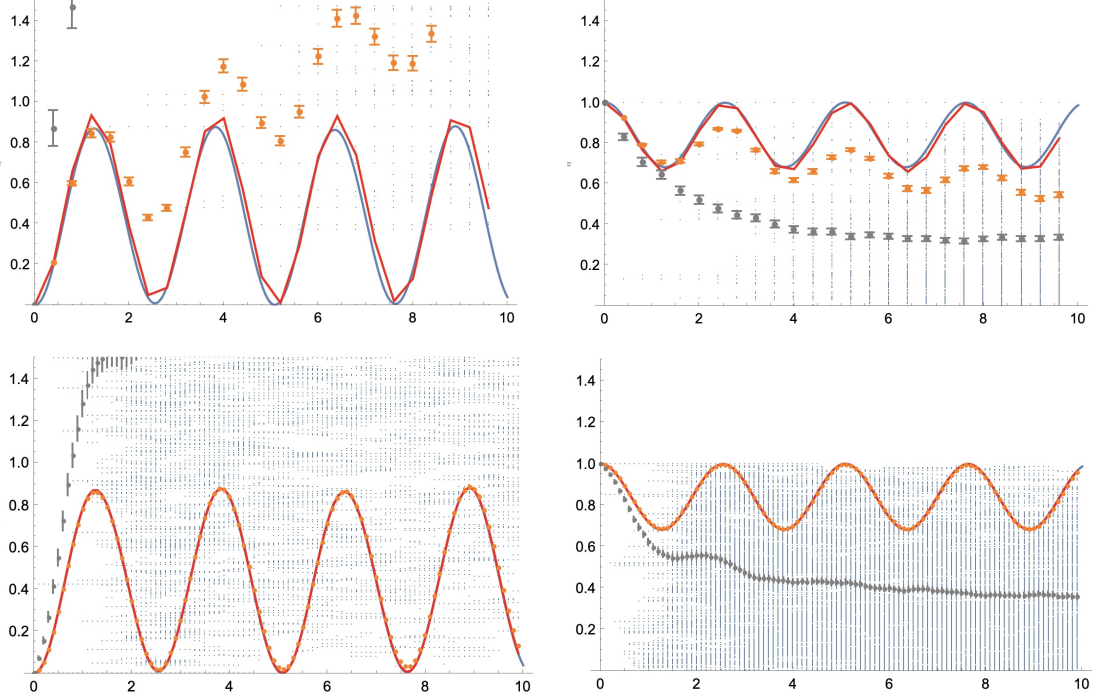


FIG. 29: qDrift sampling of the Trotterized evolution operator associated with one plaquette of SU(3) Yang-Mills flux truncated at 8 (as given in Eq. (238)) for  $\Delta T = 0.4$  (upper panels) and  $\Delta T = 0.1$  (lower panels). The left panels show the energy in the electric field and the right panels show the vacuum-to-vacuum persistence probability. The solid blue lines are the exact time evolution, while the red curves correspond to the result from a fixed-ordering LO Trotter evolution. The blue points correspond to the results obtained by qDrift sampling the Trotter ordering at each Trotter step. The gray points with error bars correspond to the mean of the 400 trajectories. The operator sampling rate is the same for the two analyses, where nominally, in the qDrift algorithm, the sampling rate (and hence inverse step size) should be increased by the number of operators.

system and unitary transformations are performed within the larger system, and measurements are performed on the parts of the system outside of the one of interest (of ancilla qubits). An important aspect of this approach is that it starts us thinking about the impact and potential utility of projective measurements at the end, or during, quantum simulations, which are now well known to be an effective element of quantum computation.

Consider a simple example of how this algorithm works in the context of LO Trotter evolution, one that we have discussed previously. Two unitary operators that give rise to LO Trotter evolution are,

$$\begin{aligned}\hat{U}_1 &= \hat{U}_{\hat{K}}(t)\hat{U}_{\hat{V}}(t) = e^{-i[(\hat{K}+\hat{V})t+i\frac{t^2}{2}[\hat{K},\hat{V}]]} + \mathcal{O}(t^3) \\ \hat{U}_2 &= \hat{U}_{\hat{V}}(t)\hat{U}_{\hat{K}}(t) = e^{-i[(\hat{K}+\hat{V})t-i\frac{t^2}{2}[\hat{K},\hat{V}]]} + \mathcal{O}(t^3) .\end{aligned}\quad (244)$$

If their average could be formed, it would parametrically reduce the systematic error in LO Trotter evolution, where the leading impact of the commutator would be eliminated, i.e.,

$$\frac{1}{2} \left[ \hat{U}_{\hat{K}}(t)\hat{U}_{\hat{V}}(t) + \hat{U}_{\hat{V}}(t)\hat{U}_{\hat{K}}(t) \right] = e^{-i(\hat{K}+\hat{V})t} + \mathcal{O}(t^3) .\quad (245)$$

To be able to construct a linear combination of the two unitaries  $\hat{U}_{1,2}$ , one ancilla qubit is added, expanding the system from  $n_Q$  qubits to  $n_Q + 1$  qubits. A single qubit rotation operator in

the ancilla space is also added, and controlled-unitaries in the physical space, see Fig. 30 (where the use of "V" as a circuit element is not to be confused with the potential energy term in the Hamiltonian). Stepping through this circuit, with an ancillary unitary of the form

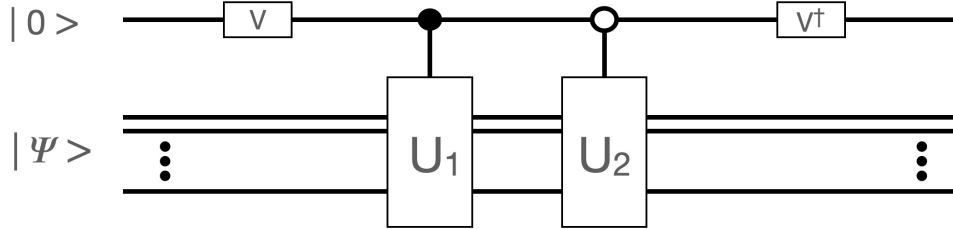


FIG. 30: A circuit to implement a linear combination of two unitaries using an ancilla qubit.

$$V = \begin{pmatrix} \sqrt{\frac{\lambda}{\lambda+1}} & -\sqrt{\frac{1}{\lambda+1}} \\ \sqrt{\frac{1}{\lambda+1}} & \sqrt{\frac{\lambda}{\lambda+1}} \end{pmatrix}$$

$$V|0\rangle = \sqrt{\frac{\lambda}{\lambda+1}}|0\rangle + \sqrt{\frac{1}{\lambda+1}}|1\rangle , \quad V|1\rangle = -\sqrt{\frac{1}{\lambda+1}}|0\rangle + \sqrt{\frac{\lambda}{\lambda+1}}|1\rangle , \quad (246)$$

such that the action of this circuit is

$$\begin{aligned} |0\rangle \otimes |\psi\rangle &\rightarrow \left( \sqrt{\frac{\lambda}{\lambda+1}}|0\rangle + \sqrt{\frac{1}{\lambda+1}}|1\rangle \right) \otimes |\psi\rangle \\ &\rightarrow \sqrt{\frac{\lambda}{\lambda+1}}|0\rangle \otimes |\psi\rangle + \sqrt{\frac{1}{\lambda+1}}|1\rangle \otimes \hat{U}_1|\psi\rangle \\ &\rightarrow \sqrt{\frac{\lambda}{\lambda+1}}|0\rangle \otimes \hat{U}_2|\psi\rangle + \sqrt{\frac{1}{\lambda+1}}|1\rangle \otimes \hat{U}_1|\psi\rangle \\ &\rightarrow \sqrt{\frac{\lambda}{\lambda+1}} \left( \sqrt{\frac{\lambda}{\lambda+1}}|0\rangle - \sqrt{\frac{1}{\lambda+1}}|1\rangle \right) \otimes \hat{U}_2|\psi\rangle + \sqrt{\frac{1}{\lambda+1}} \left( \sqrt{\frac{1}{\lambda+1}}|0\rangle + \sqrt{\frac{\lambda}{\lambda+1}}|1\rangle \right) \otimes \hat{U}_1|\psi\rangle \\ &\rightarrow \frac{1}{\lambda+1}|0\rangle \otimes (\lambda\hat{U}_2 + \hat{U}_1)|\psi\rangle + \frac{\sqrt{\lambda}}{\lambda+1}|1\rangle \otimes (\hat{U}_1 - \hat{U}_2)|\psi\rangle . \end{aligned} \quad (247)$$

By measuring the ancilla qubit, and only keeping members of the ensemble that measure  $|0\rangle$ , the wavefunction in the physical system has collapsed to

$$|\psi_f\rangle \rightarrow \alpha |0\rangle \otimes (\lambda\hat{U}_2 + \hat{U}_1)|\psi\rangle , \quad (248)$$

where  $\alpha$  is the appropriate normalization constant. For the case that we are interested in,  $\lambda = 1$  accomplished by a rotation of the ancilla around the y-axis by  $\theta = \frac{\pi}{2}$ . As the controls used to form combinations of the physical systems do not alter the ancilla qubit, this rotation gives rise to a 50% probability a measurement of the ancilla yielding a 0 or a 1.

It is not difficult to imagine how this method generalizes to linear combinations of multiple unitaries controlled by multiple ancillas, with/requiring "state preparation" in the ancillar space along the lines that we have discussed previously for scalar field theory.

### F. Quantum Imaginary Time Evolution (QITE)

Another creative algorithm for time evolution, that is related to, but different from, LCU, which can be used in the state-preparation of the physical system that parallels algorithms that are used for classical computing is Quantum Imaginary Time Evolution (QITE). One of the challenges for quantum simulation, that we have discussed, is state preparation, and the fact that it generically resides in **QMA** complexity class, putting generic preparation of an arbitrary systems naively beyond the capabilities of quantum computers. There has been increasing progress exploring QITE, for example, see Ref. [70].

One finds unitary operators in a larger space that, through entangling operations with the ancilla space and subsequent measurement(s), allows for non-unitary operators on the physical (subsystem) space, at the cost of having a probability of success that is less than unity. As you might imagine, all of the important elements of QITE are in the control/ancilla sector. We start by defining a non-unitary operator and embedding it into a larger space and identifying a unitary operator in the larger space,

$$\begin{aligned} \hat{Q} &= \frac{e^{-(H-E_o)\tau}}{\sqrt{\hat{I} + e^{-2(H-E_o)\tau}}} = A(\tau) e^{-(H-E_o)\tau} \rightarrow e^{-(H-E_o)\tau} \\ \hat{U}(\tau) &= \begin{pmatrix} \hat{Q}(\tau) & A(\tau) \\ A(\tau) & -Q(\tau) \end{pmatrix} = \hat{Z} \otimes \hat{Q}(\tau) + \hat{X} \otimes \hat{A}(\tau) , \end{aligned} \quad (249)$$

where  $E_o$  is an *offset* energy that is tuned for the calculation, but with  $E_o \lesssim E_{gs}$ . Clearly,  $\hat{Q}$  is not a unitary operator because at large  $\tau$  it behaves as the exponential of the ground state for  $E_o = 0$ , but  $\hat{U}^\dagger \hat{U} = \hat{I}$  !!. Application of  $\hat{U}$  to the combined system gives (for the ancilla prepared in the initial state  $|0\rangle$ ),

$$\hat{U}(\tau)|0\rangle \otimes |\psi\rangle = |0\rangle \otimes \hat{Q}(\tau)|\psi\rangle + |1\rangle \otimes \hat{A}(\tau)|\psi\rangle , \quad (250)$$

and thus performing a measurement of the ancilla qubit collapses the wavefunction down to

$$|\psi_f\rangle \rightarrow \alpha |0\rangle \otimes \hat{Q}(\tau)|\psi\rangle , \quad (251)$$

with a normalization factor  $\alpha$  (unrelated to previous usages) and hence one has generated system that is evolved in imaginary time, shifting it toward the ground state. The non-unitary nature of evolution in the physical space is implemented by the non-unitary nature of quantum measurement [71].

The probability for success of this process, defined by the fraction of events in the ancilla with  $|0\rangle$ , depends upon the spectrum of the physical system, and tunings are required to increase this probability to make the algorithm feasible with finite resources and finite fidelities, particularly for unknown systems. Thus, if a wavefunction can be initialized in the physical space that is close to the true ground state wavefunction, then such a protocol can provide a better wavefunction after some imaginary time  $\tau$  (that will be defined by the spectrum of the system Hamiltonian).

For small systems it is easy to find the quantum circuits that reproduce the desired unitary matrix. It is also the case, that it can also be helpful to consider Trotterizing this evolution in a similar way to that which we have discussed previously. What this means is that at the end of each Trotter step, a measurement is performed and members of the ensemble that are closer to the ground state are retained, and hence the projective measurement removes energy from the physical system at each step. This resembles cooling the physical system, as opposed to asking which are *really cold* and which are *hot/warm* at the end of the imaginary time interval.

### G. Other

There are a number of other important algorithms that we could discuss, which include:

1. Feynman Clock (Annealers)
2. Fast-Forwarding
3. Simulating Hamiltonian dynamics with a truncated Taylor series
4. low-energy spaces

These are left for you to explore on your own.

## VI. QUANTUM SIMULATIONS OF LATTICE GAUGE THEORIES

In simulating quantum field theories that are relevant to Nature, and in particular relevant to nuclear and particle physics, discretizations of fermion fields onto the spatial or spacetime lattice are required. In the context of four-dimensional Euclidean-space lattice field theory, there is significant understanding about how to implement fermion fields. Importantly, in that context which utilizes classical computation, the fermion fields not included explicitly as stochastically evaluated fields directly, but their effect is included stochastically in sampling of a determinant and explicitly in the computation of "valence" quark propagators. There are many nice discussions about fermions in the continuum and in lattice formulations. There has been a long history associated with constructing lattice actions for fermions, and you will likely have heard about the *doubling problem* for lattice QCD calculations (in 4 Euclidean dimensions), which was resolved more than twenty years ago. Quantum simulation is different because fermion degrees of freedom are available in quantum registers, permitting the inclusion of fermion fields explicitly.

### A. Fermions in 1+1 Dimensions

Let us begin by considering fermions in 1+1 dimensions. A nice summary for 1+1 dimensions can be found in a foundational paper by Banks, Susskind and Kogut [72], but there are many others, including in text books. We consider a 1-dimensional spatial lattice with continuum time evolution, with spatial sites 1 to  $N$ , and lattice spacing  $a$ . The fermion field operators at each site are labeled by  $\phi(n)$  and  $\phi^\dagger(n)$  which satisfy the equal-time anti-commutation relations<sup>43</sup>

$$\{\phi(n), \phi^\dagger(k)\} = \delta_{n,k}, \quad \{\phi(n), \phi(k)\} = 0. \quad (252)$$

This is in analogy with 3+1 dimensional equal-time anticommutation relations,  $\{\psi_a(\mathbf{x}), \psi_b^\dagger(\mathbf{y})\} = \delta^{(3)}(\mathbf{x} - \mathbf{y}) \delta_{ab}$ .

In analogy with the previous construction of a finite-difference operator that recovers  $\nabla$  and  $\nabla^2$  in scalar field theory, we consider constructing an operator that recovers the 1-dimensional non-interacting Dirac equation in the continuum and infinite-volume limits. As a starting point, consider a Hamiltonian constructed from nearest-neighbor interactions between the fermions, of the form

$$\hat{H} = \frac{i}{2a_n} \sum_n \left[ \phi^\dagger(n) \phi(n+1) - \phi^\dagger(n+1) \phi(n) \right], \quad (253)$$

---

<sup>43</sup> There is a variable overload of  $\phi$ , by having it denote a fermion field in this initial discussion.

and the time-evolution of the field is given via the Heisenberg operator

$$i \frac{d}{dt} \phi(n) = \left[ \phi(n), \hat{H} \right] = \frac{i}{2a_n} (\phi(n+1) - \phi(n-1)) . \quad (254)$$

The instantaneous dynamics of the field at even sites is determined by the field at odd sites, and vice versa. If we construct a 2-spinor from an adjacent even and odd sites, we can construct an object that satisfies the 1+1 dimensional Dirac equation in the continuum limit. Explicitly, writing  $\psi = (\phi_e, \phi_o)^T$  which means  $\psi(x) = (\phi(n), \phi(n+1))^T = (\psi_L(x), \psi_R(x))^T$  for  $n$ -even only with  $x = n/2$ , and recognizing that the spatial lattice spacing is twice the "fermion site" lattice spacing,  $a_x = 2a_n$ , and setting  $a_x = 1$ ,

$$\begin{aligned} \frac{d}{dt} \psi_L(x) &= \frac{d}{dx} \psi_R(x) , \quad \frac{d}{dt} \psi_R(x) = \frac{d}{dx} \psi_L(x) \\ \frac{d}{dt} \psi(x) &= \alpha_x \frac{d}{dx} \psi(x) , \quad \alpha_x = \begin{pmatrix} 0 & 1 \\ 1 & 0 \end{pmatrix} , \end{aligned} \quad (255)$$

where a leading finite-difference discretization of the fermion field has been used to connect the discrete differences between lattice sites and the continuum spatial-derivative operator. This is sufficient to make the connection between the lattice theory in the limit of lattice spacing that is much smaller than lengths scales associated with physics of interest and the analogous continuum theory results.  $\gamma_\mu$  matrices can be defined for this 1+1D theory,

$$\gamma_0 = \begin{pmatrix} 1 & 0 \\ 0 & -1 \end{pmatrix} , \quad \gamma_x = \begin{pmatrix} 0 & 1 \\ -1 & 0 \end{pmatrix} , \quad \{\gamma_\mu, \gamma_\nu\} = 2g_{\mu\nu} , \quad (256)$$

which can be shown to satisfy the usual anti-commutation relation by explicit multiplication, where  $g_{00} = +1$  and  $g_{xx} = -1$  employing the *West-Coast metric*. Because  $\alpha_x = \gamma_0 \gamma_x$  and  $(\gamma_0)^2 = I$ ,

$$\begin{aligned} \frac{d}{dt} \psi(x) &= \alpha_x \frac{d}{dx} \psi(x) , \\ \gamma_0 \frac{\partial}{\partial t} \psi(x) &= \gamma_x \frac{\partial}{\partial x} \psi(x) , \\ \not{\partial} \psi(x) &= 0 , \end{aligned} \quad (257)$$

which is the 1+1 dimensional analog of the more familiar 3+1D Dirac equation. With this construction, including distinguishing between even and odd lattice sites, that in the continuum limit, via a finite-difference operator, the Dirac equation can be recovered without any pathologies. The only somewhat odd aspect of the formulation is the identification of "hypercubes" consisting of two (fermion) lattice sites per "physical" spatial site in order to recover the correct continuum, i.e., the Dirac spinor has two degrees of freedom, 1 time and 1 space from the upper and lower components of the spinor, emerging from a single field at each lattice site. Correspondingly, to match degrees of freedom, the lattice sites pair-up (or conspire) in such a way to recover the correct continuum limit.

Naively, this looks like we have a problem because of **doublers**. What is a doubler? The target lattice action describes one massless Dirac fermion in the continuum and infinite-volume limits, and the potential issue (which is/was a real issue in higher dimensions) can be seen by considering the action of the Hamiltonian in Eq. (253) on a plane-wave state,

$$\chi(n) = A e^{-ika_n n} , \quad \langle H \rangle = |A|^2 \frac{1}{a_n} \sin ka_n . \quad (258)$$

$\langle H \rangle$  behaves as  $|k|$  for  $k \sim 0$ ,  $\frac{\pi}{a_n}$  for  $k$  within the first Brillouin zone  $0 \leq k < \pi/a_n$ . Therefore, it would naively appear that this Hamiltonian is providing two massless particles and not just one. However, the spatial hypercube provides an upper limit of  $k < \pi/(2a_n) = \pi/a_x$ , and not  $k < \pi/a_n$ , and shifts in momentum can be used in such a way to combine the two massless single component fermions into the two-component spinor. Therefore, the construction faithfully reproduces the behavior of one species of two-component fermions in 1+1D. In higher dimensions, analogous combinations of components on the hypercube can be performed, e.g., in 4+0 dimensions, there are  $2^4 - 1 = 15$  doublers on the hypercube and combinations form four 4-component Dirac spinors, which are called four *tastes*. The effective lagrange density density exhibits an  $SU(4)_{\text{taste}}$  symmetry (defined at the discretized quark level), and a single pion (e.g.,  $\sim \bar{q}_1 \gamma_5 q_2$ ), for example, becomes a member of a 16 dimensional taste multiplet. For quantum simulations in 3+1D, where the time direction is continuous, and only discretization of the spatial directions is required, there are  $2^3 = 8$  degrees of freedom defining two 4-component Dirac spinors. This means that for each fermion field, there are two lights degrees of freedom, and not just one, suggesting that it might be possible to accommodate  $n_f = 2$  flavor theories in 3+1D more easily than expected.

As the theory is described by a two-component spinor in the continuum limit, "chirality" is defined by left-handed and right-handed movers, and the 1+1D equivalent of the  $\gamma_5$  matrix can be defined. In 3+1D,  $\gamma_5$  is defined by  $\gamma_5 = i\gamma_0\gamma_x\gamma_y\gamma_z$ , which can be directly modified into 1+1 dimensions, as

$$\gamma_5 = i\gamma_0\gamma_x = \begin{pmatrix} 0 & i \\ i & 0 \end{pmatrix}, \quad \{\gamma_5, \gamma_\nu\} = 0. \quad (259)$$

We are now in a position to consider, for instance, bilinear operators of the form, e.g.,  $\bar{\psi}(x)\psi(x) = \psi^\dagger(x)\gamma_0\psi(x)$ .

Fermion fields in 1+1D can be mapped to spin systems, as uncovered by Jordan and Wigner. That is to say that all aspects of a 1+1D fermion system can be faithfully reproduced by simulations of spin systems. This is great news for quantum computers and qubits, as such mappings are direct and easy, but not necessarily optimally efficient. By mapping an occupied fermion state at  $n$  to spin- $\uparrow$  and an unoccupied fermion state at  $n$  to spin- $\downarrow$ , one JW mapping<sup>44</sup> is (and the  $\psi(x)$  field has been re-distributed into its lattice  $\phi(n)$  components):

$$\begin{aligned} \phi(n) &= (-i\hat{Z}_1)(-i\hat{Z}_2) \dots (-i\hat{Z}_{n-1}) \sigma_n^- \\ \phi^\dagger(n) &= (+i\hat{Z}_1)(+i\hat{Z}_2) \dots (+i\hat{Z}_{n-1}) \sigma_n^+, \end{aligned} \quad (260)$$

where  $-\hat{Z}_j$  provides a phase of  $-1$  if a site is occupied and  $+1$  if it is unoccupied. This corresponds to  $|1\rangle$  being the unoccupied states and  $|0\rangle$  occupied - which is entirely convention and is entirely up to you to define before mapping the problem to qubits. The Pauli matrices have already been

---

<sup>44</sup> There is no unique way to accomplish this mapping, and so conventions must be defined.

defined, but a reminder is helpful,

$$\begin{aligned}\sigma^- &= \frac{1}{2}(\sigma_x - i\sigma_y) = \begin{pmatrix} 0 & 0 \\ 1 & 0 \end{pmatrix} = \frac{1}{2}(X - iY) \\ \sigma^+ &= \frac{1}{2}(\sigma_x + i\sigma_y) = \begin{pmatrix} 0 & 1 \\ 0 & 0 \end{pmatrix} = \frac{1}{2}(X + iY) \\ \sigma_z &= \begin{pmatrix} 1 & 0 \\ 0 & -1 \end{pmatrix} = Z \\ \sigma_i \sigma_j &= \delta_{ij} I_2 + i\varepsilon_{ijk} \sigma_k, \quad \{\sigma_i, \sigma_j\} = 2\delta_{ij} I_2, \quad [\sigma_i, \sigma_j] = 2i\varepsilon_{ijk} \sigma_k.\end{aligned}\quad (261)$$

It is instructive to work through a few straightforward examples to see how this mapping works. Consider a lattice with four (staggered) fermion sites, that describe two spatial sites. The field operators for this system are

$$\begin{aligned}\phi(0) &= \sigma^- \otimes I \otimes I \otimes I, \quad \phi^\dagger(0) = \sigma^+ \otimes I \otimes I \otimes I \\ \phi(1) &= -i\hat{Z} \otimes \sigma^- \otimes I \otimes I, \quad \phi^\dagger(1) = +i\hat{Z} \otimes \sigma^+ \otimes I \otimes I \\ \phi(2) &= -\hat{Z} \otimes \hat{Z} \otimes \sigma^- \otimes I, \quad \phi^\dagger(2) = -\hat{Z} \otimes \hat{Z} \otimes \sigma^+ \otimes I \\ \phi(3) &= +i\hat{Z} \otimes \hat{Z} \otimes \hat{Z} \otimes \sigma^-, \quad \phi^\dagger(3) = -i\hat{Z} \otimes \hat{Z} \otimes \hat{Z} \otimes \sigma^+\end{aligned},\quad (262)$$

and a couple of examples of operations are

$$\begin{aligned}\{\phi(1), \phi^\dagger(1)\} &= \{-i\hat{Z} \otimes \sigma^- \otimes I \otimes I, +i\hat{Z} \otimes \sigma^+ \otimes I \otimes I\} \\ &= I \otimes \{\sigma^-, \sigma^+\} \otimes I \otimes I = I \otimes I \otimes I \otimes I \\ &= I \\ \{\phi(1), \phi(1)\} &= 0 \\ \{\phi(0), \phi^\dagger(1)\} &= \{\sigma^- \otimes I \otimes I \otimes I, +i\hat{Z} \otimes \sigma^+ \otimes I \otimes I\} \\ &= \{\sigma^-, +i\hat{Z}\} \otimes \sigma^+ \otimes I \otimes I \\ &= 0.\end{aligned}\quad (263)$$

Bilinears can be mapped onto the spin system via, e.g.,

$$\begin{aligned}\sum_x \bar{\psi}(x)\psi(x) &= \sum_x \psi^\dagger(x)\gamma_0\psi(x) = \sum_n \phi_n^\dagger \phi_n (-1)^n = \sum_n (-1)^n \sigma^+ \sigma^- = \sum_n (-1)^n \frac{1}{2} (1 + \hat{Z}_n) \\ &= \frac{1}{2} \sum_n (-1)^n \hat{Z}_n,\end{aligned}\quad (264)$$

where the sum  $\sum_n (-1)^n = 0$ .

The non-interacting Hamiltonian given in Eq. (253), describes a massless Dirac fermion in 1+1D. Including a mass term for this fermion, and mapping onto spins or qubits through the JW mapping leads to,

$$\hat{H} = -\frac{1}{2a} \sum_n [\sigma_n^+ \sigma_{n+1}^- + \sigma_{n+1}^+ \sigma_n^-] + \frac{m}{2} \sum_n (-)^n \hat{Z}_n,\quad (265)$$

to describe a massive non-interacting fermion. It is helpful to understand this form in more detail, to be able to discern the strengths and weaknesses of the JW mapping for quantum field theories

more generally general. Let's start by considering the ground state of a theory with a large mass, such that the mass term dominates over the kinetic term.

Thinking about Dirac theory, with a full Dirac sea, when we promote a particle from the Dirac sea into a particle with +ve energy, we also leave a hole in the Dirac sea that we identify as an antiparticle, e.g., an  $e^+e^-$  pair is created that conserves the electric charge of the universe. So in the JW mapping, the even sites correspond to +ve energy particle states which are unoccupied in the trivial vacuum, and the odd sites correspond to -ve energy states which are fully occupied in the trivial vacuum. Creating an  $e^+e^-$  pair from the vacuum corresponds to adding a particle to an even site (creating a particle) and removing a particle from the odd sites (creating a hole). The trivial ground state from the mass term is

$$|\psi\rangle_{\text{trivial}} = |\downarrow\uparrow\downarrow\uparrow\downarrow\dots\downarrow\uparrow\rangle = |101010\dots10\rangle , \quad (266)$$

and contains zero  $e^+e^-$  pairs. If an  $e^+e^-$  pair is created at the  $x=1$  site, the state becomes

$$|\psi\rangle_{e^+e^-;n=1} = |\downarrow\uparrow\uparrow\downarrow\downarrow\uparrow\dots\downarrow\uparrow\rangle = |100110\dots10\rangle , \quad (267)$$

An operator that measures the electric charge at each site is (electrons on even sites and positrons on odd sites),

$$\hat{Q}(n) = -\frac{1}{2} \left( \hat{Z} + (-)^n \right) , \quad (268)$$

which, on the trivial vacuum yields zero at for each  $n$ . On the other hand

$$\hat{N}_p(n) |\downarrow\uparrow\uparrow\downarrow\downarrow\uparrow\dots\downarrow\uparrow\rangle , \quad (269)$$

gives -1 for  $n=2$  and +1 for  $n=3$ , as expected for an  $e^+e^-$  pair residing at these sites.

### 1. Time Evolution of Free fermions using a JW Mapping

One of the first questions to ask is that if we have a given configuration of fermions, how do we evolve it forward in time implementing the Hamiltonian in Eq. (265)? The terms that we need to understand how to implement, assuming Trotter the evolution, are

$$\begin{aligned} \hat{U}_{\text{kin}} &= e^{iH_{\text{kin}}t} = e^{it\frac{1}{2}\sum_n [\sigma_n^+\sigma_{n+1}^- + \sigma_n^-\sigma_{n+1}^+]} \\ \hat{U}_{\text{mass}} &= e^{-iH_{\text{mass}}t} = e^{-it\frac{m}{2}\sum_n (-)^n \hat{Z}_n} , \end{aligned} \quad (270)$$

where  $a = 1$  has been used. Thus, we are required to find circuit representations of

$$\begin{aligned} \hat{U}_{\text{kin},n} &= e^{it\frac{1}{2} [\sigma_n^+\sigma_{n+1}^- + \sigma_n^-\sigma_{n+1}^+]} \\ \hat{U}_{\text{mass},n} &= e^{-it\frac{m}{2}(-)^n \hat{Z}_n} . \end{aligned} \quad (271)$$

The mass terms are straightforward, as they can be implemented with single-qubit phases, but less so the kinetic (hopping) terms. However, we have already seen how to implement such operators,

$$\sigma^+\sigma^- + \sigma^-\sigma^+ = \frac{1}{2} (\hat{X}\hat{X} + \hat{Y}\hat{Y}) . \quad (272)$$

Figure 31 shows the circuits for implementing the unitary  $e^{-i\frac{1}{2}\alpha(\hat{X}\hat{X} + \hat{Y}\hat{Y})}$ , and thus by choosing  $\alpha = -\frac{1}{2}$ , we now have the circuits to implement a single Trotter step of the free evolution. As

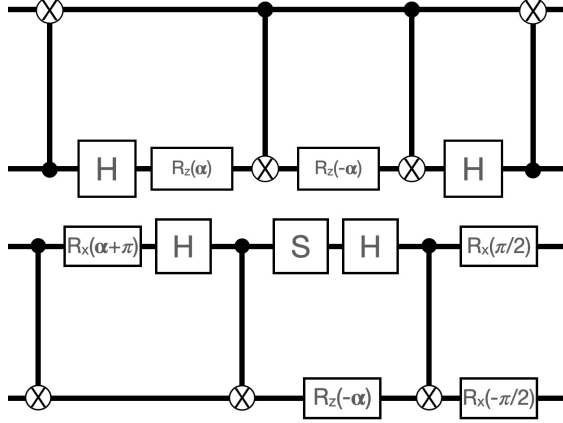


FIG. 31: Circuits with 3 and 4 CNOTs that implement the unitary  $e^{-i\frac{1}{2}\alpha(\hat{X}\hat{X}+\hat{Y}\hat{Y})}$ .

discussed previously, Trotterization of the Hamiltonian into kinetic (hopping) and potential (mass) generates systematic errors which can be mitigated through various procedures. It is also the case that further Trotterization of the hopping term also generates errors because the actions on adjacent sites do not commute. Consider a sub-system of 2 lattice sites with 4 fermion sites, and lets consider the action of the hopping term, which includes terms of the form,

$$\hat{A} = \sigma^+ \otimes \sigma^- \otimes \hat{I} + \sigma^- \otimes \sigma^+ \otimes \hat{I}, \quad \hat{B} = \hat{I} \otimes \sigma^+ \otimes \sigma^- + \hat{I} \otimes \sigma^- \otimes \sigma^+, \quad (273)$$

which have commutators

$$[\hat{A}, \hat{B}] = \sigma^- \otimes \hat{Z} \otimes \sigma^+ - \sigma^+ \otimes \hat{Z} \otimes \sigma^-, \quad (274)$$

which is 3-body operator generated from the non-commutativity of 2-body operators. As discussed previously, this higher-body operator could be included into a modified Hamiltonian with a coefficient designed to cancel the corresponding Trotterization errors (an improved “Symanzik” action), or it could be used as a way to include 3-body operators explicitly through the implementation of 2-body evolution operators.

Now we have a complete implementation of the free fermion time evolution of a multi-fermion system. It has a number of important features that are essential in the control and quantification of systematic errors, but we know, in principle, how to systematically improve calculations. It is clear that if one is looking to perform a calculation within a given error bound, significant effort is required to determine how to actually accomplish that.

Now, the inclusion of interactions. There are a number of different forms of interactions that are relevant to quantum simulation. Common are interactions that are local 4-fermion interactions, that result from general forms of operators

$$\mathcal{O} = \bar{\psi}_i \psi_j \bar{\psi}_k \psi_l, \quad (275)$$

that generate a contribution to the Hamiltonian that transition particles between states or orbitals. This is a generic type of interaction, and all of the complexity is typically in the form of the coefficients. A local interaction, as in particle physics or the pionless theory in nuclear physics, has all interactions at single spacetime point, but in chemistry, by not including explicit electromagnetic interactions, gives non-local interactions. For example, consider an interaction of the form, after JW mapping

$$\hat{\mathcal{O}} = \sigma^+ \otimes \sigma^- \otimes \sigma^- \otimes \sigma^+ + \sigma^- \otimes \sigma^+ \otimes \sigma^+ \otimes \sigma^-, \quad (276)$$

For this type of operator contribution to the time evolution, we will be requiring a unitary of the form

$$\hat{U}_{\hat{\mathcal{O}}}(t) = e^{-it\frac{1}{2}\beta\hat{\mathcal{O}}} \quad , \quad (277)$$

for some coefficient  $\beta$  that is dictated by the theory. To better understand the action of this

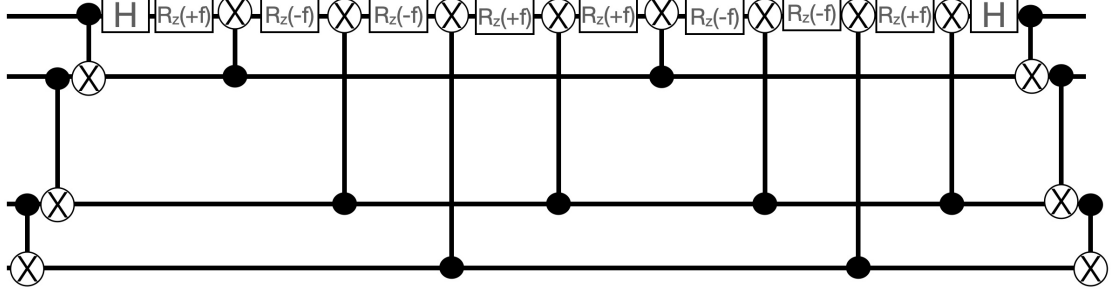


FIG. 32: Circuit with 14 CNOTs that implements the unitary  $e^{-i\frac{1}{2}\beta(\sigma^+\otimes\sigma^-\otimes\sigma^-\otimes\sigma^+ + \sigma^-\otimes\sigma^+\otimes\sigma^+\otimes\sigma^-)}$ , where for shorthand we have used  $f = \beta/8$ .

operator, we note that the operator annihilates all but two possible configurations of spins, so that for most of the states,  $\hat{U}|\phi\rangle = |\phi\rangle$ . However, there are two states for which it acts non-trivially,

$$\begin{aligned} \sigma^+ \otimes \sigma^- \otimes \sigma^- \otimes \sigma^+ |\downarrow\uparrow\downarrow\downarrow\rangle &= |\uparrow\downarrow\downarrow\uparrow\rangle \\ \sigma^- \otimes \sigma^+ \otimes \sigma^+ \otimes \sigma^- |\uparrow\downarrow\downarrow\uparrow\rangle &= |\downarrow\uparrow\uparrow\downarrow\rangle \end{aligned} \quad , \quad (278)$$

which furnishes the matrix form of the operator as given in Fig. (33). The 14-CNOT circuit in

Out[12896]//MatrixForm=	
1	0 0 0 0 0 0 0
0	1 0 0 0 0 0 0
0	0 1 0 0 0 0 0
0	0 0 1 0 0 0 0
0	0 0 0 1 0 0 0
0	0 0 0 0 1 0 0
0	0 0 0 0 0 1 0
0	0 0 0 0 0 0 1
0	0 0 0 0 0 0 0
Cos	[ $\frac{\beta}{2}$ ]
0	0 0 -i Sin [ $\frac{\beta}{2}$ ] 0 0 0 0 0 0
0	0 0 0 0 0 0 0
0	0 0 0 0 0 0 0
0	0 0 0 0 0 0 0
-i Sin	[ $\frac{\beta}{2}$ ] 0 0 Cos [ $\frac{\beta}{2}$ ] 0 0 0 0 0 0
0	0 0 0 0 0 0 0
0	0 0 0 0 0 0 0
0	0 0 0 0 0 0 0
0	0 0 0 0 0 0 0
0	0 0 0 0 0 0 0
0	0 0 0 0 0 0 0
0	0 0 0 0 0 0 0

FIG. 33: Matrix representation of  $e^{-i\frac{1}{2}\beta(\sigma^+\otimes\sigma^-\otimes\sigma^-\otimes\sigma^+ + \sigma^-\otimes\sigma^+\otimes\sigma^+\otimes\sigma^-)}$  on a four-qubit register. [Generated using Mathematica.]

Fig. (32) is the simplest way, in terms of the number of CNOT gates, to implement this specific 4-qubit operator. All that the circuit is doing is implementing the two-state rotation given in Eq. (278)!! This is clearly quite cumbersome to implement using this gate set. The circuit logic,

embedded in the circuit, has to "decide" if it will operate on the state or not, and must select only 2 of the 16 states to act on nontrivially. In reality the circuit moves information around, including between states that are beyond the two in question, before arriving at the correct transformation. In this sense, the circuit is quite clunky, but there is nothing special about this operator, such types of circuits are generically clunky.

There have been interesting papers (for example, by Andrade, Davoudi, Grass, Hafezi and Pagano [73], and Katz, Cetina and Monroe [74] that motivate and show how to create "native" N-body gates on trapped-ion systems. These allow for the implementation of such operators in the same way (or similar) to how one, at the software level, *asks the system* to perform that operation. These works were both driven, in part, by the needs of quantum field theories.

Considering now CNOT-gate counts. The hopping term requires 3 per implementation, and so for a site with L-spatial sites, and hence 2L fermion sites, 1 Trotter step requires 3 (2L-1) CNOTs. A local, nearest neighbor four-Fermi interaction, of the form discussed above, requires 14 CNOTs for (2L-1) sites, and so 1 Trotter step requires a total of 17 (2L-1) CNOT gates. On the other hand, if the interaction is nonlocal, then a total of 14 (2L)(2L-1)/2 are required, giving a total of (2L-1)( 14 L + 3), which scales as  $\mathcal{O}(L^2)$  as expected.

## B. Yukawa Theory in 1+1 Dimensions: 1 Fermion and 1 Scalar

Our newly acquired knowledge about how to include fermions in 1+1D lattice simulations, Jordan-Wigner and the associated quantum circuitry required for time evolution, can be combined with the scalar field theory framework to describe a fermion interacting with a scalar field. In nuclear physics, this is analogous to the low-energy interactions between nucleons mediate by the exchange of a (pseudo-)scalar particle (but with an important difference dictated by chiral symmetry<sup>45</sup>), while in high-energy physics this parallels interactions between the fermions and Higgs field, as an example. The Hamiltonian for this two-species field theory (one spin- $\frac{1}{2}$  fermion interacting with one spin-0 boson) is

$$H_{\psi,\phi} = H_\phi + H_\psi + g \bar{\psi}\psi \phi , \quad (280)$$

where  $H_\phi$  is the Hamiltonian for a scalar particle (with or without the  $\lambda\phi^4$  self interactions),  $H_\psi$  is the free fermion Hamiltonian, and the third term denotes the lowest dimension interaction between  $\psi$  and  $\phi$ . The Yukawa<sup>46</sup> coupling of the scalar field to the fermion scalar density can be included in the latticized, JW-mapped Hamiltonian straightforwardly (as the fermion part is the same as the mass term in the Hamiltonian). In particular, under the mapping to quantum registers

$$g \int d^3\mathbf{x} \bar{\psi}(\mathbf{x})\psi(\mathbf{x})\phi(\mathbf{x}) \rightarrow \tilde{g} \sum_{n=even}^{2L} \left( \frac{1}{2}(-)^n \hat{Z}(n) + \frac{1}{2}(-)^{n+1} \hat{Z}(n+1) \right) \hat{\phi}(n) , \quad (281)$$

where there are half the number of sites for the scalar field, one for each spatial lattice site, and the JLP mapping of the scalar field is utilized. The strength of the Yukawa interaction in the

<sup>45</sup> The interactions between nucleons  $N = (p, n)^T$  and a single pion is of the form, in the non-relativistic limit,

$$\delta H_{N,\pi} = \frac{\sqrt{2}g_A}{f} \bar{N} \sigma \cdot \nabla \Pi N , \quad \Pi = \begin{pmatrix} \pi^0/\sqrt{2} & \pi^+ \\ \pi^- & -\pi^0/\sqrt{2} \end{pmatrix} , \quad f \sim 93 \text{ MeV} . \quad (279)$$

<sup>46</sup> This interaction is called a *Yukawa* interaction as it is named after the person who first suggested it, **Hideki Yukawa**.

continuum is determined by the coupling constant,  $g$ , which is *matched* to the lattice coupling,  $\tilde{g}$ , in such a way to recover the correct continuum interaction as  $a \rightarrow 0$ .

Figure 34 shows the mapping of the  $\psi$  and  $\phi$  fields in a 1-dimensional lattice with 4 spatial lattice sites to qubits using the Jordan-Wigner mapping of  $\psi$ , and the Jordan-Lee-Preskill basis for the scalar field. <sup>47</sup> For reasonable parameters and truncations, 3 qubits per site (corresponding

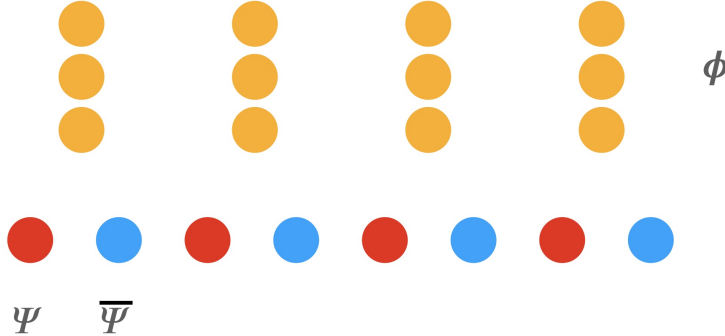


FIG. 34: The qubit-mapping of a scalar field coupled to a fermion field  $\psi$  in 1+1 dimensions using the Jordan-Wigner mapping and the Jordan-Lee-Preskill basis for the scalar field  $\phi$ . This cartoon shows a theory with  $L = 4$  spatial lattice sites (and hence 4 fermion and 4 anti-fermion sites in the Kogut-Susskind/Jordan-Wigner discretization) and the scalar field digitized with 3 qubits per spatial site.

to 8 states in the Hilbert space at each site) is sufficient for low/reasonable precision in simulating the low-energy dynamics of the scalar field with mass, coupling and maximum field of order unity. Hence for  $L = 4$  spatial sites, we expect to be able to achieve reasonable precision for low-energy dynamics with a total of 20 qubits.

One of the nice aspects of this construction is that both the qubit-interactions in the fermion and scalar sectors from their coupling map to diagonal operators on the qubit register, and hence can be implemented with products of  $\hat{Z}\hat{Z}$  operators, one acting on the scalar field register and one on fermion qubits. If we had chosen different bases for  $\phi$  and  $\psi$ , this would not have been the case, and more complex quantum circuits would have been required.

### C. 1+1 QED - The Schwinger Model in the Continuum

The Schwinger model is the 1+1D theory of quantum electrodynamics (QED), and is quite remarkable as it shares a number of features of 3+1D QCD that are important to simulate with high precision. There is an extensive literature on this subject, and I point you to a really good and recent book by *Frishman and Sonnenschein* [75]. The Lagrange density describing 1+1D QED in the continuum and in infinite volume is

$$\mathcal{L} = \bar{\psi} [ i\partial^\mu - m ] \psi - \frac{1}{4} F^{\mu\nu} F_{\mu\nu} = \bar{\psi}_L i\partial^\mu \psi_L + \bar{\psi}_R i\partial^\mu \psi_R - m \bar{\psi} \psi - \frac{1}{4} F^{\mu\nu} F_{\mu\nu}, \quad (282)$$

where the covariant derivative and field strength are

$$D_\mu = \partial_\mu + ie\hat{Q}A_\mu, \quad F_{\mu\nu} = \partial_\mu A_\nu - \partial_\nu A_\mu, \quad (283)$$

---

<sup>47</sup> The JPL basis simplifies the quantum circuitry, but in principle any basis could have been chosen and the cartoon would have been the same.

with  $\hat{Q}$  the charge operator. The left- and right-handed (chirality) fields are defined via projection using the  $\gamma_5$  matrix,

$$\psi_L(x) = \frac{1}{2}(1 - \gamma_5)\psi(x) , \quad \psi_R(x) = \frac{1}{2}(1 + \gamma_5)\psi(x) , \quad \psi(x) = \psi_L(x) + \psi_R(x) . \quad (284)$$

The Lagrange density in Eq. (282) is invariant under the local transformations

$$\psi(x) \rightarrow \psi'(x) = e^{i\alpha(x)\hat{Q}}\psi(x) , \quad A_\mu(x) \rightarrow A_\mu(x) - \partial_\mu\alpha(x) , \quad (285)$$

at each spacetime point.

In addition to local symmetries, it is also interesting to consider global transformations,  $\alpha(x) \rightarrow \alpha$  independently for the left and right handed fields. In the case of a massless theory, the Lagrange density in Eq. (282) is invariant under,

$$\psi_L(x) \rightarrow \psi'_L(x) = e^{i\alpha_L\hat{Q}}\psi(x) , \quad \psi_R(x) \rightarrow \psi'_R(x) = e^{i\alpha_R\hat{Q}}\psi(x) . \quad (286)$$

The chiral transformation can also be written in terms of other (related) angles,

$$\psi(x) \rightarrow \psi'(x) = e^{i\eta_V\hat{Q}}\psi(x) , \quad \psi(x) \rightarrow \psi'(x) = e^{i\eta_A\gamma_5\hat{Q}}\psi(x) . \quad (287)$$

At the classical level, the Lagrangian and all S-matrix elements (amplitudes) are invariant under these two chiral transformations, either  $L, R$  or  $V, A$ . The associated conserved vector and axial-vector Noether currents at the classical level are

$$J^\mu = \bar{\psi}\gamma^\mu\psi , \quad J_5^\mu = \bar{\psi}\gamma^\mu\gamma_5\psi . \quad (288)$$

Now, in the gauge sector alone, there are only two components to consider, the time and the space directions,  $F_{01}$  and  $F_{10}$ , which are (trivially) related, and hence there is no magnetic field. In the absence of fermions, there is an electric field satisfying  $E_1 = -F_{10} = F_{01} = \partial_0 A_1 - \partial_1 A_0$ . The equations of motion are  $\partial^\mu F_{\mu\nu} = 0$ , which yields,

$$\partial_t E_x = \partial_x E_x = 0 , \quad (289)$$

and hence the electric field is constant in spacetime, and hence this theory of only gauge dynamics is trivial.

Including the fermions changes this. In particular, the axial symmetry does not survive quantum fluctuations and hence the classical symmetry is actually not a symmetry and the current is anomalous. This is easily seen by considering the point-split operator in the limit of vanishing separation,  $\epsilon$ , <sup>48</sup>

$$J_5^\mu = \bar{\psi}(x + \frac{\epsilon}{2}) \gamma^\mu\gamma_5 e^{-ie\int_{x-\epsilon/2}^{x+\epsilon/2} dz_\alpha A_\alpha(z)} \psi(x - \frac{\epsilon}{2}) , \quad (290)$$

taking derivatives and noting that the contraction of the product of fermion fields is singular,

$$T[\psi(x)\bar{\psi}(y)] = -\frac{i}{2\pi}\gamma^\nu \frac{(x-y)_\nu}{(x-y)^2} + \text{normal ordered} . \quad (291)$$

---

<sup>48</sup> Some of the “user-friendly” manipulations in *Peskin and Schroeder* are reproduced here.

It can then be shown that

$$\begin{aligned}
\partial_\mu J_5^\mu &= \left( \partial_\mu \bar{\psi}(x + \frac{\epsilon}{2}) \right) \gamma^\mu \gamma_5 e^{-ie \int_{x-\epsilon/2}^{x+\epsilon/2} dz_\alpha A_\alpha(z)} \psi(x - \frac{\epsilon}{2}) \\
&\quad + \bar{\psi}(x + \frac{\epsilon}{2}) \gamma^\mu \gamma_5 e^{-ie \int_{x-\epsilon/2}^{x+\epsilon/2} dz_\alpha A_\alpha(z)} \left( \partial_\mu \psi(x - \frac{\epsilon}{2}) \right) \\
&\quad + \bar{\psi}(x + \frac{\epsilon}{2}) \gamma^\mu \gamma_5 (-ie A_\nu \epsilon^\nu) e^{-ie \int_{x-\epsilon/2}^{x+\epsilon/2} dz_\alpha A_\alpha(z)} \psi(x - \frac{\epsilon}{2}) + \mathcal{O}(\epsilon^2) \\
&= \left( ie \bar{\psi}(x + \frac{\epsilon}{2}) \gamma^\nu A_\nu \right) \gamma^\mu \gamma_5 e^{-ie \int_{x-\epsilon/2}^{x+\epsilon/2} dz_\alpha A_\alpha(z)} \psi(x - \frac{\epsilon}{2}) \\
&\quad + \bar{\psi}(x + \frac{\epsilon}{2}) \gamma^\mu \gamma_5 e^{-ie \int_{x-\epsilon/2}^{x+\epsilon/2} dz_\alpha A_\alpha(z)} \left( -ie \gamma^\nu A_\nu \psi(x - \frac{\epsilon}{2}) \right) \\
&\quad + \bar{\psi}(x + \frac{\epsilon}{2}) \gamma^\mu \gamma_5 (-ie A_\nu \epsilon^\nu) e^{-ie \int_{x-\epsilon/2}^{x+\epsilon/2} dz_\alpha A_\alpha(z)} \psi(x - \frac{\epsilon}{2}) + \mathcal{O}(\epsilon^2) \\
&= -ie \epsilon^\nu \bar{\psi}(x + \frac{\epsilon}{2}) \gamma^\mu \gamma_5 F_{\mu\nu} \psi(x - \frac{\epsilon}{2}) \\
&= \frac{e}{2\pi} \epsilon^{\mu\nu} F_{\mu\nu} , \tag{292}
\end{aligned}$$

and hence  $J_5^\mu$  is not a conserved current<sup>49</sup>. Looking at this term, we realize that we did not include all of possible terms that are gauge invariant and relevant and marginal in the Lagrange density in Eq. (282). A term of the form  $\epsilon^{\mu\nu} F_{\mu\nu}$  is gauge invariant by itself, should have been included in Eq. (282). Therefore, the Lagrange density to be considered going forward is,

$$\mathcal{L} = \bar{\psi} [ iD - m ] \psi - \frac{1}{4} F^{\mu\nu} F_{\mu\nu} + \frac{e\theta}{4\pi} \epsilon^{\mu\nu} F_{\mu\nu} , \tag{294}$$

and we recognize that while the vector current is conserved, the axial current is anomalous with its conservation violated by quantum fluctuations. The (coupling) constant  $\theta$  is not predicted by the theory, it is an additional constant that is to be fit to “Nature”, or utilized in simulation. Further, this terms is proportional to  $E_x$ , and gives rise to a background electric field,<sup>50</sup> see Eq. (296). The electric field at each point of the system can be related to an integral over the charges. For example, if the line is semi-infinite, the electric field at some point of the system is,

$$E_x = -e \int dx \bar{\psi} \gamma_0 \psi - \frac{e\theta}{2\pi} , \tag{296}$$

where the  $\theta$ -term enters as, or is responsible for, a background electric field.

The Schwinger model can be bosonized, see, for example, Ref. [75].<sup>51</sup> That is to say that there is a one-to-one correspondence between observables in the gauge field theory defined in Eq. (294)

---

<sup>49</sup> We have used

$$\text{Tr} (\gamma^\alpha \gamma^\beta \gamma_5) = 2\epsilon^{\alpha\beta} . \tag{293}$$

<sup>50</sup>

$$\epsilon^{\mu\nu} F_{\mu\nu} = F_{01} - F_{10} . \tag{295}$$

<sup>51</sup> This is just one example, one of the simplest, of bosonization that can be readily extended to non-Abelian systems. See Ref. [75], and references therein.

and in the scalar field theory defined by the Hamiltonian,

$$\begin{aligned} H &= \frac{1}{2}\Pi^2 + \frac{1}{2}(\partial_x\phi)^2 - \frac{cm^2}{\pi} \cos(2\sqrt{\pi}\phi) + \frac{e^2}{2\pi} \left( \frac{\theta}{2\sqrt{\pi}} - \phi \right)^2 , \\ &\rightarrow \frac{1}{2}\Pi^2 + \frac{1}{2}(\partial_x\phi)^2 + \frac{1}{2}\mu^2\phi^2 - \frac{cm\mu}{\pi} \cos(\theta + 2\sqrt{\pi}\phi) , \\ c &= \frac{1}{2}e^{\gamma_E} \sim 0.891 , \quad \mu = \frac{e}{\sqrt{\pi}} , \end{aligned} \quad (297)$$

where there is a correspondance of the form  $\psi_L(x) \leftrightarrow e^{-i\phi(x)}$  and  $\psi_R(x) \leftrightarrow e^{+i\phi(x)}$ . We have obtained this result by a shift in the field variable  $\phi' = \phi - \frac{\theta}{2\sqrt{\pi}}$ . This theory has a number of interesting aspects to it. One of particular note is that the massless Schwinger model,  $m = 0$ , is the same as a massive non-interacting scalar field. In the massive case, the potential is  $2\pi$ -periodic in  $\theta$  (the background electric field), and can support non-trivial topologically-stabilized states.

The sine-Gordon equation derives from a Hamiltonian of the form

$$H = \frac{1}{2}\Pi^2 + \frac{1}{2}(\partial_x\phi)^2 - \frac{m^4}{\lambda} \left[ \cos\left(\frac{\sqrt{\lambda}}{m}\phi\right) - 1 \right] , \quad (298)$$

(a different  $m$  than above) which is periodic in  $\phi$ . There are eigenstates that are non-trivial mapping between the phase (field) and spatial location, of the form

$$\phi(x) = \frac{4m}{\sqrt{\lambda}} \tan^{-1}\left(e^{\pm m(x-x_0)}\right) , \quad (299)$$

defining kinks and anti-kinks centered at  $x_0$ . Under the bosonization map, the vector current becomes

$$J^\mu = \bar{\psi}\gamma^\mu\psi \rightarrow \frac{1}{\sqrt{\pi}}\epsilon^{\mu\alpha}\partial_\alpha\phi . \quad (300)$$

As this involves a single derivative, a topological charge can be defined as

$$Q_{\text{top}} = \sqrt{\pi} \int_{-\infty}^{+\infty} dx J^0(x) , \quad (301)$$

which depends on the difference between field values at  $\pm\infty$  only, and are constants of the motion. From a quantum simulation perspective, which has started to be explored in spin-models [76] (a first step toward a gauge theory), one can pursue simulations of kink-kink or kink-antikink scattering at higher energies to enable inelasticities producing multiple hadrons in the final states, as a prototype for QCD collisions.

#### D. The Lattice Schwinger Model in $A_0 = 0$ Gauge

From a physics discovery perspective within the Standard Model, the Schwinger model seems too far afield to be useful, but that is actually not true, depending on what we define to be useful. Charges in the Schwinger model are screened. That is to say that if we place an electric charge at some point, the electric field observed far from the charge vanishes. The vacuum state re-organizes itself in the same way that a dielectric responds to screen electric fields in classical electromagnetism. This is analogous to the screening of color charges, being confined into hadrons in QCD. The vacuum state has a non-zero expectation value of fermion condensate,  $\langle\bar{\psi}\psi\rangle \neq 0$ , as

is the case for QCD. The spectrum of states is that of composite particles, containing two-body and three-body bound states of these composites, analogous to the proton, the deuteron and the triton of QCD. So we see that while 1+1 QED cannot be compared with nature, it shares many of the key features of QCD, and as such, performing quantum simulations of observables within the Schwinger model will provide a sandbox for developing algorithms and protocols for simulations of QCD. This is particularly so for observables that are challenging to compute classically, such as hadronization, fragmentation and finite-density phases.

The last year, during 2023-2024, a significant amount of progress has been made in simulating the Schwinger model using quantum computers. Our group (IQuS) has introduced scalable quantum circuits as elements of the pool implemented using ADAPT-VQE, which we call SC-ADAPT-VQE, which we will discuss later. This made use charge screening and the associated exponential decay of correlation functions and entanglement as a function of distance to converge quantum circuits to some predetermined level of precision. Using this method, we prepared the vacuum state of the Schwinger model using 100 qubits of IBM's quantum computers, and then time-evolved a wavepacket into back-to-back hadrons over 14 Trotter steps. An artist's impression of the simulation of the vacuum is shown in Fig. 35. This required a circuit with  $\sim 14k$  CNOT gates and circuit depth of 370, which is the largest simulation performed to date. These techniques are applicable to higher dimensions, and guide the way forward for 3+1D simulations of lattice gauge theories.

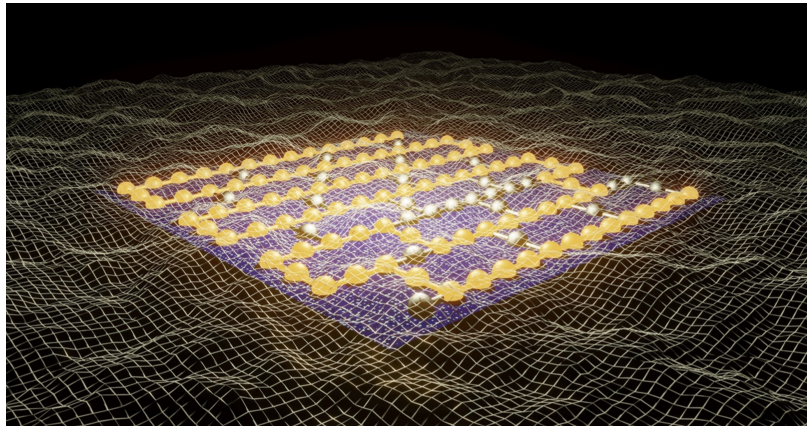


FIG. 35: The Schwinger model vacuum. A cartoon of qubit layout used to prepare the Schwinger model vacuum using IBM's quantum computers. [Image created by Marc Illa (IQuS)]

To construct a corresponding lattice Hamiltonian that recovers the continuum Hamiltonian as the lattice spacing vanishes, the non-interacting Hamiltonian considered previously must be modified to produce the gauge-covariant kinetic term in the continuum limit. This is accomplished naturally through parallel transporters in gauge space, defining the link variables.

$$\begin{aligned}
 \hat{H} &= \frac{i}{2a} \sum_n \left[ \phi^\dagger(n) \phi(n+1) - \phi^\dagger(n+1) \phi(n) \right] \\
 &\rightarrow \frac{i}{2a} \sum_n \left[ \phi^\dagger(n) \hat{U} \phi(n+1) - \phi^\dagger(n+1) \hat{U}^\dagger \phi(n) \right] \\
 &= \frac{i}{2a} \sum_n \left[ \phi^\dagger(n) e^{iae\hat{Q}A_x} \phi(n+1) - \phi^\dagger(n+1) e^{-iae\hat{Q}A_x} \phi(n) \right] \\
 &\rightarrow \bar{\psi}(x) [-i\gamma_x D_x + m] \psi(x) , \quad D_x = -\nabla_x + iea\hat{Q}A_x , \tag{302}
 \end{aligned}$$

as desired<sup>52</sup>.

What is the link operator actually doing? It is helpful to consider some field commutators. Absorbing the couplings into the fields, and working in  $A_0 = 0$  gauge,<sup>53</sup>

$$\begin{aligned} [\hat{A}_x(\mathbf{x}), \partial_0 \hat{A}_x(\mathbf{y})] &= [\hat{A}_x(\mathbf{x}), \hat{E}_x(\mathbf{y})] = i\delta_{x,y} \\ [\hat{E}_x(\mathbf{x}), e^{+i\hat{A}_x(\mathbf{y})}] &= +i[\hat{E}_x(\mathbf{x}), \hat{A}_x(\mathbf{y})] e^{+i\hat{A}_x(\mathbf{y})} = +e^{+i\hat{A}_x(\mathbf{x})} \\ [\hat{E}_x(\mathbf{x}), \hat{U}(\mathbf{y})] &= \hat{U}\delta_{x,y} , \end{aligned} \quad (305)$$

from which we see a discrete set of eigenstates of  $\hat{E}_x$  at each position, with integer eigenvalues,  $|n\rangle$ , such that  $\hat{E}_x|n\rangle = n|n\rangle$ , and the action of  $\hat{U}$  is that of a raising operator,  $\hat{U}|n\rangle = |n+1\rangle$ . Explicitly,

$$\hat{E}_x \hat{U}|n\rangle = \hat{U}\hat{E}_x|n\rangle + \hat{U}|n\rangle = (n+1)\hat{U}|n\rangle . \quad (306)$$

One potential Hilbert space layout for the lattice Schwinger model is now obvious—the Kogut-Susskind fermion mapping via Jordan-Wigner with a infinite-discrete Hilbert space between each of these fermion sites to describe the state of the electric field.

The Hamiltonian describing the contribution from the electric field itself is,

$$H_E = \frac{1}{2} \sum_n |E_x|^2 , \quad (307)$$

and therefore, the lattice Schwinger model can be written as

$$H_{1+1QED}^{\text{latt.}} = \frac{1}{2a} \sum_{n=0}^{N_{fs}-1} (\sigma_n^+ L_n^- \sigma_{n+1}^- + \sigma_n^- L_n^+ \sigma_{n+1}^+) + \frac{m}{2} \sum_{n=0}^{N_{fs}-1} (-)^n \hat{Z}_n + \frac{ag^2}{2} \sum_{n=0}^{N_{fs}-1} l_n^2 , \quad (308)$$

where  $L^\pm|l\rangle = |l\pm 1\rangle$ , and  $g$  is the electric coupling (in a given scheme). Figure 36 shows the lattice layout for the Schwinger model with explicit degrees of freedom for the gauge-field, i.e.,  $A_0 = 0$  gauge. The Gauss's law constraint is that the flux-difference at any fermion site corresponds to the charge at that site. For instance, the action of the hopping term can, for example, couple the trivial vacuum to one with a  $e^-e^+$  pair and corresponding gauge link,

$$|\downarrow\uparrow\rangle \otimes |n,n,n\rangle \rightarrow |\uparrow\downarrow\rangle \otimes |n,n-1,n\rangle , \quad (309)$$

Figure 37 shows a cartoon of states that satisfy Gauss's law, before and after the action of the hopping term. A created  $e^-e^+$  pair is coupled to a change in the electric field between the sites of the pair.

<sup>52</sup> For small lattice spacings,

$$e^{+iae\hat{Q}A_x} \rightarrow 1 + iae\hat{Q}A_x - \dots , \phi(n+1) = \phi(n) + a\partial\phi(n) + \dots . \quad (303)$$

<sup>53</sup> Recall that, for non-commuting operators,

$$[\hat{A}, f(\hat{B})] = [\hat{A}, \hat{B}] \frac{\partial f(\hat{B})}{\partial \hat{B}} . \quad (304)$$

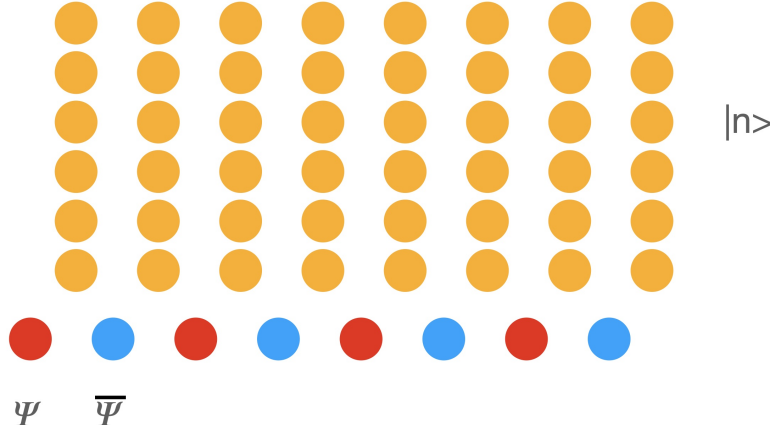


FIG. 36: Qubit layout for 1+1D lattice QED (the lattice Schwinger model) where the gauge field is included explicitly as local degrees of freedom ( $A_0 = 0$  gauge). The red circles denote electron sites, while the blue denote positron sites. The orange circles denote ladder states for the local gauge fields.

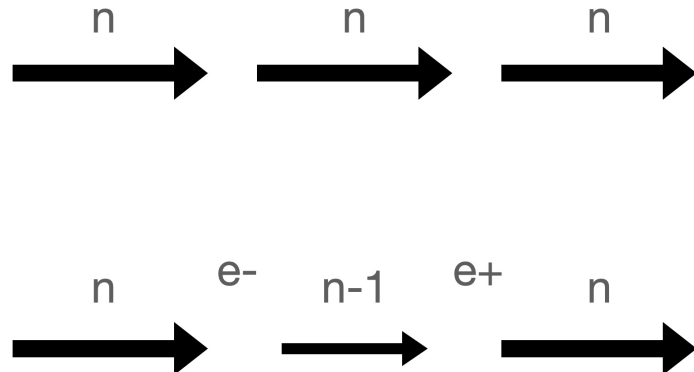


FIG. 37: An artist's impression of implementing Gauss's Law in the Schwinger model.

This implementation is local as all operations by the Hamiltonian depend only on the fields at individual sites. Even though Gauss's law fully constrains the electric field once the field at one end of the system is defined, there are quantum registers for the electric field at each fermion site that are acted on. This seems quite an expensive overhead to include. A different mapping exists through a different choice of gauge fixing, e.g.,  $A_x = 0$  gauge (axial gauge).

Including the  $\theta$ -term can be accomplished straightforwardly, and entails shifting the electric field values by the amount of the background field,

$$\sum_{n=0}^{N_{fs}-1} l_n^2 \rightarrow \sum_{n=0}^{N_{fs}-1} \left( l_n + \frac{\theta}{2\pi} \right)^2 , \quad (310)$$

Something to keep in mind, that we have not dwelt upon, but will return to in the context of non-Abelian gauge theories, is how the gauge invariant spaces are “dealt with”. In particular, the link variable transforms in such a way to preserve gauge invariance at each lattice site, and there are independent *left* and *right* actions of the gauge transformations,

$$U_{n,n+1} \rightarrow V_{L,n} U_{n,n+1} V_{R,n+1} . \quad (311)$$

1. *Eliminating the (Spatial) Gauge-Field from the Outset : A Non-Local Mapping of the Schwinger Model using Axial Gauge:  $A_x = 0$*

There are mappings of 1+1D QED that do not require explicit Hilbert spaces (qubits or qudits) for the gauge field. The electric field adjacent to each site is uniquely constrained by the flux that enters and exits the site and the charges at the site, without any unconstrained degrees of freedom (unlike in higher spatial dimensions). A nice review of the general construction for U(1) and SU(N) lattice theories in 1+1D can be found, for example, in Ref. [77]. From a non-lattice point of view, this corresponds to a different choice of gauge, discussions of which can be in quantum field theory textbooks, for example, Weinberg's text [78]. Before JW mapping, a gauge transformation can be performed on the field at each lattice site in which the system is stepped through (from left to right), defining the n+1 site field relative to the n-site field by

$$\phi_n^\dagger U_{n,n+1} \phi_{n+1} \rightarrow \tilde{\phi}_n^\dagger \tilde{\phi}_{n+1} , \quad (312)$$

which changes only the hopping term, and returns the model back to that of a non-interacting theory (except for the energy in the gauge field, defined by  $A_0$ ), and leaves the mass term unchanged. The gauge-field term for the lattice model is of the form

$$\sum_{n=0}^{N_{fs}-1} l_n^2 = l_0^2 + l_1^2 + \dots \sim |E_0|^2 + |E_1|^2 + \dots , \quad (313)$$

and starting with an external field,  $\mathcal{E}$ , at the left of the lattice, becomes

$$\begin{aligned} \sum_{n=0}^{N_{fs}-1} l_n^2 &\rightarrow |\mathcal{E} + Q_0|^2 + |\mathcal{E} + Q_0 + Q_1|^2 + |\mathcal{E} + Q_0 + Q_1 + Q_2|^2 + \dots \\ &= \sum_{n=0}^{N-2} (N - 1 - n) Q_n^2 + 2 \sum_{n=0}^{N-3} \sum_{m=n+1}^{N-2} (N - 1 - m) Q_n Q_m , \end{aligned} \quad (314)$$

where we have made explicit use of Gauss's law, and  $Q_n$  is the electric charge at site- $n$ . Therefore, the complete lattice Hamiltonian for the Schwinger model formulated without explicit gauge-field degrees of freedom encoded on a quantum register ( $A_x = 0$  gauge) is

$$\begin{aligned} H_{1+1QED}^{\text{latt.}(without)} &= \frac{1}{2a} \sum_{n=0}^{N_{fs}-1} (\sigma_n^+ \sigma_{n+1}^- + \sigma_n^- \sigma_{n+1}^+) + \frac{m}{2} \sum_{n=0}^{N_{fs}-1} (-)^n \hat{Z}_n \\ &+ \frac{ag^2}{2} \left( \sum_{n=0}^{N_{fs}-2} (N_{fs} - 1 - n) \hat{Q}_n^2 + 2 \sum_{n=0}^{N_{fs}-3} \sum_{m=n+1}^{N_{fs}-2} (N_{fs} - 1 - m) \hat{Q}_n \hat{Q}_m \right) , \\ \hat{Q}_n &= -\frac{1}{2} (\hat{Z}_n + (-)^n) , \end{aligned} \quad (315)$$

where the global sign of  $\hat{Q}$  is unphysical, and we are assuming that the particles are electrons (and antiparticles are positrons). Figure 38 shows a cartoon of the types of non-local interactions required to define the energy in the electric field in  $A_x = 0$  gauge,

There is a trade-off between the local and nonlocal mappings. In the local mapping, corresponding to  $A_0 = 0$  gauge, explicit degrees of freedom are included to define the gauge field, all interactions in the Hamiltonian are local and the number of operations required in simulation scales with the length of the lattice, consistent with one of the criteria that are required to be satisfied in

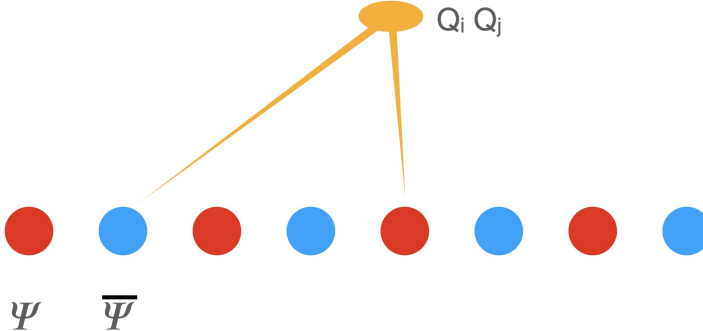


FIG. 38: A nonlocal operator with structure  $\hat{Q}_i \hat{Q}_j$  that is required to define the energy in the electric field in the lattice Schwinger model when the gauge-field is not included explicitly.

order to perform simulations at scale. In contrast, the non-local mapping, corresponding to  $A_x = 0$  gauge, requires far fewer qubits as the formally infinite dimensional Hilbert spaces at each site are not required. However, this comes at the cost of requiring non-local interactions between the sites to define the energy in the electric field, which scales quadratically with the lattice extent - naively violating the quantum simulation criterion.

However, in simulation, the question is to the resources required to compute a quantity of interest, for example, a scattering cross section, to a certain level of precision. In some of our recent work [64, 65], we realized that confinement (an emergent phenomenon, that is unobvious at the level of the Hamiltonian) exponentially suppresses correlations that are more than a few confinement-lengths separated, and hence changes the resource requirement  $\mathcal{O}(L^2)$  scaling to  $\mathcal{O}(\xi L)$ , where  $\xi$  is the confinement length scale, for simulations of bounded error. So, while it is not obvious from the nature of the JW mapping to spins, the fact that the theory is confining at low-temperatures means that it can be simulated efficiently at scale. The high-temperature regime needs to be analyzed in a similar way. Another interesting observation that we have made is that, somewhat counter-intuitively, the resources (operations) required to evolve such a lattice field theory forward in time, scale in the same way for both choices of gauge,  $A_0 = 0$  and  $A_x = 0$  gauges, i.e., the local and non-local mappings require the similarly-scaling resources per spacetime volume evolution [79, 80]. Therefore, both mappings are viable for quantum simulation, with one requiring fewer qubits at the expense of post-simulation verification of exponentially decaying charge-charge correlation functions (in the low-energy regime).

## 2. More than one species: $e^-$ and $\mu^-$

One question that we need to answer before going to non-Abelian gauge theories is about how to simulate more than one charged species. Recall the two different formulations of the Hamiltonian, corresponding to two choices of gauge fixing, given in Eq. (308) in  $A_0 = 0$  gauge and in Eq. (315) in  $A_x = 0$  gauge,

$$H_{A_0=0}^{\text{latt.}} = \frac{1}{2a} \sum_{n=0}^{N_{fs}-1} (\sigma_n^+ L_n^- \sigma_{n+1}^- + \sigma_n^- L_n^+ \sigma_{n+1}^+) + \frac{m}{2} \sum_{n=0}^{N_{fs}-1} (-)^n \hat{Z}_n + \frac{ag^2}{2} \sum_{n=0}^{N_{fs}-1} l_n^2 \quad (316)$$

and

$$\begin{aligned} H_{A_x=0}^{\text{latt.}} = & \frac{1}{2a} \sum_{n=0}^{N_{fs}-1} (\sigma_n^+ \sigma_{n+1}^- + \sigma_n^- \sigma_{n+1}^+) + \frac{m}{2} \sum_{n=0}^{N_{fs}-1} (-)^n \hat{Z}_n \\ & + \frac{ag^2}{2} \left( \sum_{n=0}^{N_{fs}-2} (N_{fs} - 1 - n) \hat{Q}_n^2 + 2 \sum_{n=0}^{N_{fs}-3} \sum_{m=n+1}^{N_{fs}-2} (N_{fs} - 1 - m) \hat{Q}_n \hat{Q}_m \right) \end{aligned} \quad (317)$$

respectively.

When describing the dynamics of two charged species, e.g.,  $e^-$  and  $\mu^-$ , it is a little easier to understand what has to be done with the local ( $A_0 = 0$ ) gauge construction. Recalling the strings of  $\hat{Z}$ 's that accompany fermions to accommodate Fermi statistics, the Hamiltonian becomes,

$$\begin{aligned} H_{N_f=2}^{\text{latt.}, A_0=0} \rightarrow & -\frac{1}{2a} \sum_{n=0}^{N_{fs}-1} (\sigma_{n,e}^+ \sigma_{n,\mu}^z \sigma_{n+1,e}^- L_n^- + \sigma_{n,e}^- \sigma_{n,\mu}^z \sigma_{n+1,e}^+ L_n^+) + \frac{m_e}{2} \sum_{n=0}^{N_{fs}-1} (-)^n \hat{Z}_{n,e} \\ & - \frac{1}{2a} \sum_{n=0}^{N_{fs}-1} (\sigma_{n,\mu}^+ \sigma_{n+1,e}^z \sigma_{n+1,\mu}^- L_n^- + \sigma_{n,\mu}^- \sigma_{n+1,e}^z \sigma_{n+1,\mu}^+ L_n^+) + \frac{m_{\mu^-}}{2} \sum_{n=0}^{N_{fs}-1} (-)^n \hat{Z}_{n,\mu^-} \\ & + \frac{ag^2}{2} \sum_{n=0}^{N_{fs}-1} l_n^2 . \end{aligned} \quad (318)$$

The  $\sigma^z$  between the  $\sigma^\pm$  are to take into account the occupation of the “other” species. If it is occupied, there is an additional –ve sign compared to when it is unoccupied.

Figure 39 shows one basis configuration of the  $N_f = 2$  system that satisfies Gauss’s law. From

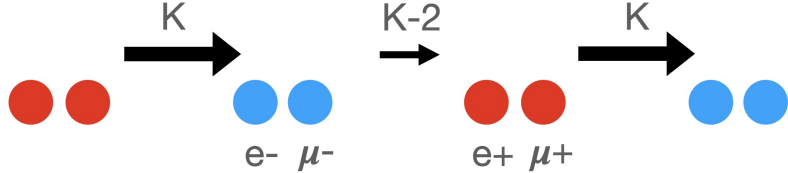


FIG. 39: One basis configuration of the 1+1 QED with both electrons and muons.  $K = l_n$  is the winding number of the electric field.

this figure, it is obvious how to construct Gauss’s law at each site - it is the sum over charges at each site that dictates the discontinuity between adjacent gauge fields. This also enables a ready construction of the Hamiltonian in  $A_x = 0$  gauge,

$$\begin{aligned} H_{N_f=2}^{\text{latt.}, A_x=0} \rightarrow & -\frac{1}{2a} \sum_{n=0}^{N_{fs}-1} (\sigma_{n,e}^+ \sigma_{n,\mu}^z \sigma_{n+1,e}^- + \sigma_{n,e}^- \sigma_{n,\mu}^z \sigma_{n+1,e}^+) + \frac{m_{e^-}}{2} \sum_{n=0}^{N_{fs}-1} (-)^n \hat{Z}_{n,e^-} \\ & - \frac{1}{2a} \sum_{n=0}^{N_{fs}-1} (\sigma_{n,\mu}^+ \sigma_{n+1,e}^z \sigma_{n+1,\mu}^- + \sigma_{n,\mu}^- \sigma_{n+1,e}^z \sigma_{n+1,\mu}^+) + \frac{m_{\mu^-}}{2} \sum_{n=0}^{N_{fs}-1} (-)^n \hat{Z}_{n,\mu^-} \\ & + \frac{ag^2}{2} \left( \sum_{n=0}^{N_{fs}-2} (N_{fs} - 1 - n) \hat{Q}_n^2 + 2 \sum_{n=0}^{N_{fs}-3} \sum_{m=n+1}^{N_{fs}-2} (N_{fs} - 1 - m) \hat{Q}_n \hat{Q}_m \right) , \end{aligned} \quad (319)$$

where  $\hat{Q}_n \rightarrow \hat{Q}_{n,e^-} + \hat{Q}_{n,\mu^-}$ . The extension to an arbitrary number of charged particles, with arbitrary charges, is now straightforward.

### 3. Background Charges

In general, the inclusion of background charges (or classical sources) is the mechanism by which different aspects and different charge sectors of the theory are probed, particularly the detection of charge confinement and screening. The inclusion of background charges into 1+1D QED is accomplished through a discontinuity in Gauss's Law at given sites, and, importantly, without including a new species of fermions being included into the (simulation) dynamics, as seen in Figure 40. The physics reasons for being able to include the heavy-field in this way are deeply

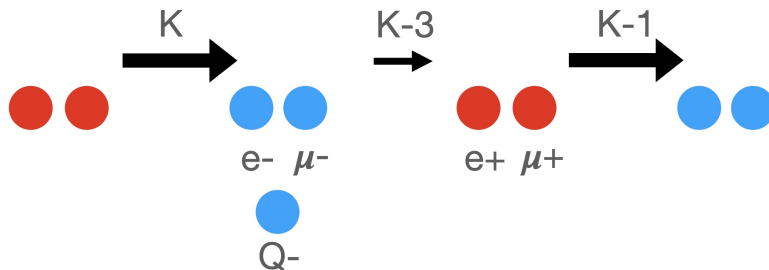


FIG. 40: One basis configuration of the 1+1 QED with electrons, muons and a background -ve static charge,  $Q^-$ , at one site. The integer  $K$  denotes the electric field leaving the left-most (antiparticle) lattice site, and entering the particle site containing a total charge of  $-3$ , which reduces the electric field by  $\Delta K = -3$ . While the electron and muon fields are dynamical, the background static charge is included as a discontinuity in Gauss's law.

rooted in quantum field theory. First, there may simply be a fixed background charge. Second, it is also a way to consider the *heavy-meson* spectrum of a theory with a large mass hierarchy, such that  $m_Q \gg \Lambda_{QED}, m_e, m_\mu, E$ , where  $\Lambda_{QED}$  is the typical energy scale of the bound states of the  $e - \mu$  sector,  $m_{e,\mu}$  are the masses of the  $e$  and  $\mu$ , and  $E$  is the energy being probed in the system. Discovery and implementation of heavy-quark effective field theory (HQET), by Mark Wise, David Politzer, Nathan Isgur [81–84] and others in the mid- to late-1980s pioneered this line of thinking and organization of effective field theories with mass hierarchies, including the discovery of heavy-quark spin-symmetry. Heavy-baryon chiral perturbation theory (HB $\chi$ PT), the low-energy EFT describing the light-baryon sector(s), developed by Jenkins and Manohar [85, 86], followed directly from HQET. The latter is the most general covariant low-energy EFT describing baryons, from which other constructions, such as the low-velocity expansions are derived and are a subset thereof.

In 1+1D QED, by including a background static charge corresponds to including an infinitely massive charge (compared with the other mass scales), and hence the large dimensionless ratios that would naively arise, e.g.,  $m_Q/m_e$ , are all explicitly removed, with the knowledge that any computation in the low energy theory with  $N_Q$  static charges gives energy eigenvalues that are shifted by  $N_Q m_Q$ , with recoil-type corrections that are suppressed by powers of  $m_e/m_Q, m_\mu/m_Q, E/m_Q, \Lambda_{QED}/m_Q$ .

There are a series of calculations that can be (and have been) performed [87], including the vacuum energy, the mass of a single heavy hadron, and the potential energy between a heavy hadron and heavy anti-hadron, in the theory of a background charge and a dynamical electron field. The methodology used in those calculations is [87]:

1. The ground state energy of the electronic system without any background charges is computed,  $E_0$ .

2. The ground state energy of the system with one  $Q^-$  charge is computed,  $E^{(Q)}$ . From this, the (non-perturbative) mass of the *hadron* containing one  $Q^-$  charge is determined to be  $M_Q = E^{(Q)} - E_0$ . The mass of the hadron with  $Q^-$  background charge will be the same as that with a  $Q^+$  background charge.
3. The ground state energy of the system with one  $Q^-$  charge at  $x = 0$  and one  $Q^+$  charge at  $x = R$  is computed,  $E^{(Q^-Q^+)}(R)$ . The potential energy between the hadrons is determined by the difference between this energy and that of the rest mass of two hadrons,  $V^{(Q^-Q^+)}(R) = E^{(Q^-Q^+)}(R) - 2M_Q$ . For screened charges, this vanishes as  $R \rightarrow \infty$ .
4. Similarly, the potential between two hadrons containing same-sign static charges can be determined.

The eigenstates of each of these systems can be used to determine the local charge configurations and entanglement within the states, in the hadrons and the changes due to the forces between them, using state tomography and partial tracing, e.g., Refs. [79, 87]

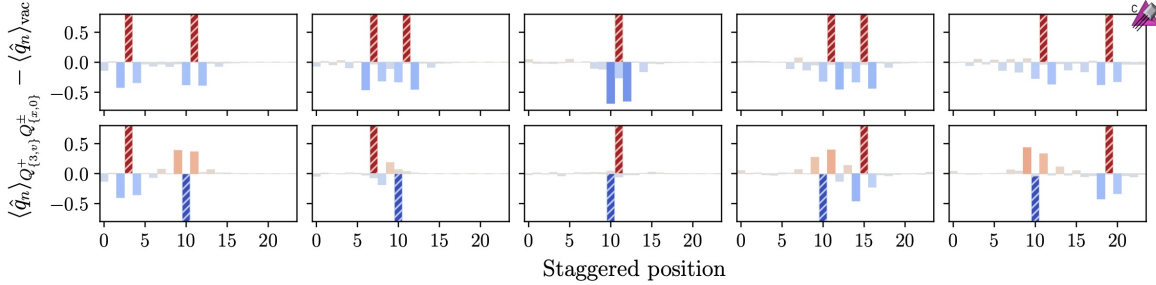


FIG. 8. The vacuum subtracted charge distribution in the light degrees of freedom (solid bars) shown for when the moving heavy- $Q^+$  is at  $x = \{3, 7, 11, 15, 19\}$  (left-to-right). The results in the upper (bottom) panels are for a static heavy- $Q^+$  ( $Q^-$ ) located at  $x = 11$  ( $x = 10$ ). The dashed bars denote the location of the heavy-charges, and simulation parameters  $v_{\max} = 0.2$ ,  $m = 0.1$ ,  $g = 0.8$ , and  $L = 12$  have been used.

FIG. 41: Classical simulations of the collision of two hadrons (upper panels) and a hadron and anti-hadron (lower panels). See Ref. [88] for details.

Figure 41 shows the charge density associated with two background heavy –ve charges (top panels) and one +ve and one –ve heavy charge (bottom panels), as computed in Ref. [88]. The ground state of the system with the background charges at rest and well separated is two hadrons with their associated light degrees of freedom not overlapping.

#### 4. Quantum Circuits

Without detail, it is worth thinking about the quantum circuits for implementing multi-flavor 1+1D QED. In  $A_x = 0$  gauge, with hopping and mass terms being identical in form to the non-interacting theory (that we have discussed in detail previously), the quantum circuits for time evolution are those of the non-interacting theory with only changes to couplings and masses required. With multiple flavors, the number of bodies touched by the hopping term increase due to Pauli statistics, such that there are  $\hat{Z}$  operators acting on all fermions between the particle and corresponding anti-particle site. So with  $N_f$  species of charged particles, the hopping operators are of the form

$\sigma^+ \otimes \hat{Z}^{\otimes N_f - 1} \otimes \sigma^-$ , and hence the associated circuits are more complicated, but straightforward variations of what we have considered previously.<sup>54</sup>

Implementing the gauge field is also straightforward because the charge operators at each spatial site are combinations of  $\hat{I}$  and  $\hat{Z}$  (and background charges). The charge operators sum over the charges at each site, and are at most quadratic in  $\hat{Z}$ , but their numbers proliferate with increasing  $N_f$ .<sup>55</sup>

### E. Non-Abelian Gauge Theories in 1+1 Dimensions

1+1D QED shares many features of QCD that are valuable to explore. Its utility in quantum simulations related to high-energy physics and nuclear physics will continue as simulation capabilities increase. Perhaps the most important lesson so far was that the choice of gauge fixing makes a significant difference in the form of the lattice theory, while the scaling of required quantum resources remain essentially unchanged for evolving through a given spacetime volume.

We can delay dealing with some of the complexity on non-Abelian gauge theories in 1+1D by working in  $A_x^a = 0$  gauge, where each of the gauge fields in the spatial direction associated with the generators of  $SU(N_c)$  are set equal to zero, leaving constrained  $A_0^a$  fields. In this way, link operators and considerations related to local gauge links can be avoided, and the equivalent non-local construction can be used to begin with.

Consider the  $SU(2)$  lattice gauge theory (that is invariant under local  $SU(2)$  color transformations) with one flavor of quark, arranged in an  $SU(2)$  color doublet [89]. In the continuum, the Lagrange density and components are,

$$\begin{aligned} \mathcal{Q} &= \begin{pmatrix} r \\ g \end{pmatrix}, \quad \mathcal{Q} \rightarrow \mathcal{Q}' = \hat{U}(x)\mathcal{Q}, \\ \mathcal{L} &= \overline{\mathcal{Q}}i\cancel{D}\mathcal{Q} - m\overline{\mathcal{Q}}\mathcal{Q} - \frac{1}{4}\sum_{a=1}^3 G_{\mu\nu}^a G^{a,\mu\nu}, \quad D_\mu = \partial_\mu + igT^a W_\mu^a, \\ W_\mu^a &\rightarrow W_\mu^{a'} = UW_\mu^a U^\dagger - \partial_\mu UU^\dagger, \quad T^a = \frac{1}{2}\sigma^a. \end{aligned} \quad (320)$$

In  $A_x^a = 0$  gauge, the JW mapping is similar to the two-species QED case,

$$\begin{aligned} H_{N_c=2, N_f=1}^{\text{latt.}, A_x=0} &\rightarrow -\frac{1}{2} \sum_{n=0}^{N_{fs}-1} \left( \sigma_{n,r}^+ \sigma_{n,g}^z \sigma_{n+1,r}^- + \sigma_{n,r}^- \sigma_{n,g}^z \sigma_{n+1,r}^+ + \sigma_{n,g}^+ \sigma_{n+1,r}^z \sigma_{n+1,g}^- + \sigma_{n,g}^- \sigma_{n+1,r}^z \sigma_{n+1,g}^z \right) \\ &+ \frac{m}{2} \sum_{n=0}^{N_{fs}-1} (-)^n (\hat{Z}_{n,r} + \hat{Z}_{n,g}) + N_{fs} \\ &+ \frac{g^2}{2} \sum_{a=1}^3 \left( \sum_{n=0}^{N_{fs}-2} (N_{fs} - 1 - n) (\hat{Q}_n^a)^2 + 2 \sum_{n=0}^{N_{fs}-3} \sum_{m=n+1}^{N_{fs}-2} (N_{fs} - 1 - m) \hat{Q}_n^a \hat{Q}_m^a \right), \end{aligned} \quad (321)$$

where the gauge terms recovers the  $\sum_a |E^a|^2$  contribution, and the lattice spacing is set equal to unity,  $a = 1$ . We have gone straight to the final result, but should consider some of the steps. In

<sup>54</sup> It is important to keep track (make sure you are completely happy) of the signs associated with particle and anti-particle sites (due to the fact that the *occupied* state differs between the two).

<sup>55</sup> The situation is significantly different for non-Abelian theories, as the generators of the transformations act on the states in non-trivial ways.

particular, the Hamiltonian must be a color singlet, and as such mixed terms, such as  $E^a E^b$ , are not present.

The Gauss's law constraints are more complicated, as they apply to each component of the SU(2) gauge field,

$$E_<^a + Q^a = E_>^a , \quad (322)$$

at each fermion site, but are sufficiently simple in 1+1D, that the general construction for the Schwinger model translates to the non-Abelian lattice theory straightforwardly with only slight modifications. The SU(2) charge operators are defined by, along with their JW mapping,

$$\begin{aligned} \hat{Q}^1 &= \phi^\dagger T^1 \phi \rightarrow \frac{1}{2} (\sigma_{n,r}^+ \sigma_{n,g}^- + \sigma_{n,r}^- \sigma_{n,g}^+) , \\ \hat{Q}^2 &= \phi^\dagger T^2 \phi \rightarrow -i \frac{1}{2} (\sigma_{n,r}^+ \sigma_{n,g}^- - \sigma_{n,r}^- \sigma_{n,g}^+) , \\ \hat{Q}^3 &= \phi^\dagger T^3 \phi \rightarrow \frac{1}{4} (\sigma_{n,r}^z - \sigma_{n,g}^z) . \end{aligned} \quad (323)$$

The additional complication due to the non-Abelian nature of the theory is readily visible. While  $\hat{Q}^3$  multiplies basis states by phases corresponding to the occupation of the site, the  $\hat{Q}^{1,2}$  transform basis states into other basis states. So computing the charge of a given state is complex, and states of *good* SU(2) charge are typically entangled states—entangled in color space. The classical computational resource requirements for simulations are significantly more than for QED for this reason. This is at the heart of the difference between simulating Abelian and non-Abelian gauge theories, and more generally the different physical manifestations of the two. It is also the case that  $N_C = 2$  theories are fundamentally different from  $N_C = 3, 4, 5$  theories, for reasons that we will return to later.

In the  $A_0 = 0$  gauge, there are parallel transporters between the lattice sites (that act on qubits or qudits that are additionally included in the mapping), defined by

$$\hat{U}_n = e^{i\theta_n^a \hat{T}^a} , \quad \hat{U}_n^{(r)} = e^{i\theta_n^a T^{(r),a}} , \quad (324)$$

where in the case of the fundamental representation of SU(2),  $T^a = \sigma^a/2$ . For the sake of simplicity, we examine SU(2), and simply state results for a general SU(N) group. The action of  $\hat{U}$  does not produce a single complex number, but is matrix valued, and appears equivalent to an SU(2) rotation operator with a basis defined by the conjugate momentum,  $|j, m\rangle$ . However, this is not actually the case because this operator acts in two different Hilbert spaces, one on the left and one on the right (or the tip and tail of an arrow). The transporter is designed to connect two different Hilbert spaces, such that

$$\psi_n^\dagger \hat{U}_{n,n+1} \psi_{n+1} \rightarrow \psi_n^\dagger V_n^\dagger \left( V_n \hat{U}_{n,n+1} V_{n+1}^\dagger \right) V_{n+1} \psi_{n+1} , \quad (325)$$

is invariant under independent SU(N) transformations in the left-handed and right-handed spaces at  $n$  and  $n+1$ ,  $V_n$  and  $V_{n+1}$ , respectively. So the link operator has to be thought of in a fundamentally different way from, say, the quark operators that act in a single Hilbert space....the link operator acts in two spaces in order to parallel transport between them.

The actions of left-acting and right-acting SU(2) electric field operators are, one in each of the two spaces (either end of the link operator),

$$\begin{aligned} [\hat{L}_n^a, \hat{U}_n] &= \hat{T}^a \hat{U}_n , \quad [\hat{R}_n^a, \hat{U}_n] = \hat{U}_n \hat{T}^a \\ [\hat{R}_n^a, \hat{R}_n^b] &= if^{abc} \hat{R}_n^c , \quad [\hat{L}_n^a, \hat{L}_n^b] = -if^{abc} \hat{L}_n^c , \quad [\hat{L}_n^a, \hat{R}_n^b] = 0 . \end{aligned} \quad (326)$$

To make sense of the form of these relations, particularly the operator orderings, the state that it is acting on  $|j, m_L, m_R\rangle$  has the form  $|j, m_L\rangle\langle j, m_R|$ . The subscript denotes the location of the link, as opposed to the site label. We see that the  $\hat{L}$  and  $\hat{R}$  define the transformations of the parallel transporter at the two sites that it connects, and each have the commutation relations of an SU(N) algebra. Because the parallel transporter preserves the SU(N) charges between sites, a conjugate-variable basis can be defined for each  $\hat{U}$  by, for example, for SU(2)

$$\begin{aligned} & \{ |j, m_L, m_R\rangle \}, \\ & \hat{L}^2 |j, m_L, m_R\rangle = \hat{\mathbf{R}}^2 |j, m_L, m_R\rangle = j(j+1) |j, m_L, m_R\rangle, \\ & \hat{L}_z |j, m_L, m_R\rangle = m_L |j, m_L, m_R\rangle, \quad \hat{R}_z |j, m_L, m_R\rangle = m_R |j, m_L, m_R\rangle. \end{aligned} \quad (327)$$

From the action of generators on the trivial vacuum, in particular the action  $\hat{U}$  on a given representation of SU(2), gives

$$\begin{aligned} \hat{L}^a \hat{U} |0\rangle &= \hat{U} \hat{L}^a |0\rangle + T^a \hat{U} |0\rangle = T^a \hat{U} |0\rangle \\ \sum_a \hat{L}^a \hat{L}^a \hat{U} |0\rangle &= \sum_a (T^a)^2 \hat{U} |0\rangle \rightarrow j_r(j_r+1) \hat{U}^{(r)} |0\rangle, \end{aligned} \quad (328)$$

and similarly  $\sum_a (\hat{R}^a)^2 \hat{U}^{(r)} |0\rangle = j_r(j_r+1) \hat{U}^{(r)} |0\rangle$ . This shows that the parallel transporter connecting quarks in the fundamental representation of SU(2) transforms as a  $j = 1/2$  operator, such that the action of the link operator on a given link state is,

$$\hat{U}_{\alpha\beta}^{(1/2)} |j, a, b\rangle = \sum_{\oplus K} \sqrt{\frac{(2j+1)}{(2K+1)}} |K, a+\alpha, b+\beta\rangle \langle K, b+\beta | j, b, \frac{1}{2}, \beta \rangle \langle K, a+\alpha | j, a, \frac{1}{2}, \alpha \rangle \quad (329)$$

This shows that the action of the link operator corresponds to raising and lowering operations in SU(2) irreps, with coefficients determined by products of Clebsch-Gordon coefficients.<sup>56</sup> It is important to note that the action of the link operator on a state of fixed  $j$  produces a coherent sum of states with  $K = j \pm 1/2$  (with generally different amplitudes), but that the value of  $K$  is shared between the left-handed and right-handed spaces, and there are no mixed states produced. This has to be the case by the conservation of electric flux along the link. While the orientation of the electric field in the SU(2) space can differ between the spaces, the magnitude of the flux cannot. The Hilbert space layout of this problem ( $A_0 = 0$  gauge) can be seen in Fig. 42.

The JW mapping in  $A_0 = 0$  gauge is similar to that in  $A_x^a = 0$  gauge (in Eq. (321)),

$$\begin{aligned} H_{N_c=2, N_f=1}^{\text{latt.}, A_0^a=0} &\rightarrow -\frac{1}{2} \sum_{n=0}^{N_{fs}-1} \left( \sigma_{n,r}^+ \sigma_{n,g}^z \sigma_{n+1,r}^- \left( \hat{U}^{(\frac{1}{2})} \right)_r^r + \sigma_{n,g}^+ \sigma_{n+1,r}^z \sigma_{n+1,g}^- \left( \hat{U}^{(\frac{1}{2})} \right)_g^g \right. \\ &\quad \left. - \sigma_{n,r}^+ \sigma_{n,g}^z \sigma_{n+1,r}^z \sigma_{n+1,g}^- \left( \hat{U}^{(\frac{1}{2})} \right)_g^r - \sigma_{n,g}^+ \sigma_{n+1,r}^- \left( \hat{U}^{(\frac{1}{2})} \right)_r^g + \text{h.c.} \right) \\ &\quad + \frac{m}{2} \sum_{n=0}^{N_{fs}-1} (-)^n (\hat{Z}_{n,r} + \hat{Z}_{n,g}) + N_{fs} + \frac{g^2}{2} \sum_{n=0}^{N_{fs}-1} \sum_{a=1}^3 (\hat{j}^a)^2, \end{aligned} \quad (330)$$

but with important differences. Specifically, the hopping term involves non-trivial connections between different colored quarks induced by the parallel transporter, and the link states are local. The trivial vacuum, for 2 spatial sites is

$$|\Omega\rangle = |\downarrow\uparrow\downarrow\uparrow\rangle \otimes |0, 0, 0\rangle \otimes |0, 0, 0\rangle \otimes |0, 0, 0\rangle, \quad (331)$$

---

<sup>56</sup> Clearly, I have not attempted to prove this, which is left as an *exercise for the reader*.

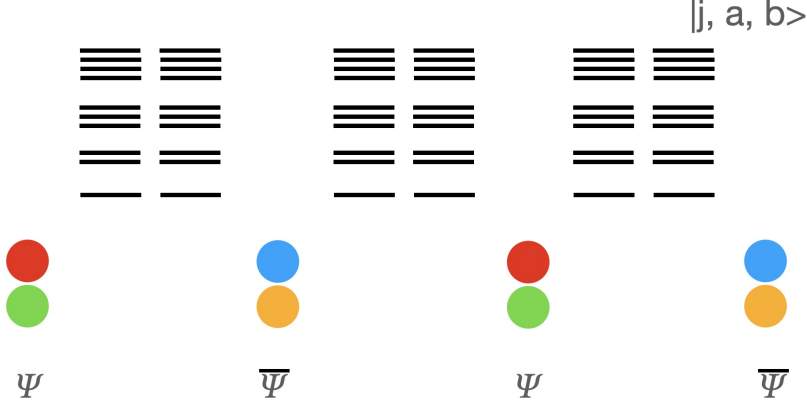


FIG. 42: The Hilbert space layout of  $SU(2)$  lattice gauge theory in  $A_0^a = 0$  gauge. The fermions are encoded in two qubits per lattice site with a JW mapping of the Kogut-Susskind Hamiltonian (as usual, with each encoding the occupation of the different quark colors), while the three gauge fields are encoded into states  $|j, a, b\rangle$  for all possible values of  $j$  (which in practice is limited by a cut-off in  $j$ -space tuned to the desired precision of the simulation).

with open boundary conditions and

$$|\Omega\rangle = |\downarrow\uparrow\downarrow\uparrow\rangle \otimes |0,0,0\rangle \otimes |0,0,0\rangle \otimes |0,0,0\rangle \otimes |0,0,0\rangle , \quad (332)$$

with PBCs.

### 1. The Extension to $SU(3)$ in 1+1D

The extension of the  $SU(2)$  construction to  $SU(3)$  and  $SU(N)$  gauge groups follows straightforwardly. We detail the extensions to  $SU(3)$ , which includes all of the (conceptual) differences between  $SU(2)$  and which can be generalized to  $SU(N)$  without new elements. The electric basis is defined by states of the form

$$|\mathbf{R}, a, b\rangle , \quad (333)$$

where  $\mathbf{R}$  denotes an irrep of  $SU(3)$ , for example **3**, or **10** or **27**, and the  $a, b$  denote states in the given irrep, which can also be denoted in terms of the Cartan subalgebra of  $SU(3)$ ,

$$|\mathbf{R}, \{\mathbf{I}, I_z, Y\}_l, \{\mathbf{I}, I_z, Y\}_r\rangle = |\mathbf{R}, \{\mathbf{I}, I_z, Y\}\rangle_l \otimes_r |\mathbf{R}, \{\mathbf{I}, I_z, Y\}| , \quad (334)$$

The action of the link operator in the fundamental representation of  $SU(3)$ , **3**, is given by

$$\hat{U}_{\alpha\beta}^{(\mathbf{3})} |\mathbf{R}, a, b\rangle = \sum_{\mathbf{R}', \Gamma_{1,2}, a', b'} \sqrt{\frac{d_{\mathbf{R}}}{d_{\mathbf{R}'}}} |\mathbf{R}', a', b'\rangle \langle \mathbf{R}, a, \mathbf{3}, \alpha | \mathbf{R}', a' \rangle_{\Gamma_1} \langle \mathbf{R}', b' | \mathbf{R}, b, \mathbf{3}, \beta \rangle_{\Gamma_2} , \quad (335)$$

where  $\Gamma_i$  denotes irrep multiplicities, and  $d_{\mathbf{R}}$  the dimensionality of the irrep. The  $\langle \mathbf{R}', b' | \mathbf{R}, b, \mathbf{3}, \beta \rangle_{\Gamma}$  denote  $SU(3)$  Clebsch-Gordon coefficients, which can be a little tricky to compute when combining high-dimensional irreps, but luckily they are quite simple when forming tensor products with the **3** or **3̄**.

As the gauge space is infinite dimensional, associated with continuous  $SU(3)$  transformations, which in irrep space, corresponds to arbitrarily high-dimensional irreps, a truncation must be

imposed (somehow). From a physics perspective, the large irreps correspond to large electric field (with an associated high energy density), and a cut off in  $\mathbf{R}$  is a well-motivated choice of truncation. It should be kept in mind that how this is accomplished is not specified. For instance, a hard cut off could be imposed, which is what is generally done today, where irreps above a certain dimensionality are excluded from the simulation. Another choice could be to impose a Gaussian cut off with a width defined by some dimensionality. Whichever regulation is imposed, it is critical that the predictions of target physical observables do not depend on how it is done and the parameters chosen to do it. For example, the value of the average electric field obtained during the time evolution from some given initial state should be independent of the cut off in  $\mathbf{R}$ . This can be verified by repeating the simulations with a number of different cut offs and looking for stability in the final result. It should also be kept in mind that this only needs to be the case within a given uncertainty tolerance. Further, the gauge space at each link grows substantially with the cut-off if it is truncated by the magnitude of the electric field.

$\mathbf{E}^{(a)}$  is the color electric field which can be formed in the basis of irreps of SU(3), such that an irrep with tensor representation  $T_{b_1 \dots b_q}^{a_1 \dots a_p}$ , and states denoted by  $|p, q\rangle$ , with the Casimir and dimensionality given by

$$\sum_{a=0}^8 |\hat{\mathbf{E}}^{(a)}|^2 |p, q\rangle = \frac{1}{3} (p^2 + q^2 + pq + 3p + 3q) |p, q\rangle$$

$$\hat{\dim}|p, q\rangle = \frac{1}{2}(p+1)(q+1)(p+q+2) |p, q\rangle . \quad (336)$$

For the lowest-lying irreps, **1, 3, 8, 6, 15**..., the values of the Casimir are  $1, \frac{4}{3}, 3, \frac{10}{3}, \frac{16}{3} \dots$ . The (number of) states that are required to describe an irrep. sector of the link space are,

$$|\mathbf{1}, 0, 0\rangle : 1 , \quad |\mathbf{3}, a, b\rangle : 3^2 = 9 , \quad |\overline{\mathbf{3}}, a, b\rangle : 3^2 = 9 , \quad |\mathbf{8}, a, b\rangle : 8^2 = 64 ,$$

$$|\mathbf{6}, a, b\rangle : 6^2 = 36 , \quad |\overline{\mathbf{6}}, a, b\rangle : 6^2 = 36 , \quad |\mathbf{15}, a, b\rangle : 15^2 = 225 , \quad |\overline{\mathbf{15}}, a, b\rangle : 15^2 = 225 \quad (337)$$

corresponding to the number of states in the left-space multiplied by the number in the right space.

## F. Yang-Mills Lattice Gauge Theory in Higher Dimensions

We have now developed much of the machinery that we need to start building the framework for quantum simulations in higher numbers of spatial dimensions, but complications remain. The Gauss's law constraints are no longer sufficient to uniquely define all of the components of the gauge field, and therefore dynamical degrees of freedom have to be included. They cannot be gauged away, but they can be transformed. More complicated gauge invariant structures can be formed, such as plaquettes and clusters of plaquettes (overlapping or not) of gauge flux. Figure 43 provides a schematic of formulating Yang-Mills lattice gauge theory using the Kogut-Susskind formulation.

### 1. Plaquettes

The formulations of 1+1D lattice gauge theory considered in previous sections were in terms of parallel transporters that implemented the gauge degrees of freedom as explicit degrees of freedom connecting adjacent lattice sites. Figure 44 shows a generic 2-D spatial lattice layout showing link operators, a generic plaquette and fermion fields. In higher numbers of dimensions, gauge-invariant operators can be constructed for non-Abelian and Abelian gauge theories that do not involve

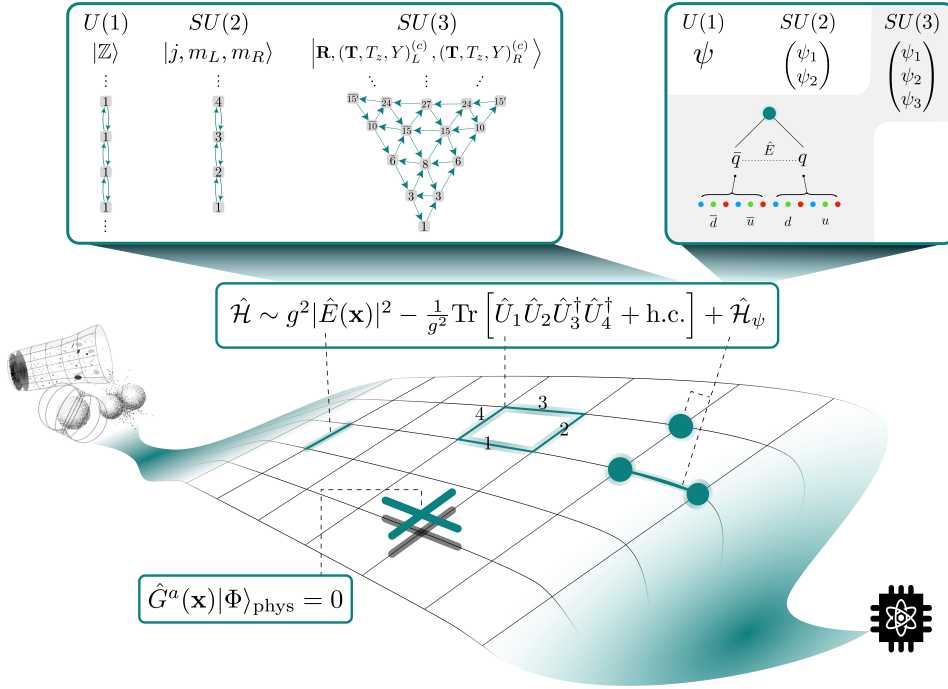


FIG. 43: A schematic of formulating Yang-Mills lattice gauge theory using the Kogut-Susskind formulation. The connectivity in group space is shown at the top for U(1), SU(2) and SU(3). [Image assembled by Natalie Klco, with consultation with Christian Bauer, Zohreh Davoudi and Martin Savage [13].]

fermions, but implement the (unconstrained) dynamics of the gauge-field itself. The minimal (and simplest) structure that can be used to tessellate (pixelate) a surface is the square plaquette, which is efficient to implement.<sup>57</sup> This is not a unique way to tessellate, and other structures such as triangle and hexagonal gauge-invariant operators are also used. For example, for the plaquette operator with corners at  $(x, y) = (0, 0), (0, 1), (1, 1), (1, 0)$ , with flux in the fundamental representation of SU(3),

$$\begin{aligned} & \left( \hat{U}_{00,01}^{(3)} \right)_\beta^\alpha \left( \hat{U}_{01,11}^{(3)} \right)_\gamma^\beta \left( \hat{U}_{11,10}^{(3)} \right)_\rho^\gamma \left( \hat{U}_{10,00}^{(3)} \right)_\alpha^\rho \rightarrow \\ & \text{Tr} \left[ \left( \hat{U}_{00,01}^{(3)} \right) V_{01} V_{01}^\dagger \left( \hat{U}_{01,11}^{(3)} \right) V_{11} V_{11}^\dagger \left( \hat{U}_{11,10}^{(3)} \right) V_{10} V_{10}^\dagger \left( \hat{U}_{10,00}^{(3)} \right) V_{00} V_{00}^\dagger \right] , \end{aligned} \quad (338)$$

is a gauge-invariant operator. Taylor expanding the operator in terms of the gauge-field centered at the middle of the plaquette gives,

$$\begin{aligned} P_{xy} &= e^{-ig \int_0^{a\hat{x}} dz A_x(z)} e^{-ig \int_{a\hat{x}}^{a\hat{x}+a\hat{y}} dz A_y(z)} e^{-ig \int_{a\hat{x}+a\hat{y}}^{a\hat{y}} dz A_x(z)} e^{-ig \int_{a\hat{y}}^0 dz A_y(z)} \\ &= e^{-iga(A_x(c) - \frac{a}{2}\partial_y A_x(c) + \dots)} e^{-iga(A_y(c) + \frac{a}{2}\partial_x A_y(c) + \dots)} e^{+iga(A_x(c) + \frac{a}{2}\partial_y A_x(c) + \dots)} e^{+iga(A_y(c) - \frac{a}{2}\partial_x A_y(c) + \dots)} \\ &= e^{-iga^2(\partial_x A_y(c) - \partial_y A_x(c) + \dots)} = e^{-iga^2(G_{xy}(c) + \dots)} = 1 - ig a^2 G_{xy} - \frac{g^2 a^4}{2} (G_{xy})^2 + \dots , \end{aligned} \quad (339)$$

<sup>57</sup> Recent work has suggested other space-filling structures, such as Triamond lattices could be beneficial for quantum simulation [90]. This is because they limit the link-connectivity to three links in 3+1D, as opposed to six links for hypercubic lattices.

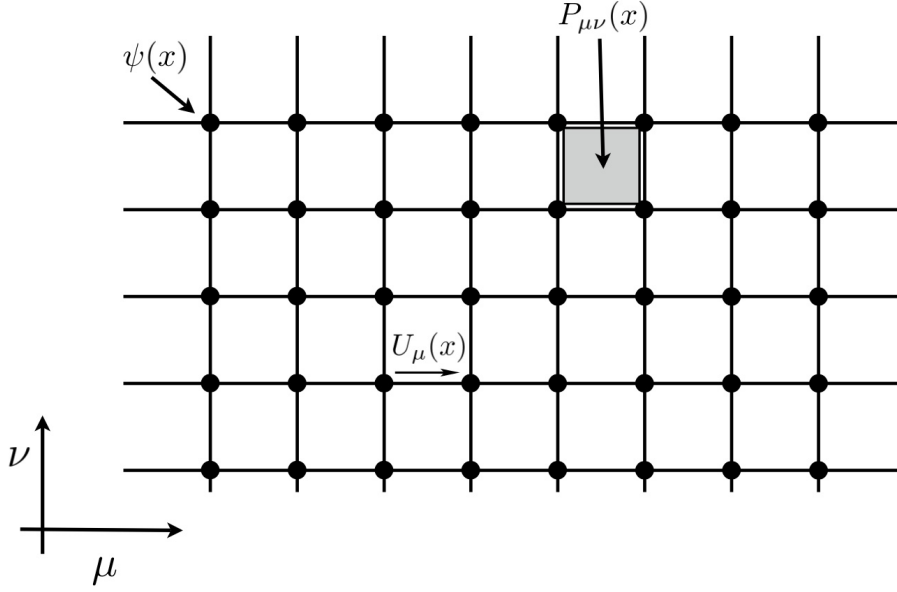


FIG. 44: A 2D lattice of links and sites. Fermions are defined at the lattice sites, the parallel transporters between sites are defined on the links, and plaquettes are formed from squares of link operators.

where the fields are expanded around the center of the plaquette,  $c$ , for example,  $A_x(x + a\hat{x}/2, y) = A_x(c) - \frac{a}{2}\partial_y A_x(c) + \frac{a^2}{8}\partial_y \partial_y A_x(c) + \dots$ , where  $c = (x + a\hat{x}/2, y + a\hat{y}/2)$ . The leading contribution to deviation from unity of the plaquette operator, when expanded around its center, for small lattice spacing is the field strength tensor,  $G_{\mu\nu}$ . Recalling that these are matrix-valued functions, with vanishing trace, we see that

$$\frac{1}{g^2} \sum_{\mathbf{x}, \mu > \nu} [N_c - \text{Tr}[P_{\mu\nu}]] \rightarrow -\frac{1}{8} \int d^3\mathbf{x} \text{Tr} [ G_{\mu\nu} G^{\mu\nu} ] + \dots = -\frac{1}{4} \sum_a \int d^3\mathbf{x} G_{\mu\nu}^a G^{a,\mu\nu}(\mathbf{x}) \quad (340)$$

Classical Euclidean space calculations are performed in this basis, by Monte Carlo'ing over the matrix-valued link  $U$ , and using the plaquette construction above, keeping or rejecting configurations based upon the value of the action.

In the basis defined by eigenstates of the electric operator, the variables conjugate to the link operator, this Hamiltonian is recovered, as shown by Kogut and Susskind [91] in the 1970s, by

$$\hat{H} = \frac{g^2}{2a^{d-2}} \sum_{b, \text{links}} |\hat{\mathbf{E}}^{(b)}|^2 + \frac{1}{2a^{4-d}g^2} \sum_{\text{plaquettes}} \left[ 2N_c - \hat{\square}(\mathbf{x}) - \hat{\square}^\dagger(\mathbf{x}) \right] , \quad (341)$$

The plaquette operator,  $\hat{\square}(\mathbf{x})$ , is defined for SU(3) as

$$\begin{aligned} \hat{\square}(\mathbf{x}) &= \text{Tr} \left[ \hat{U}^3(\mathbf{x}, \mathbf{x} + a\boldsymbol{\mu}) \hat{U}^3(\mathbf{x} + a\boldsymbol{\mu}, \mathbf{x} + a\boldsymbol{\mu} + a\boldsymbol{\nu}) \hat{U}^3(\mathbf{x} + a\boldsymbol{\mu} + a\boldsymbol{\nu}, \mathbf{x} + a\boldsymbol{\nu}) \hat{U}^3(\mathbf{x} + a\boldsymbol{\nu}, \mathbf{x}) \right] \\ &= \hat{U}_{\alpha, \beta}^3 \hat{U}_{\beta, \gamma}^3 \left( \hat{U}_{\gamma, \delta}^3 \right)^\dagger \left( \hat{U}_{\delta, \alpha}^3 \right)^\dagger , \end{aligned} \quad (342)$$

The electric contribution from each link is proportional to the Casimir operator acting on the link  $|\mathbf{R}, \alpha, \beta\rangle$ , without changing the color irrep,  $\mathbf{R}$ , while the plaquette operators,  $\hat{\square} + \hat{\square}^\dagger$ , add color

fluxes **3** and  $\bar{\mathbf{3}}$  to each of the links in the plaquette, which change the irrep of each link, subject to Gauss's law. The action of the plaquette operator on a link in the electric-basis has the form,

$$\hat{U}_{\alpha,\beta}^{\mathbf{r}} |\mathbf{R}, a, b\rangle = \sum_{\substack{\oplus \mathbf{R}', \Gamma \\ a'b'}} \sum_{a'b'} \sqrt{\frac{\dim(\mathbf{R})}{\dim(\mathbf{R}')}} |\mathbf{R}', a', b'\rangle \langle \mathbf{R}, a, \mathbf{r}, \alpha | \mathbf{R}', a'\rangle_{\Gamma_1} \langle \mathbf{R}', b' | \mathbf{R}, b, \mathbf{r}, \beta \rangle_{\Gamma_2} . \quad (343)$$

Consider the form of a three-point vertex where states of irreps **C** and **Q** enter and **R** leaves, as shown in Fig. 45. Without colored matter fields at the site, Gauge invariance at the vertex

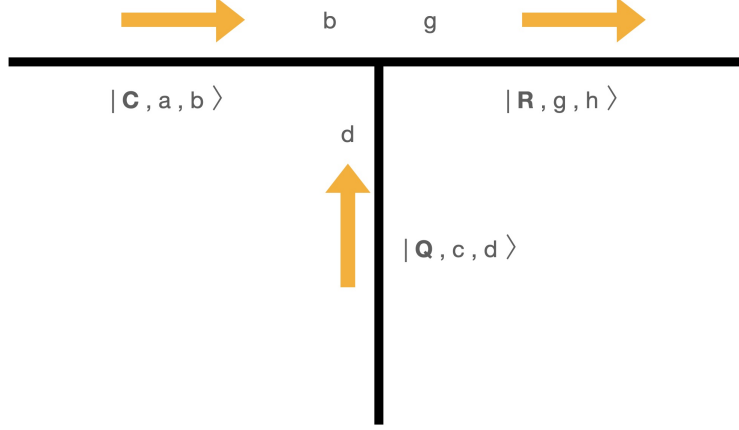


FIG. 45: A 3-pt vertex of non-abelian gauge links.

(Gauss's law) requires that the vertex is a singlet under color transformations. That is to say that **C**  $\otimes$  **Q** must contain **R** so that **C**  $\otimes$  **Q**  $\otimes$   $\bar{\mathbf{R}}$  contains a **1**. Further, gauge rotations at the vertex requires specific couplings fixed by SU(3) Clebsch-Gordon coefficients, such that, corresponding to Fig. 45,

$$|vertex(a, c, h)\rangle = \sum_{b, d, g, \Gamma} \langle \mathbf{C}, b, \mathbf{Q}, d | \mathbf{R}, g \rangle_{\Gamma} |\mathbf{C}, a, b\rangle \otimes |\mathbf{Q}, c, d\rangle \otimes |\mathbf{R}, g, h\rangle , \quad (344)$$

where  $\langle \mathbf{C}, b, \mathbf{Q}, d | \mathbf{R}, g \rangle_{\Gamma}$  is the associated CG-coefficient, with the subscript labelling the possible multiple states with the same dimensionality, *e.g.*,  $\mathbf{8} \otimes \mathbf{8} = \mathbf{27} \oplus \mathbf{10} \oplus \bar{\mathbf{10}} \oplus \mathbf{8} \oplus \bar{\mathbf{8}} \oplus \mathbf{1}$ . For a given lattice, the total state is given by a sum of products of all links multiplied by the CG coefficients required to make each contribution a color singlet.

While the action of the electric operator is proportional to the Casimir, by design in the electric basis, the magnetic field operator is given by the sum of the plaquette and hermitean conjugate operators, and the relevant terms acting on this vertex are (for the plaquette operator acting on the rhs of the diagram in Fig. 45)

$$\sum_{\beta} \left( \hat{U}^{(3)} \right)_{\beta}^{\alpha} \left( \hat{U}^{(3)} \right)_{\gamma}^{\beta} |vertex\rangle = \sum_{\beta, b, d, g, \Gamma} \langle \mathbf{C}, b, \mathbf{Q}, d | \mathbf{R}, g \rangle_{\Gamma} |\mathbf{C}, a, b\rangle \otimes \left( \hat{U}^{(3)} \right)_{\beta}^{\alpha} |\mathbf{Q}, c, d\rangle \otimes \left( \hat{U}^{(3)} \right)_{\gamma}^{\beta} |\mathbf{R}, g, h\rangle . \quad (345)$$

Using Eq. (343),

$$\left( \hat{U}^{(3)} \right)_{\beta}^{\alpha} |\mathbf{Q}, c, d\rangle = \sum_{\mathbf{Q}', c', d'} |\mathbf{Q}', c', d'\rangle \langle \mathbf{Q}, c, \mathbf{3}, \alpha | \mathbf{Q}', c'\rangle \langle \mathbf{Q}', d' | \mathbf{Q}, d, \mathbf{3}, \beta \rangle \sqrt{\frac{\dim \mathbf{Q}}{\dim \mathbf{Q}'}} . \quad (346)$$

There are indices and summations to keep track of. Of particular importance is the sum over  $\beta$  in Eq. (345). This sum is required by gauge invariance, as discussed previously in constructing the plaquette operator. At the level of this vertex, this means that the action of the plaquette operator is a color singlet, and hence conserves color flux at the vertex. As the vertex has been constructed to be a singlet, the action of the plaquette operator leaves it a singlet. The important point to note is that persistence of the vertex as a color singlet manifests itself through the cancellations of amplitudes between different color irreps created by the action of the operator.

A *simple* example of this can be found by considering the vertex

$$|vertex\rangle = \sum_b |\mathbf{3}, a, b\rangle \otimes |\mathbf{1}, 0, 0\rangle \otimes |\mathbf{3}, b, h\rangle , \quad (347)$$

and acting with the plaquette operator gives,

$$\begin{aligned} \left(\hat{U}^{(3)}\right)_\beta^\alpha |\mathbf{1}, 0, 0\rangle &= \frac{1}{\sqrt{3}} |\mathbf{3}, \alpha, \beta\rangle \\ \left(\hat{U}^{(3)}\right)_\gamma^\beta |\mathbf{3}, b, h\rangle &= \frac{1}{\sqrt{2}} |\mathbf{6}, b + \beta, h + \gamma\rangle \langle \mathbf{3}, b, \mathbf{3}, \beta | \mathbf{6}, b + \beta \rangle \langle \mathbf{6}, h + \gamma | \mathbf{3}, h, \mathbf{3}, \gamma \rangle \\ &\quad + |\bar{\mathbf{3}}, b + \beta, h + \gamma\rangle \langle \mathbf{3}, b, \mathbf{3}, \beta | \bar{\mathbf{3}}, b + \beta \rangle \langle \bar{\mathbf{3}}, h + \gamma | \mathbf{3}, h, \mathbf{3}, \gamma \rangle \\ \sum_\beta \left(\hat{U}^{(3)}\right)_\beta^\alpha \left(\hat{U}^{(3)}\right)_\gamma^\beta |vertex\rangle &= \sum_{b, \beta} |\mathbf{3}, a, b\rangle \otimes \frac{1}{\sqrt{3}} |\mathbf{3}, \alpha, \beta\rangle \\ &\otimes \left( \frac{1}{\sqrt{2}} |\mathbf{6}, b + \beta, h + \gamma\rangle \langle \mathbf{3}, b, \mathbf{3}, \beta | \mathbf{6}, b + \beta \rangle \langle \mathbf{6}, h + \gamma | \mathbf{3}, h, \mathbf{3}, \gamma \rangle \right. \\ &\quad \left. + |\bar{\mathbf{3}}, b + \beta, h + \gamma\rangle \langle \mathbf{3}, b, \mathbf{3}, \beta | \bar{\mathbf{3}}, b + \beta \rangle \langle \bar{\mathbf{3}}, h + \gamma | \mathbf{3}, h, \mathbf{3}, \gamma \rangle \right) . \end{aligned} \quad (348)$$

The action of the plaquette operator has generated entanglement between two adjacent vertices, with the superposition of  $\mathbf{6}$  and  $\bar{\mathbf{3}}$  links on the right-hand side of the vertex. Recall that these are states with different Casimirs.

There are situations that may look like the theory is generating violations of Gauss's Law implicitly, but this is not the case, for all of the physics reasons that we have already discussed. For example, consider

$$|vertex\rangle = \sum_b |\mathbf{1}, 0, 0\rangle \otimes |\mathbf{3}, a, b\rangle \otimes |\mathbf{3}, b, h\rangle , \quad (349)$$

and acting with the same plaquette operator.

$$\begin{aligned} \sum_\beta \left(\hat{U}^{(3)}\right)_\beta^\alpha \left(\hat{U}^{(3)}\right)_\gamma^\beta |vertex\rangle &= \sum_{b, \beta} |\mathbf{3}, a, b\rangle \otimes \\ &\otimes \left( \frac{1}{\sqrt{2}} |\mathbf{6}, a + \alpha, b + \beta\rangle \langle \mathbf{3}, a, \mathbf{3}, \alpha | \mathbf{6}, a + \alpha \rangle \langle \mathbf{6}, b + \beta | \mathbf{3}, b, \mathbf{3}, \beta \rangle \right. \\ &\quad \left. + |\bar{\mathbf{3}}, a + \alpha, b + \beta\rangle \langle \mathbf{3}, a, \mathbf{3}, \alpha | \bar{\mathbf{3}}, a + \alpha \rangle \langle \bar{\mathbf{3}}, b + \beta | \mathbf{3}, b, \mathbf{3}, \beta \rangle \right) \\ &\otimes \left( \frac{1}{\sqrt{2}} |\mathbf{6}, b + \beta, h + \gamma\rangle \langle \mathbf{3}, b, \mathbf{3}, \beta | \mathbf{6}, b + \beta \rangle \langle \mathbf{6}, h + \gamma | \mathbf{3}, h, \mathbf{3}, \gamma \rangle \right. \\ &\quad \left. + |\bar{\mathbf{3}}, b + \beta, h + \gamma\rangle \langle \mathbf{3}, b, \mathbf{3}, \beta | \bar{\mathbf{3}}, b + \beta \rangle \langle \bar{\mathbf{3}}, h + \gamma | \mathbf{3}, h, \mathbf{3}, \gamma \rangle \right) , \end{aligned} \quad (350)$$

which naively appears to have terms of the form  $|\mathbf{1}, 0, 0\rangle \otimes |\mathbf{6}, w, z\rangle \otimes |\bar{\mathbf{3}}, w, z\rangle$ , which would (obviously) violate Gauss's law. However, because of the CG coefficients, explicitly the symmetry of

the **6** and the antisymmetry of the  $\bar{\mathbf{3}}$ , the coefficients of these cross terms explicitly vanish,<sup>58</sup> leaving only contributions of the form  $|\mathbf{1}, 0, 0\rangle \otimes |\mathbf{6}, w, z\rangle \otimes |\mathbf{6}, w, z\rangle$ , and  $|\mathbf{1}, 0, 0\rangle \otimes |\bar{\mathbf{3}}, w, z\rangle \otimes |\bar{\mathbf{3}}, w, z\rangle$ , as required to satisfy Gauss's law.

## 2. In the Beginning....There was One Plaquette of Glue

As the scientific community is essentially at time  $t = 0$  with regard to the quantum simulations of QCD, the first place to start is the quantum simulation of a single plaquette of Yang-Mills lattice gauge theory. This is the fundamental building block of quantum simulations of the Standard Model. The constraints of color conservation are so stringent that this is the simplest nontrivial system to consider, and there are lessons to be learned, from constructing the system through to its quantum simulation, that provide useful lessons for going forward. This was system was studied in detail by Anthony Ciavarella, Natalie Klco and myself in Ref. [92] using IBM's quantum computers, with follow-up works, *e.g.*, Ref. [93] using D-Waves quantum annealers. For a single plaquette of SU(3) glue, the Hamiltonian is given by

$$\hat{H} = \frac{g^2}{2} \sum_{b, \text{links}} |\hat{\mathbf{E}}^{(b)}|^2 + \frac{1}{2g^2} (6 - \hat{\square} - \hat{\square}^\dagger) , \quad (352)$$

and Gauss's law dictates that the color of each of the 4 links is the same, leading to a (global) basis defined by

$$|\mathbf{R}\rangle = \frac{1}{\dim(\mathbf{R})^2} \sum_{\alpha, \beta, \gamma, \delta} |\mathbf{R}, \alpha, \beta\rangle_1 |\mathbf{R}, \beta, \gamma\rangle_2 |\mathbf{R}, \gamma, \delta\rangle_3 |\mathbf{R}, \delta, \alpha\rangle_4 , \quad (353)$$

For this system, matrix elements between basis states  $\langle \mathbf{R}_f | \hat{\square} | \mathbf{R}_i \rangle = 1$  if  $\mathbf{R}_f$  is present in the decomposition of  $\mathbf{R}_i \otimes \mathbf{3}$ , and 0 otherwise, by the completeness of CG coefficients.

## 3. Global Basis

It is informative to study a simple, but nontrivial, global basis truncation of  $p, q \leq 1$ , which contains the irreps  $\{\mathbf{1}, \mathbf{3}, \bar{\mathbf{3}}, \mathbf{8}\}$ . These can be straightforwardly mapped to two qubits as  $\{|00\rangle, |10\rangle, |01\rangle, |11\rangle\} = \{|\mathbf{1}\rangle, |\mathbf{3}\rangle, |\bar{\mathbf{3}}\rangle, |\mathbf{8}\rangle\}$ .<sup>59</sup> The four states of the plaquette (that satisfy Gauss's law) are each mapped to a state in the Hilbert space, and the Hamiltonian is

$$\hat{H} = \frac{g^2}{2} \begin{pmatrix} 0 & 0 & 0 & 0 \\ 0 & \frac{16}{3} & 0 & 0 \\ 0 & 0 & \frac{16}{3} & 0 \\ 0 & 0 & 0 & 12 \end{pmatrix} + \frac{1}{g^2} \left( 3 \hat{\mathbb{I}} - \frac{1}{2} \begin{pmatrix} 0 & 1 & 1 & 0 \\ 1 & 0 & 1 & 1 \\ 1 & 1 & 0 & 1 \\ 0 & 1 & 1 & 0 \end{pmatrix} \right) . \quad (354)$$

In terms of operators acting on a two-qubit system, the electric Hamiltonian operator can be decomposed as

$$\hat{H}_E = \frac{g^2}{6} (17 \hat{\mathbb{I}} \otimes \hat{\mathbb{I}} - 9 \hat{Z} \otimes \hat{\mathbb{I}} - 9 \hat{\mathbb{I}} \otimes \hat{Z} + \hat{Z} \otimes \hat{Z}) , \quad (355)$$

<sup>58</sup>

$$\sum_{b, \beta} \langle \bar{\mathbf{3}}, b + \beta | \mathbf{3}, b, \mathbf{3}, \beta \rangle \langle \mathbf{3}, b, \mathbf{3}, \beta | \mathbf{6}, b + \beta \rangle = 0 . \quad (351)$$

<sup>59</sup> Which, for this special case, maps the number of up and down indices to the qubits.

where  $\hat{\mathbb{I}}$  is the identity operator. The magnetic Hamiltonian can be similarly decomposed as

$$\hat{H}_B = \frac{3}{g^2} \hat{\mathbb{I}} \otimes \hat{\mathbb{I}} - \frac{1}{2g^2} \left( \hat{X} \otimes \hat{\mathbb{I}} + \hat{\mathbb{I}} \otimes \hat{X} + \frac{1}{2} (\hat{X} \otimes \hat{X} + \hat{Y} \otimes \hat{Y}) \right) . \quad (356)$$

Neglecting terms proportional to the identity, the one-plaquette Hamiltonian can be separated into Trotterized operators, with 1-body and 2-body structure,  $\hat{H} = \hat{H}_1 + \hat{H}_2$ , with

$$\begin{aligned} \hat{H}_1 &= \left( \frac{17g^2}{6} + \frac{3}{g^2} \right) \hat{\mathbb{I}} \otimes \hat{\mathbb{I}} - \frac{g^2}{6} (9 \hat{Z} \otimes \hat{\mathbb{I}} + 9 \hat{\mathbb{I}} \otimes \hat{Z}) - \frac{1}{2g^2} (\hat{X} \otimes \hat{\mathbb{I}} + \hat{\mathbb{I}} \otimes \hat{X}) \\ \hat{H}_2 &= \frac{g^2}{6} \hat{Z} \otimes \hat{Z} - \frac{1}{4g^2} (\hat{X} \otimes \hat{X} + \hat{Y} \otimes \hat{Y}) . \end{aligned} \quad (357)$$

The panels of Fig. 46 show the probability of a single plaquette remaining in the trivial vacuum,  $|00\rangle$ , and its electric energy fluctuations for a color irrep basis truncated to  $\{\mathbf{1}, \mathbf{3}, \bar{\mathbf{3}}, \mathbf{8}\}$ , as computed in 2021 using IBM's quantum computers. The results of the same calculation performed a

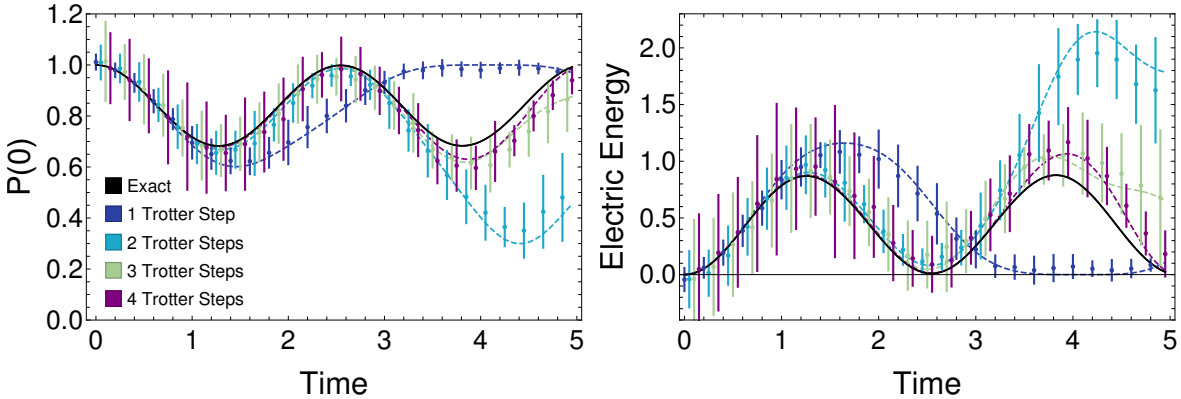


FIG. 46: Results from 2021 by Ciavarella, Klco, Savage [92]. The (trivial-) vacuum-to-vacuum persistence probability  $|\langle 00 | \hat{U}(t) | 00 \rangle|^2$  (left panel) and the energy in the electric field (right panel) of the one-plaquette system derived from the Hamiltonian given in Eq. (354) for color irreps  $\mathbf{1}, \mathbf{3}, \bar{\mathbf{3}}, \mathbf{8}$ . Dashed lines correspond to the exact results for 2nd-order Trotterization with  $\Delta t = t, t/2, t/3, t/4, 0$ . Points correspond to quadratic extrapolations of results obtained from IBM's **Athenes** quantum processor, with systematic and statistical uncertainties.

year later using new error-mitigation techniques, including dynamic decoupling, Pauli-twirling and decoherence renormalization, are shown in Fig. 47.

A comment is in order regarding how the Trotterized time evolution is performed. In Fig. 46, the notation is that the curve/results from k-Trotter steps means that for each point (time) on the curve, k Trotter steps were employed (regardless of time). The time interval between applications of the time-evolution operator,  $\Delta t$  increases with  $t$ , and hence so do the systematic Trotterization errors. Therefore, the Trotterized evolution for a given number of Trotter steps should be (and is) rapidly converging when compared with later times, and consequently, there is a time for which the Trotter errors are large enough for the approximation to fail (for a given k). The advantage of this implementation is that the number of entangling (CNOT) gates is a fixed number as a function of time for a given k. In Fig. 47, the more standard implementation of Trotterized time evolution is employed. There is a fixed  $\Delta t$  between points shown in the figure, and hence a fixed systematic Trotterization error. The advantage is that the systematic error is independent of time, and therefore easily interpretable, but the downside is that the number of entangling gates increases for each subsequent application of the evolution operator.

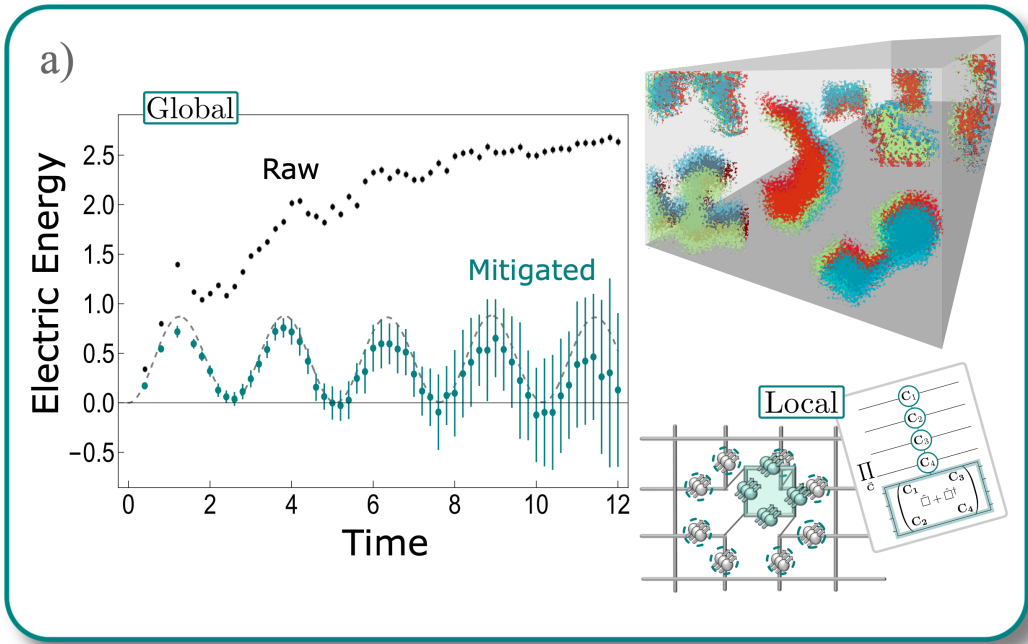


FIG. 47: The time evolution of one plaquette using leading order Trotter computed in late 2022. A fixed- $\Delta t$  evolution operator is repeatedly applied. Employed error-mitigation techniques included measurement error correction, dynamic decoupling, Pauli-twirling and decoherence renormalization. Quality results were obtained for circuits with up to approximately 400 CNOT gates. [Results obtained by Anthony Ciavarella, and image assembled by Natalie Klco, with consultation with Christian Bauer, Zohreh Davoudi and Martin Savage [13].]

The uncertainties in the results shown in Fig. 46 are significantly larger than in Fig. 47 for two reasons. The first is that the IBM processors used in the simulations were different, the former using `ibmq_athens` and the latter `ibmq_manilla`. The processors have different gate fidelities, decoherence times, and other characteristics, which means the results and errors differ. A major difference in the quality of the results is the different set of error mitigation techniques that were used, each were the best available at the time. In Fig. 46, the well-known CNOT extrapolation method was used. This method relies upon the fact that two applications of the CNOT gate corresponds to the identity operator ( $\text{CNOT.CNOT} = \text{identity}$ ) for an ideal quantum device and circuit. Therefore, in its most naive form, the results obtained with the quantum circuit are computed, giving rise to results with statistical errors, and device errors, one of which results from the imperfections of the CNOT gates in the circuit. Next, each CNOT gate in the circuit is replaced by three (adjacent) CNOT gates, which would give the same results for an ideal quantum computer. On a real device, the CNOT errors are magnified by a factor of three for the same ensemble size. This process can be repeated for larger numbers of CNOT replacements. For a sufficiently small CNOT error, and extrapolation to zero CNOT gates can be performed. This was first performed by an IBM team in some chemistry simulations, with a number of follow-up works exploring variants thereof, *e.g.*, Ref. [94], and an early example of such extrapolations can be seen in Fig. 48. It is the result of such extrapolations (for each time slice) that are shown in Fig. 46. There are well known variants on this method of extrapolation, including increasing the number of CNOT gates for a select number of CNOT gates in the circuit, which reduces the overall CNOT error in any given circuit, but increases the dimensionality of the extrapolation to a (potentially large) surface [96].

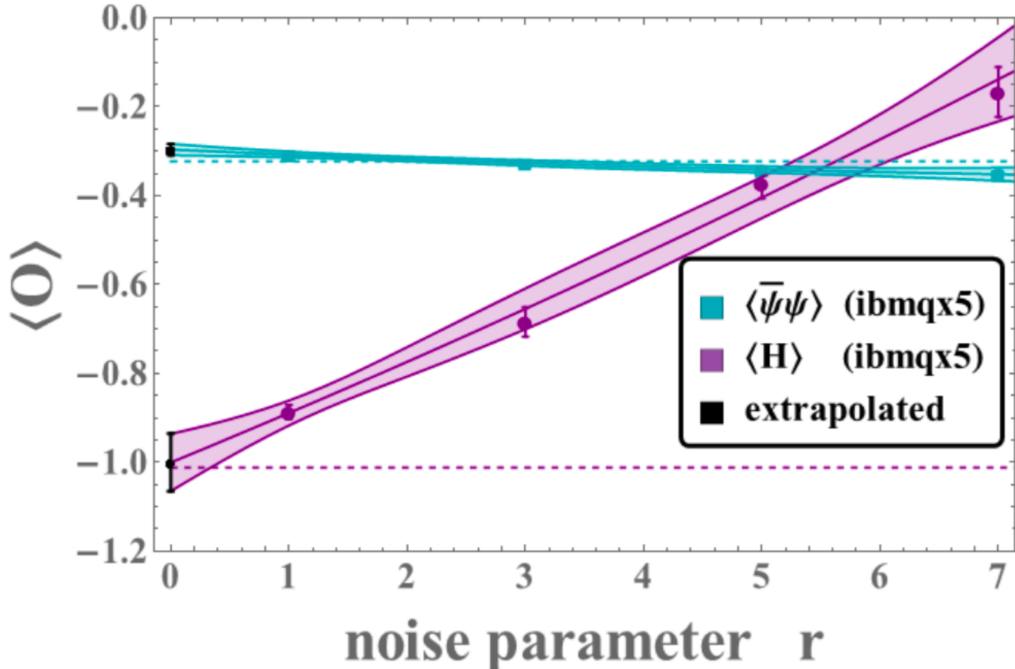


FIG. 48: An early example of a CNOT error-mitigation extrapolation [95]. The horizontal axis displays the *noise parameter*,  $r$ , which indicates the number of CNOT-gates per CNOT-gate (see the main text). Results were obtained using IBM's `ibmqx5` quantum computer in 2017-2018. The sensitivity of different observables to the (coherent) CNOT errors is obvious.

In Fig. 47, a combination of multiple error mitigation strategies were employed.<sup>60</sup> The main techniques used were: Measurement Error Mitigation, Dynamic Decoupling, Pauli-Twirling and Decoherence Renormalization.<sup>61</sup>

#### 4. Measurement Error Mitigation

This is one of the techniques that are essential in arriving at meaningful results from present-day quantum simulations, and mitigates SPAM errors (state preparation and measurement errors). Conceptually, the idea is the following: imagine first preparing an  $n$ -qubit quantum register in  $|0\rangle^{\otimes n}$  and then actually measuring the state of the register. The results obtained will not always be  $|0\rangle^{\otimes n}$  because of SPAM errors, and the decoherence of the device itself. The result will be a function of the time interval between preparation and measurement. The results obtained (the mean values and uncertainties) are used to form the first *row* of a matrix, lets call it  $V$ . Next, the

<sup>60</sup> As a side note: this combination of error mitigation strategies was arrived at from discussions occurring at the IQuS workshop on **Quantum Error Mitigation for Particle and Nuclear Physics**, organized by Benjamin Nachman (LBNL), Christian Bauer (LBNL), Wibe de Jong (LBNL), Kristan Temme (IBM), Abhinav Kandala (IBM) and Raphael Pooser (ORNL), that was held during May 9-13 in 2022..... the first post-covid in-person workshop held at IQuS. These were combined with recent results displaying the potential of a new technique, decoherence renormalization [97].

<sup>61</sup> It has been interesting to witness the evolution of techniques in the community during the last six years, and particularly the built-in functionality of software for quantum simulation, *e.g.*, `qiskit`. New techniques first appear in the literature through being executed *by hand*, and then shortly afterward, appear as a *function call* so that the user no longer needs expertise in the method, and can simply use/implement it as a *black box*.

register can be prepared in the state  $|0\rangle^{\otimes n-1} \otimes |1\rangle$ , generating another row of  $V$  upon subsequent measurements, and so forth. These  $n$ -sets of measurements populate all elements in the matrix  $V$ . In order to mitigate the SPAM errors, the inverse matrix,  $V^{-1}$  can be applied to the results

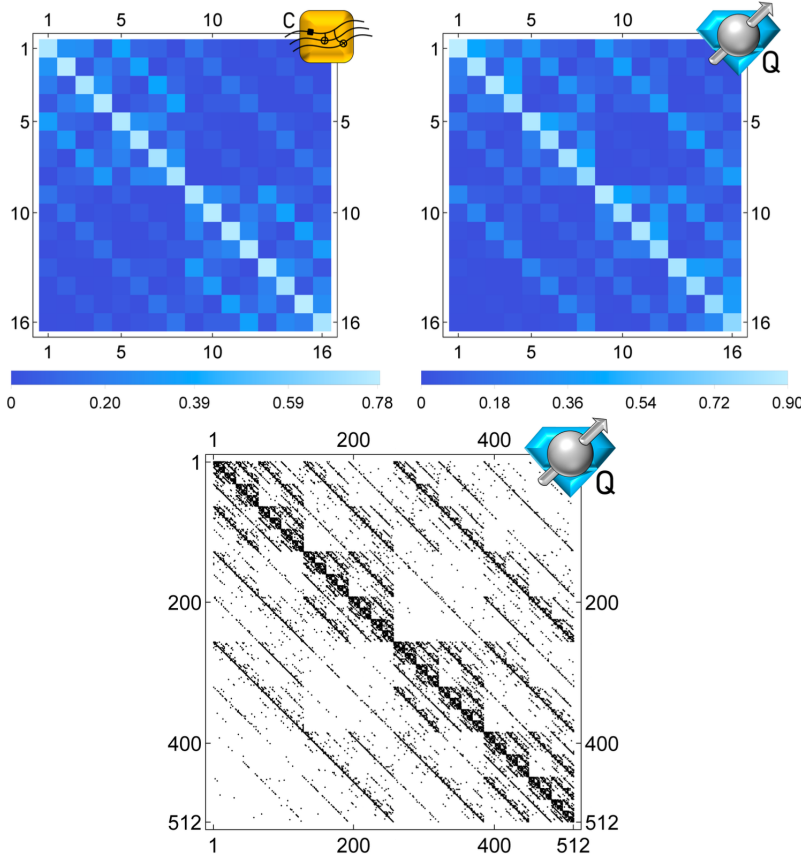


FIG. 15. Measurement-error calibration matrices extracted from the simulator (upper-left) with the extracted `Poughkeepsie` noise model and from the `Poughkeepsie` quantum hardware (upper-right) for 4-qubit systems. Lower panel shows the measurement-error calibration matrix for the 9-qubit system utilized for 3-site state preparation with a monochrome color scheme to support clear visualization of the 512-dimensional space.

FIG. 49: An example of SPAM errors obtained on IBM's `poughkeepsie` in 2019 by Natalie Klco and myself [62]. The yellow icon represents results obtained using the `qiskit` classical simulator, while the blue icon denotes results obtained from the quantum device.

obtained in any simulation, to provide *first level* results from the device with which to begin to perform analysis. An example of SPAM errors measured on IBM quantum computers in 2019 are shown in Fig. 49.

##### 5. Dynamic Decoupling

This is a mitigation technique of a different character to the mitigation of SPAM errors. In many quantum circuits, there are sections of the circuit over which the sequence of gate applications is limited to a number of qubits that is less than that of the full quantum register, or of the *active* part of the register used in the simulation. The qubits not involved are *idle*, and hence susceptible to anisotropies, and associated depolarization, of their local environments. The impact of such

depolarization is circuit and QPU dependent. In superconducting QPUs this is significantly more important than in trapped-ion device, for example. One fairly primitive way to mitigate such errors is dynamic decoupling, which, as the name suggests, suppresses such couplings to the local environment by *un-idling* (my word) the nominally idle qubits in such a way that leaves them unchanged when they once again become an active element of the quantum circuit (on an ideal quantum computer). In its simplest form, this is implemented by acting with an even number of  $\hat{X}$ -gates on each qubit during the time they are idle. As such gates are also imperfect, a tuning is required to determine the optimal number of applications to minimize errors.

### 6. Pauli-Twirling or Randomized Compiling

The action of the CNOT gates has specific *directions* in the two-qubit Hilbert space, and as such acts an-isotropically in the space. The errors that it introduces on each member of the measurement ensemble are the same - they are systematic errors and not statistical in nature. As a result, their net impact depends upon the state of the quantum device and not just the circuit itself, and worse, they accumulate with each CNOT in a circuit, leading to larger systematic deviations as more are included. Pauli-twirling is a way to change the CNOT errors from systematic errors to statistical errors, that can then be mitigated by increasing ensemble sizes. By randomly changing the orientation of the errors of each CNOT gate, while preserving the action of an ideal CNOT gate, the largest impact of CNOT errors can be statistically averaged to zero. While one could simply act with randomly selected SU(4) transformations,  $S_r$ , such that the CNOT is a circuit is replaced by  $S_r.\text{CNOT}.S_r^\dagger$ , it is more efficient to simply select randomly from the 15 generators of SU(4), along with the identity operator. For example, each CNOT in the circuit is randomly replaced by one of the 16 following structures.

$$\begin{aligned} \text{CNOT} &\rightarrow \text{CNOT} , \\ \text{CNOT} &\rightarrow (\hat{I} \otimes \hat{Y}) . \text{CNOT} . (\hat{Z} \otimes \hat{Y}) , \\ \text{CNOT} &\rightarrow (\hat{Y} \otimes \hat{Y}) . \text{CNOT} . (\hat{X} \otimes \hat{Z}) , \\ &\dots \end{aligned} \tag{358}$$

A complete list of the 16 operators can be found in Ref. [97]. This is found to dramatically reduce the errors introduced by imperfect CNOT gates, but at the expense of requiring much larger ensembles, something that is practical for simulations using IBM quantum computers, but not yet practical for trapped-ion quantum computers.

### 7. Decoherence Renormalization

This is a mitigation strategy that was recently introduced, sometime in 2022 for practical purposes [97]. Conceptually, it removes the leading effect of qubit decoherence by identifying observables that should remain unity, or a fixed number, throughout the evolution of the system, and the deviations from unity can be used to correct the observables of interest. Consider the time evolution of an initial state over some time interval, and an equivalent forward-backward evolution,

$$|\psi\rangle(t) = \hat{U}(t)|\psi\rangle , \quad |\chi\rangle(t) = \hat{U}(-t/2)\hat{U}(t/2)|\psi\rangle . \tag{359}$$

Imagine the situation where there were 8 states defining the Hilbert space. Upon complete decoherence of the quantum device, each is likely with the same probability of  $P_j = \frac{1}{8}$ . If we have a

quantity that we know to have  $p_a = 1$ , for some  $a$ , then the ideal distance from de-coherence is  $1 - \frac{1}{8}$ . After all of the previously discussed error-mitigation is implemented, we can construct the quantity,

$$p_a(t) = |\langle \psi_a | \hat{U}(-t/2) \hat{U}(t/2) | \psi_a \rangle|^2. \quad (360)$$

which is the probability of returning to the initial state after a forward-backward evolution, which for an ideal quantum computer would be  $p_a = 1$ , but will tend toward  $1/8$  from above as the device decoheres (for this example). Therefore, the ratio

$$r_a(t) = \frac{1 - \frac{1}{8}}{p_a(t) - \frac{1}{8}}, \quad (361)$$

is a scale factor that can be used to remove the leading impact of decoherence from the vacuum-to-vacuum persistence probability  $P(t)$ ,

$$P(t)^{\text{mitigated}} - \frac{1}{8} = r_a(t) \left( P(t)^{\text{raw}} - \frac{1}{8} \right), \quad (362)$$

for  $P(t)^{\text{raw}} > \frac{1}{8}$ .

It is these combinations of error-mitigation strategies that transform the *raw* results in Fig. 47 to the mitigated results shown in that figure. It is obvious, from that figure, that without such mitigation, the results obtained from the device are not representative of the underlying physics that being simulated. However, the suite of error mitigation techniques allow for a meaningful signal to be extracted, with quantified uncertainties that encompass the true result.

### 8. Local Basis

We have made progress in simulating a single plaquette of glue by implementing Gauss's law at the level of states before considering the action of the evolution operator, *i.e.*, using a global basis. Now, if this were performed using a local basis, each link is mapped to qubits, and in this case each link would be mapped to 2 qubits and the system is then described by  $2 \times 4 = 8$  qubits. The Hilbert space of physical states in this mapping is  $2^8 = 256$ , and we recall that there are only 4 physical states that satisfy Gauss's law. So we are starting to see, on a small scale, the redundancies that are possible in mapping lattice gauge theories to quantum devices. The gauge-invariant space is exponentially smaller than the total state space (and the gauge-variant space).

What are the actions of the operators? First let's consider the electric operator. The total electric energy in the system is the sum of energies in each link.

$$\begin{aligned} \hat{H}_E &= \frac{g^2}{2} \sum_{b=1}^8 \sum_{\text{links}=1}^4 |\hat{\mathbf{E}}^{(b)}|^2 \\ &= \frac{g^2}{2} \begin{pmatrix} 0 & 0 & 0 & 0 \\ 0 & \frac{4}{3} & 0 & 0 \\ 0 & 0 & \frac{4}{3} & 0 \\ 0 & 0 & 0 & 3 \end{pmatrix} \otimes \hat{I}_4^{\otimes 3} + \frac{g^2}{2} \hat{I}_4 \otimes \begin{pmatrix} 0 & 0 & 0 & 0 \\ 0 & \frac{4}{3} & 0 & 0 \\ 0 & 0 & \frac{4}{3} & 0 \\ 0 & 0 & 0 & 3 \end{pmatrix} \otimes \hat{I}_4^{\otimes 2} \\ &\quad + \frac{g^2}{2} \hat{I}_4^{\otimes 2} \otimes \begin{pmatrix} 0 & 0 & 0 & 0 \\ 0 & \frac{4}{3} & 0 & 0 \\ 0 & 0 & \frac{4}{3} & 0 \\ 0 & 0 & 0 & 3 \end{pmatrix} \otimes \hat{I}_4 + \frac{g^2}{2} \hat{I}_4^{\otimes 3} \otimes \begin{pmatrix} 0 & 0 & 0 & 0 \\ 0 & \frac{4}{3} & 0 & 0 \\ 0 & 0 & \frac{4}{3} & 0 \\ 0 & 0 & 0 & 3 \end{pmatrix}. \end{aligned} \quad (363)$$

The magnetic term is more complicated because Gauss's law couples actions on adjacent links. Neglecting the identity terms,

$$\hat{H}_B = -\frac{1}{2g^2} \begin{pmatrix} 0 & 1 & 0 & 0 \\ 0 & 0 & 0 & 0 \\ 0 & 0 & 0 & 0 \\ 0 & 0 & 0 & 0 \end{pmatrix}^{\otimes 4} - \frac{1}{2g^2} \begin{pmatrix} 0 & 0 & 0 & 0 \\ 1 & 0 & 0 & 0 \\ 0 & 0 & 0 & 0 \\ 0 & 0 & 0 & 0 \end{pmatrix}^{\otimes 4} + \dots . \quad (364)$$

It is therefore useful to think in terms of qu4its for this system, a 4-state qudit ( $d = 4$ ), and consider Given operators and generators of Givens transformations, e.g.

$$\mathcal{X}_{13} = \begin{pmatrix} 0 & 1 & 0 & 0 \\ 1 & 0 & 0 & 0 \\ 0 & 0 & 0 & 0 \\ 0 & 0 & 0 & 0 \end{pmatrix}, \quad \mathcal{Y}_{13} = \begin{pmatrix} 0 & i & 0 & 0 \\ -i & 0 & 0 & 0 \\ 0 & 0 & 0 & 0 \\ 0 & 0 & 0 & 0 \end{pmatrix}$$

$$G_{13}^{\mathcal{X}}(\beta) = e^{-i\beta\mathcal{X}_{13}}, \quad G_{13}^{\mathcal{Y}}(\beta) = e^{-i\beta\mathcal{Y}_{13}} . \quad (365)$$

These are more natural operators to think about with regard to hardware, as it is easy to imagine an atomic transition that interchanges states **1** → **3**, without impacting other states in the system. These can also be clearly identified with generators of SU(4). So for transitions of interest will require, for example,

$$\left[ \frac{1}{2} (\mathcal{X}_{13} + i\mathcal{Y}_{13}) \right]^{\otimes 4} . \quad (366)$$

While generally true, this is overly messy when working within the gauge-invariant space. Consider the action of  $\mathcal{X}_{13}^{\otimes 4}$ , this can give rise to a cornucopia of gauge non-invariant terms, but, importantly, it will remain in a gauge invariant space if it is initially in a gauge invariant state. For example,

$$\mathcal{X}_{13}^{\otimes 4} |\mathbf{1111}\rangle = |\mathbf{3333}\rangle, \quad \mathcal{X}_{13}^{\otimes 4} |\mathbf{3333}\rangle = |\mathbf{1111}\rangle , \quad (367)$$

producing a gauge invariant state. So we see that the action of  $\square + \square^\dagger$  can be recovered by the action of unitaries of the form

$$e^{-i\alpha(\square+\square^\dagger)} \rightarrow e^{-i\beta(\mathcal{X}_{13}^{\otimes 4} + \mathcal{X}_{13}^{\otimes 4} + \mathcal{X}_{38}^{\otimes 4} + \mathcal{X}_{38}^{\otimes 4})} . \quad (368)$$

This looks somewhat disturbing before we think more deeply about it.

The first concern is about building circuits for each of the exponentials, e.g.  $e^{-i\beta\mathcal{X}_{13}^{\otimes 4}}$ . It transpires that it is straightforward to systematically construct circuits of this form from ones with one less  $\mathcal{X}$ , and iteratively construct circuits that will faithfully reproduce the desired unitary action.

The second concern is about the impact of Trotterization. Unless one is lucky, which is generically untrue (in this instance), circuits can't be identified that furnish the complete evolution without Trotterization. The question then becomes - does Trotterization preserve gauge invariance. As each pair of operators is gauge invariant by themselves, the Trotterization of the sum leaves a gauge invariant state. Which means that we can Trotterize without causing damage to gauge invariance. The coefficients of the states will be modified away from their continuous time evolution values, *i.e.*, there remain systematic errors due to Trotterization, but the state remains gauge invariant and in the physical space.

### 9. Insights from $SU(2)$ Lattice Gauge Theory

To develop intuition for these systems, we return to  $SU(2)$  lattice gauge theory. The connectivity in group space is straightforward as the link operator can take any given state to two possible (and different) final states,  $j' = j \pm \frac{1}{2}$ . The Hamiltonian is

$$\begin{aligned}\hat{H} &= \frac{g^2}{2} \sum_{a,\text{links}} |\mathbf{E}^a|^2 + \frac{1}{2g^2} (4 - \hat{\square} - \hat{\square}^\dagger) \\ H_{j,j'} &= \frac{1}{2} g^2 j(j+1) \delta_{j,j'} + \frac{1}{g^2} (2\delta_{j,j'} - \delta_{j+1,j'} - \delta_{j-1,j'}) \\ &\rightarrow \frac{1}{2} g^2 \hat{j}^2 - \frac{1}{g^2} \nabla_j^2 ,\end{aligned}\quad (369)$$

where a finite-difference relation is used (perhaps oddly?) to connect to a continuum  $\nabla$  operator acting in  $j$  space. In order for this replacement/approximation to become accurate,  $j$  must become large, in which limit we expect this to describe the asymptotic behavior of the wavefunction in  $j$  space. This corresponds to a Weber type-A differential equation, with Parabolic Cylinder functions as solutions. Asymptotically for large  $j$ , these functions scale as

$$\psi \rightarrow e^{-\frac{g^2}{2\sqrt{2}}(j+\frac{1}{2})^2} ,\quad (370)$$

demonstrating Gaussian convergence in field space at large- $j$ . So, in the  $SU(2)$  gauge theory of one plaquette, the contribution to the ground state wavefunction, and the low-lying states in general, is Gaussian suppressed with increasing  $j$ , which is a much stronger suppression than a naive power law (that would be arrived at from operator scaling alone). Studying the analogous behavior of the  $SU(3)$  plaquette shows the same scaling suppression with increasing dimensionality of the irrep. Figure 50 shows the scaling of contributions to the 1-plaquette ground state wavefunction from

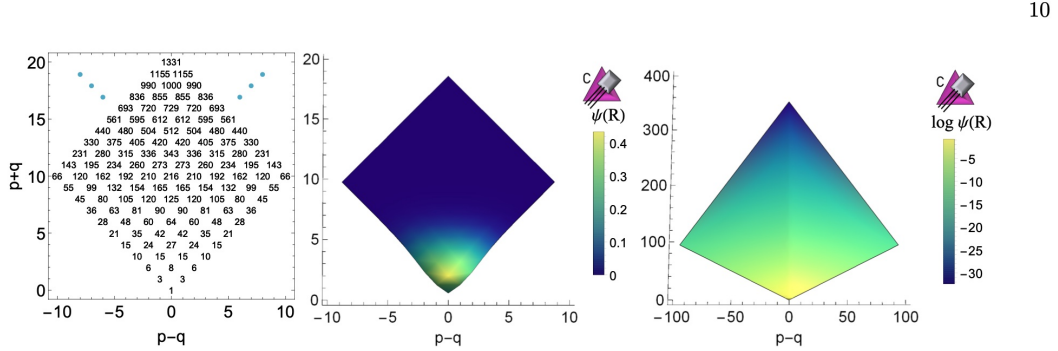


FIG. 3. On a grid (left panel) of irreducible representations organized by their dimensionality and plaquette connectivity (as shown in Fig. 2), support of the ground state wavefunction  $\psi(\mathbf{R})$ , shown for  $g = 0.5$ , is localized to low irrep dimensionalities (center panel). Conjugate irreps appear on the left half of the grid with real irreps appearing along the center vertical. The right panel shows  $\log \psi(\mathbf{R})$  on a scaled quadratic grid for visual clarity of the convergence structure.

FIG. 50: The contributions from irreps of  $SU(3)$  to the ground state wavefunction of a single plaquette [92].

increasing dimensionality irreps.

## VII. APPLIED QUANTUM COMPUTATIONAL COMPLEXITY

To end this course, I would like to give an overview of emerging understanding of quantum computational complexity. Once again, this is something that the QIS community has been pushing

the boundaries of for more than 20 years, but has not really been discussed in the nuclear and high-energy communities. There are many ways that this could be approached, but I will take a somewhat pedestrian approach via classical and quantum gate sets.

### A. Stabilizer States

Stabilizer states are one of the key elements of quantum error correction [36, 98]., and up to this point we have not spent any time discussing them. They currently are not impacting the development of quantum simulations using NISQ-era devices, and we expect that this situation changes as the devices become more fault-tolerant and error correcting, and the users become more sophisticated. Here, we begin to introduce the general outline of stabilizer states, with an eye to better understanding the computational complexity of quantum systems, with a focus of developing techniques that will be advantageous in performing future quantum simulations more efficiently.

Some comments about a general qudit system, before specializing to qubits and qutrits. A single qudit, with the  $\mathbf{d}$ , states, has  $\mathbf{d}(\mathbf{d}+1)$  stabilizer states, i.e. 6 for qubits and 12 for qutrits. For  $n_Q = 2$  qudits, there are  $\mathbf{d}^2(\mathbf{d}^2+1)(\mathbf{d}+1)$  stabilizer states, i.e. 60 for qubits and 360 for qutrits. For  $n_Q = 3$  qudits, there are  $\mathbf{d}^3(\mathbf{d}^3+1)(\mathbf{d}^2+1)(\mathbf{d}+1)$  stabilizer states, i.e. 1080 for qubits and 30240 for qutrits, and generally, for  $n_Q$ -qudits, the number of pure stabilizer states is [99],

$$N_{\text{stab}} = d^{n_Q} \prod_{i=1}^{n_Q} (d^i + 1) . \quad (371)$$

It is interesting to note that for  $\mathbf{d}$  a prime number, the stabilizer states are equivalent to undirected graph states.

#### 1. Stabilizer States for Qubit Systems

Imagine that we have a wavefunction with support across  $n_Q$  qubits, which corresponds to a  $d = 2^{n_Q}$  dimensional Hilbert space. Working with the generalized set of Pauli operators that includes the identity matrix,

$$P = \{ \hat{X}, \hat{Y}, \hat{Z}, \hat{I} \} , \quad (372)$$

then there are  $d^2 = 4^{n_Q}$  possible non-zero matrix elements required to fully reconstruct the most general density matrix,  $\hat{\rho}$ ,

$$\begin{aligned} \hat{\rho} &= \frac{1}{d} \sum_P c_P \hat{P} , \quad \hat{P} = P_{i_1} \otimes P_{i_2} \otimes \dots \otimes P_{i_{n_Q}} \\ c_P &= \text{Tr} \left[ \hat{\rho} \hat{P} \right] = \langle \psi | \hat{P} | \psi \rangle . \end{aligned} \quad (373)$$

However, there are states for which there are only  $d$  non-zero  $c_P$ , which take values  $\pm 1$ , which are called stabilizer states. These are states than can be prepared efficiently using classical computers, and interestingly include entangled states for  $n_Q > 1$ .

Let us start by considering one qubit to begin with. There are six stabilizer states for a single qubit, corresponding to the eigenstates of  $\hat{X}, \hat{Y}, \hat{Z}$ . If we re-cast this discussion in a way that generalizes to qutrits and beyond, we should consider working with a basis defined by  $\hat{X}$  and  $\hat{Z}$ .

For qubits, we introduce a complex phase  $\omega = i = e^{i\pi/2}$ , and the Pauli operator basis<sup>62</sup>

$$P = \{ \hat{X}, \omega \hat{X} \hat{Z}, \hat{Z}, \hat{I} \} , \quad (374)$$

from which the stabilizer states can be written as

$$(1, 0), (0, 1), \frac{1}{\sqrt{2}}(1, 1), \frac{1}{\sqrt{2}}(1, \omega), \frac{1}{\sqrt{2}}(1, \omega^2), \frac{1}{\sqrt{2}}(1, \omega^3) . \quad (375)$$

One can easily verify that the density matrices associated with these six states can be written as sums over just  $d = 2$  Pauli strings, out of the possible  $d^2 = 4$ . Obviously, because  $\text{Tr}\hat{\rho} = 1$ ,  $c_I = 1$ . In the case of the Pauli-operator basis defined in Eq. (374), the coefficients  $c_P$  are real numbers, and complex conjugation is not required.

For a pure state, for which  $\hat{\rho} = \hat{\rho}.\hat{\rho}$ , it is helpful to define the quantities

$$\Xi_P = c_P^2/d , \quad \sum_P \Xi_P = 1 . \quad (376)$$

To see that these states can be prepared efficiently using classical computers, it is sufficient to start with a simple state,  $|0\rangle$ , which is stabilized by  $\hat{I}$  and  $\hat{Z}$  ( $\hat{I}|0\rangle = +|0\rangle$  and  $\hat{Z}|0\rangle = +|0\rangle$ ) and use only Clifford gates to generate the classically accessible states (i.e., no T-gates). It is straightforward to show that by applying the H-gate and S-gate in all possible combinations, that only these six states are generated. Note that we could have started with another stabilizer state, for example,  $|1\rangle$  which is stabilized by  $\hat{I}$  and  $-\hat{Z}$  ( $\hat{I}|1\rangle = +|1\rangle$  and  $-\hat{Z}|1\rangle = +|1\rangle$ ).

To move beyond a single qubit, we add the CNOT gate to this gate set. As we discussed earlier, as this is a classical operator, adding this to the H-gate and S-gate provides a complete gate set for classical computation. If we begin with two qubits in the tensor-product state of  $|00\rangle$ , then applying S-gates, H-gates and CNOT-gates in all possible orderings to the two qubits generate all of the two-qubit stabilizer states, for which there are 60. These states can be classified into two categories, tensor-product states and entangled states. There are  $6^2 = 36$  tensor-product states and 24 entangled states, giving a total of 60 two-qubit stabilizer states. This has been explored in great detail, e.g., for  $n_Q = 3$  there are 1080 stabilizer states, and the number grows exponentially with the number of qubits. This can be generalized to  $n$  qubits using a recursive formula:  $\mathcal{N}_{ss}(n) = 2(2^n + 1)\mathcal{N}_{ss}(n - 1)$  [100].

From a physics quantum simulation perspective, stabilizer states are fascinating because it means that there are states that are maximally entangled that we might be able to prepare classically on the quantum computer to provide a starting point for a quantum simulation that actually requires a quantum computer!! Entanglement alone is not sufficient to automatically dictate that a quantum computer is needed for simulation [36, 98], as we have discussed previously. From a more “theoretical” standpoint, it suggests, as we have discussed previously, that we should pursue the development of perturbation theories around leading order states that are stabilizer states, expanding our starting points from the 20th Century that have been so successful.

## 2. Qutrits

We are currently witnessing quantum devices and architectures expand beyond qubits, and to have control over coherence and entanglement of systems with multiple levels per “unit Hilbert space”. Recent results from the Innsbruck team [101, 102], for example, demonstrated a  $d = 7$  state qudit

---

<sup>62</sup> We are using a quite awkward way to write  $\hat{Y} = \omega \hat{X} \hat{Z}$ .

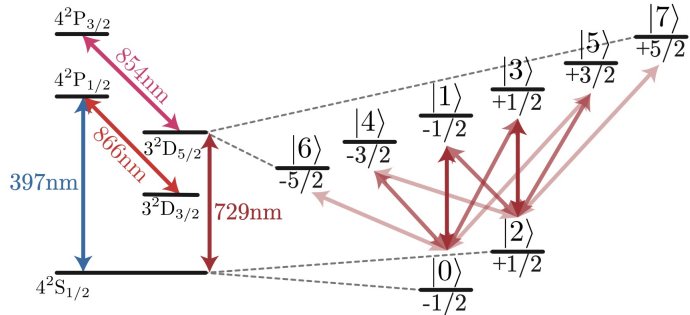


FIG. 51: The energy-level diagram of the atoms used in an experimental demonstration of a  $d = 7$  qudit quantum computer using trapped ions [101].

system using a trapped-ion system, using the atomic energy levels shown in Fig. 51. There is also significant progress in using superconducting systems for qutrits and higher, see for example, Refs. [103, 104] along with the efforts at Fermilab and Lawrence Livermore National Laboratory to develop superconducting radio frequency (SRF) cavity systems, which can support multiple level qudits (electromagnetic) per cavity<sup>63</sup>. This progress motivates the exploration of qudit systems as potential platforms for quantum simulations of fundamental physics. Just as importantly, qudit systems have been theoretically identified as being of utility, beyond qudits, for QIST applications, for error correction (including erasure) with entanglement properties beyond qubits. They have also been motivated as natural elements to simulate some physically interesting systems, such as systems with nucleon-pairing [105] and quantum chromodynamics [106, 107]. It turns out that qudit systems with  $d$  a prime number, have special attributes that distinguish them from non-prime systems. Therefore  $d = 2, 3, 5, 7, 11, 13, \dots$  are low dimensional systems of special interest.

Let us review some of the features of qutrits,  $d = 3$ , which exhibit features that are not present in qubit systems. A nice discussion of the features I will discuss here can be found in papers by Dan Harlow and collaborators [108, 109]. We have discussed the utility of repetition codes (and quantum circuits) for qubits previously, and extending to qutrits adds symmetry to system. Labeling the states of a single qutrit as  $\{|0\rangle, |1\rangle, |2\rangle\}$ , logical states,  $|\tilde{j}\rangle$ , can be constructed using three qutrits as,

$$\begin{aligned} |\tilde{0}\rangle &= \frac{1}{\sqrt{3}} [ |000\rangle + |111\rangle + |222\rangle ] , \\ |\tilde{1}\rangle &= \frac{1}{\sqrt{3}} [ |012\rangle + |120\rangle + |201\rangle ] , \\ |\tilde{2}\rangle &= \frac{1}{\sqrt{3}} [ |021\rangle + |102\rangle + |210\rangle ] , \end{aligned} \quad (377)$$

and any single-qutrit wavefunction can be written in terms of these logical states as

$$|\tilde{\psi}\rangle = \sum_{i=1}^3 c_i |\tilde{i}\rangle . \quad (378)$$

Imagine trying to recover information about the encoded state in the situation where one only has access to two of the three qutrits of the logical qutrit. Remarkably, there exists a two-qutrit

<sup>63</sup> <https://sqmscenter.fnal.gov/>

operation that permits the extraction of the wavefunction. This two-qutrit operation, for example acting on qutrits 1,2,  $\hat{U}_{12}$ , acts such that

$$\hat{U}_{12} \otimes \hat{I} |\tilde{\psi}\rangle = |\psi\rangle \otimes \frac{1}{\sqrt{3}} [ |00\rangle + |11\rangle + |22\rangle ] , \quad (379)$$

and thus the wavefunction can be determined from qutrit-1 unambiguously. Analogously, the same can be determined when acting on the other pairs of qutrits. It is straightforward to identify the action of  $\hat{U}_{12}$ , a  $9 \times 9$  matrix,

$$\begin{aligned} |\text{00}\rangle &\rightarrow |\text{00}\rangle , |\text{11}\rangle \rightarrow |\text{01}\rangle , |\text{22}\rangle \rightarrow |\text{02}\rangle \\ |\text{01}\rangle &\rightarrow |\text{12}\rangle , |\text{12}\rangle \rightarrow |\text{10}\rangle , |\text{20}\rangle \rightarrow |\text{11}\rangle \\ |\text{02}\rangle &\rightarrow |\text{21}\rangle , |\text{10}\rangle \rightarrow |\text{22}\rangle , |\text{21}\rangle \rightarrow |\text{20}\rangle , \end{aligned}$$

$$\hat{U}_{12} = \begin{pmatrix} 1 & 0 & 0 & 0 & 0 & 0 & 0 & 0 & 0 \\ 0 & 0 & 0 & 0 & 1 & 0 & 0 & 0 & 0 \\ 0 & 0 & 0 & 0 & 0 & 0 & 0 & 0 & 1 \\ 0 & 0 & 0 & 0 & 0 & 0 & 1 & 0 & 0 \\ 0 & 0 & 0 & 0 & 0 & 0 & 0 & 1 & 0 \\ 0 & 0 & 0 & 0 & 0 & 0 & 0 & 0 & 1 \\ 0 & 1 & 0 & 0 & 0 & 0 & 0 & 0 & 0 \\ 0 & 0 & 0 & 0 & 0 & 0 & 0 & 1 & 0 \\ 0 & 0 & 1 & 0 & 0 & 0 & 0 & 0 & 0 \end{pmatrix} \quad (380)$$

This means that one of the physical qutrits can be lost from the logical qutrit, and the encoded wavefunction can be recovered by performing a unitary transformation.

There is a second feature about qutrits that adds to their potential utility. Imagine that an evedropper gains access to (an ensemble of) one of the physical qutrits in a logical qutrit, and seeks to extract information. How much information can be extracted? It is remarkable that by tracing over two qutrits, and forming the eigenvalues of the reduced density matrix, all three eigenvalues are equal to  $\lambda = \frac{1}{3}$ , independent of the encoded wavefunction. This is a maximally mixed state, with each basis state contributing with equal probability and without quantum correlations between them.

These two features, distinguishes qutrits from qubits in important ways from a information security and error correction standpoint, and also from a quantum simulation standpoint.

From the standpoint of simulating systems relevant to fundamental physics, qutrits appear natural, but relatively unexplored, in a number of areas, including to encode three flavors of neutrinos, and the three colors of quarks. It remains early days in simulating these systems, and others, and so the full utility of qutrits awaits discovery.

### 3. Stabilizer States for Qutrit Systems

Now that the motivation for pursuing qudit systems is clear, with the qutrit most understood at this point in time, it is useful to develop the stabilizer formalism, including stabilizer states and their properties. We have already seen in the context of quantum simulation that SU(2) is more similar to U(1) than SU(3) and higher, we expect that the qutrit will be closer in form to higher qudit systems than qubits are. Let us consider a qutrit, with wavefunction (forgetting about

physical Vs logical at the moment) and density matrix,

$$|\psi\rangle = \sum_{i=1}^3 c_i |j\rangle , \quad \hat{\rho} = |\psi\rangle\langle\psi| . \quad (381)$$

On general grounds,  $\hat{\rho}$  can be decomposed into generators of SU(3) and the identity matrix. Being trained as a particle physicist, it is natural to decompose  $\hat{\rho}$  into the identity and a sum of Gell-Mann matrices or generators of SU(3). For example,

$$\hat{\rho} = c_I \hat{I} + \sum_{a=1}^8 c_a T^a , \quad c_I = \frac{1}{3} \text{Tr}[\hat{\rho}] , \quad c_a = 2 \text{Tr}[\hat{\rho} T^a] , \quad (382)$$

where  $T^a = \lambda^a/2$  are the generators of SU(3) and  $\lambda^a$  are the Gell-Mann matrices define in App. A. However, one can immediately see that this is not an optimal way to proceed because of the different normalizations of the identity operator and the generators. They are the same in SU(2), but differ for a general SU(N). So, while they can be certainly used, there are better ways to proceed, which have been developed in detail in the QIS community.

A better way to proceed is to work with operators formed from  $\hat{X}$  and  $\hat{Z}$  operators (for example, see Refs. [110–112]), as hinted at previously, and the Pauli-basis formulation introduced in subsection VII A 1 can be readily generalized. To begin the discussion, a generalization of the  $\hat{X}$  and  $\hat{Z}$  operators from qubits to qutrits (and higher) is sufficient to develop the general framework. It is convenient to define the action of the operators (assuming PBCs in qudit space)

$$\begin{aligned} \hat{X}|j\rangle &= |j+1\rangle , \quad \hat{Z}|j\rangle = \omega^j |j\rangle , \quad \omega = e^{i2\pi/d} , \quad d=3 \\ \hat{X} &= \begin{pmatrix} 0 & 0 & 1 \\ 1 & 0 & 0 \\ 0 & 1 & 0 \end{pmatrix} , \quad \hat{Z} = \begin{pmatrix} 1 & 0 & 0 \\ 0 & e^{\frac{2i\pi}{3}} & 0 \\ 0 & 0 & e^{-\frac{2i\pi}{3}} \end{pmatrix} . \end{aligned} \quad (383)$$

Both matrices are traceless, the first trivially, while the second uses  $1 + e^{\frac{2i\pi}{3}} + e^{\frac{4i\pi}{3}} = 0$ . Requiring 9 basis operators, in analogy with the identity and 8 generators of SU(3), we define the Pauli-basis for qutrits to be

$$\hat{P} = \{\hat{I}, \hat{X}, \hat{Z}, \hat{X}^2, \omega \hat{X} \hat{Z}, \hat{Z}^2, \omega^2 \hat{X} \hat{Z}^2, \hat{X}^2 \hat{Z}, \hat{X}^2 \hat{Z}^2\} . \quad (384)$$

This operator basis does not have the usual orthogonality under traces, because of the  $Z_3$ -nature of the system. These operators satisfy the orthogonality condition under tracing,

$$\begin{aligned} \text{Tr} \left[ \hat{P}_i \hat{P}_j \right] &= 3h_{i,j} \\ h_{1,1} = h_{2,4} = h_{4,2} = h_{3,6} = h_{6,3} = h_{5,9} = h_{9,5} = h_{7,8} = h_{8,7} &= 1, \quad \text{and } h_{i,j} = 0 \text{ else} . \end{aligned} \quad (385)$$

To reconstruct a density matrix using this operator basis, the process is similar, but the off-diagonal trace relation means that the construction requires using a “key”, e.g.

$$\begin{aligned} c_i &= \text{Tr} \left[ \hat{\rho} \hat{P}_i \right] \\ \hat{\rho} &= \frac{1}{3} \sum_{i,j} h_{i,j} c_i \hat{P}_j \\ &= \frac{1}{3} \left( c_1 \hat{P}_1 + c_2 \hat{P}_4 + c_3 \hat{P}_6 + c_4 \hat{P}_2 + c_5 \hat{P}_9 + c_6 \hat{P}_3 + c_7 \hat{P}_8 + c_8 \hat{P}_7 + c_9 \hat{P}_5 \right) . \end{aligned} \quad (386)$$

This address the fact that the expansion in terms of Gell-Mann matrices does not have a uniform set of trace coefficients, but at the expense of having off-diagonal operator traces. However, this construction generalizes to higher dimension qudits, with the basis spanned by operators of the form  $\hat{X}^\alpha \hat{Z}^\beta$ , where  $0 \leq \alpha, \beta < d$ .

Creating the set of stabilizer states for a single qutrit proceeds along the same lines as for the single qubit. We perform all possible applications of the qutrit Hadamard-gate and S-gate, which are

$$\hat{H} = \frac{1}{\sqrt{3}} \begin{pmatrix} 1 & 1 & 1 \\ 1 & \omega & \omega^2 \\ 1 & \omega^2 & \omega \end{pmatrix}, \quad \hat{S} = \begin{pmatrix} 1 & 0 & 0 \\ 0 & 1 & 0 \\ 0 & 0 & \omega \end{pmatrix}. \quad (387)$$

This procedure realizes 12 stabilizer states, of the form

$$\begin{aligned} & (1, 0, 0), (0, 1, 0), (0, 0, 1), \\ & \frac{1}{\sqrt{3}}(1, 1, 1), \frac{1}{\sqrt{3}}(1, 1, \omega), \frac{1}{\sqrt{3}}(1, 1, \omega^2), \frac{1}{\sqrt{3}}(1, \omega, 1), \frac{1}{\sqrt{3}}(1, \omega^2, 1), \\ & \frac{1}{\sqrt{3}}(1, \omega, \omega), \frac{1}{\sqrt{3}}(1, \omega, \omega^2), \frac{1}{\sqrt{3}}(1, \omega^2, \omega), \frac{1}{\sqrt{3}}(1, \omega^2, \omega^2) , \end{aligned} \quad (388)$$

which, interesting, does not contain states with a single zero. The density matrix associated with each of these stabilizer states has a decomposition in terms of the XZ-Pauli basis in Eq. (384), with  $d = 3$  non-zero  $c_P$  coefficients, with a single appearance of each of  $1, \omega, \omega^2$ , out of the possible  $d^2 = 9$   $c_P$ . Thus, for these states  $|c_P| = 1$  (3 of them) or 0 (6 of them).

For universal classical computation involving more than one qudit, we need to generalize the CNOT gate from qubits to qudits. That is, we need to identify classically efficient entangling gates, for example for a recent experimental realization using transmons, see Ref. [113]. The simplest generalization of the CNOT gate beyond that defined for qubits is

$$\text{CNOT}_{12}|a, b\rangle = |a, a + b \bmod(3)\rangle , \quad (389)$$

where the subscript denotes  $\{\text{control}, \text{target}\}$ , leading to two distinct contributions for a 2-qutrit system, with the control on qutrit-1,  $\text{CNOT}_{12}$ , or on qutrit-2,  $\text{CNOT}_{21}$ . The Clifford gate set for 2 qutrits is

$$\{ \hat{I} \otimes \hat{I}, \hat{I} \otimes \hat{H}, \hat{I} \otimes \hat{S}, \hat{H} \otimes \hat{I}, \hat{S} \otimes \hat{I}, \hat{H} \otimes \hat{H}, \hat{H} \otimes \hat{S}, \hat{S} \otimes \hat{H}, \hat{S} \otimes \hat{S}, \text{CNOT}_{12}, \text{CNOT}_{21} \} . \quad (390)$$

Applying this gate set in all possible combinations to an initial state  $|00\rangle$  generates the complete set of 2-qutrit stabilizer states, for which there are 360.<sup>64</sup> The stabilizers are of the form of a power of 3 number of coefficients, i.e., 1, 3, 9, and are of the form, for example,

$$(0, 0, 0, 0, 0, 0, 0, 0, 1), (0, 0, 0, 0, 0, 0, 1, 1, \omega), (1, 1, 1, 1, 1, 1, \omega, \omega, \omega) . \quad (391)$$

Taking matrix elements of the the complete set of  $\hat{P}_i \otimes \hat{P}_j$  (defined in Eq. (384)) in each of these states results in  $d = 3^2 = 9$  non-zero matrix elements out of the  $d^2 = 9^2 = 81$  possible combinations. This is the generalization from the qubit case. However, one finds that the elements for each are from  $1, \omega, \omega^2$ .

---

<sup>64</sup> When I do this by randomly selecting gates and applying, I find that I need more than 3K trials (on average) to generate the 360 independent stabilizer states.

## B. Magic

### 1. Magic for Qubit Systems

Given the above discussion, it is helpful to develop measures that indicate the quantum complexity of a system. This can take many forms, of course, but a quantity that measures the distance to the nearest stabilizer state is a good place to start. The point to note is that for each stabilizer state,  $d$  of the  $d^2$  matrix elements of Paulis strings are  $\pm 1$ , as discussed around Eq. (376). There are many functional forms to consider when defining the non-stabilizerness of a given state, but the simplest to think about is  $\sum_P \Xi_P^2 = 1/d$  for a stabilizer state.<sup>65</sup> Therefore, we can define the “magic” in any state [114–116] by the deviation of  $d \sum_P \Xi_P^2$  from unity,

$$\mathcal{M} = 1 - d \sum_P \Xi_P^2 , \quad (392)$$

where this is defined to be the linear-magic. A more general set of measures are defined by the Renyi entropies,

$$\mathcal{M}_\alpha = \frac{1}{1-\alpha} \log \left( \sum_P \Xi_P^\alpha \right) - \log d , \quad (393)$$

which also vanish for stabilizer states.

Unlike entanglement, even a single qubit can contain magic, and require a T-gate to prepare. This does not mean that it is classically difficult to prepare, it is not! Consider a qubit in the state

$$|\psi\rangle = \cos \frac{\theta}{2} + e^{i\phi} \sin \frac{\theta}{2} , \quad (394)$$

from which it is straightforward to show that the magic in this state is

$$\mathcal{M} = \frac{1}{16} \sin^2 \theta (9 + 7 \cos 2\theta - 2 \sin^2 \theta \cos 4\phi) . \quad (395)$$

This is a function which vanishes in a number of places, corresponding to the state being a stabilizer state.

Two qubits is more complex as you would imagine, but the calculational strategy is the same. Given that single and few qubit magic can be computed by hand and the circuits are straightforward, the challenge is in defining a wavefunction with magic that is entangled at large scales. This is where classical computing cannot perform well, and quantum computers are required.

### 2. Magic for Qutrit Systems

The definition of magic can be extended from qubits to qudits with minor modifications. Noting that the matrix element of Pauli strings are powers of  $\omega$  for stabilizer states, we can define

$$\Xi_P = |c_P|^2/d , \quad \sum_P \Xi_P = 1 , \quad (396)$$

---

<sup>65</sup> There are  $d$  contributions, each of  $1/d^2$ .

for qutrit, and more generally qudit systems. In the same way that we defined the measure of non-stabilizerness, magic, for qubits, the same definition can be applied here

$$\mathcal{M} = 1 - d \sum_P \Xi_P^2 . \quad (397)$$

### C. The Entanglement Power and Magic Power of Unitary Operators

If we consider a simple scattering situation, such as occurs at the LHC, where we collide two hadrons, or a hadron and a nucleus, or two nuclei, with energies far exceeding their rest mass, then the final state typically has a very high multiplicity of light hadrons. The simulation of such processes is far beyond the capabilities of classical computing and requires quantum computers. As such, the system has evolved from a simple tensor-product state of two (composite) particles, to a high-multiplicity final states that is entangled and requiring T-gates to prepare. This change in entanglement and T-gate counts between the initial and final states is induced by the interactions, in this case the strong interactions. From well-known quantum field theory techniques, we know that that the asymptotic final state is evolved from the asymptotic initial state by the S-matrix. The initial state corresponds to well-separated (exponentially vanishing overlap) particles (wavepackets) directed at each other with high momentum, and the final state is a large number of well-isolated particles. Therefore, all of the information about the change of entanglement and the change in magic is contained in the S-matrix. As the S-matrix results from a unitary operator  $\hat{S}$ , we can use the developments in QIS regarding the entangling power and magic power of unitary operators. The entangling power of the S-matrix is the average amount of entanglement that is induced by the S-matrix across the Hilbert space. In Ref. [117], the two-particle entangling power was defined in terms of integrated averages over the block sphere of each particle, followed by forming the entanglement entropy of the one-particle reduced density matrix. Recently, we showed that this was equivalent to the average entanglement induced over the average 36 tensor-product stabilizer states, formed from the 6 single-qubit stabilizer states given in Eq. (375),

$$\bar{\mathcal{E}}(\hat{S}) \equiv \frac{1}{\mathcal{N}_{ss}^{TP}} \sum_{i=1}^{\mathcal{N}_{ss}^{TP}} \mathcal{E}\left(\rho_i^{(1)}(\hat{S})\right) , \quad (398)$$

where  $\mathcal{N}_{ss}^{TP}$  is the number of tensor-product stabilizer states, and  $\rho_i^{(1)}(\hat{S}) = \text{Tr}_2 [\rho_i^{(12)}(\hat{S})]$  is the outgoing reduced density matrix for particle 1, obtained by tracing the full outgoing density matrix  $\rho_i^{(12)}(\hat{S}) = \hat{S}|\Psi_i\rangle\langle\Psi_i|\hat{S}^\dagger$  over particle 2. The entangling power of the nucleon-nucleon and hyperon-nucleon S-matrix were computed in Ref. [117], and shown to reveal interesting structures. In particular, points of vanishing  $\bar{\mathcal{E}}(\hat{S})$  were shown to correspond to points of enhanced (emergent) symmetries in the system. For NN, vanishing entanglement power coincides with points of SU(4) spin-flavor symmetry that have been shown to emerge in the large- $N_c$  limit of QCD [118].

In the case of magic, a similar definition can be made for the magic-power of the S-matrix [116]. One starts from a stabilize state that has vanishing magic and measure the amount of magic in the final state,

$$\bar{\mathcal{M}}(\hat{S}) \equiv \frac{1}{\mathcal{N}_{ss}} \sum_{i=1}^{\mathcal{N}_{ss}} \mathcal{M}\left(\hat{S}|\Psi_i\rangle\right) , \quad (399)$$

where  $\mathcal{N}_{ss}$  denotes the total number of  $n$ -qubit stabilizer states. Generally, the magic power and the entangling power differ for the NN and YN forces, but they are similar across a large energy interval.

## VIII. ASSIGNMENT-1

### A. A One-Qubit Effective Hamiltonian and Time Evolution

As we will learn later, the Hamiltonian associated with a single plaquette in SU(2) lattice gauge theory, truncated down to a two dimensional Hilbert space, spanned by  $\{ |0\rangle, |\frac{1}{2}\rangle \}$ , has the form:

$$\hat{H} = c_E \begin{pmatrix} 0 & 0 \\ 0 & 1 \end{pmatrix} + \frac{1}{2} c_B \begin{pmatrix} 2 & -1 \\ -1 & 2 \end{pmatrix} , \quad (400)$$

for electric and magnetic coefficients  $c_{E,B}$ . The first term corresponds to the electric energy in the SU(2) field, while the second term corresponds to the magnetic energy.

The time-evolution operator,  $\hat{U}(t)$  can be constructed in terms of Euler angles. This is helpful in designing a quantum circuit that does not have errors associated with the non-commutation of Pauli matrices. Using the general Euler decomposition of rotations,  $\hat{U}(t)$  can have the form:

$$\hat{U}(t) = e^{i\phi} e^{i\alpha\hat{Z}} e^{i\beta\hat{X}} e^{i\gamma\hat{Z}} , \quad (401)$$

1. Find analytic expressions for  $\alpha, \beta, \gamma, \phi$  as a function of the coupling,  $c_{E,B}$ , and time,  $t$ .
2. Find the quantum circuit that implements  $\hat{U}(t)$ .
3. Using `qiskit` or `cirq` (your choice), implement this circuit on a quantum simulator.
4. For  $c_E = 1$  and  $c_B = 1$ , plot the energy in the electric field as a function of time, from  $t = 0, 2$  starting from an initial state of  $|0\rangle$  (the *trivial vacuum* for this system).
5. For  $c_E = 1$  and  $c_B = 1$ , determine how many measurements are required to obtain a 0.5% precision determination of the (trivial) vacuum-to-vacuum survival probability at  $t = 1.3$  starting from an initial state of  $|0\rangle$ .

### B. State Preparation: A Real Function on Two Qubits

Starting in the 2-qubit state  $|0\rangle = |00\rangle$ .

1. Find the angles  $\theta_{00}, \theta_{10}, \theta_{11}$ , required to prepare the 2-qubits in the state

$$|\psi\rangle = \frac{5}{\sqrt{54}} |0\rangle + \frac{4}{\sqrt{54}} |1\rangle + \frac{3}{\sqrt{54}} |2\rangle + \frac{2}{\sqrt{54}} |3\rangle . \quad (402)$$

2. Design the quantum circuit to prepare this state
3. Implement the circuit using the `qiskit` or `cirq` simulators, and perform measurements to verify you have prepared the correct state. Comment on any deviations you may observe.
4. Design the corresponding circuit using Molmer-Sorensen gates, and without CNOT-gates.

## IX. ASSIGNMENT-2

### A. Question 1: Entanglement

Consider the wavefunction describing two entangled regions, each containing two qubits,

$$|\psi\rangle = \frac{1}{3\sqrt{10}} [ 6|00,00\rangle + 3|01,00\rangle + 4|01,10\rangle + 5|01,11\rangle + 2|11,00\rangle ] . \quad (403)$$

1. After constructing the density matrix  $\hat{\rho}_{AB}$ , determine the reduced density matrices  $\hat{\rho}_A$ ,  $\hat{\rho}_B$ . What is the Schmidt rank of each density matrix?
2. Find the eigenvalues and eigenvectors of both reduced matrices, and use them to reconstruct the wavefunction using the Schmidt decomposition.
3. What is the entanglement entropy between the two regions?
4. What is the concurrence between the two qubits in region-A?
5. What is the negativity and the upper limit to distillable entanglement between the two qubits in region-A?
6. Compute the 4-tangle,  $\tau_4$ .

### B. Question 2: Non-Interacting and Interacting Scalar Field Theory

Consider a 2-site non-interacting scalar field theory in 1-dimension with a bare mass of  $m_0 = 1.0$  in lattice units that is digitized onto  $n_Q = 3$  qubits per lattice site, with a  $\phi_{\max} = 4.0$  and using PBCs in the spatial direction.

1. In the basis defined by eigenstates of the field operator at sites 1 and 2,  $|\phi_1, \phi_2\rangle$ , give the ground state wavefunction (i.e. provide a 64 component list of values of the amplitudes of the possible values of  $|\phi_1, \phi_2\rangle$ ).
2. Using `cirq` or `qiskit`, initialize your 6-qubit quantum register into this ground state (using the methods we discussed in class and extending last week's homework).
3. Now include a self coupling of the form  $\lambda_0 \phi^4$  with  $\lambda_0 = 8.0$ . Evolve the non-interacting ground state forward using leading order and second-order Trotter evolution for a time interval of  $t = 3.0$ . Show the wavefunction at site-1 as a function of time.

## X. ASSIGNMENT-3

### A. Question 1: Time Evolution

Consider a system with a Hamiltonian that is the sum of seven terms,

$$\hat{H} = \sum_{j=1}^7 \hat{H}_j , \quad (404)$$

with

$$\begin{aligned} \hat{H}_0 &= g^2 \left( \frac{14}{3} \hat{\mathbb{I}} \otimes \hat{\mathbb{I}} \otimes \hat{\mathbb{I}} - \frac{11}{6} \hat{Z} \otimes \hat{\mathbb{I}} \otimes \hat{\mathbb{I}} - \frac{3}{2} \hat{\mathbb{I}} \otimes \hat{\mathbb{I}} \otimes \hat{Z} - \frac{3}{2} \hat{Z} \otimes \hat{Z} \otimes \hat{\mathbb{I}} + \frac{1}{6} \hat{\mathbb{I}} \otimes \hat{Z} \otimes \hat{Z} \right) , \\ \hat{H}_1 &= -\frac{1}{4g^2} \hat{\mathbb{I}} \otimes \hat{\mathbb{I}} \otimes \hat{X} , \\ \hat{H}_2 &= -\frac{1}{4g^2} (\hat{\mathbb{I}} + \hat{Z}) \otimes \hat{X} \otimes \hat{\mathbb{I}} , \\ \hat{H}_3 &= -\frac{1}{4g^2} (\hat{\mathbb{I}} \otimes \hat{X} \otimes \hat{X} + \hat{\mathbb{I}} \otimes \hat{Y} \otimes \hat{Y}) , \\ \hat{H}_4 &= -\frac{1}{4g^2} (\hat{X} \otimes \hat{\mathbb{I}} \otimes \hat{X} + \hat{Z} \otimes \hat{\mathbb{I}} \otimes \hat{X}) , \\ \hat{H}_5 &= -\frac{1}{4g^2} \hat{Y} \otimes \hat{Z} \otimes \hat{Y} , \\ \hat{H}_6 &= -\frac{1}{2g^2} (\hat{b}^\dagger \otimes \hat{b} \otimes \hat{b} + \hat{b} \otimes \hat{b}^\dagger \otimes \hat{b}^\dagger) , \\ \hat{H}_7 &= -\frac{1}{8g^2} \hat{X} \otimes (\hat{\mathbb{I}} - \hat{Z}) \otimes (\hat{\mathbb{I}} - \hat{Z}) , \end{aligned} \quad (405)$$

where  $\hat{b} = (\hat{X} + i\hat{Y})/2$ .

Imagine that you have access to a perfect quantum computer with 10 qubits and a coherence time such that an integrated number of 1000 CNOT gates can be implemented in any given computation (for each member of an ensemble). The initial wavefunction of the system is the trivial state with all qubits in  $|0\rangle$ , and assume perfect qubit readout.

1. Find the groups of mutually commuting terms in the Hamiltonian.
2. Explore leading and subleading order Trotterized evolution, qDrift, random statistical sampling and any other method that you might invent, and determine the quantum circuits and workflow to provide the highest most accurate and precise determination of the vacuum-to-vacuum amplitude between  $t = 8\text{s}$  and  $t = 10\text{s}$ . (Provide extensive details on your studies, and provide a complete quantification of uncertainties.)

## XI. ASSIGNMENT-4

### A. Question 1: The Schwinger Model

Consider the lattice Schwinger model, quantum electrodynamics (QED) in 1+1 dimensions.

1. For a system in  $A_x = 0$  gauge, give the Hamiltonian for the lattice Schwinger model that can be mapped onto 8 qubits with open boundary conditions (OBCs).
2. By exact diagonalization of the Hamiltonian, find couplings for which there are single hadrons, bound-states of 2 hadrons, and 3-body bound states. Comment on the localization/containment of these states within the lattice?
3. Find the energy of the light degrees of freedom in a heavy meson comprised of static electric charge and compensating light charges. Comment on the spatial distribution of charge.
4. Starting in the trivial vacuum, time evolve the system forward (for a set of couplings you have chosen), and determine the energy in the electric field as a function of time. Use `qiskit` or `circ` for this calculation. Comment on approximations you have made and quantify the fidelity of your calculation.
5. Estimate the parameters required to compute the simplest inelastic scattering process of two hadrons in this theory.
6. What is the entanglement entropy across a bi-partition of the vacuum state?
7. What is the 4-tangle in the electron sector?

## Appendix A: Gell-Mann Matrices

For the sake of clarity and completeness, the Gell-Mann matrices are given in this appendix. Those already familiar with particle and nuclear physics will have seen them before, but others may not have. We present them here explicitly using Gell-Mann's convention, and this is but one choice of matrix representation that is found in the literature. The generators of SU(3) transformations,  $T^a$  in the fundamental representation of SU(3) are related to the Gell-Mann matrices via  $T^a = \frac{1}{2}\lambda^a$ , such that  $\text{Tr}[T^a T^b] = \frac{1}{2}\delta^{ab}$ .

$$\begin{aligned} \lambda^1 &= \begin{pmatrix} 0 & 1 & 0 \\ 1 & 0 & 0 \\ 0 & 0 & 0 \end{pmatrix}, \quad \lambda^2 = \begin{pmatrix} 0 & -i & 0 \\ i & 0 & 0 \\ 0 & 0 & 0 \end{pmatrix}, \quad \lambda^3 = \begin{pmatrix} 1 & 0 & 0 \\ 0 & -1 & 0 \\ 0 & 0 & 0 \end{pmatrix} \\ \lambda^4 &= \begin{pmatrix} 0 & 0 & 1 \\ 0 & 0 & 0 \\ 1 & 0 & 0 \end{pmatrix}, \quad \lambda^5 = \begin{pmatrix} 0 & 0 & -i \\ 0 & 0 & 0 \\ i & 0 & 0 \end{pmatrix}, \quad \lambda^6 = \begin{pmatrix} 0 & 0 & 0 \\ 0 & 0 & 1 \\ 0 & 1 & 0 \end{pmatrix}, \quad \lambda^7 = \begin{pmatrix} 0 & 0 & 0 \\ 0 & 0 & -i \\ 0 & i & 0 \end{pmatrix} \\ \lambda^8 &= \frac{1}{\sqrt{3}} \begin{pmatrix} 1 & 0 & 0 \\ 0 & 1 & 0 \\ 0 & 0 & -2 \end{pmatrix}. \end{aligned} \quad (\text{A1})$$

### 1. Side Note

$T^3$  and  $T^8$  represent the Cartan subalgebra of SU(3) with two elements, represented by traceless, diagonal, commuting matrices. In extending to larger N, the pattern extends naturally. For instance, the Cartan algebra of SU(4) has three elements and can be spanned by,

$$T^3 = \frac{1}{2} \begin{pmatrix} 1 & 0 & 0 & 0 \\ 0 & -1 & 0 & 0 \\ 0 & 0 & 0 & 0 \\ 0 & 0 & 0 & 0 \end{pmatrix}, \quad T^8 = \frac{1}{\sqrt{12}} \begin{pmatrix} 1 & 0 & 0 & 0 \\ 0 & 1 & 0 & 0 \\ 0 & 0 & -2 & 0 \\ 0 & 0 & 0 & 0 \end{pmatrix}, \quad T^{15} = \frac{1}{\sqrt{24}} \begin{pmatrix} 1 & 0 & 0 & 0 \\ 0 & 1 & 0 & 0 \\ 0 & 0 & 1 & 0 \\ 0 & 0 & 0 & -3 \end{pmatrix} \quad (\text{A2})$$

but also by

$$T^3 = \frac{1}{2} \begin{pmatrix} 1 & 0 & 0 & 0 \\ 0 & 1 & 0 & 0 \\ 0 & 0 & -1 & 0 \\ 0 & 0 & 0 & -1 \end{pmatrix}, \quad T^8 = \frac{1}{2} \begin{pmatrix} 1 & 0 & 0 & 0 \\ 0 & -1 & 0 & 0 \\ 0 & 0 & -1 & 0 \\ 0 & 0 & 0 & 1 \end{pmatrix}, \quad T^{15} = \frac{1}{2} \begin{pmatrix} 1 & 0 & 0 & 0 \\ 0 & -1 & 0 & 0 \\ 0 & 0 & 1 & 0 \\ 0 & 0 & 0 & -1 \end{pmatrix}, \quad (\text{A3})$$

with diagonal elements corresponding to a Welch-Hadamard Transform.

- [1] N. Klco and M. J. Savage, Phys. Rev. A **99**, 052335 (2019), 1808.10378.
- [2] S. P. Jordan, K. S. M. Lee, and J. Preskill, Quant. Inf. Comput. **14**, 1014 (2014), 1112.4833.
- [3] E. Campbell, Physical Review Letters **123** (2019), URL <https://doi.org/10.1103%2Fphysrevlett.123.070503>.
- [4] J. Carlson, M. J. Savage, R. Gerber, K. Antypas, D. Bard, R. Coffey, E. Dart, S. Dosanjh, J. Hack, I. Monga, et al. (2017), URL <https://www.osti.gov/biblio/1369223>.
- [5] J. Preskill, Quantum **2**, 79 (2018), 1801.00862.

- [6] S. M. Hengstenberg, C. E. P. Robin, and M. J. Savage, Eur. Phys. J. A **59**, 231 (2023), 2306.16535.
- [7] M. C. Bañuls et al., Eur. Phys. J. D **74**, 165 (2020), 1911.00003.
- [8] W. Guan, G. Perdue, A. Pesah, M. Schuld, K. Terashi, S. Vallecorsa, and J.-R. Vlimant, Mach. Learn. Sci. Tech. **2**, 011003 (2021), 2005.08582.
- [9] N. Klco, A. Roggero, and M. J. Savage, Rept. Prog. Phys. **85**, 064301 (2022), 2107.04769.
- [10] A. Delgado et al., in *Snowmass 2021* (2022), 2203.08805.
- [11] P. Alsing et al. (2022), 2210.14757.
- [12] C. W. Bauer et al., PRX Quantum **4**, 027001 (2023), 2204.03381.
- [13] C. W. Bauer, Z. Davoudi, N. Klco, and M. J. Savage, Nature Rev. Phys. **5**, 420 (2023).
- [14] D. Beck et al. (2023), 2303.00113.
- [15] A. Di Meglio et al., *Quantum Computing for High-Energy Physics: State of the Art and Challenges. Summary of the QC4HEP Working Group* (2023), 2307.03236.
- [16] S. R. Beane and M. J. Savage, Nucl. Phys. A **713**, 148 (2003), hep-ph/0206113.
- [17] S. R. Beane and M. J. Savage, Nucl. Phys. A **717**, 91 (2003), nucl-th/0208021.
- [18] S. R. Beane, P. F. Bedaque, K. Orginos, and M. J. Savage, Phys. Rev. Lett. **97**, 012001 (2006), hep-lat/0602010.
- [19] S. R. Beane, K. Orginos, and M. J. Savage, Int. J. Mod. Phys. E **17**, 1157 (2008), 0805.4629.
- [20] S. R. Beane, W. Detmold, K. Orginos, and M. J. Savage, Prog. Part. Nucl. Phys. **66**, 1 (2011), 1004.2935.
- [21] S. R. Beane, E. Chang, W. Detmold, H. W. Lin, T. C. Luu, K. Orginos, A. Parreno, M. J. Savage, A. Torok, and A. Walker-Loud (NPLQCD), Phys. Rev. D **85**, 054511 (2012), 1109.2889.
- [22] S. R. Beane, E. Chang, S. D. Cohen, W. Detmold, H. W. Lin, T. C. Luu, K. Orginos, A. Parreno, M. J. Savage, and A. Walker-Loud (NPLQCD), Phys. Rev. D **87**, 034506 (2013), 1206.5219.
- [23] M. L. Wagman, F. Winter, E. Chang, Z. Davoudi, W. Detmold, K. Orginos, M. J. Savage, and P. E. Shanahan, Phys. Rev. D **96**, 114510 (2017), 1706.06550.
- [24] E. Chang, Z. Davoudi, W. Detmold, A. S. Gambhir, K. Orginos, M. J. Savage, P. E. Shanahan, M. L. Wagman, and F. Winter (NPLQCD), Phys. Rev. Lett. **120**, 152002 (2018), 1712.03221.
- [25] Z. Davoudi, W. Detmold, K. Orginos, A. Parreño, M. J. Savage, P. Shanahan, and M. L. Wagman, Phys. Rept. **900**, 1 (2021), 2008.11160.
- [26] M. A. Nielsen and I. L. Chuang, *Quantum Computation and Quantum Information: 10th Anniversary Edition* (Cambridge University Press, 2011), ISBN 9781107002173.
- [27] R. P. Feynman, International Journal of Theoretical Physics **21**, 467 (1982), URL <https://doi.org/10.1007/BF02650179>.
- [28] P. A. Boyle, D. Chen, N. H. Christ, M. A. Clark, S. D. Cohen, C. Cristian, Z. Dong, A. Gara, B. Joo, C. Jung, et al., IBM Journal of Research and Development **49**, 351 (2005).
- [29] G. Parisi, Phys. Rept. **103**, 203 (1984).
- [30] G. P. Lepage, in *Theoretical Advanced Study Institute in Elementary Particle Physics* (1989).
- [31] S. R. Beane, W. Detmold, K. Orginos, and M. J. Savage, J. Phys. G **42**, 034022 (2015), 1410.2937.
- [32] M. L. Wagman and M. J. Savage, Phys. Rev. D **96**, 114508 (2017), 1611.07643.
- [33] S. R. Beane, W. Detmold, T. C. Luu, K. Orginos, A. Parreno, M. J. Savage, A. Torok, and A. Walker-Loud, Phys. Rev. D **79**, 114502 (2009), 0903.2990.
- [34] Cirq Developers, *Cirq* (2022), See full list of authors on Github: <https://github.com/quantumlib/Cirq/graphs/contributors>, URL <https://doi.org/10.5281/zenodo.7465577>.
- [35] M. Treinish, J. Gambetta, S. Thomas, qiskit bot, P. Nation, P. Kassebaum, E. Arellano, D. M. Rodríguez, S. de la Puente González, L. Bello, et al., *Qiskit/qiskit-metapackage: Qiskit 0.43.3* (2023), URL <https://doi.org/10.5281/zenodo.8165419>.
- [36] D. Gottesman, *The heisenberg representation of quantum computers* (1998), quant-ph/9807006.
- [37] C. M. Dawson and M. A. Nielsen, *The solovay-kitaev algorithm* (2005), quant-ph/0505030.
- [38] N. J. Ross and P. Selinger, *Optimal ancilla-free clifford+t approximation of z-rotations* (2016), 1403.2975.
- [39] N. Khaneja and S. Glaser, *Cartan decomposition of su(2<sup>n</sup>), constructive controllability of spin systems and universal quantum computing* (2000), quant-ph/0010100.
- [40] G. Vidal and C. M. Dawson, Physical Review A **69** (2004), URL <https://doi.org/10.1103/PhysRevA.69.010301>.
- [41] D. Maslov, New Journal of Physics **19**, 023035 (2017), URL <https://doi.org/10.1088/1367-263X/aa6d4c>.

- 10882F1367–26302Faa5e47.
- [42] Y. Wang, Z. Hu, B. C. Sanders, and S. Kais, Front. Phys. **8**, 479 (2020), 2008.00959.
  - [43] R. F. Werner, Phys. Rev. A **40**, 4277 (1989), URL <https://link.aps.org/doi/10.1103/PhysRevA.40.4277>.
  - [44] C. H. Bennett, G. Brassard, S. Popescu, B. Schumacher, J. A. Smolin, and W. K. Wootters, Phys. Rev. Lett. **76**, 722 (1996), URL <https://link.aps.org/doi/10.1103/PhysRevLett.76.722>.
  - [45] S. A. Hill and W. K. Wootters, Phys. Rev. Lett. **78**, 5022 (1997), URL <https://link.aps.org/doi/10.1103/PhysRevLett.78.5022>.
  - [46] W. K. Wootters, Quantum Information and Computation **1**, 27 (2001).
  - [47] S. P. Jordan, K. S. M. Lee, and J. Preskill, Science **336**, 1130 (2012), 1111.3633.
  - [48] S. P. Jordan, H. Krovi, K. S. M. Lee, and J. Preskill, Quantum **2**, 44 (2018), 1703.00454.
  - [49] J. Kempe and O. Regev, Quantum Information & Computation **3**, quant-ph/0302079 (2003), quant-ph/0302079.
  - [50] J. Kempe, A. Kitaev, and O. Regev, Siam journal on computing **35**, quant-ph/0406180 (2004), quant-ph/0406180.
  - [51] K. Symanzik, Nucl. Phys. **B226**, 187 (1983).
  - [52] K. Symanzik, Nucl. Phys. **B226**, 205 (1983).
  - [53] P. F. Bedaque, Physics Letters B **593**, 82 (2004), URL <https://doi.org/10.1016%2Fj.physletb.2004.04.045>.
  - [54] P. F. Bedaque and J.-W. Chen, Physics Letters B **616**, 208 (2005), URL <https://doi.org/10.1016%2Fj.physletb.2005.04.045>.
  - [55] G. de Divitiis, R. Petronzio, and N. Tantalo, Physics Letters B **595**, 408 (2004), URL <https://doi.org/10.1016%2Fj.physletb.2004.06.035>.
  - [56] C. T. Sachrajda and G. Villadoro, Phys. Lett. B **609**, 73 (2005), hep-lat/0411033.
  - [57] R. A. Briceño, Z. Davoudi, T. C. Luu, and M. J. Savage, Phys. Rev. D **89**, 074509 (2014), 1311.7686.
  - [58] R. A. Briceño, Z. Davoudi, T. Luu, and M. J. Savage, Phys. Rev. D **88**, 114507 (2013), 1309.3556.
  - [59] S. Lloyd, Science **273**, 1073 (1996).
  - [60] N. Klco and M. J. Savage, Phys. Rev. A **104**, 062425 (2021), 2109.01953.
  - [61] R. D. Somma, Quantum Info. Comput. **16**, 1125 (2016), ISSN 1533-7146, URL <http://dl.acm.org/citation.cfm?id=3179430.3179434>.
  - [62] N. Klco and M. J. Savage, Phys. Rev. A **102**, 012619 (2020), 1912.03577.
  - [63] N. Klco and M. J. Savage, Phys. Rev. A **102**, 052422 (2020), 2002.02018.
  - [64] R. C. Farrell, M. Illa, A. N. Ciavarella, and M. J. Savage, PRX Quantum **5**, 020315 (2024), 2308.04481.
  - [65] R. C. Farrell, M. Illa, A. N. Ciavarella, and M. J. Savage (2024), 2401.08044.
  - [66] W. Janke and T. Sauer, Phys. Lett. A **165**, 199 (1992).
  - [67] N. Hatano and M. Suzuki, Lect. Notes Phys. **679**, 37 (2005), math-ph/0506007.
  - [68] A. M. Childs and N. Wiebe, Journal of Mathematical Physics **54**, 062202 (2013), URL <https://doi.org/10.1063%2F1.4811386>.
  - [69] A. M. Childs and N. Wiebe (2012), URL <https://doi.org/10.26421%2Fqic12.11-12>.
  - [70] F. Turro, A. Roggero, V. Amitrano, P. Luchi, K. A. Wendt, J. L. DuBois, S. Quaglioni, and F. Pederiva, Phys. Rev. A **105**, 022440 (2022), 2102.12260.
  - [71] H. TERASHIMA and M. UEDA, International Journal of Quantum Information **03**, 633 (2005), URL <https://doi.org/10.1142%2Fs0219749905001456>.
  - [72] T. Banks, L. Susskind, and J. B. Kogut, Phys. Rev. **D13**, 1043 (1976).
  - [73] B. Andrade, Z. Davoudi, T. Graß, M. Hafezi, G. Pagano, and A. Seif, Quantum Sci. Technol. **7**, 034001 (2022), 2108.01022.
  - [74] O. Katz, M. Cetina, and C. Monroe (2022), 2202.04230.
  - [75] Y. Frishman and J. Sonnenschein, Cambridge Monographs (2010).
  - [76] A. Milsted, J. Liu, J. Preskill, and G. Vidal, PRX Quantum **3**, 020316 (2022), 2012.07243.
  - [77] P. Sala, T. Shi, S. Kühn, M. C. Bañuls, E. Demler, and J. I. Cirac, Phys. Rev. D **98**, 034505 (2018), 1805.05190.
  - [78] S. Weinberg, *The Quantum Theory of Fields*, vol. 1 (Cambridge University Press, 1995).
  - [79] R. C. Farrell, I. A. Chernyshev, S. J. M. Powell, N. A. Zemlevskiy, M. Illa, and M. J. Savage, Phys. Rev. D **107**, 054512 (2023), 2207.01731.
  - [80] R. C. Farrell, I. A. Chernyshev, S. J. M. Powell, N. A. Zemlevskiy, M. Illa, and M. J. Savage, Phys.

- Rev. D **107**, 054513 (2023), 2209.10781.
- [81] H. D. Politzer and M. B. Wise, Phys. Lett. B **206**, 681 (1988).
- [82] H. D. Politzer and M. B. Wise, Phys. Lett. B **208**, 504 (1988).
- [83] N. Isgur and M. B. Wise, Phys. Lett. B **232**, 113 (1989).
- [84] N. Isgur and M. B. Wise, Phys. Lett. B **237**, 527 (1990).
- [85] E. E. Jenkins and A. V. Manohar, Phys. Lett. B **255**, 558 (1991).
- [86] E. E. Jenkins and A. V. Manohar, Phys. Lett. B **259**, 353 (1991).
- [87] H.-H. Lu et al., Phys. Rev. A **100**, 012320 (2019), 1810.03959.
- [88] R. C. Farrell, M. Illa, and M. J. Savage (2024), 2405.06620.
- [89] Y. Y. Atas, J. Zhang, R. Lewis, A. Jahanpour, J. F. Haase, and C. A. Muschik, Nature Commun. **12**, 6499 (2021), 2102.08920.
- [90] A. H. Z. Kavaki and R. Lewis (2024), 2401.14570.
- [91] J. Kogut and L. Susskind, Phys. Rev. D **11**, 395 (1975), URL <https://link.aps.org/doi/10.1103/PhysRevD.11.395>.
- [92] A. Ciavarella, N. Klco, and M. J. Savage, Phys. Rev. D **103**, 094501 (2021), 2101.10227.
- [93] M. Illa and M. J. Savage, Phys. Rev. A **106**, 052605 (2022), 2202.12340.
- [94] M. Urbanek, B. Nachman, V. R. Pascuzzi, A. He, C. W. Bauer, and W. A. de Jong (2021), 2103.08591.
- [95] N. Klco, E. F. Dumitrescu, A. J. McCaskey, T. D. Morris, R. C. Pooser, M. Sanz, E. Solano, P. Lougovski, and M. J. Savage, Phys. Rev. A **98**, 032331 (2018), 1803.03326.
- [96] N. Klco, J. R. Stryker, and M. J. Savage, Phys. Rev. D **101**, 074512 (2020), 1908.06935.
- [97] S. A. Rahman, R. Lewis, E. Mendicelli, and S. Powell, Phys. Rev. D **106**, 074502 (2022), 2205.09247.
- [98] D. Gottesman, *Stabilizer codes and quantum error correction* (1997), quant-ph/9705052.
- [99] V. Veitch, S. A. Hamed Mousavian, D. Gottesman, and J. Emerson, New Journal of Physics **16**, 013009 (2014), ISSN 1367-2630, URL <http://dx.doi.org/10.1088/1367-2630/16/1/013009>.
- [100] H. J. García, I. L. Markov, and A. W. Cross, Quantum Info. Comput. **14**, 683–720 (2014), ISSN 1533-7146, 1711.07848.
- [101] M. Ringbauer, M. Meth, L. Postler, R. Stricker, R. Blatt, P. Schindler, and T. Monz, Nature Phys. **18**, 1053 (2022), 2109.06903.
- [102] P. Hrmo, B. Wilhelm, L. Gerster, M. W. van Mourik, M. Huber, R. Blatt, P. Schindler, T. Monz, and M. Ringbauer, Nature Commun. **14**, 2242 (2023), 2206.04104.
- [103] A. Morvan, V. V. Ramasesh, M. S. Blok, J. M. Kreikebaum, K. O'Brien, L. Chen, B. K. Mitchell, R. K. Naik, D. I. Santiago, and I. Siddiqi, Phys. Rev. Lett. **126**, 210504 (2021), URL <https://link.aps.org/doi/10.1103/PhysRevLett.126.210504>.
- [104] E. Champion, Z. Wang, R. Parker, and M. Blok (2024), 2405.15857.
- [105] M. Illa, C. E. P. Robin, and M. J. Savage, Phys. Rev. C **108**, 064306 (2023), 2305.11941.
- [106] M. Illa, C. E. P. Robin, and M. J. Savage (2024), 2403.14537.
- [107] M. Meth et al. (2023), 2310.12110.
- [108] A. Almheiri, X. Dong, and D. Harlow, Journal of High Energy Physics **2015** (2015), ISSN 1029-8479, URL [http://dx.doi.org/10.1007/JHEP04\(2015\)163](http://dx.doi.org/10.1007/JHEP04(2015)163).
- [109] D. Harlow, Communications in Mathematical Physics **354**, 865–912 (2017), ISSN 1432-0916, URL <http://dx.doi.org/10.1007/s00220-017-2904-z>.
- [110] M. Howard, E. Brennan, and J. Vala, Entropy **15**, 2340–2362 (2013), ISSN 1099-4300, URL <http://dx.doi.org/10.3390/e15062340>.
- [111] S. X. Cui and Z. Wang, Journal of Mathematical Physics **56** (2015), ISSN 1089-7658, URL <http://dx.doi.org/10.1063/1.4914941>.
- [112] Q. Wang, Electronic Proceedings in Theoretical Computer Science **266**, 58 (2018).
- [113] N. Goss, A. Morvan, B. Marinelli, B. K. Mitchell, L. B. Nguyen, R. K. Naik, L. Chen, C. Jünger, J. M. Kreikebaum, D. I. Santiago, et al., Nature Communications **13** (2022), ISSN 2041-1723, URL <http://dx.doi.org/10.1038/s41467-022-34851-z>.
- [114] L. Leone, S. F. Oliviero, and A. Hamma, Physical Review Letters **128** (2022), ISSN 1079-7114, URL <http://dx.doi.org/10.1103/PhysRevLett.128.050402>.
- [115] L. Leone and L. Bittel (2024), 2404.11652.
- [116] C. E. P. Robin and M. J. Savage (2024), 2405.10268.
- [117] S. R. Beane, D. B. Kaplan, N. Klco, and M. J. Savage, Phys. Rev. Lett. **122**, 102001 (2019), 1812.03138.
- [118] D. B. Kaplan and M. J. Savage, Phys. Lett. B **365**, 244 (1996), hep-ph/9509371.